Aus dem
CharitéCentrum für Grundlagenmedizin
Fächerverbund Anatomie
Institut für Funktionelle Anatomie
Direktor: Prof. Dr. med Matthias Ochs

Habilitationsschrift

Lung surfactant in the pathophysiology and treatment of lung fibrosis

zur Erlangung der Lehrbefähigung für das Fach Anatomie mit Schwerpunkt Zellbiologie und mikroskopische Anatomie

vorgelegt dem Fakultätsrat der Medizinischen Fakultät
Charité-Universitätsmedizin Berlin
von

Elena Lopez-Rodriguez, PhD

Eingereicht: Oktober 2021
Dekan: Prof. Dr. med. Axel R. Pries
1. Gutachter/in: Frau Prof.Dr. Gabriela Krasteva-Christ
2. Gutachter/in: Herr Prof.Dr. Peter König

TABLE OF CONTENTS

1 GENERAL INTRODUCTION

The main function of the lung is gas exchange. This function is essential for life and optimized combining a large surface area in contact with air and a thin barrier for gas (O_2/CO_2) diffusion. An array of conductive tubes (conductive airways: trachea and bronchi) leads atmospheric air through convection to the distal (alveolar) side of the lung, where gas exchange happens by diffusion (through a pressure gradient). The thinnest part of this diffusion barrier (air-blood barrier) is composed by just three elements: a very thin alveolar epithelial type 1 cell (AE1C) facing the air; an endothelial cell facing the blood; and the shared basal lamina between both (1).

This large surface area (around 140m^2 of alveolar surface) exposed to the environment makes the lung susceptible, not only to environmental changes (temperature, humidity) but also to changes in air composition or potential pathogens/particles travelling through the air. The lung is also exposed to many physical forces to mechanically renew the air inside, pushing out the CO_2-saturated air during expiration and pulling in O_2-saturated air during inspiration. Pressure is required to make the gas flow through the conductive airways during the breathing cycle. Therefore during inspiration the breathing muscles and movement of the chest and pleura creates a slightly negative pressure at alveoli (2). The elastic recoil of the lung ensures deflation during expiration, where the pressure along the entire tracheobronchial tree to alveoli is equal to atmospheric pressure. At the alveoli level, many physical forces also play a key role during the respiratory cycle. To the elastic recoil of the lung, due to the pleura and chest recoil forces, elastic properties of the connective tissue of the alveolar septa should also be taken into account. In addition, alveoli should also overcome interfacial forces from the air-liquid interface they are exposed to. This is mainly the surface tension at the liquid lining layer or hypophase. This force is mainly counteracted by lung surfactant, a specific mix of lipids and proteins synthesized and secreted by specialized cells, the alveolar epithelial type 2 cell (AE2C) (3). These cells are also the progenitor cells of the alveolar epithelium. Changes in either elastic properties of the lung tissue or surface tension, may lead to impaired lung mechanics and function.

If surface tension is not properly regulated by deficiency or inactivity of lung surfactant (see section 1.1 Lung surfactant), lung mechanics may also be compromised. Lung surfactant deficiency is the main contributing factor to the neonatal respiratory distress syndrome (NRDS) and leads to collapse of alveoli after birth and death. In this case, the premature neonates are born before lung surfactant is synthesized in sufficient amounts in the AE2C in the developing lung, before the 24-26th week of gestational age (4). In the same direction, changes in either quantity or type of fibers in the connective tissue of the alveolar septa and peripheral and peribronchiolar connective tissue have, thus a great impact in lung mechanics. An example of such a change is lung fibrosis (see section 1.2 Lung fibrosis), where an aberrant wound healing

leads to an abnormal accumulation of collagen fibers (5, 6). Mechanical stress, at the same time, leads to epithelial injury, contributing to the development of many lung diseases (7, 8).

1.1 LUNG SURFACTANT

Even though the lung comprises more than 40 different types of cells, the epithelium covering the alveoli is simply composed of two types of epithelial cells. The AE1C covers around the 90% of the alveolar surface and builds the surface through which gas diffusion happens. The AE2C is specialized in the production of lung surfactant, its degradation and recycling also occurs in the AE2C and partially in the alveolar macrophage (AM). Lung surfactant is mainly composed of phospholipids (approx. 80-90%) and proteins (approx. 5-15%) and AE2Cs are enriched in endoplasmic reticulum (7). In addition, the distinctive feature that characterize an AE2C are the organelles where surfactant is stored, the lamellar bodies (LB), which form a tightly packed structure and is secreted into the alveolar spaces (9). LB are secreted after proper stimuli, such as such as ATP (10, 11), calcium (12) or stretching forces (13). LB bodies unravel in the alveolar space and lamella are interconnected with the help of the surfactant protein A (SP-A) in a mesh or network of square tubular arrays, called tubular myelin (TM) (3, 14). TM opens up in interconnected multilamellar and multilayer structures, which reach the interface, forming the surface-active interfacial film (15). Surfactant composition shows a high proportion of dipalmitoyl phosphatidylcholine (DPPC), which has the unique property of higher lateral packing, when compared to unsaturated acyl chains. The palmitoyl (C16) acyl chains densely pack at the interface, reducing surface tension of the liquid at the hypophase surface. However, the process for DPPC to reach the interface is intrinsically energetically not favorable and proteins, such as surfactant protein B (SP-B) and C (SP-C), help these surface-active amphiphilic components to reach and stably pack at the interface.

Surface tension is the result of the cohesive forces between water molecules, which are unbalanced at the interface, creating a net force towards the center of a drop of water. This means that surface tension tends to minimize the surface of water or liquid exposed to another face, resulting in a spherical geometry in the case of water drops or the collapsing of alveoli due to the high adherence of the liquid lining layer.

Modeling an alveolus as a sphere, we can apply LaPlace law. This means that the intra-alveolar pressure is directly proportional to the surface tension and inversely proportional to its size (radius). Therefore, at a constant pressure, smaller alveoli, or alveoli at the end of the expiration, tend to have higher surface tension. This means that the cohesive forces of the alveolar wall will tend to close or collapse it. The main effect of surfactant is the stabilization of alveoli, so surfactant is able to “regulate” surface tension depending on alveolar size. This means that, especially during low lung volumes at the end of expiration, surfactant is able to lower down surface tension, by highly packing DPPC at the interface, to minimum values,

avoiding alveolar collapse. In this way, surfactant also maintains intra-alveolar pressure almost constant through the breathing cycle, ensuring surface tension is matched to alveolar size (16).

1.2 LUNG FIBROSIS

Respiratory disease causes an immense worldwide health burden (16). Each year 4 million people die prematurely from chronic respiratory diseases (17). Healthcare costs for respiratory diseases are an increasing burden on the economies of all countries. For example, across the 28 countries of the EU, the total costs of respiratory diseases amount to more than €380 billion annually (18).

Idiopathic pulmonary fibrosis (IPF) is a severe disease characterized by chronic inflammation, myofibroblast accumulation, and excessive extracellular matrix deposition, resulting in the damage of lung structure and respiratory failure. In Europe alone, approximately 40,000 new cases are diagnosed each year; however, its prognosis is overall poor, with a median survival of 3–4 years (17-19). Even though, two different drugs have been approved for the treatment of IPF, Nintedanib and Pirfenidone, results from clinical studies showed that they slow down the progression of the disease (20, 21), leaving lung transplantation as the only curative treatment. Therefore, this disease remains as incurable due to its complex and not known etiology (22-24).

Histologically, IPF is characterized by being spatially heterogeneous, meaning that healthy areas of the lung tissue can be found next to completely remodeled areas (25, 26). In the remodeled areas, accumulation of extracellular matrix components, such as collagen, and fibroblast foci are the typical histological feature. Fibrosis is thought to be the result of abnormal wound repair and tissue remodeling resulting from chronic epithelial injury leading to chronic inflammation and finally fibrosis (25). Pirfenidone is supposed to have an anti-fibrotic effect by blocking transforming growth factor beta 1 (TGF-β1), in an unknown molecular mechanism (27-29). This cytokine plays a key role in the development of fibrosis by inducing fibroblast migration and differentiation, extracellular matrix deposition and collagen accumulation (30, 31). However, recent data points to a defective paracrine-lipid cross-talking between alveolar cells as contributing factor to development and progression of the disease (32, 33). Moreover, immune cells also play a key role in the progression and development of the disease, especially in the transition point from inflammation to fibrotic development. Where, for example, macrophages change from a pro-inflammatory state to a pro-fibrotic state, which includes the production of TGF-β1 (34-36).

1.3 CONTEXT OF THIS WORK

The influence of lung surfactant in the development of lung fibrosis has not been deeply studied. Even though, some other research groups have pointed at surfactant dysfunction, in

terms of surfactant protein deficiency, changes in lipid profile, or higher surface tension in patient samples (37-39), a direct relation to the pathophysiology is still missing. When looking at human lung material, we should take into account that this material comes from either end-stage explanted lungs or biopsies directed to highly remodeled areas of the lung. This means that this material is not appropriate to understand dynamic changes through the development of the disease. For this purpose, animal models allow us to run time dependent analysis of the different events/changes happening in the lung, in very early stages throughout the fibrotic development phase. In this way, we can understand the dynamics and timing of the changes leading to the end-stage lung in the human. Understanding the order of events and its timing is also essential to develop targeted therapies.

As explained before, lung surfactant is essential to stabilize alveoli, preventing alveolar collapse and reducing the work of breathing. Therefore, we hypothesized that surfactant dysfunction/deficiency may contribute to the pathophysiology of lung fibrosis by inducing collapse, collapse induration (or permanent collapse) and mechanical stress in the epithelium triggering or contributing to aberrant wound healing. For surfactant dysfunction to have a triggering effect it has to occur very early in the development of the disease.

Therefore, in the next chapters we focused on time dependent changes after induction of lung disease. More specifically, we used animal models of lung fibrosis such as the TGF-β1 adenoviral transfection in mice ((40), see Chapter 2.1), genetically modified SP-C deficient mice ((41), see Chapter 2.2) and the widely used bleomycin induced rat model ((42), see Chapter 2.3). We analyzed early stages in every model, in a time course relevant for each, and focusing on time dependent changes of the lung surfactant system, immune cells such as alveolar macrophages, alveolar structure and lung mechanical properties.

Investigating early phases of fibrotic development will help us elucidate the mechanisms triggering aberrant fibrotic remodeling before the onset of fibrotic non-reversible wounds. This may be an important step towards early diagnosis of the disease and preventive treatment development. In addition, we propose a therapeutic strategy targeting lung surfactant deficiency, by either applying a surfactant replacement therapy (SRT) ((43), see Chapter 3.1) or directly replacing dysfunctional AE2C by healthy ones, for them to secrete and synthesize new surfactant ((44), see Chapter 3.2).

2 LUNG SURFACTANT AND LUNG FIBROSIS: COMMON PATHWAYS

2.1 TRANSFORMING GROWTH FACTOR BETA 1 (ORIGINAL WORK 1)

Lopez-Rodriguez E., Boden C., Echaide M., Perez-Gil J., Kolb M., Gauldie J., Maus U.A., Ochs M. & Knudsen L. "*Surfactant dysfunction during overexpression of TGF- β1 precedes profibrotic lung remodeling in vivo"* American Journal of Physiology - Lung Cell and Molecular Physiology. 2016; 310(11): L1260-71.

Transforming growth factor-beta (TGF-β) is a widely distributed growth factor with multiple biological functions in different organs, from lung organogenesis and homeostasis to tissue re-generation, tumorigenesis, and immune response. It is also involved in many respiratory diseases, such as pulmonary fibrosis but also emphysema, asthma, and cancer (45-47).

In 1985, the first human TGF-β molecular cloning was reported (48) and later its receptors were discovered (49). Today the TGF superfamily includes the Activin, Nodal, bone morphogenic proteins (BMPs), growth and differentiation factors (GDFs) and the three isoforms of TGF-β (TGF-β1, TGF-β2 and TGF-β3), between others with a total of 33 proteins in mammals (50). TGF-β is involved in a wide range of cellular and molecular mechanisms including cell proliferation, migration and differentiation, apoptosis, extracellular matrix (ECM) production and cell fate. Thereby, influencing the above-mentioned biological functions in multiple organs (45).

TGF-β1 is synthesized as a bigger (391 amino-acid) precursor molecule. After proteolytic cleavage, a 112 amino acid subunit results of approx. 25 kDa dimeric protein, linked by a sulfide bond. TGF-β1 is secreted in an inactive form. In addition, this latent (inactive form) is non-covalently bounded to another peptide, the latency associated peptide (LAP), which is derived from the N-terminal region of the TGF-β1 precursor, forming the small latent complex (SLC). The SLC is located in the cytoplasm of its producing cell until it binds to another protein called latent TGF-β-binding protein (LTBP), which is then secreted. TGF-β1 activation pathway is currently not well understood. Integrins, pH, reactive oxygen species (ROS) and proteases are some of the known factors, which have been shown to activate TGF-β1 (51-53). Active TGF-β1 binds and induces the oligomerization of the serine/threonine TGF-β receptor I and II. Consequently, a cascade of phosphorylation signals is initiated and the proteins of the Smad family are activated (phosphorylated). Smad2 and Smad3 are involved in the TGF-β1 pathway, while Smad1/5/9 in the BMP pathway. Phosphorylated Smads bind to Smad4 and are translocated to the nucleus. In the nucleus they, together with other co-receptors and transcription factors, will up-regulate the expression of numerous genes related to cell cycle arrest, apoptosis, epithelial to mesenchymal transition (EMT) and ECM deposition (54).

The accumulation of ECM in tissue is the histologic hallmark of fibrotic remodeling. Cells produce and attach to components of the ECM, such as fibronectin, collagen, laminin or elastin and proteoglycans (31). In addition, different secreted enzymes, such as matrix metalloproteinases (MMPs) or plasmin, can also degrade the ECM. The balance between production and degradation of the ECM matrix components is essential for the proper function of the organs. After injury, cells release plenty of cytokines, such as TGF-β1, to initiate normal tissue repair. However, both the excess and sustained production and secretion of TGF-β1 stimulates an aberrant tissue repair, resulting in the fibrotic remodeling of the wounded tissue (31, 55).

In IPF, the origin of the disease or the injury triggering event resulting in aberrant tissue repair is yet unknown. In addition, how the production of TGF-β1 is chronically sustained in order to end in a fibrotic remodeling is a question yet to answer. Others proposed that epithelial injury, either from chronic infection or from mechanical stress, might trigger fibrotic remodeling (56-59). As explained before, surfactant dysfunction/deficiency may influence mechanical properties of the lung, therefore potentially contributing to lung fibrosis development. However, the connection between TGF-β1 and lung surfactant has not been deeply investigated to date.

The aim of this work was to investigate the potential link between TGF-β1 signaling pathway and lung surfactant regulation *in vivo*. For this purpose, we used a well-established animal model, where TGF-β1 overexpression is induced in the lung by adenoviral vector transfection (containing the sequence coding for the active TGF-β1 protein) into the lung. As we were interested in the direct interaction between TGF- β1 and surfactant regulation, we analyzed the lungs at an early fibrosis development state, during TGF-β1 overexpression (one week after transfection), and later during fibrosis onset, where TGF-β1 overexpression already disappeared (two weeks after transfection). In this way, we could observe: 1) if there are changes in surfactant regulation in the presence of TGF-β1; 2) investigate where in the molecular pathway, there may be an interaction between both pathways, TGF-β1 signaling and lung surfactant regulation; 3) if any changes are restored to normal in the absence of overexpressed TGF-β1. In addition, if lung surfactant is dysregulated early in the induction of fibrotic remodeling, we also aimed to investigate the potential injury and changes in AE2C.

Am J Physiol Lung Cell Mol Physiol 310: L1260–L1271, 2016.
First published April 22, 2016; doi:10.1152/ajplung.00065.2016.

CALL FOR PAPERS | *Translational Research in Acute Lung Injury and Pulmonary Fibrosis*

Surfactant dysfunction during overexpression of TGF-β1 precedes profibrotic lung remodeling in vivo

Elena Lopez-Rodriguez,[1] Caroline Boden,[1] Mercedes Echaide,[3] Jesus Perez-Gil,[3] Martin Kolb,[4] Jack Gauldie,[4] Ulrich A. Maus,[2,5] Matthias Ochs,[1,5,6] and Lars Knudsen[1,5]

[1]*Institute of Functional and Applied Anatomy, Hannover Medical School, Hannover, Germany;* [2]*Department of Experimental Pneumology, Hannover Medical School, Hannover, Germany;* [3]*Department of Biochemistry and Molecular Biology, Faculty of Biology, Universidad Complutense de Madrid, Madrid, Spain;* [4]*Firestone Institute of Respiratory Health, McMaster University, Hamilton, Ontario, Canada;* [5]*Biomedical Research in Endstage and Obstructive Lung Disease Hannover (BREATH), Member of the German Center for Lung Research (DZL), Hannover, Germany; and* [6]*REBIRTH Cluster of Excellence, Hannover, Germany*

Submitted 10 February 2016; accepted in final form 17 April 2016

Lopez-Rodriguez E, Boden C, Echaide M, Perez-Gil J, Kolb M, Gauldie J, Maus UA, Ochs M, Knudsen L. Surfactant dysfunction during overexpression of TGF-β1 precedes profibrotic lung remodeling in vivo. *Am J Physiol Lung Cell Mol Physiol* 310: L1260–L1271, 2016. First published April 22, 2016; doi:10.1152/ajplung.00065.2016.—Transforming growth factor-β_1 (TGF-β1) is involved in regulation of cellular proliferation, differentiation, and fibrogenesis, inducing myofibroblast migration and increasing extracellular matrix synthesis. Here, TGF-β1 effects on pulmonary structure and function were analyzed. Adenovirus-mediated gene transfer of TGF-β1 in mice lungs was performed and evaluated by design-based stereology, invasive pulmonary function testing, and detailed analyses of the surfactant system 1 and 2 wk after gene transfer. After 1 wk decreased static compliance was linked with a dramatic alveolar derecruitment without edema formation or increase in the volume of septal wall tissue or collagen fibrils. Abnormally high surface tension correlated with downregulation of surfactant proteins B and C. TTF-1 expression was reduced, and, using PLA (proximity ligand assay) technology, we found Smad3 and TTF-1 forming complexes in vivo, which are normally translocated into the nucleus of the alveolar epithelial type II cells (AE2C) but in the presence of TGF-β1 remain in the cytoplasm. AE2C show altered morphology, resulting in loss of total apical surface area per lung and polarity. These changes of AE2C were progressive 2 wk after gene transfer and correlated with lung compliance. Although static lung compliance remained low, the volume of septal wall tissue and collagen fibrils increased 2 wk after gene transfer. In this animal model, the primary effect of TGF-β1 signaling in the lung is downregulation of surfactant proteins, high surface tension, alveolar derecruitment, and mechanical stress, which precede fibrotic tissue remodeling and progressive loss of AE2C polarity. Initial TTF-1 dysfunction is potentially linked to downregulation of surfactant proteins.

TGF-β1; TTF-1; AE2C polarity; surfactant; pulmonary fibrosis

TRANSFORMING GROWTH FACTOR-β_1 (TGF-β1) is a cytokine with a pivotal role in development of lung fibrosis (1, 47). TGF-β1 has been previously related to fibroblast migration, extracellular matrix deposition, and collagen accumulation (22). Molecular pathways of TGF-β1 start with the activation of two receptors, followed by numerous signaling cascades, one of which includes activation of members of the Smad family. Complexes of Smad2, Smad3, and Smad4 translocate to the nucleus and are responsible, together with other transcription factors, for the expression of different genes in the cell (30, 31). Adenoviral transfection of active TGF-β1 has already been studied in rats and mice, where development of a fibrotic phenotype after a minor inflammatory phase showed a prolonged deposition of collagen and recruitment of myofibroblast (2, 12, 40, 48). On the other hand, TGF-β1 effects have also been deeply studied in vitro, especially concerning alveolar epithelial cells and surfactant regulation. Surfactant proteins B (SP-B) and C (SP-C) are physiologically important components of pulmonary surfactant, playing a key role in the maintenance of opened alveoli, reducing surface tension, and avoiding alveolar collapse (45, 62). The effect of TGF-β1 overexpression in the regulation of SP-B has been described in alveolar epithelial-like cells, NCI H441 and A549 cells (24, 27, 32), but never before in an in vivo model. SP-B is essential for surfactant activity, and SP-B conditional knockout models showed increased surface tension leading to abnormal mechanical stress in the alveolar epithelium (36). Moreover, SP-B levels are reduced in patients suffering different lung diseases such as lung fibrosis (15). In addition to surfactant impairment, TGF-β1 has also been directly related to mechanical stress (7, 17) in the lung and closely linked to epithelial-to-mesenchymal transition (EMT) (6, 21, 28, 35, 57, 59), leading to loss of epithelial integrity (with deficiencies on cadherins and integrins to maintain proper cell-cell and cell-basal membrane adhesions) and remodeling of the lung tissue components (such as increased deposition of collagen) (3, 11, 46). The order of the events triggering and enhancing remodeling of the lung is still unclear, but there is growing evidence that surfactant dysfunction and alveolar collapse may be events preceding fibrotic remodeling in the lung (29). As a result alveolar epithelial cells show diverse phenotypes, from cells suffering endoplasmatic reticulum (ER) stress and apoptosis, through those migrating and transitioning to a wound-

Address for reprint requests and other correspondence: L. Knudsen, Institute of Functional and Applied Anatomy, Hannover Medical School, Carl-Neuberg-Str-1, 30625 Hannover, Germany (e-mail: knudsen.lars@mh-hannover.de).

healing phenotype, to those displaying a partial EMT-like process (46). Moreover, since alveolar epithelial type II cells (AE2C) hyperplasia is a feature of idiopathic pulmonary fibrosis (IPF) (9), of special interest would be to analyze both the temporal development and the effects of TGF-β1 on AE2C in vivo. Studying early stages in development of fibrotic phenotype, we aim to help elucidating the mechanisms undergoing changes in AE2C, surfactant function, mechanical stress, and chronic lung injury, thought to be one of the triggering events leading to lung fibrotic remodeling.

MATERIALS AND METHODS

Animals. Eighty male C57BL/6 mice (8 wk old; 20–25 g) were obtained from Charles River Laboratories (Sulzfeld, Germany). The study protocol was approved by the authorities of Lower Saxony LAVES (Niedersächsisches Landesamt für Verbraucherschutz und Lebensmittelsicherheit, which houses the German equivalent of an institutional animal care and use committee) following European Animal Welfare Regulations (approval TVA 12/0799).

Adenoviral transfection and sample collection. We instilled 10^8 plaque-forming units of AdTGFβ1$^{223–225}$ (48) or empty control vector intratracheally. Mice were euthanized 1 wk and 2 wk after adenoviral transfection.

Invasive pulmonary function testing. Animals were anesthetized with intraperitoneal (ip) injection of 80 mg/kg ketamine (Anesketin, Albrech, Aulendorf, Germany) and 5 mg/kg xylazine (Rompun 2%, Bayer, Leverkusen, Germany), diluted in physiological NaCl. Following the cessation of pain reflexes, a cannula was surgically inserted in the trachea. The animal was then connected to the flexiVent and an additional ip injection of the same anesthesia solution was applied to maintain the animal deep in narcosis during the mechanical ventilation. Additionally, 0.8 mg/kg pancuronium bromide (Pancuronium-Actavis 2 mg/ml, Actavis, Munich, Germany) was ip injected to prevent spontaneous breathing. Following a 5- to 10-min stabilization period ventilating the animal at positive end-expiratory pressure (PEEP) 3 cmH_2O, derecruitability tests were conducted as described before (29). First two recruitment maneuvers (deep inflation of the lung consisting of a 3-s increasing ramp to 30 cmH_2O followed by 3-s pressure hold to standardize the volume history) were applied. Then forced oscillation technique (FOT), consisting of baseline ventilation for 5 min with 30-s intervals of 8-s broadband, low amplitude of 17 sinusoidal frequency (0.5–19 Hz) perturbations, was conducted. Respiratory impedance was calculated for each frequency by Fourier transform and fit to the constant phase model to compute tissue elastance (H). Tissue hysteresivity (η) is calculated dividing tissue damping (G) (data not shown) by tissue elastance (H). The Flexiware software calculates therefore tissue hysteresivity (G/H) values within the 5 min of FOT. We calculated an average per animal and plotted the average per group. Finally, three pressure-controlled quasi-static pressure-volume loops were performed and quasi-static compliance (Cst) was calculated. The reported H values are the mean value of all the animals per group, whereas Cst values are mean values from three measurements in each animal. Inflation of the lung before fixation was performed by deep inflation of the lung (up to 30 cmH_2O) and subsequently decreased to 10 cmH_2O pressure, at which the trachea was closed. Since mechanical differences between healthy controls and empty vector controls (EV control) are not recognizable, next assays were performed with both healthy and EV controls, which are referred to from now on as control group to reduce the number of animal experiments.

Tissue preparation and fixation. Vascular perfusion-fixation was performed right after inflation of the lungs to 30 cmH_2O during the deflation limb at a constant airway opening pressure of 10 cmH_2O by use of the flexiVent. Perfusion of the lungs was carried out with 0.9% NaCl and 0.25% heparin at a constant pressure of 25 cmH_2O and followed by perfusion with the fixation solution (1.5% glutaraldehyde, 1.5% paraformaldehyde in 0.15 M HEPES buffer). Then the whole lung-heart block was excised and further fixed by immersion in the same fixing solution for 24 h at 4°C. Afterward all tissue not belonging to the lungs was eliminated and lung volume was determined by fluid displacement. Sampling of the fixing lungs was performed following systematic uniform random sampling as described before (52) and lung sections were embedded in Technovite 8,100 (Kulzer Hereaus, Wehrheim, Germany) (43) and further stained with 0.1% toluidine or 0.2% orceine for stereological analysis at light microscopy level. Lung cubes were also randomly sampled, embedded in Epon (Serva, Heidelberg, Germany), and contrasted with 1% osmium tetroxide (EMS, Hatfield, PA) and 4% uranyl acetate (Serva, Heidelberg, Germany) for stereological analysis under electron microscopy (19, 34, 37). Following the same procedure, another set of lungs were instillation-fixed with 10% formalin and sampled before being embedded in paraffin (Paraplast, Leica, Wetzlar, Germany) and used for immunohistochemistry and proximity ligand assay (PLA).

Histological sections and staining. Formalin-fixed paraffin-embedded tissue was stained with a Masson-Goldner staining kit (Merck, Darmstadt, Germany) for visualization of connective tissue (green).

Design-based stereology in light microscopy and electron microscopy. A list of recommended and determined stereological parameters (34, 37) is given in Table 1. At the light microscopic level, a newCAST-system (Viopharm, Horsholm, Denmark) was used to perform systematic uniform random area sampling and to superimpose an appropriate test system on the fields of view. Generally a point grid was used and points hitting the structure of interest or the reference volume were counted so that the ratio of the counted points resulted in the volume fraction of the given structure within the reference space. Since the volume of the reference space (volume of the lung) is known, volume fractions were converted to total volumes in all cases. At light microscopy level from eight animals per group, six to eight sections each and at least 60 fields of view to obtain 100–200 counting events per lung were analyzed. At electron micros-

Table 1. *Stereological parameters determined in this study*

Parameter	Determination	Magnification
Lung volume V(lung)	Fluid displacement	
Volume of septal wall V(sep, lung)	Point counting	×5
Total alveolar surface area S(alv, lung)	Intersection counting	×20
Thickness of the septal wall τ(sep)	V(sep, par) × 2/S(alv, par)	×20
Number of alveoli in the lung *N*(alv, lung)	Physical disector	×20
Volume of collagen in the lung V(collagen, lung)	Point counting	×8,900
Volume of alveolar edema in the lung V(ed, lung)	Point counting	×8,900
Volume of AE2C in the lung V(AE2C, lung)	Point counting	×8,900
Volume of LB in the lung V(LB, lung)	Point counting	×8,900
Volume density of LB in AE2C Vv(LB/AE2C)	Point counting	×8,900
Apical-basal ratio in AE2C	Intersection counting Sv(apical/AE2C)/Sv(basal/AE2C)	×8,900
Total AE2C apical surface in the lung S(apical, lung)	Vv(apical/AE2C)×V(AE2C, lung)	

AE2C, alveolar epithelial type 2 cells; alv, alveolar; col, collagen; ed, alveolar edema; LB, lamellar bodies; par, parenchyma; sep, septal wall; S, total surface area; Sv, surface area density; τ, thickness; V, volume; Vv, volume density.

Table 2. *List of antibodies used for Western blot analyses in BAL and lung homogenate samples*

Primary Antibody	Source	Dilution
Rabbit anti-SP-B	WRAB-48604 (Seven Hills Bioreagents, Cincinnati, OH)	1:1,000
Rabbit anti-SP-C	WRAB-76694 (Seven Hills Bioreagents, Cincinnati, OH)	1:1,000
Rabbit anti-proSP-B	WRAB-55522 (Seven Hills Bioreagents, Cincinnati, OH)	1:1,000
Rabbit anti-proSP-C	WRAB-9337 (Seven Hills Bioreagents, Cincinnati, OH)	1:1,000
Rabbit anti-TGF-β1 (mAB)	3709 (Cell Signaling Technology, Leiden, Netherlands)	1:1,000

copy level a transmission electron microscope (Morgagni, Eindhoven, Netherlands) equipped with a digital camera (Olympus Soft Imaging Systems, Münster, Germany) was used to obtain representatives fields of view from five animals per group. Five to seven sections per lung and at least 60 fields of view were analyzed to obtain 100–200 counting events per lung, providing appropriate precision of the stereological parameters. For superimposing a test system, a STEPanizer stereology tool (53) was used.

Western blot. For bronchoalveolar lavage (BAL) sample preparation ($n = 5$ per group), equal volumes of BAL samples were taken and mixed with loading buffer [2% SDS, 10% glycerol, 0.1% bromophenol blue, 10% β-mercaptoethanol in 12.5 μl Tris·HCl (pH 6.8)] and boiled for 10 min. Then 20 μl of BAL samples were loaded in the 16% polyacrylamide (PA) electrophoresis gel for detection of SP-B and SP-C and 10% PA gels to detect proSP-B and proSP-C. Proteins were transferred into Immun-Blot PVDF membrane (Bio-Rad Laboratories, Munich, Germany) and following 2 h of blocking (TBS-0.1% Tween 20, 5% nonfat milk, pH 7.4) at room temperature (RT), primary antibodies were incubated overnight at 4°C. Table 2 shows the list of primary antibodies used for Western blot from BAL samples.

After washing with TBS-T (TBS-0.1% Tween 20), secondary antibody (1:2000, polyclonal swine anti-rabbit, DAKO, Glostrup, Denmark) was incubated for 1 h at RT. Blot membranes were developed with ECL Prime Western blotting detection reagent (Amersham Bioscience, Buckinghamshire, UK) and band density of exposed films (Amersham Bioscience) was analyzed by densitometry using Image J (Rasband WS, ImageJ, U. S. National Institutes of Health, Bethesda, MD, http://imagej.nih.gov/ij/).

For lung homogenate samples ($n = 5$ per group), little pieces of lung tissue (~15 mg) were mixed with lysis buffer (50 mM Tris·HCl pH 7.5, 150 mM NaCl, 1% Triton, 0.5% Na-deoxycholate, 5 mM EDTA and protease inhibitor cocktail (complete mini, Roche, Mannheim, Germany). A TissueLyser II (Qiagen, Hilden, Germany) was used to disrupt the tissue. Soluble proteins were isolated from the supernatant of the disrupted tissue after centrifugation (10,000 *g*, 10 min, 4°C). Total protein content was determined by BCA protein assay (Thermo Scientific, Waltham, MA), and total 20 μg of proteins per well in loading buffer were loaded in 12% PA gels. Proteins were transferred into Immun-Blot PVDF membrane (Bio-Rad Laboratories) and after 2 h of blocking (TBS-0.1% Tween 20, 5% BSA, pH 7.4) at RT, primary antibodies were incubated overnight at 4°C. A list of primary antibodies is shown in Table 3. After washing with TBS-T (TBS-0.1% Tween 20), secondary antibodies (1:2,000, polyclonal swine anti-rabbit-horseradish peroxidase (HRP) or 1:1,000 polyclonal rabbit anti-goat-HRP, DAKO, Glostrup, Denmark) were incubated for 1 h at RT. Blot membranes were developed with ECL Prime Western blotting detection reagent (Amersham Bioscience) and band density of exposed high-performance ECL X-ray films (Amersham Bioscience) was analyzed by densitometry using Image J (ImageJ, U. S. National Institutes of Health).

RT-PCR. Total cell RNA was isolated from frozen lung tissue by use of ISOLATE RNA Mini Kit (Bioline, Berlin, Germany) and quantified by spectrometry at 260 nm. Reverse transcription was performed with 1 μg of total RNA and the iScript cDNA Synthesis Kit (Bio-Rad Laboratories) in a thermocycler (MasterCycler, Eppendorf, Hamburg, Germany). Real-time PCR was performed with iQ SYBR Green Supermix (Bio-Rad Laboratories) at a final primer concentration of 100 nm and 50 ng cDNA. Antibody-mediated hotstart iTaq DNA polymerase was activated after an initial 3-min denaturation step at 95°C. Denaturation of DNA was performed by holding further 95°C for 10 s. Annealing and extension temperature was set to 59°C (30 s) for 40 cycles in a Bio-Rad CFX96 RT-PCR system (Bio-Rad Laboratories). Primer design was performed with the GeneFisher software from the University Bielefeld (Bielefeld, Germany) (13) and primer sequences are shown in Table 4. RT-PCR data are represented as normalized expression (ΔΔCq), which corresponds to the relative quantity of the target gene normalized to the quantity of the reference gene (GAPDH). Bars correspond to the mean and standard error of $n = 6$ animals per group.

Captive bubble surfactometer. Surfactant membranes were isolated from BAL samples and were assayed at 20 mg/ml phospholipid concentration in a captive bubble surfactometer as described before (44).

Proximity ligand assay and quantification. PLA and quantification allow us to detect and quantify protein interactions using two specific primary antibodies for the proteins of interest and two different secondary antibodies that contain unique DNA strands, which are ligated, when closed enough (<40 nm), with the help of a ligase to form a circular template. This template (anchored to the antibody) is amplified by use of fluorescently labeled oligonucleotides, which hybridize to the template and the subsequent rolling-circle amplification products (49). The signal is easily visible as a fluorescence spot and analyzed by fluorescence microscopy. Formalin-fixed paraffin-embedded sections were processed for PLA by the same protocol described above for immunohistochemistry until incubation with primary antibodies. Primary anti-TTF-1 and anti-Smad3 were used as indicated in Table 5 and incubated overnight at 4°C. After washing (0.01 M Tris, 0.15 M NaCl, and 0.05% Tween 20), 1 h incubation at 37°C in a wet chamber with PLA anti-rabbit MINUS and anti-goat PLUS (Duolink kit, OLink Biosciences, Uppsala, Sweden) (1:5 dilution) was performed. Ligation of the PLA probes minus and plus was achieved by using ligation solution (1:40 dilution) provided by OLink Biosciences and incubated for 30 min at 37°C in a wet chamber. Finally, for amplification, incubation of the samples with amplification solution (1:5, containing the fluorescently labeled oligonucleotides) and polymerase (1:80) was done during 100 min at 37°C in a wet chamber. DAPI was used to counterstain nuclei. Negative controls for cross-reactivity between antibodies showed that no positive fluorescence signal was detected (not shown). Pictures were taken with a fluorescence microscope (Leica DM6000B, Leica, Wetzlar, Germany). Quantification of the complexes was done by counting single dots and their location relative to the nucleus within one cell. Enough numbers of fields of view were taken to count a total of 50 cells per animal ($n = 3$) and data are expressed as relative quantity of complexes (relative to control), divided by location.

Table 3. *List of primary antibodies used for Western blot and tissue homogenate*

Primary Antibody	Source	Dilution
Goat anti-TTF-1	sc-8761 (Santa Cruz Biotechnology, Heidelberg, Germany)	1:500
Rabbit anti-Smad3	sc-8332 (Santa Cruz Biotechnology, Heidelberg, Germany)	1:1,000
Rabbit anti-β-actin	ab8229 (abcam, Cambridge, UK)	1:1,000

Table 4. *List of primers used for RT-PCR*

Gene	Protein	Accesion Number	Forward Primer	Reverse Primer
Sftpa	SP-A	NM_023134.4	TGT CTA AGA AGC CAG AGA ACC A	GGG TGG CTG CTA TTA GGT CA
Sftpb	SP-B	NM_001282071.1	CAA TCC GGA AGT TCC TGG AA	TAA TCT GGC TCT GGA AGT AGT CA
Sftpc	SP-C	NM_011359.2	AGA TGG TCC TTG AGA TGA GCA	ATA CAC AAC GAT GCC AGT GGA
Sftpd	SP-D	NM_009160.2	GCC ATA CAG CAA CTC ATC ACA	GGA GCC CAA TTA GAA TAG ACC A
Abca3	ABCA3	NM_013855.2	TAA GGA CAA GAT GCG CAT CAG A	AGA GCC CTG TCA GCA GAG A
Napsa	NAPSIN A	NM_008437.1	CAC AGG CCA GGA CTA TGT CA	AGA CGT CCC CAA GGA TCC A
Tgfb1	TGF-b1 murine	NM_011577.1	AGT GTG GAG CAA CAT GTG GA	CGT CAA AAG ACA GCC ACT CA
Tgfb1	TGF-B1 porcine	NM_214015.1	CGT TGG CTG CTA GTG CTG A	GAC AGA ATC TGG CCG CGA A
Tgfbr1	TGF-bRI	NM_009370.2	GTT GAT ACT AGG AGA AGC AGC AA	CTA ACT CCA GCA GCA GTG AGA
Smad3	SMAD-3	NM_016769.4	CCT TTG GAG AAG TTG TAA TGG A	TCC CGT CTC TCT GCA TCC TA
Nkx2-1	TTF-1	NM_009385.3	GCG ACG TTT CAA GCA ACA GA	CTT GTA GCG GTG GTT CTG GA
P2ry2	P2Y2	NM_008773.3	GCC TAA CAG AAC TGT GAG GAA	GAC ACC TGA CTG AGG TGC TA
P2rx4	P2X4	NM_011026.2	CCA GAT CAA GTG GGA CTG CA	ACC TGA AAT TGT AGC CAG GAG A
Slc34a2	IIb Na-Pi	NM_011402.3	CTG ATG GCA TAC AGA CCT GGA	GTA AGC AAG ATG ATG CCC ACA

Statistical analysis. Statistical tests and data plotting were assessed with GraphPad Prism 6.0 (GraphPad Software). Data are presented as means ± SE and analyzed by one-way ANOVA corrected for multiple comparison by Bonferroni test with confidence interval 95%. Correlation analyses were performed using Pearson's test and linear regression. P values <0.05 were considered statistically significant.

RESULTS

Structural and mechanical changes after TGF-β1 transfection. Structural changes can be observed in Fig. 1, *A* and *B*. Masson-Goldner trichrome staining shows nonaerated areas of lung parenchyma 1 and 2 wk after transfection of TGF-β1. Although 2 wk after gene transfer an increase in collagen fibers can be found in these regions, this appears not to be the case 1 wk after gene transfer, when we observe an increased cellularity. Using perfusion-fixed lungs we were able to clearly identify capillaries usually found in the septal walls of the lung (Fig. 1*B*). Alveolar ducts are enlarged and the septal walls appear to be piled up, manifesting as thickened septal walls corresponding to microatelectases in the presence of high surface tension, findings we have previously documented in the bleomycin model as well. Both alveolar collapse (Fig. 1*B*, TGF-β1 1 wk) and the later deposition of collagen fibrils contribute to the thickening of the septal walls (Fig. 1*B*, TGF-β1 2 wk). Further analysis of the tissue hysteresivity (Fig. 1*C*) shows virtually no change in η-value between controls and the 1-wk group, suggesting that increase in H 1 wk after transfection is related to pure derecruitment of distal air space and therefore impaired alveolar dynamics (4), whereas at later time points (2-wk group) differences in tissue hysteresivity suggest the contribution of changes in the rheological properties of lung parenchyma, which can result from beginning profibrotic remodeling. In line with this observation, collagen deposition, quantified by design-based stereology using electron micrographs (Fig. 1*D*) within the septal walls is first noticeable 2 wk after TGF-β1 transfection (Fig. 1*E*). Accordingly, 1 wk after TGF-β1 transfection, static compliance demonstrates an increased stiffness of the respiratory system (Fig. 2*A*): both 1 and 2 wk after transfection groups show decreased static compliance. Moreover, lung mechanics as seen in tissue elastance H measured during ventilation at PEEP 3 cmH_2O (Fig. 2*B*) shows a further increase in lung stiffness 2 wk after transfection compared with group 1-wk and control groups. Using pooled data, the thickening of the septal walls (as seen in Fig. 1, *A* and *B*) is statistically significantly correlated with the decreased static compliance of lungs, independent if it results from pure derecruitment (*week 1*) or interstitial remodeling with collagen deposition or both of these factors (*week 2*) (Fig. 2*C*). Both lung volume and alveolar surface at an airway opening pressure of 10 cmH_2O are significantly decreased in 1-wk group and show a slight recovery 2 wk after transfection (Fig. 2, *D* and *E*). Although volumes of septal wall and alveolar edema per lung do not differ from controls at 1 wk, these parameters increase 2 wk after transfection (Fig. 2, *F* and *G*). In summary, after 1 wk decreased static compliance can be correlated with pure derecruitment of alveoli without increase in septal wall tissue per lung. After 2 wk an increase in septal wall tissue including the volume of collagen fibrils results in an additional increase in tissue elastance H and hysteresivity while static compliance is unchanged compared with *week 1*.

Regulation of surfactant protein expression and function by TGF-β1. We investigated whether the two associated surfactant proteins B and C suffered changes due to the presence of TGF-β1. Figure 3*A* shows SP-B and SP-C partial deficiency 1 wk after transfection of TGF-β1, associated with the presence of active TGF-β1 in the BAL. Therefore it seems that during overexpression of active porcine TGF-β1 (1-wk group) the two most important proteins for activity of surfactant are underexpressed (Fig. 3*B*). To depict whether this deficiency comes from downregulation of the corresponding genes, we performed RT-PCR of surfactant proteins A-D (*Sftpa*, *Sftpb*, *Sftpc*, *Sftpd*) and genes involved in surfactant synthesis (ABCA3) or surfactant protein processing (napsin A). Figure 3*C* demonstrates a downregulation of surfactant-related genes not only 1 wk but also 2 wk after gene transfer with a trend toward recovery at the time point 2 wk. However, there is a full recovery of protein level of SP-B and SP-C 2 wk after transfection coinciding with the disappearance of active TGF-β1 in the BAL. Surprisingly, not only are the BAL levels of mature

Table 5. *List of antibodies used for fluorescence immunhistochemistry*

Primary Antibody	Source	Dilution
Rabbit anti-TTF-1	sc-13040 (Santa Cruz Biotechnology, Heidelberg, Germany)	1:50
Goat anti-Smad3	sc-6033 (Santa Cruz Biotechnology, Heidelberg, Germany)	1:50

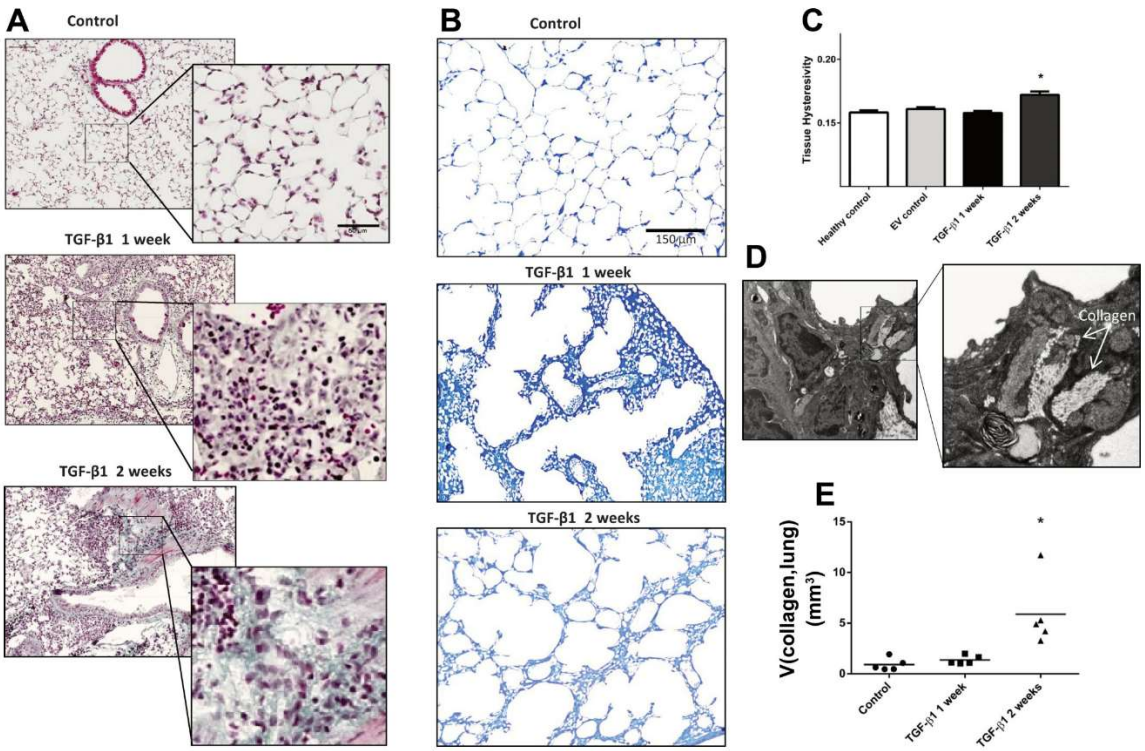

Fig. 1. Structural changes after TGF-β1 transfection. *A*: Masson-Goldner trichrome staining, showing nonaerated areas in lung parenchyma with increased cellularity 1 wk and increased amounts of collagen (green) 2 wk after TGF-β1 expression (scale bar = 100 μm, high-magnification images scale bar = 50 μm). *B*: perfusion-fixed and toluidine blue-stained representative pictures showing microatelectases at an airway opening pressure of 10 cmH_2O (TGF-β1 1 wk). The alveolar ducts are enlarged and alveoli are not visible anymore with thickened interalveolar septal walls as sign of high surface tension. *C*: tissue hysteresivity before and after TGF-β1 transfection ($n = 6$). Representative electron microscopic micrographs showing location of collagen fibrils (*D*), used to quantify volume of collagen within septal walls [V(collagen, lung); *E*]. $^*P < 0.05$ vs. control.

SP-B and SP-C recovered but there is also a noticeable aberrant accumulation of the surfactant protein precursors in the tissue homogenate (lung homogenate) (Fig. 3*D*) 2 wk after transfection, potentially originating from dysfunctional AE2C. Since the adenoviral vector used contains the porcine sequence of the active TGF-β1, differentiation between murine (endogenous) and porcine (exogenous) expression of the protein is possible (Fig. 3*E*). In the case of the adenoviral sequence, it appears overexpressed 1 wk after transfection and disappears with time, correlated with the level of the active protein in BAL. Since the vector is given intratracheally, an important source for intra-alveolar active TGF-β1 are epithelial cells of the respiratory system whereas endogenous TGF-β1 is produced by different cell types including interstitial cells. The endogenous murine sequence seems to decrease while the adenoviral sequence is overexpressed and comes back to slightly increased levels of expression 2 wk after transfection, not affecting surfactant protein levels in the BAL anymore but coinciding with still elevated Smad3 expression in lung homogenate. Both SP-B and SP-C proteins are essential for surfactant function; hence we analyzed the activity of lung surfactant with a captive bubble surfactometer. Figure 3*F* shows minimal surface tension reached upon compression during dynamic cycling of the bubble. Minimal surface tension shows deficient activity of surfactant 1 wk after transfection of TGF-β1 at normalized phospholipid concentration. Thus minimal surface tension correlates with the deficiency in SP-B and SP-C during TGF-β1 expression (Fig. 3, *A* and *B*). Moreover, quantification of the total number of open alveoli shows a marked loss of alveoli due to alveolar collapse, which is not reversible 2 wk after transfection (Fig. 3*G*). Since the complete surfactant system seems to be impaired by TGF-β1 and the proteins studied here are regulated by the same transcription factor in AE2C (*Nkx2-1* or TTF-1), we investigated TTF-1 in deeper detail.

Smad3/TTF-1 complexes during TGF-β1 overexpression. At the protein level (Fig. 4, *A* and *B*) simultaneously to the upregulation of Smad3, we can observe the downregulation of TTF-1, which can partially explain SP-B and SP-C deficiency. RNA expression levels of genes involved in the TGF-β1 signaling pathway can be observed in Fig. 4*C*. On the other hand, TTF-1 has already been described to interact with Smad3 and locate to the nucleus (20) in A549 cells. In our in vivo model we investigated whether these Smad3/TTF-1 complexes form and whether they locate exclusively to the nucleus of AE2C. In Fig. 4*D*, positive red fluorescence dots can be observed demonstrating the existence of Smad3/TTF-1 complexes in vivo. Moreover, we quantified the location of these

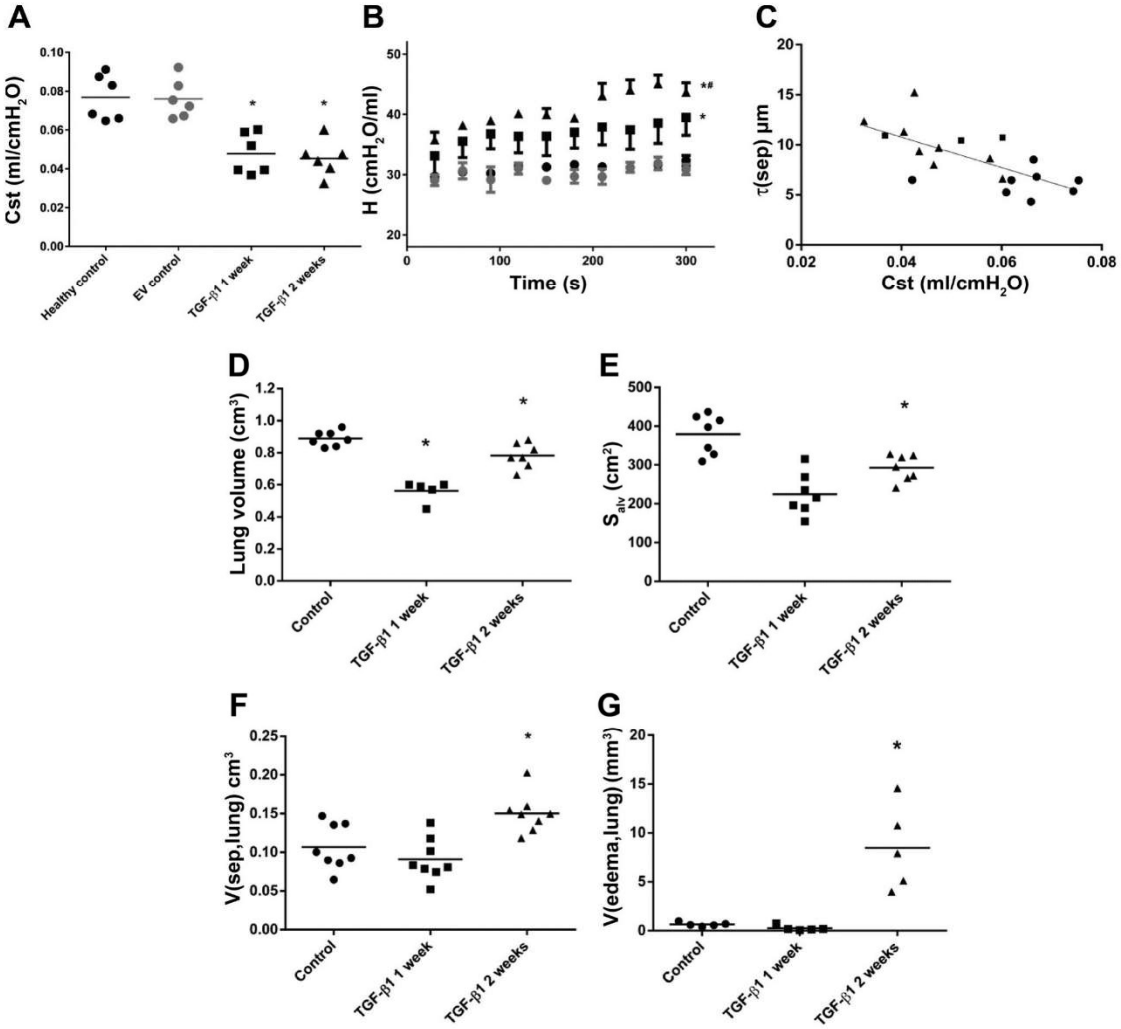

Fig. 2. Mechanical changes after TGF-β1 transfection. Static compliance (Cst; *A*) and tissue elastance (*H*; *B*) values measured repetitively after recruitment maneuver during PEEP 3 cmH_2O ventilation ($n = 6$). EV, empty vector. *C*: statistically significant correlation between Cst and thickness of the septal wall [τ(sep)] $P < 0.01$, $r^2 = 0.48$ (●, controls; ■, 1 wk after TGF-β1 transfection; ▲, 2 wk after TGF-β1 transfection), by means of design-based stereology. *D*: lung volume as measured by fluid displacement in the different groups. Total alveolar surface per lung (S_{alv}, *E*) and absolute volume of septal wall in the lung [V(sep,lung); *F*] as measured by design-based stereology at light microscopic level. *G*: absolute volume of alveolar edema in the lung [V(edema,lung)] measured by design-based stereology at the electron microscopy level. $*P < 0.05$ vs. controls; $\#P < 0.05$ vs. 1 wk.

complexes relative to the nucleus (Fig. 4*E*). Interestingly, in addition to a reduced total relative number of complexes, correlating with the partial deficiency of TTF-1, we found fewer complexes located in the nucleus (red arrows in Fig. 4*D*) with the associated increase in complexes located in the cytoplasm (white arrows in Fig. 4*D*) during overexpression of TGF-β1 (1-wk group). Once overexpression of porcine TGF-β1 disappears (2-wk group), both the relative amount of complexes and their nuclear location increases; even though TTF-1 protein levels are not back to normal (Fig. 4, *A* and *B*), it seems that sufficient amount of TTF-1 is actively translocated to the nucleus. Nevertheless, whereas BAL levels of SP-B and SP-C as well as the surfactant function recover, the expression of related genes showed only a tendency for recovery.

Loss of apical surface and polarity on AE2C after TGF-β1 transfection. Even though changes in total volume of AE2C are not that noticeable (Fig. 5*E*), we observed differences in morphology and location of these cells between the different groups. Figure 5, *A–D* shows different AE2C profiles 2 wk after gene transfer by electron microscopy. Although AE2C are mostly classified as such by the existence of lamellar bodies (LB; white arrows), some of these cells do not show a clear AE2C morphology and, most importantly, location. Although some AE2C (Fig. 5, *A* and *B*) show LB together with apical membranes with microvilli in contact with air spaces corre-

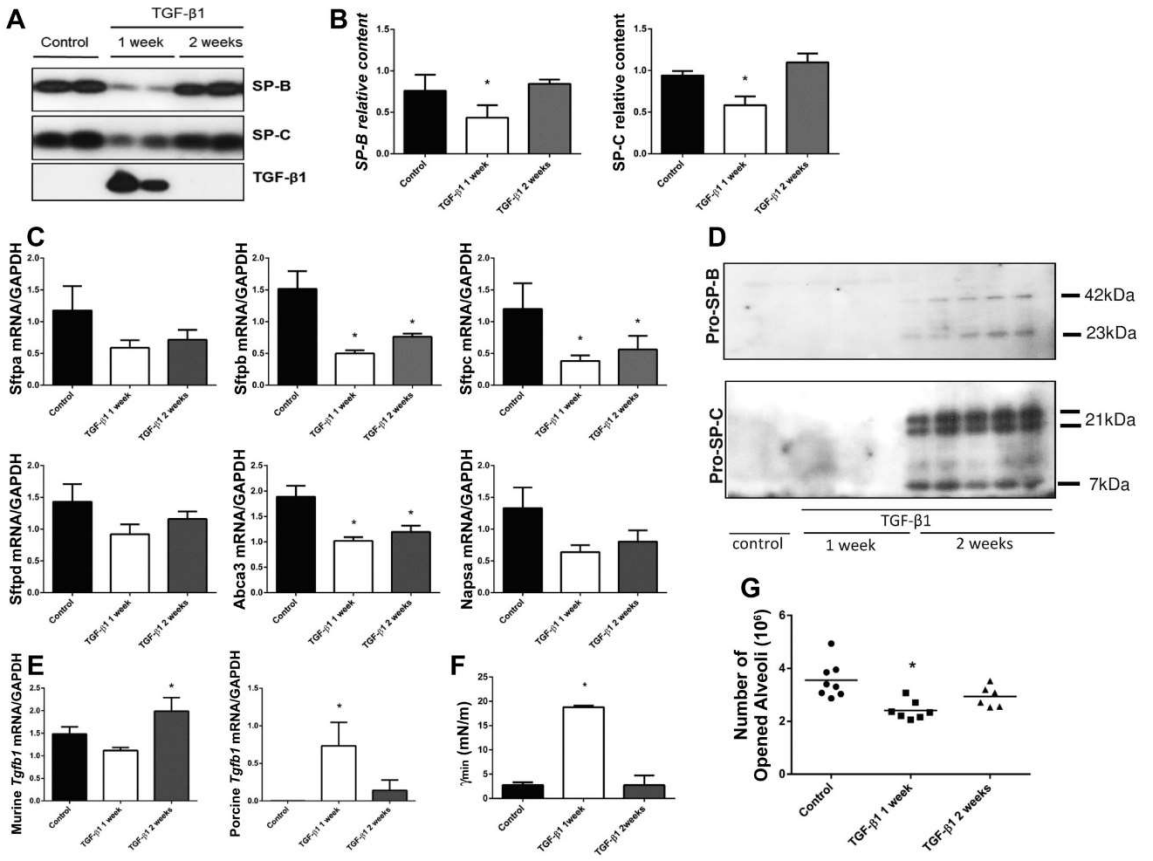

Fig. 3. Regulation of surfactant protein expression and function by TGF-β1. *A*: representative Western blot of surfactant proteins B and C and TGF-β1 on bronchoalveolar lavage from mice lungs 1 and 2 wk after transfection of TGF-β1. *B*: quantification of relative protein content (by band densitometry, $n = 5$). *C*: RT-PCR analysis of different genes related to surfactant function and processing (*Sftpa*, *Sftpb*, *Sftpc*, *Sftpd*, *Abca3*, and *Napsa*). *D*: representative Western blot of SP-B and SP-C precursors in lung homogenate from mice lungs 1 and 2 wk after transfection of TGF-β1. *E*: normalized expression of murine *Tgfb1* and porcine *Tgfb1* (adenoviral *Tgfb1*) by RT-PCR. *F*: surfactant function measured by captive bubble surfactometer (CBS): minimum surface tension (γmin) reached by surfactant in the different groups at the end of the compression of the bubble in the CBS. *G*: reduction on total number of opened alveoli due to the effect of TGF-β1, quantified by design-based stereology. $^*P < 0.05$ vs. controls.

sponding to a normal control phenotype, other AE2C-like cells (Fig. 5, *C* and *D*) show also LB, but in a different location, deep inside in the septal wall, therefore without obvious contact with the alveolar air spaces and no clear typical apical membrane. Stereological quantification of the apical-to-basal membrane ratio (Fig. 5*F*) in AE2C (or LB-containing cells) shows a decreasing proportion of apical membrane after transfection of TGF-β1. Further analysis (Fig. 5*G*) shows a total decrease in apical surface of AE2C in the lung leading to ~1/3 of the normal total apical AE2C surface. In addition, static compliance values correlate with total apical surface of AE2C (Fig. 5*H*) better than volume of AE2C (Fig. 5*E*), since the apical surface of AE2C is the functional surface of these cells. Moreover, expression of different apical AE2C membrane proteins showed also to be strongly downregulated (Fig. 5*I*: P2ry2, P2rx4, Slc34a2), correlating with total loss of polarity of AE2C. In addition, LB content in the septal wall (Fig. 5*J*) varies after transfection with TGF-β1. Simultaneously to surfactant dysfunction, a decrease is found 1 wk after gene transfer, whereas 2 wk after gene transfer an intracellular LB accumulation in AE2C coincides with the loss of apical surface (Fig. 5*J*).

DISCUSSION

Progressive fibrosis in lung diseases such as IPF is a result of chronic epithelial injury and cumulative aberrant repair. The origin and order of events leading to fibrotic remodeling of the lung is still unknown. Animal models give us the opportunity to study very early stages of diseases and effects of single profibrotic agents in vivo. Hence, we investigated short-term effects (1–2 wk) of the overexpression of TGF-β1 on pulmonary structure and function. Changes in mechanical properties of the lung such as elastance, hysteresivity, and static compliance lead us to the conclusion that one of the very immediate effects of the overexpression of TGF-β1 is alveolar collapse in

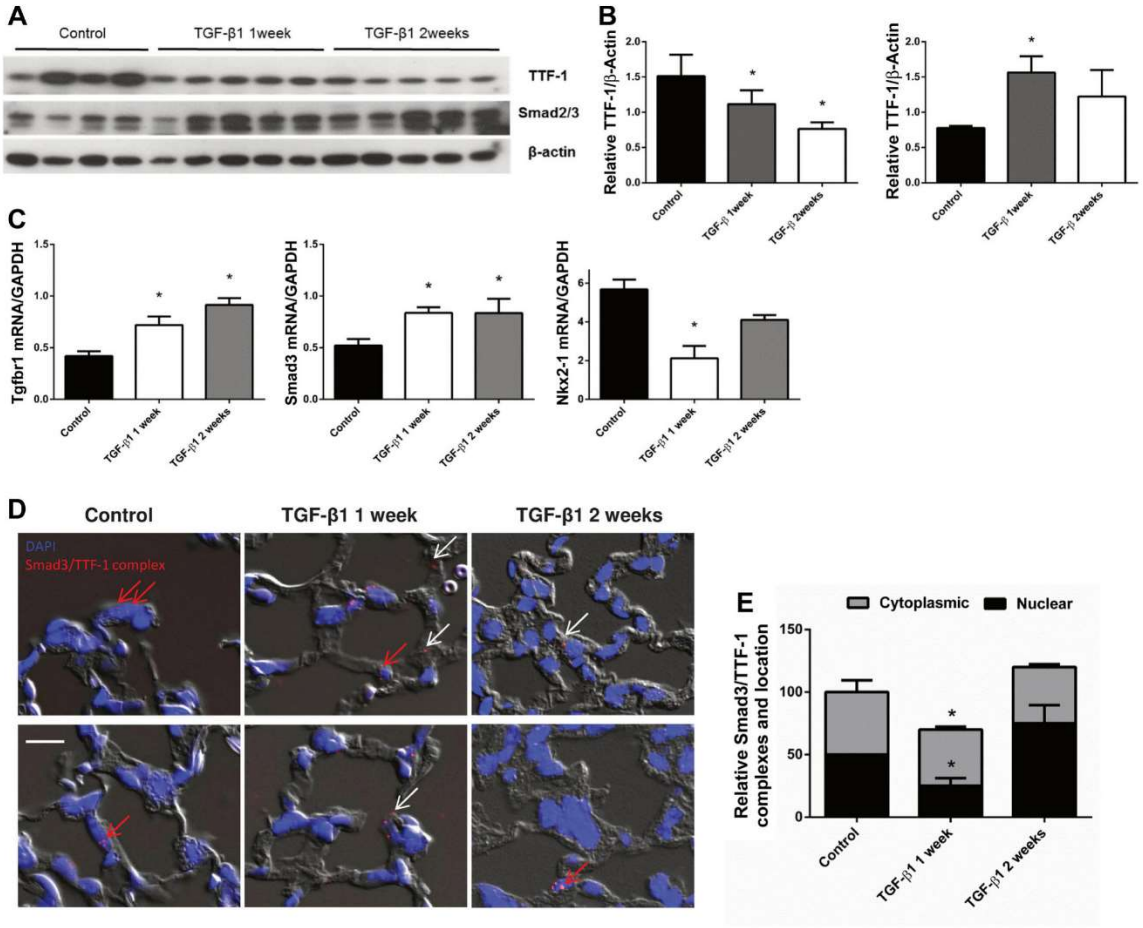

Fig. 4. Smad3/TTF-1 complexes during TGF-β1 overexpression. *A*: representative Western blot against TTF-1, Smad3, and β-actin from lung homogenates. *B*: quantification of relative protein content (by band densitometry, $n = 5$), normalized by β-actin levels. *C*: RT-PCR gene expression of TGF-β1 receptor II, Smad3, and TTF-1 in control, 1-wk, and 2-wk TGF-β1 groups. *D*: Smad3/TTF-1 complexes as seen by PLA using anti-TTF-1 and anti-Smad2/3 antibodies. Representative images under fluorescence microscopy showing Smad3/TTF-1 complexes (red) and their relative location to the nucleus [red arrows, complexes colocalized in the nucleus (DAPI); white arrows, complexes located in the cytoplasm) of the cell (blue) (scale bar = 10 μm). *E*: quantification of Smad3/TTF-1 complexes and relative location within the cell. Red dots were quantified and assigned to a cytoplasmic or nuclear location; values were corrected by the number of cells measured. $^*P < 0.05$ vs. control.

the absence of fibrosis as shown by the stereological data (Fig. 2, *A–C*). Accordingly, the number of open alveoli at an airway opening pressure of 10 cmH_2O was significantly reduced 1 wk after gene transfer (Fig. 3*G*), while volumes of septal wall tissue and collagen fibrils were not increased in the lung. Alveolar collapse or intratidal alveolar recruitment/derecruitment has already been described as possible chronic lung injury trigger (58). Inspiratory crackles as heard during lung auscultation represent an early sign of pulmonary fibrosis (8). Inspiratory Velcro crackles have been discussed as resulting from explosive and energy-rich reopenings of distal air spaces during inspiration (55). The underlying reason for this behavior of distal air spaces might be the increased collapsibility of the alveoli due to major alterations in the surfactant system. Surfactant proteins SP-B and SP-C partial deficiency has already been found in patient samples suffering from IPF (14, 15, 26) and other animal fibrosis models (41). Because of the effect of TGF-β1 on the collapsibility of alveoli, it seems reasonable to investigate lung surfactant activity and its regulation under overexpression of this profibrotic cytokine. Downregulation of SP-B and -C has already been shown and correlated with the expression of TGF-β1 in vitro (24, 27, 33, 62). It has been already proposed that SP-B is possibly regulated in vitro by TGF-β1 through Smad3 interactions with TTF-1 (thyroid transcription factor 1, part of homeobox domain transcription factors family, also named NKX2.1) and HNF-3 (hepatocyte nuclear factor 3, part of forkhead/winged helix transcription factors, also named FOXA1/FOXA2) (33). Here we demonstrate for the first time that overexpression of bioactive TGF-β1 also acts as a negative regulator of SP-B and SP-C in vivo (Fig. 3), which correlates with impaired surface activity, structural changes, and impairment of the lung function. SP-B

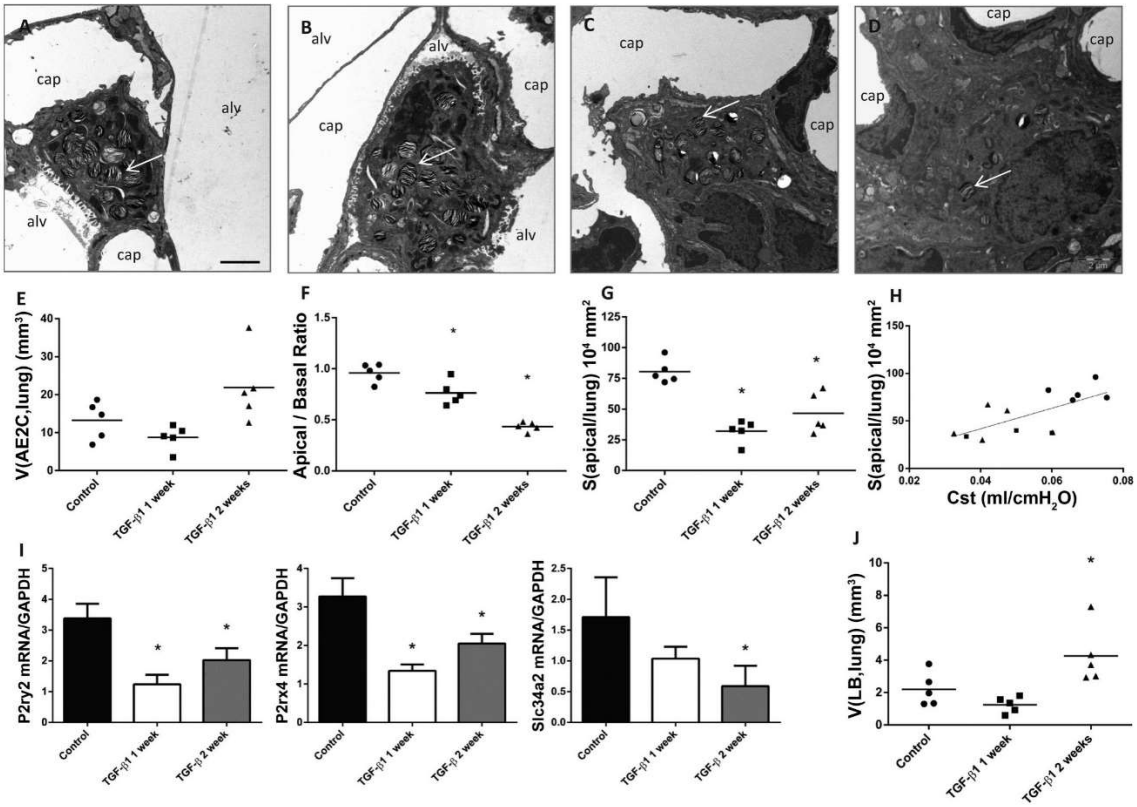

Fig. 5. Loss of apical surface and polarity on AE2C after TGF-β1 transfection. *A–D*: representative images of AE2C 2 wk after transfection of TGF-β1. AE2C showing typical apical surface with microvilli (*left*) and LB-containing cells (*right*) in the middle of the interstitial space, with no contact with the air and no typical apical surface (scale bar = 2 μm). AE2 cells were found in control (*A* and *B*), 1 wk (*C*), and 2 wk (*D*) after gene transfer. White arrows point at lamellar bodies; alv, alveolar air space; cap, capillary lumen. *E*: total volume of AE2C per lung. *F*: stereological quantification of the apical-to-basal ratio on AE2C 1 and 2 wk after transfection of TGF-β1. *G*: loss of total AE2C apical surface in the lung. *H*: statistically significant correlation between loss of total apical surface and loss of compliance after transfection with TGF-β1, $P < 0.05$, $r^2 = 0.46$ (●, controls; ■, 1 wk after TGF-β1 transfection; ▲, 2 wk after TGF-β1 transfection). *I*: downregulation of the expression of AE2C apical-specific proteins. *J*: accumulation of lamellar bodies within the septal wall, quantified by design-based stereology at electron microscopic level. *$P < 0.05$ vs. control.

and SP-C at equal lipid concentration and composition have been demonstrated to be of importance for surface tension reducing properties of synthetic surfactant preparations (44) so that it seems to be very likely that decreased surfactant protein levels are at least in part responsible for impaired surface activity of pulmonary surfactant during TGF-β1 overexpression. Nevertheless, our data cannot rule out that differences in lipid composition and concentration also contribute to the TGF-β1 effects on surfactant function, lung structure, and mechanics. Furthermore, when TGF-β1 levels reduce to normal, lung injuries are not reversible in short term and progress into a fibrotic remodeling of the lung, including deposition of collagen. Surprisingly, surfactant impairment occurs simultaneously to TGF-β1 overexpression and precedes any kind of fibrotic remodeling in our model in vivo, similar to our previous findings in the bleomycin-induced lung fibrosis model (29). As described before (15, 18, 29, 42), abnormally high surface tension may contribute to mechanical stress due to collapse and reopening of alveoli. Surfactant isolated from IPF patients show abnormally high surface tension (15, 26). This abnormal mechanical stress acting on alveolar epithelium is described to lead to fibrotic remodeling in various animal models (7, 17), including bleomycin-induced lung fibrosis (41). In addition, we found that other surfactant-related proteins were also downregulated such as ABCA3, a lipid transporter essential for correct storage of surfactant in lamellar bodies. On the other hand, downregulation of other surfactant-related proteins, such as SP-A and napsin A, led us to investigate a further upstream pathway in the synthesis of surfactant components up to TTF-1 (thyroid transcription factor 1), responsible for the regulation of surfactant synthesis and specific to lung epithelium. According to previous results (16), in our in vivo model we observed partial deficiency in TTF-1 (Fig. 3, *A* and *B*) and downregulation of the gene (*Nkx2.1*) during TGF-β1 overexpression. Interestingly not only the protein level of TTF-1 but also its location determines its activity, since TTF-1 protein level remain downregulated (Fig. 3), but enough TTF-1 seems to be actively translocated into the nucleus, potentially contributing to enhancement of SP-B and SP-C BAL levels back to normal 2 wk after transfection (Fig.

3, *A* and *B*). However, the expression of SP-B and SP-C genes shows only a slight trend for recovery 2 wk compared with 1 wk after gene transfer. These findings indicate that other TGF-β1-related mechanisms including, e.g., increased degradation of surfactant proteins might also be involved in the dramatic decline in BAL levels we observed 1 wk after gene transfer. Many previous attempts tried to show interaction between TTF-1 and Smad3 (a signaling protein within TGF-β1 pathway) by means of EMSA (electrophoretic mobility shift assay) (24, 27, 32, 33), coimmunoprecipitation (32) or PLA (20) in vitro. It has already been proposed that Smad3 is able to bind directly to the MH1 and MH2 domains of TTF-1, therefore preventing binding of TTF-1 to SP-B gene promoter (33). We have shown not only the existence of a direct interaction between TTF-1 and Smad3, but also the location of these complexes in the cell in an in vivo model (Fig. 4, *D* and *E*). Since Smad3 plays a key role in fibrosis (6, 59, 60), we hypothesized that part of the profibrotic effect of Smad3 would include the downregulation of the surfactant system, contributing to mechanical stress in lung epithelium and abnormal alveolar recruitment and derecruitment as indicated by the loss of ventilated alveoli in the context of high surface tension and the virtually unchanged hysteresivity. Alveolar derecruitment 1 wk after gene transfer also explains the significant increase in septal wall thickness in concert with a decrease in alveolar surface area per lung without an increase in the total volume of septal wall tissue. The finding that during TGF-β1 overexpression Smad3 and TTF-1 complexes form and, instead of in the nucleus, are in increased proportion found extranuclearly provided a potential mechanism by which TGF-β1 interferes with gene expression of components of the surfactant system, preceding collagen deposition and progressive loss of polarity of AE2 cells. A failure of TTF-1 to translocate to the nucleus of AE2C has been linked to surfactant dysfunction and infant respiratory distress syndrome in a recent study and is therefore likely to be of relevance in our model as well (38). Therefore we could demonstrate for the first time in an in vivo model that TGF-β1 is able to contribute to the mechanical stress produced by surfactant dysfunction that lead to fibrotic remodeling of the lung.

Since TTF-1 is a transcription factor specific for lung epithelium and present in AE2C, we investigated whether there is a noticeable effect of TGF-β1 in AE2C. AE2C are key cells for the function of the lung, not only because they are responsible of surfactant synthesis and secretion, but also as origin of alveolar epithelial lining cells (54). Injury of AE2C has already been described to happen during development of a fibrotic phenotype (63) and includes changes in morphology (hypertrophy) and location (45), ER stress, and apoptosis (23, 25, 50, 61). Abnormal or nonfunctional AE2C have already been found in patients suffering from lung fibrosis, and therefore therapy strategies have been proposed to regenerate the deficient nonfunctional AE2C (14). Accordingly, we found in our in vivo model various morphologies and locations of AE2C within the lung tissue, where some "interstitial AE2C or LB-containing cells" can also be observed (Fig. 5, *A–D*). Interestingly, the only feature to identify these cells as AE2C is the remaining LB in their cytoplasm. Whether they are still "AE2C" in terms of metabolism or function is a question yet to be answered. In addition to the unique feature of synthetizing and storing surfactant in these particular compartments, AE2C are polarized cells showing apical and basolateral membrane completely different in location and function. These components can be clearly identified at the electron microscopic level since tight junctions separate the apical from the basolateral membrane. Although the apical membrane of AE2C presents microvilli and is the surface in contact with the alveolar lumen, in which surfactant metabolism occurs, the basolateral membrane is in charge of keeping the cell attached to the basal lamina and to other cells, as well as the communication with the neighboring epithelial and interstitial cells. In addition to the quantification of apical membrane surface area, we studied the expression levels of specific AE2C apical membrane proteins, such as P2Y2, P2X4 (10), and IIb Na-Pi cotransporter (*Slc34a2*) (51). In all cases, downregulation of expression of the proteins can be correlated with loss of apical surface, representing loss of polarity of these cells since total AE2C volume is not decreased but instead increased (Fig. 5). The effect of TGF-β is noticeable up to 2 wk after transfection in AE2C, and endogenous TGF-β is upregulated (Fig. 3) in lung tissue. Furthermore, the total volume of lamellar bodies per lung increases and this in concert with the occurrence of intracellular precursors of SP-B and SP-C in lung homogenate can be considered as correlates of dysfunctional AE2 cells.

In conclusion, these findings link for the first time the TGF-β1 signaling pathway with increased tissue elastance due to high surface tension and alveolar derecruitment. In this model, these alterations represent initial effects of the TGF-β1 signaling and occur without any signs of pulmonary fibrosis during the first week as evaluated by means of design-based stereology. During the expression of bioactive TGF-β1, surfactant proteins are downregulated by concomitant reduction of the expression of TTF-1 and potentially a Smad3-mediated failure of TTF-1 to translocate to the nucleus of AE2C. Hence the primary effect of TGF-β1 overexpression on lung structure is surfactant dysfunction, alveolar derecruitment, and associated mechanical stress. These observations precede and contribute to the loss of AE2 cell polarity and interstitial profibrotic remodeling as demonstrated by loss of apical AE2C surface area 2 wk after gene transfer. At 2 wk after gene transfer surface tension returned to normal and lung mechanical impairment results from interstitial remodeling with septal wall thickening and deposition of collagen fibrils.

ACKNOWLEDGMENTS

The authors thank Sarah Knippenberg, Karin Westermann, Sabine Fiedler, and Susanne Fassbender for excellent technical support.

GRANTS

This research was supported by grants from Biomedical Research in Endstage and Obstructive Lung Disease Hannover (BREATH), Member of the German Center for Lung Research (DZL) (to U. A. Maus, M. Ochs, and L. Knudsen), Cluster of Excellence REBIRTH (Regenerative Biology to Reconstructive Therapy) (to M. Ochs), the Alexander von Humboldt Foundation (to E. Lopez-Rodriguez), and the German Research Foundation (DFG: KN 916/1-1 to L. Knudsen). M. Echaide and J. Perez-Gil acknowledge grants from Spanish Ministry of Economy (BIO2012-30733) and the Regional Government of Madrid (P2013/MIT-2807).

DISCLOSURES

M. Kolb reports grants from the Canadian Institute for Health Research, during the conduct of the study; grants and personal fees from Roche, grants and personal fees from Boehringer Ingelheim, personal fees from GSK, personal fees from Gilead, grants from Actelion, grants from Respivert,

personal fees from Astra Zeneca, personal fees from Prometic, and personal fees from Genoa, outside the submitted work.

The other authors have nothing to disclose.

AUTHOR CONTRIBUTIONS

E.L.-R., C.B., M.E., J.P.-G., M.R.K., J.G., U.A.M., M.O., and L.K. conception and design of research; E.L.-R., C.B., M.E., J.P.-G., M.R.K., J.G., U.A.M., M.O., and L.K. performed experiments; E.L.-R., C.B., M.E., J.P.-G., M.R.K., J.G., U.A.M., M.O., and L.K. analyzed data; E.L.-R., C.B., M.E., J.P.-G., M.R.K., J.G., U.A.M., M.O., and L.K. interpreted results of experiments; E.L.-R. and L.K. prepared figures; E.L.-R., M.O., and L.K. drafted manuscript; E.L.-R., J.P.-G., M.R.K., J.G., U.A.M., M.O., and L.K. edited and revised manuscript; E.L.-R., C.B., M.E., J.P.-G., M.R.K., J.G., U.A.M., M.O., and L.K. approved final version of manuscript.

REFERENCES

1. **Ask K, Bonniaud P, Maass K, Eickelberg O, Margetts PJ, Warburton D, Groffen J, Gauldie J, Kolb M.** Progressive pulmonary fibrosis is mediated by TGF-beta isoform 1 but not TGF-beta3. *Int J Biochem Cell Biol* 40: 484–495, 2008.
2. **Ask K, Labiris R, Farkas L, Moeller A, Froese A, Farncombe T, McClelland G, Inman M, Gauldie J, Kolb M.** Comparison between conventional and "clinical" assessment of experimental lung fibrosis. *J Transl Med* 6: 1–10, 2008.
3. **Bartis D, Mise N, Mahida RY, Eickelberg O, Thickett DR.** Epithelial-mesenchymal transition in lung development and disease: does it exist and is it important? *Thorax* 69: 760–765, 2014.
4. **Bates JHT.** *Lung Mechanics: An Inverse Modeling Approach*. Cambridge, UK: Cambridge University Press, 2009.
5. **Bilek AM, Dee KC, Gaver DP.** Mechanisms of surface-tension-induced epithelial cell damage in a model of pulmonary airway reopening. *J Appl Physiol* 94: 770–783, 2003.
6. **Bonniaud P, Kolb M, Galt T, Robertson J, Robbins C, Stampfli M, Lavery C, Margetts PJ, Roberts AB, Gauldie J.** Smad3 null mice develop airspace enlargement and are resistant to TGF-β-mediated pulmonary fibrosis. *J Immunol* 173: 2099–2108, 2004.
7. **Cabrera-Benítez NE, Parotto M, Post M, Han B, Spieth PM, Cheng WE, Valladares F, Villar J, Liu M, Sato M, Zhang H, Slutsky AS.** Mechanical stress induces lung fibrosis by epithelial-mesenchymal transition. *Crit Care Med* 40: 510–517, 2012.
8. **Cottin V, Cordier JF.** Velcro crackles: the key for early diagnosis of idiopathic pulmonary fibrosis? *Eur Respir J* 40: 519–521, 2012.
9. **Datta A, Scotton CJ, Chambers RC.** Novel therapeutic approaches for pulmonary fibrosis. *Br J Pharmacol* 163: 141–172, 2011.
10. **Dietl P, Haller T, Frick M.** Spatio-temporal aspects, pathways and actions of Ca^{2+} in surfactant secreting pulmonary alveolar type II pneumocytes. *Cell Calcium* 52: 296–302, 2012.
11. **Fernandez IE, Eickelberg O.** The impact of TGF-β on lung fibrosis. *Proc Am Thorac Soc* 9: 111–116, 2012.
12. **Gauldie J, Sime PJ, Xing Z, Marr B, Tremblay GM.** Transforming growth factor-β gene transfer to the lung induces myofibroblast presence and pulmonary fibrosis. In: *Tissue Repair and Fibrosis: The Role of the Myofibroblast*, edited by Desmoulière A, Tuchweber B. Berlin: Springer, 1999, p. 35–45.
13. **Giegerich R, Meyer F, Schleiermacher C.** GeneFisher—software support for the detection of postulated genes. *Proc Int Conf Intell Syst Mol Biol* 4: 68–77, 1996.
14. **Günther A, Korfei M, Mahavadi P, von der Beck D, Ruppert C, Markart P.** Unravelling the progressive pathophysiology of idiopathic pulmonary fibrosis. *Eur Respir Rev* 21: 152–160, 2012.
15. **Günther A, Schmidt R, Nix F, Yabut-Perez M, Guth C, Rosseau S, Siebert C, Grimminger F, Morr H, Velcovsky HG, Seeger W.** Surfactant abnormalities in idiopathic pulmonary fibrosis, hypersensitivity pneumonitis and sarcoidosis. *Eur Respir J* 14: 565–573, 1999.
16. **Guzy RD, Stoilov I, Elton TJ, Mecham RP, Ornitz DM.** Fibroblast growth factor 2 is required for epithelial recovery, but not for pulmonary fibrosis, in response to bleomycin. *Am J Respir Cell Mol Biol* 52: 116–128, 2014.
17. **Heise RL, Stober V, Cheluvaraju C, Hollingsworth JW, Garantziotis S.** Mechanical stretch induces epithelial-mesenchymal transition in alveolar epithelia via hyaluronan activation of innate immunity. *J Biol Chem* 286: 17435–17444, 2011.
18. **Horiuchi T, Ikegami M, Cherniack RM, Mason RJ.** Increased surface tension of the lung and surfactant in bleomycin-induced pulmonary fibrosis in rats. *Am J Respir Crit Care Med* 154: 1002–1005, 1996.
19. **Hsia CCW, Hyde DM, Ochs M, Weibel ER.** An official research policy statement of the American Thoracic Society/European Respiratory Society: standards for quantitative assessment of lung structure. *Am J Respir Crit Care Med* 181: 394–418, 2010.
20. **Isogaya K, Koinuma D, Tsutsumi S, Saito RA, Miyazawa K, Aburatani H, Miyazono K.** A Smad3 and TTF-1/NKX2-1 complex regulates Smad4-independent gene expression. *Cell Res* 24: 994–1008, 2014.
21. **Kasai H, Allen JT, Mason RM, Kamimura T, Zhang Z.** TGF-beta1 induces human alveolar epithelial to mesenchymal cell transition (EMT). *Respir Res* 6: 56, 2005.
22. **Kim IY, Kim MM, Kim SJ.** Transforming growth factor-beta: biology and clinical relevance. *J Biochem Mol Biol* 38: 1–8, 2005.
23. **Korfei M, Ruppert C, Mahavadi P, Henneke I, Markart P, Koch M, Lang G, Fink L, Bohle RM, Seeger W, Weaver TE, Guenther A.** Epithelial endoplasmic reticulum stress and apoptosis in sporadic idiopathic pulmonary fibrosis. *Am J Respir Crit Care Med* 178: 838–846, 2008.
24. **Kumar AS, Gonzales LW, Ballard PL.** Transforming growth factor-β1 regulation of surfactant protein B gene expression is mediated by protein kinase-dependent intracellular translocation of thyroid transcription factor-1 and hepatocyte nuclear factor 3. *Biochim Biophys Acta* 1492: 45–55, 2000.
25. **Lawson WE, Cheng DS, Degryse AL, Tanjore H, Polosukhin VV, Xu XC, Newcomb DC, Jones BR, Roldan J, Lane KB, Morrisey EE, Beers MF, Yull FE, Blackwell TS.** Endoplasmic reticulum stress enhances fibrotic remodeling in the lungs. *Proc Natl Acad Sci USA* 108: 10562–10567, 2011.
26. **Lawson WE, Crossno PF, Polosukhin VV, Roldan J, Cheng DS, Lane KB, Blackwell TR, Xu C, Markin C, Ware LB, Miller GG, Loyd JE, Blackwell TS.** Endoplasmic reticulum stress in alveolar epithelial cells is prominent in IPF: association with altered surfactant protein processing and herpesvirus infection. *Am J Physiol Lung Cell Mol Physiol* 294: L1119–L1126, 2008.
27. **Li C, Zhu NL, Tan RC, Ballard PL, Derynck R, Minoo P.** Transforming growth factor-β inhibits pulmonary surfactant protein B gene transcription through SMAD3 interactions with NKX2.1 and HNF-3 transcription factors. *J Biol Chem* 277: 38399–38408, 2002.
28. **Li M, Krishnaveni MS, Li C, Zhou B, Xing Y, Banfalvi A, Li A, Lombardi V, Akbari O, Borok Z, Minoo P.** Epithelium-specific deletion of TGF-β receptor type II protects mice from bleomycin-induced pulmonary fibrosis. *J Clin Invest* 121: 277–287, 2011.
29. **Lutz D, Gazdhar A, Lopez-Rodriguez E, Ruppert C, Mahavadi P, Günther A, Klepetko W, Bates JH, Smith B, Geiser T, Ochs M, Knudsen L.** Alveolar derecruitment and collapse induration as crucial mechanisms in lung injury and fibrosis. *Am J Respir Cell Mol Biol* 52: 232–243, 2015.
30. **Massagué J, Seoane J, Wotton D.** Smad transcription factors. *Genes Dev* 19: 2783–2810, 2005.
31. **Massagué J, Wotton D.** Transcriptional control by the TGF-β/Smad signaling system. *EMBO J* 19: 1745–1754, 2000.
32. **Minoo P, Hu L, Xing Y, Zhu NL, Chen H, Li M, Borok Z, Li C.** Physical and functional interactions between homeodomain NKX2.1 and winged helix/forkhead FOXA1 in lung epithelial cells. *Mol Cell Biol* 27: 2155–2165, 2007.
33. **Minoo P, Hu L, Zhu N, Borok Z, Bellusci S, Groffen J, Kardassis D, Li C.** SMAD3 prevents binding of NKX2.1 and FOXA1 to the SpB promoter through its MH1 and MH2 domains. *Nucleic Acids Res* 36: 179–188, 2008.
34. **Mühlfeld C, Ochs M.** Quantitative microscopy of the lung: a problem-based approach. Part 2: stereological parameters and study designs in various diseases of the respiratory tract. *Am J Physiol Lung Cell Mol Physiol* 305: L205–L221, 2013.
35. **Nakao A, Fujii M, Matsumura R, Kumano K, Saito Y, Miyazono K, Iwamoto I.** Transient gene transfer and expression of Smad7 prevents bleomycin-induced lung fibrosis in mice. *J Clin Invest* 104: 5–11, 1999.
36. **Nesslein LL, Melton KR, Ikegami M, Na CL, Wert SE, Rice WR, Whitsett JA, Weaver TE.** Partial SP-B deficiency perturbs lung function and causes air space abnormalities. *Am J Physiol Lung Cell Mol Physiol* 288: L1154–L1161, 2005.

37. **Ochs M, Mühlfeld C.** Quantitative microscopy of the lung: a problem-based approach. Part 1: basic principles of lung stereology. *Am J Physiol Lung Cell Mol Physiol* 305: L15–L22, 2013.
38. **Peca D, Petrini S, Tzialla C, Boldrini R, Morini F, Stronati M, Carnielli VP, Cogo PE, Danhaive O.** Altered surfactant homeostasis and recurrent respiratory failure secondary to TTF-1 nuclear targeting defect. *Respir Res* 12: 1–8, 2011.
39. **Possmayer F, Hall SB, Haller T, Petersen NO, Zuo YY, Bernardino de la Serna J, Postle AD, Veldhuizen RAW, Orgeig S.** Recent advances in alveolar biology: some new looks at the alveolar interface. *Respir Physiol Neurobiol* 173 *Suppl*: S55–S64, 2010.
40. **Rodt T, von Falck C, Dettmer S, Halter R, Maus R, Ask K, Kolb M, Gauldie J, Länger F, Hoy L, Welte T, Galanski M, Maus UA, Borlak J.** Micro-computed tomography of pulmonary fibrosis in mice induced by adenoviral gene transfer of biologically active transforming growth factor-β1. *Respir Res* 11: 181, 2010.
41. **Savani RC, Godinez RI, Godinez MH, Wentz E, Zaman A, Cui Z, Pooler PM, Guttentag SH, Beers MF, Gonzales LW, Ballard PL.** Respiratory distress after intratracheal bleomycin: selective deficiency of surfactant proteins B and C. *Am J Physiol Lung Cell Mol Physiol* 281: L685–L696, 2001.
42. **Schmidt R, Meier U, Markart P, Grimminger F, Velcovsky HG, Morr H, Seeger W, Günther A.** Altered fatty acid composition of lung surfactant phospholipids in interstitial lung disease. *Am J Physiol Lung Cell Mol Physiol* 283: L1079–L1085, 2002.
43. **Schneider JP, Ochs M.** Alterations of mouse lung tissue dimensions during processing for morphometry: a comparison of methods. *Am J Physiol Lung Cell Mol Physiol* 306: L341–L350, 2014.
44. **Schürch D, Ospina OL, Cruz A, Pérez-Gil J.** Combined and independent action of proteins SP-B and SP-C in the surface behavior and mechanical stability of pulmonary surfactant films. *Biophys J* 99: 3290–3299, 2010.
45. **Selman M, Pardo A.** Role of epithelial cells in idiopathic pulmonary fibrosis. *Proc Am Thorac Soc* 3: 364–372, 2006.
46. **Selman M, Pardo A.** Revealing the pathogenic and aging-related mechanisms of the enigmatic idiopathic pulmonary fibrosis. An integral model. *Am J Respir Crit Care Med* 189: 1161–1172, 2014.
47. **Sheppard D.** Transforming growth factor β: a central modulator of pulmonary and airway inflammation and fibrosis. *Proc Am Thorac Soc* 3: 413–417, 2006.
48. **Sime PJ, Xing Z, Graham FL, Csaky KG, Gauldie J.** Adenovector-mediated gene transfer of active transforming growth factor-beta1 induces prolonged severe fibrosis in rat lung. *J Clin Invest* 100: 768–776, 1997.
49. **Soderberg O, Gullberg M, Jarvius M, Ridderstrale K, Leuchowius KJ, Jarvius J, Wester K, Hydbring P, Bahram F, Larsson LG, Landegren U.** Direct observation of individual endogenous protein complexes in situ by proximity ligation. *Nat Methods* 3: 995–1000, 2006.
50. **Tanjore H, Cheng DS, Degryse AL, Zoz DF, Abdolrasulnia R, Lawson WE, Blackwell TS.** Alveolar epithelial cells undergo epithelial-to-mesenchymal transition in response to endoplasmic reticulum stress. *J Biol Chem* 286: 30972–30980, 2011.
51. **Traebert M, Hattenhauer O, Murer H, Kaissling B, Biber J.** Expression of type II Na-picotransporter in alveolar type II cells. *Am J Physiol Lung Cell Mol Physiol* 277: L868–L873, 1999.
52. **Tschanz S, Schneider JP, Knudsen L.** Design-based stereology: planning, volumetry and sampling are crucial steps for a successful study. *Ann Anat* 196: 3–11, 2014.
53. **Tschanz SA, Burri PH, Weibel ER.** A simple tool for stereological assessment of digital images: the STEPanizer. *J Microsc* 243: 47–59, 2011.
54. **Volckaert T, De Langhe S.** Lung epithelial stem cells and their niches: Fgf10 takes center stage. *Fibrogenesis Tissue Repair* 7: 1–15, 2014.
55. **Vyshedskiy A, Alhashem RM, Paciej R, Ebril M, Rudman I, Fredberg JJ, Murphy R.** Mechanism of inspiratory and expiratory crackles. *Chest* 135: 156–164, 2009.
56. **Whitsett JA, Weaver TE.** Hydrophobic surfactant proteins in lung function and disease. *N Engl J Med* 347: 2141–2148, 2002.
57. **Willis BC, Liebler JM, Luby-Phelps K, Nicholson AG, Crandall ED, du Bois RM, Borok Z.** Induction of epithelial-mesenchymal transition in alveolar epithelial cells by transforming growth factor-β1. *Am J Pathol* 166: 1321–1332, 2005.
58. **Wilson TA, Bachofen H.** A model for mechanical structure of the alveolar duct. *J Appl Physiol* 52: 1064–1070, 1982.
59. **Zhao J, Shi W, Wang YL, Chen H, Bringas P, Datto MB, Frederick JP, Wang XF, Warburton D.** Smad3 deficiency attenuates bleomycin-induced pulmonary fibrosis in mice. *Am J Physiol Lung Cell Mol Physiol* 282: L585–L593, 2002.
60. **Zhao Y, Geverd DA.** Regulation of Smad3 expression in bleomycin-induced pulmonary fibrosis: a negative feedback loop of TGF-beta signaling. *Biochem Biophys Res Commun* 294: 319–23, 2002.
61. **Zhong Q, Zhou B, Ann DK, Minoo P, Liu Y, Banfalvi A, Krishnaveni MS, Dubourd M, Demaio L, Willis BC, Kim KJ, DuBois RM, Crandall ED, Beers MF, Borok Z.** Role of endoplasmic reticulum stress in epithelial-mesenchymal transition of alveolar epithelial cells. *Am J Respir Cell Mol Biol* 45: 498–509, 2011.
62. **Zhou B, Zhong Q, Minoo P, Li C, Ann DK, Frenkel B, Morrisey EE, Crandall ED, Borok Z.** Foxp2 inhibits Nkx-mediated transcription of SP-C via interactions with the Nkx2.1 homeodomain. *Am J Respir Cell Mol Biol* 38: 750–758, 2008.
63. **Zoz DF, Lawson WE, Blackwell TS.** Idiopathic pulmonary fibrosis: a disorder of epithelial cell dysfunction. *Am J Med Sci* 341: 435–438, 2011.

Reprinted with permission

RELEVANCE OF THIS WORK

In this paper, we demonstrated for the first time *in vivo* that TGF-β1 might regulate surfactant protein expression through Smad3 sequestration of TTF-1 into the cytoplasm. Active extracellular TGF-β1 binds to its receptor proteins and initiate a cascade of signals that include the phosphorylation of some members of the Smad protein family. The phosphorylated complex of Smad2/3, together with other transcription factors, translocate to the nucleus to regulate the expression of many genes. From our results, we can conclude that the activation of Smad2/3 prevents the translocation of TTF-1 into the nucleus, which then is not able to activate the expression of the SP-B and SP-C genes nor to regulate its own expression. Therefore, we could observe not only SP-B and SP-C deficient gene and protein expression, but also less TTF-1 gene expression. We observed this effect during TGF-β1 overexpression, one week after transfection, but not afterwards. However, it seems that the tissue injury caused during the overexpression of TGF-β1 is not reversible and aberrant wound healing continues further during the second week in the study. The initial, potential mechanical stress caused by surfactant dysfunction, seen in the abnormal alveolar dynamics and increased surface tension, seems to induce AE2C damage and alveolar collapse that are not resolved in the absence of TGF-β1. AE2C lost their apical membrane and appeared embedded in interstitial tissue, where they no longer can secrete new surfactant. Previously, many reports proposed damage and decrease in number of AE2C to contribute to lung fibrosis, even though the exact mechanisms is not known. Here we conclude that surfactant dysfunction at early stages may be contributing not only to mechanical stress and collapse, but also to injury of AE2C.

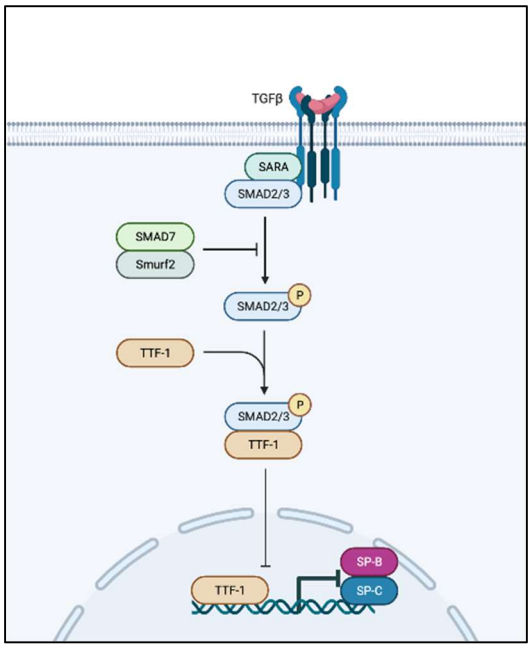

Figure 1: Proposed common molecular pathway for the regulation of surfactant proteins by TGF-β1. Created in BioRender.com.

2.2 SURFACTANT PROTEIN C (ORIGINAL WORK 2)

Ruwisch J., Sehlmeyer K., Roldan N., Garcia-Alvarez B., Perez-Gil J., Weaver T.E., Ochs M., Knudsen L. & **Lopez-Rodriguez E**. "*Air Space Distension Precedes Spontaneous Fibrotic Remodeling and Impaired Cholesterol Metabolism in the Absence of Surfactant Protein C*" American Journal of Respiratory Cell and Molecular Biology, 2020; 62(4): 466-478.

As seen in the previous chapter, TGF-β1 interacts with the regulation of surfactant related genes through one of its transcription factors, TTF-1. TTF-1 is responsible of the transcription of surfactant genes, including SFTPC, the gene coding for surfactant protein C (SP-C) (60). This protein is very hydrophobic, small (of only 35 amino acids) and accounts for approx. 1% of lung surfactant mass. SP-C is highly preserved among species (61), specifically expressed in AE2C and often used as molecular marker for the differentiation of lung tissue (62). The mature form of SP-C has a 4.3 kDa size, but it is expressed as a larger precursor, of 21 kDa in the AE2C, which is enzymatically processed to the mature form.

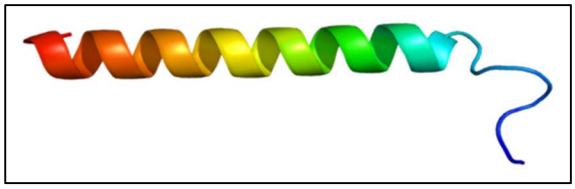

Figure 2: Proposed structure of SP-C (Wikimedia Commons, CC BY-SA 3.0).

SP-C structure, rich in valine and leucine amino acid residues, adopts a metastable α-helix, which is normally embedded in the phospholipid membrane-like structures of lung surfactant, due to its hydrophobic nature. It also contains a high proportion of branched residues, which, in more polar or hydrophilic environments, makes this protein susceptible to adopt more β-sheet structures and fibrillogenic amyloid-like structures (63, 64). These aggregates are a common feature in several interstitial lung diseases. It is also palmitoylated in the N-terminal site (not shown in figure 2) and the two palmitoyl-residues are described to anchor the protein to the phospholipid membrane-like structures (65, 66). Therefore, SP-C interacts very closely and stably with phospholipids and has a great influence in the structure and dynamics of the surfactant membrane structures. More specifically, SP-C is able to alter lipid packing by both influencing the lipid motion and lateral distribution (67, 68) and membrane permeability in vitro (69-71). Within the context of the lung surfactant function, SP-C is able to promote interfacial lipid adsorption and lipid transfer between different lipid membrane-like structures (72-74). In addition, it also interconnects multilayered stacks that serve as a surfactant reservoir, storing newly secreted surfactant complexes and surfactant molecules squeezed out from the interface upon compression to the interfacial film (73, 75). In this way, SP-C may facilitate the insertion of surfactant material, during surface area expansion (inhalation) and exclusion of excess material, during the surface area compression (during exhalation).

Therefore, in the absence of SP-C this recycling of surface-active material into and out of the interfacial film may be impaired. This has a very important physiological meaning, as not low enough surface tension may be reached upon compression of small alveoli, the most susceptible ones to collapse, as explained in section 1.2. This may lead to alveolar instability and collapsibility of alveoli (76). These alveoli may be re-opened, with higher pressure, but this may also initiate the response mechanisms to mechanical stress in the alveolar epithelium. Therefore, triggering aberrant tissue repair and fibrotic remodeling, as explained before.

In addition, many mutations in the SP-C gene have been already reported in familial forms of interstitial lung diseases (ILD), making SP-C a highly relevant protein in the pathophysiology of these diseases (recently reviewed in Sehlmeyer et al 2020 (77)).

Variant	Reference
L188Q	Thomas et al., 2002 (78)
R167Q	Tredano et al., 2004 (79)
I73T	Tredano et al., 2004 (79); Abou Taam et al., 2009 (80); Thouvenin et al., 2010(81) ; Cottin et al., 2011 (82); Avital et al., 2014 (83); Hevroni et al., 2015 (84); Salerno et al., 2016 (85)
G100S	Ono et al 2011 (86)
Y104H	Kuse et al., 2013 (87)
I38F	Avital et al., 2014 (83)
V39L	
C121F	van Hoorn et al., 2014 (88)
I38F	Hevroni et al., 2015 (84)
L188E	Chibbar et al., 2004 (89)
E66K	Stevens et al., 2005 (90)

Table 1: Most common mutations found in the SP-C gene in human ILD patients (adapted from Sehlmeyer, Ruwisch, Roldan & Lopez-Rodriguez, 2020 (77)).

The aim of this work was to investigate the structural and functional changes of the lungs of SP-C deficient mice with age. For this purpose, we bred and aged WT and SP-C KO mice in our animal facility. To understand the order of events and changes in the lungs with age, we took animals every 10 weeks, of an age ranging from 10 to 60 weeks old and performed different analyses *in vivo* and in the isolated lungs. We hypothesized that: 1) the alveolar instability due to the absence of SP-C will lead to a mild but chronic alveolar collapse, specially of the smallest distal alveoli; 2) this chronic alveolar collapse may lead to permanent de-recruitment of the alveoli with two consequences: 2.1) with less open alveoli, air re-organization may lead to over-distend alveoli and ductal spaces; 2.2) mechanical stress due to chronic alveolar collapse and collapse induration may lead to wound fibrotic formation; 3) these chronic but mild events may lead to the onset of fibrosis remodeling with age in the absence of SP-C.

ORIGINAL RESEARCH

Air Space Distension Precedes Spontaneous Fibrotic Remodeling and Impaired Cholesterol Metabolism in the Absence of Surfactant Protein C

Jannik Ruwisch[1,2*], Kirsten Sehlmeyer[1,2*], Nuria Roldan[3,4], Begoña Garcia-Alvarez[4], Jesus Perez-Gil[4], Timothy E. Weaver[5], Matthias Ochs[1,2,6], Lars Knudsen[1,2,6], and Elena Lopez-Rodriguez[1,2,6]

[1]Institute of Functional and Applied Anatomy, Hannover Medical School, Hannover, Germany; [2]BREATH (Biomedical Research in Endstage and Obstructive Lung Disease Hannover), Member of the German Center for Lung Research, Hannover, Germany; [3]Alveolix AG and ARTORG Center, University of Bern, Bern, Switzerland; [4]Biochemistry and Molecular Biology Department, Faculty of Biology, and Research Institute "Hospital 12 de Octubre," Complutense University Madrid, Madrid, Spain; [5]Cincinnati Children's Hospital Medical Center and the University of Cincinnati College of Medicine, Cincinnati, Ohio; and [6]Institute of Vegetative Anatomy, Charité–Universitaetsmedizin Berlin, Berlin, Germany

ORCID ID: 0000-0002-1549-8150 (E.L.-R.).

Abstract

Surfactant protein (SP)-C deficiency is found in samples from patients suffering idiopathic pulmonary fibrosis, especially in familial forms of this disease. We hypothesized that SP-C may contribute to fibrotic remodeling in aging mice and alveolar lipid homeostasis. For this purpose, we analyzed lung function, alveolar dynamics, lung structure, collagen content, and expression of genes related to lipid and cholesterol metabolism of aging SP-C knockout mice. In addition, *in vitro* experiments with an alveolar macrophage cell line exposed to lipid vesicles with/without cholesterol and/or SP-C were performed. Alveolar dynamics showed progressive alveolar derecruitment with age and impaired oxygen saturation. Lung structure revealed that decreasing volume density of alveolar spaces was accompanied by increasing of the ductal counterparts. Simultaneously, septal wall thickness steadily increased, and fibrotic wounds appeared in lungs from the age of 50 weeks. This remarkable phenotype is unique to the 129Sv strain, which has an increased absorption of cholesterol, linking the accumulation of cholesterol and the absence of SP-C to a fibrotic remodeling process. The findings of this study suggest that overall loss of SP-C results in an age-dependent, complex, heterogeneous phenotype characterized by a combination of overdistended air spaces and fibrotic wounds that resembles combined emphysema and pulmonary fibrosis in patients with idiopathic pulmonary fibrosis. Addition of SP-C to cholesterol-laden lipid vesicles enhanced the expression of cholesterol metabolism and transport genes in an alveolar macrophage cell line, identifying a potential new lipid–protein axis involved in lung remodeling.

Keywords: surfactant protein C; pulmonary fibrosis; alveolar dynamics; lipid metabolism; alveolar macrophages

Clinical Relevance

This research enables investigation of the events potentially occurring before lung fibrotic remodelling, allowing an understanding of the mechanism of a devastating disease and the development of therapeutic approaches to preventing it.

(Received in original form October 10, 2019; accepted in final form January 10, 2020)

*These authors contributed equally to this work.

Supported by BREATH (Biomedical Research in Endstage and Obstructive Lung Disease), a Member of the German Center for Lung Research, Cluster of Excellence REBIRTH (Regenerative Biology to Reconstructive Therapy Hannover), and Hochschulinterne Leistungsförderung program (Medizinische Hochschule Hannover), Spanish Ministry of Science and Universities grant RTI2018-094564-B-I00 and regional Government of Madrid grant P2018/NMT4389 (N.R., B.G.-A., and J.P.-G.), and Formación Profesorado Universitario fellowship AP2012/5099 and short-term fellowship EST15/00594 granted by the Spanish Ministry of Education, Culture, and Sport (N.R.).

Author Contributions: Conceptualization—L.K. and E.L.-R.; methodology—J.R., K.S., N.R., and E.L.-R.; formal analysis—J.R., K.S., N.R., and E.L.-R.; investigation—J.R., K.S., N.R., and E.L.-R.; writing—original draft preparation—J.R., K.S., N.R., B.G.-A., J.P.-G., T.E.W., M.O., L.K., and E.L.-R.; writing—review and editing—J.R., K.S., N.R., B.G.-A., J.P.-G., T.E.W., M.O., L.K., and E.L.-R.; supervision—L.K. and E.L.-R.; project administration—E.L.-R.; and funding acquisition—M.O., L.K., and E.L.-R.

Correspondence and requests for reprints should be addressed to Elena Lopez-Rodriguez, Ph.D., Institute of Vegetative Anatomy, Charite Universitatsmedizin zu Berlin, Philippstraße 12, 10115 Berlin, Germany. E-mail: elena.lopez-rodriguez@charite.de.

This article has a related editorial.

This article has a data supplement, which is accessible from this issue's table of contents at www.atsjournals.org.

Am J Respir Cell Mol Biol Vol 62, Iss 4, pp 466–478, Apr 2020

Originally Published in Press as DOI: 10.1165/rcmb.2019-0358OC on January 10, 2020
Internet address: www.atsjournals.org

Idiopathic pulmonary fibrosis (IPF) is a chronic, progredient, restrictive interstitial lung disease, characterized by increased collagen deposition with fatal outcome. Current pathogenetic concepts focus on the dysfunction of alveolar epithelial cell (AEC) type 2, stem cell exhaustion, and aberrant profibrotic wound repair (1). On high-resolution computer tomography (HRCT) images, IPF depicts the picture of usual interstitial pneumonia, characterized by the presence of heterogeneously distributed honeycomb cysts with basal and subpleural predominance (2–4). A range of 2–20% of patients with IPF present with a positive familial history classified as familial pulmonary fibrosis (5–8). Multiple gene studies have identified a wide set of genes that seem to drive fibrogenesis (9–12), including mutations of genes encoding surfactant proteins (SPs) (7, 13–16).

Pulmonary surfactant mainly consists of phospholipids and SP-A, -B, -C, and -D. SP-B and -C are essential for reducing surface tension at the alveolar air–liquid interface (17, 18). The hydrophobic, mature SP-C peptide has been shown to be crucial for maintaining surfactant homeostasis under dynamic conditions. During surfactant film compression, SP-C provides film stability at low lung volumes (17, 19, 20). As the respiratory cycle progresses, SP-C facilitates the reincorporation of subinterfacial phospholipids into the monolayer, promoting film expansion upon inspiration (17, 18, 21). To date, more than 60 different mutations in the human *SFTPC* gene have been associated with development of acute and chronic lung disease in infants, children, and adults (22–24). The *SFTPC* gene is exclusively expressed by AEC2 and encodes the 21-kD precursor protein, proSP-C (25, 26).

Aging is one of the main common factors in IPF, mostly affecting patients over the age of 60 years (2). With increasing age, the lung is progressively challenged with harmful biological and physical noxae (27–29). Multiple hits, such as repeated exposure to mechanical stress, as occurs during heterogenous lung ventilation in the setting of increased surface tension and alveolar instability, were further shown to compromise AEC2 integrity (30–33). Aging lungs themselves show a trend toward increasing lung stiffness and lower compliance in combination with lower surfactant volumes that, in turn, may contribute to impaired lung function in the elderly (34, 35).

In addition, impaired lipid metabolism is related to many different lung diseases, including pulmonary alveolar proteinosis and lung fibrosis. Reduced lipid metabolism has been related to endoplasmic reticulum stress (36) and as a communication axis between AE2C and alveolar macrophages (37), leading to fibrotic remodeling. Even though limited information exists on the exact mechanisms of regulation of lipid metabolism, and more specifically cholesterol metabolism (38), it may present a new therapeutic target in lung fibrosis (39).

In the current study, we aim to elucidate the role of SP-C in the development of spontaneous lung fibrosis as well as the ordering of the events leading to fibrotic remodeling in the absence of this protein. To this end, we studied the alveolar dynamics, lung structure, and function of SP-C knockout (KO) mice during 60 weeks of life, as well as the morphologic and metabolic changes experienced by alveolar macrophages with or without SP-C.

Methods

Animal Model

SP-C–deficient mice, bred on the 129Sv background, were introduced (40) and obtained with permission from Cincinnati Children's Hospital (Cincinnati, Ohio). Healthy 129Sv mice, which served as the control group, were acquired from Charles River GmbH. Details about the animal groups are presented in the METHODS in the data supplement.

Lung Mechanical and Function Measurements

All animals were weighed and anesthetized via intraperitoneal injection of 80 mg/kg ketamine and 5 mg/kg xylazine in 0.9% sodium chloride. After tracheotomy, mice were connected to a small animal ventilator (FlexiVent; SCIREQ). Mechanical ventilation was performed as described previously (41) and detailed in the METHODS in the data supplement. Oxygen saturation in percentage of functional arterial hemoglobin was determined during normal mechanical ventilation at positive end-expiratory pressure (PEEP) of 3 cm H_2O with the use of a rodent oximeter (MouseOx Plus; Starr Life Sciences Corp.). Afterwards, vascular perfusion–fixation was performed as explained in the METHODS in the data supplement.

Histological Sections and Staining

Tissue slices were embedded into hydroxyethylmethacrylate (Technovit 8100; Kulzer Heraeus). For further design-based stereology on the light microscope level, tissue sections were stained with toluidine blue, as detailed in the METHODS in the data supplement. Simultaneously, lung cubes were sampled randomly for representative electron microscope (EM) imaging, as explained in the METHODS in the data supplement. Remaining tissue slices were embedded in paraffin and stained with a Masson-Goldner staining kit (Merck). Immunostaining of human tissue sections is detailed in the METHODS in the data supplement.

Design-based Stereology

Design-based stereology is the gold standard for quantitative lung structure analysis based on histological images, enabling profound mathematical inference of 3D geometrical structures from 2D sections, as for example, compartments of the distal airways (42). All analyzed parameters for lung structure regarding fibrosis were chosen according to recommendations from Mühfeld and Ochs (43) for stereology in pulmonary fibrosis. A detailed description of investigated parameters and corresponding test systems is presented in Table 1 and in the METHODS in the data supplement.

Hydroxyproline Assay

Hydroxyproline content was measured in accordance to the protocol established by Reddy and Enwemeka (44) and detailed in the METHODS in the data supplement.

Real-Time PCR

RNA was isolated from homogenized lungs after lavage following ISOLATE II RNA Mini Kit instructions (ISOLATE RNA Mini Kit; Bioline GmbH). cDNA synthesis was performed in a Thermal Cycler (CFX96TM; Bio-Rad Laboratories). Subsequent RT-PCR was performed with iTaq Universal SYBR Green Supermix (Bio-Rad Laboratories); primer sequences are shown in detail in Table 2 and in the data supplement.

Table 1. Absolute Volumes of Lung Compartments Determined by Design-based Stereology in Surfactant Protein C Knockout Mouse Lungs

Parameter [ml]	10 wk		20 wk		30 wk		40 wk		50 wk		60 wk	
	Mean	SD	Mean	SD	Mean	SD	Mean	SD	Mean	SD	Mean	SD
V(par, lung)	0.34	0.07	0.35	0.05	0.63	0.11	0.42	0.07	0.53	0.10	0.49	0.10
V(non-par, lung)	0.05	0.02	0.06	0.02	0.09	0.02	0.05	0.01	0.07	0.02	0.08	0.03
V(vent-par, lung)	0.33	0.07	0.34	0.04	0.62	0.10	0.42	0.07	0.51	0.10	0.48	0.10
V(non-vent-par, lung)	0.008	0.006	0.009	0.004	0.010	0.006	0.006	0.003	0.013	0.006	0.010	0.006
V(alv, lung)	0.16	0.04	0.15	0.02	0.29	0.05	0.19	0.03	0.21	0.03	0.22	0.06
V(duct, lung)	0.13	0.05	0.15	0.03	0.27	0.05	0.20	0.04	0.26	0.07	0.22	0.04
V(sept, lung)	0.04	0.01	0.04	0.05	0.07	0.11	0.04	0.01	0.05	0.01	0.06	0.01

Definition of abbreviations: V(alv, lung) = absolute alveolar space volume; V(duct, lung) = absolute ductal airspace volume; V(non-par, lung) = absolute non-parenchyma volume; V(non-vent-par, lung) = absolute non-ventilated parenchyma volume; V(par, lung) = absolute lung parenchyma volume; V(sept, lung) = absolute septal volume; V(vent-par, lung) = absolute ventilated parenchyma volume.
Absolute stereological lung volumes (ml) are given with mean and SD for every age group.

Cholesterol Assay

Total cholesterol concentration was quantified following instructions of Total Cholesterol Assay Kit (Colorimetric) (Cell Biolabs, Inc.) as explained in the METHODS in the METHODS in the data supplement.

Engulfment of Cholesterol-laden Lipid Vesicles with or without SP-C

Uptake of cholesterol laden with/without SP-C lipid vesicles by alveolar macrophages was performed using a fluorescently labeled cholesterol probe and quantified as the percentage of cells presenting fluorescence in a flow cytometer. Further details can be found in the METHODS in the data supplement.

Statistical Analysis

Graphs and statistical analysis were conducted with GraphPad Prism 6.0 (GraphPad Software) and detailed in the METHODS in the data supplement.

Results

Impaired Alveolar Recruitment Is Accompanied by Increased Tissue Stiffness in the Lungs of SP-C KO Mice

Body weight gain was significantly delayed in SP-C KO mice in comparison to healthy 129Sv mice up to an age of 40 weeks (Figure 1A). Likewise, absolute lung volume was significantly reduced at early ages (10 and 20 wk; Figure 1B). Simultaneously, inspiratory capacity was significantly reduced at an age of 10 and 20 weeks in comparison to healthy mice (Figure 1C). Accordingly, static compliance (Figure 1D) was significantly reduced in comparison to age-matched healthy 129Sv mice.

Tissue elastance (H) was assessed at PEEP of 1 cm H_2O, 3 cm H_2O, and 6 cm H_2O as an indicator of distal parenchymal stiffness (Figure 1E). At the early ages of 10 and 20 weeks, lungs of SP-C KO mice exhibited significantly increased H compared with healthy controls at every applied PEEP (Figures 1F–1H), pointing at stiffer lungs in the absence of SP-C at early ages. Increasing airway pressure from 1 to 6 cm H_2O may facilitate alveolar recruitment, resulting in reduced tissue stiffness, as seen in healthy 129Sv mice (Figure E1A in the data supplement). However, an applied PEEP of 6 cm H_2O (Figure 1E) failed to further reduce H at the ages of 10, 50, and 60 weeks compared with low pressure, such as PEEP of 3 cm H_2O in the SP-C KO group. This pointed at reduced recruitability of alveolar spaces at older ages (either due to alveolar collapse, permanent derecruitment and/or a remodeling process) as a result of SP-C deficiency during abnormal lung aging. In addition, a mixed-effects statistical analysis revealed that changes were mostly an effect of both genotype and aging (Table E3).

Accordingly, tissue damping (G), assessed at PEEP of 3 cm H_2O, significantly decreased from Week 20 to Week 30 in the SP-C KO group, whereas healthy mice showed no age-dependent alterations in G (Figure 1I). Meanwhile, tissue hysteresivity (η) of SP-C KO mice exhibited only minor fluctuations in contrast to healthy controls displaying a continuous increase until 50 weeks of age (Figure 1J). Thus,

Table 2. Statistically Significant Correlations after Spearman Test and Linear Regression Comprising All Surfactant Protein C Knockout Age Cohorts

Correlating Parameters	Spearman *r*	Spearman–Sig. Two Sided	*n*	Linear Regression
Vv(non-vent-par/par), S(alvepi, lung)	−0.455*	0.001	51	Y = −1974X + 260.7
Lung volume, Sv	−0.445*	0.001	51	Y = −0.02113X + 0.06102
IC, Vv(duct/par)	0.292†	0.039	50	Y = 0.1339X + 0.3125
Lung volume, mean linear intercept	0.495*	0.000	51	Y = 37.91X + 52.61
Septal thickness, G	0.290†	0.044	49	Y = 0.2579X + 2.990
Septal thickness, Vv(vent-par/par)	−0.532*	0.000	51	Y = −0.02671X + 0.5584

Definition of abbreviations: G = tissue damping; IC = inspiratory capacity; S(alvepi, lung) = total surface of alveolar epithelium per lung; Sv = surface density; Vv(duct/par) = volume density of ductal spaces in parenchyma; Vv(non-vent-par/par) = volume density of nonventilated parenchyma in parenchyma; Vv(vent-par/par) = volume density of ventilated parenchyma in parenchyma.
*$P < 0.05$.
†$P < 0.01$.

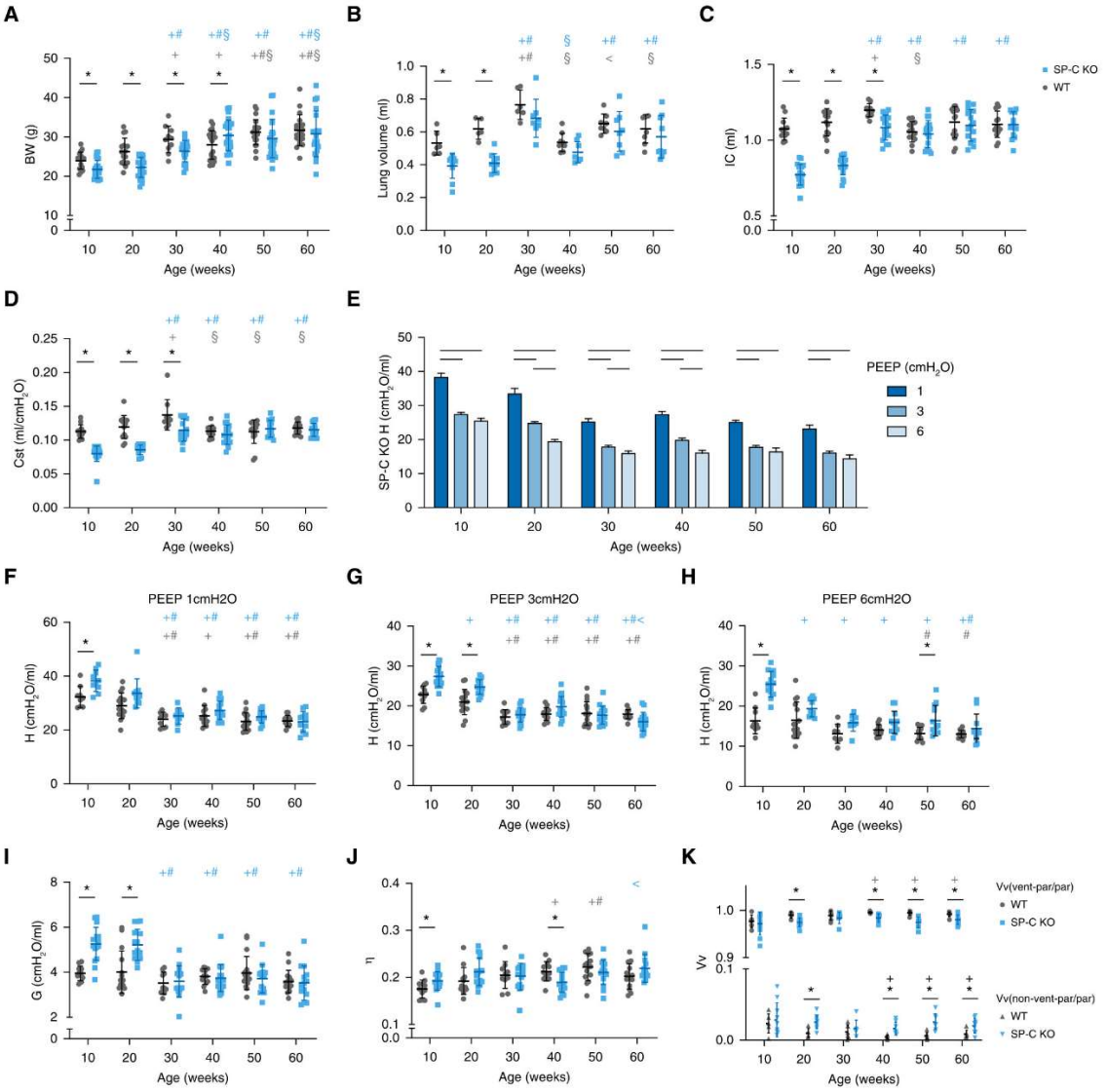

Figure 1. Impaired alveolar recruitment is accompanied by increased tissue stiffness in the lungs of surfactant protein (SP)-C knockout (KO) and healthy 129Sv mice. (*A*) Body weight (BW), (*B*) lung volume (ml), (*C*) inspiratory capacity (IC), and (*D*) static compliance (Cst) over time. (*E*) Tissue elastance (H) as an indicator of distal lung tissue stiffness was obtained during the forced oscillation technique and calculated according to the constant phase model at positive end-expiratory pressure (PEEP) of 1 cm H_2O (dark blue bars), 3 cm H_2O (blue bars), and 6 cm H_2O (light blue bars) for each age group, respectively, $n \geq 8$ (black horizontal lines indicate statistically significant differences between the groups they connect $P < 0.05$). (*F*) H at PEEP 1 cm H_2O with age. (*G*) H at PEEP 3 cm H_2O with age. (*H*) H at PEEP 6 cm H_2O with age. (*I*) Tissue damping (G). (*J*) Tissue hysteresivity (η) were assessed at 10–60 weeks of age. (*K*) Volume fraction (Vv) of ventilated parenchyma (top of the graph) and nonventilated parenchyma (bottom of the graph) within lung parenchyma. Mean ± SD, $n \geq 6$; horizontal black lines with an asterisk (*) represent a statistical difference at $P < 0.05$ between SP-C KO and healthy mice within age groups. Statistical differences with age are represented in blue for the SP-C KO group and in gray for the healthy controls. $^{+}P < 0.05$ versus 10 weeks; $^{\#}P < 0.05$ versus 20 weeks; $^{\S}P < 0.05$ versus 30 weeks; $^{<}P < 0.05$ versus 40 weeks.

significant differences between both groups were found at an age of 10 and 40 weeks, suggesting that altered rheological properties of the lung tissue. However, the main effect was due to age and not genotype (Table E3).

Stereological analysis revealed an increased volume fraction (Vv) of nonventilated parenchyma in the SP-C KO group in comparison to healthy mice, which was significant at an ages of 20, 40, 50, and 60 weeks (Figure 1K). Taken together,

deficiency of SP-C resulted in loss of ability on reopening alveoli at higher pressure and abnormal rheological properties of the lung tissue, pointing at an ongoing remodeling process. In addition, a mixed-effects statistical analysis revealed the absence of SP-C as a major contributor to the decrease of ventilated parenchyma and the increase of nonventilated parenchyma (Table E3).

Ductal Airspace Overdistension Precedes Septal Thickening in the SP-C KO Lung

General lung morphology during aging can be observed in Figure 2A. SP-C KO lungs exhibited a slight age-dependent decrease in alveolar space and an increase in ductal airspace Vv (Vv[duct/par]), which became significant at 50 weeks of age (Figures 2B and 2C). Accordingly, mean linear intercept length measurements were not significantly changed in SP-C KO versus healthy 129Sv mice, except at 50 weeks of age (Figure 2D). Healthy 129Sv mouse lungs did not reveal a major trend toward an increasing or decreasing alveolar space Vv (Figure 2B). In addition, volume-weighted mean volume values varied around the baseline observed at 10 weeks (Figure 2E) for healthy controls. In contrast, volume-weighted mean volume remained unaltered over the first 20 weeks in the SP-C KO group, but exhibited a significant increase at the end of Week 30 (Figure 2E), indicating a rearrangement in the alveolar architecture and increased alveolar size heterogeneity.

Alveolar epithelial surface was significantly reduced at 20 and 50 weeks in contrast to healthy mice (Figure 2F). In line with lung volume development, alveolar surface rose significantly in the lungs of 30-week-old SP-C KO animals, but tended to decline from Week 30 to Week 50 (Figure 2F). Simultaneously, septal thickness steadily decreased until Week 40, where a tendency toward thicker alveolar septa was observed (Figure 2G). Accordingly, SP-C KO mouse lungs showed significantly thicker septal walls in head-to-head comparison with their healthy counterparts at an age of 50 weeks (Figure 2G). Significantly, increased thickness from Week 50 coincided with the appearance of consolidated lesions, giving the first indication of fibrotic remodeling (Figure 2A; micrographs 10 and 12). In addition, overdistended ductal airspaces corresponding to increased Vv(duct/par) became particularly prominent in subpleural regions (Figure 2A; micrographs 3, 5, and 7). These features were not observed in healthy control lungs (Figure E2A).

SP-C KO Mouse Lungs Exhibit Altered Tissue Composition and Aberrant Connective Tissue Protein Gene Expression

Masson-Goldner trichrome staining provided further insight into tissue composition of observed microscopic wounds, most prominently in the lungs at 50 and 60 weeks of age. Although thickness of septa was not accompanied by staining for collagen from Weeks –20, consolidations in parenchyma stained positive for collagen at the age of 50 and 60 weeks (green, Figure 3A), especially in comparison to older healthy mice (Figure E3A). Therefore, increased septal thickness at early ages seemed to arise from alveolar collapse, whereas the later onset of thickening was associated with interstitial collagen deposition. Quantification of hydroxyproline showed a tendency toward higher levels with age, but did not demonstrate significant differences between age cohorts or genotypes (Figure 3B and Figure E3B). Relative *Col1a1*, *Col3a1*, and *Fn* expression obtained from RT-PCR analysis was significantly downregulated in the SP-C KO mice with age (Figures 3C, 3D, and 3F). Likewise, *Col2a1* and *Eln* also tended toward lower expression levels, but were not significantly different (Figures 3F and 3G). This represents a different, aberrant remodeling of fibers in comparison with the normal redistribution of fibers in healthy, aging mice (Figures E3C–E3G).

SP-C Deficiency Alters the Innate Immune System of the Lung

The total number of cells in BAL of the SP-C KO cohort declined with age (Figure 4A). In contrast, the number of cells counted in healthy BAL remained constant at a generally lower level than in BAL recovered from SP-C KO mice (Figure 4A). Statistical analysis revealed significant differences between healthy and SP-C KO at 10 and 20 weeks of age, and the effect seemed to be mainly due to the genotype and not age (Table E3). Light microscopic analysis of immune cell subtypes identified macrophages as the predominant cell type with a minor, but constant, fraction of neutrophils in the healthy mice independent of age (Figure 4B and Figure E4A). In contrast, the proportion of neutrophils was increased in SP-C KO mice at 40 weeks of age and was accompanied by the appearance of eosinophils at Week 50.

Fibrotic areas of a lung section validated the presence of electron-dense clefts in IPF lung tissue (Figure 4C). Furthermore, ultrastructural phenotype qualitative analysis of lung macrophages was performed in the SP-C KO mice for every age group. At 10 and 20 weeks of age, macrophages derived from SP-C KO lungs exhibited numerous electron-dense, lamellar body–like inclusions in the cytoplasmic cell compartment. In the successive 10 weeks, the cells further accumulated these inclusions and appeared loaded with various electron-dense clefts (Figure 4D, micrographs 7–12). Meanwhile, healthy control mice of the same strain did not show any cleft accumulation over the entire study frame (data not shown). EM micrographs of AEC2 showed no morphological alterations.

Absence of SP-C Leads to Impaired Cholesterol Metabolism in Alveolar Macrophages

Due to the notable appearance of electron-dense inclusions only in the alveolar macrophages of SP-C KO lungs, we investigated the cholesterol metabolism in these cells. Expression of cholesterol efflux transporters, such as *Abca1* (ATP binding cassette A1) and *Abcg1* (ATP binding cassette G1), as well as regulatory elements of the metabolism of cholesterol, such as the gene encoding the *Ldlr* (low-density lipoprotein) receptor, the *Lxra* (liver x receptor alpha), the *Ch25 h* (cholesterol-25-hydroxlyase), and the *Srebp2* (sterol-response element binding protein 2) steadily increased over the first 30 weeks (Figure 5A). In addition, their expression significantly dropped from Week 30 to Week 40 and was hardly detectable at 50 and 60 weeks. At the same time, total cholesterol amounts relative to total lung tissue exhibited a significant and constant increase (Figure 5B) with advancing age, as well as for the healthy 129Sv mice. In addition, the mixed-effect statistical analysis revealed that age was the main contributor to the changes in total cholesterol (Table E3).

Interestingly, expression rates of cholesterol-related genes were mirrored by gene expression of macrophage activator

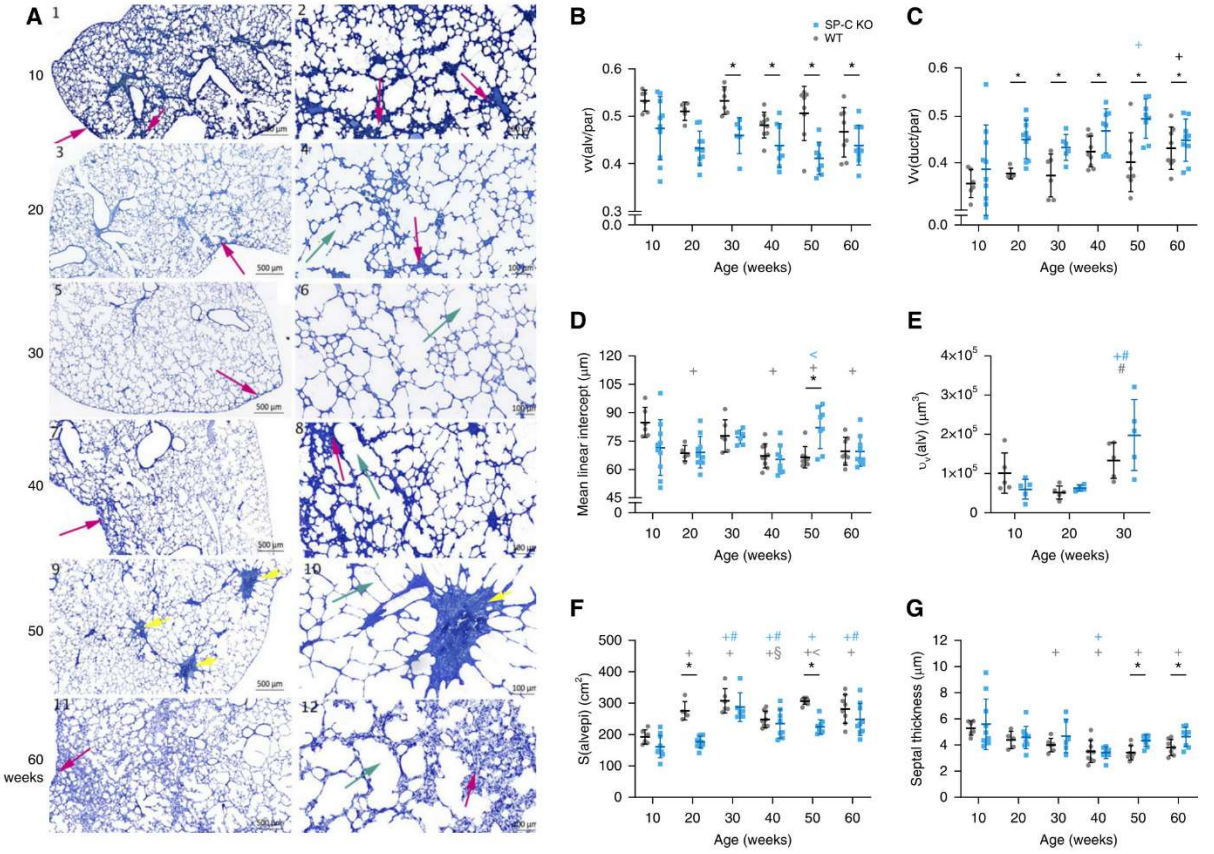

Figure 2. Ductal airspace over distension precedes septal thickening in the SP-C KO and healthy 129Sv lung. (*A*) Representative toluidine blue–stained micrographs of vascular perfused–fixed murine SP-C KO lungs (inflated with air at airway pressure = 5 cm H_2O) revealed thickened interalveolar septa as markers of microatelectasis (pink arrows; panels 1 and 2). This was followed by alveoductal overdistension (green arrow), which coincidences with alveolar size reduction in the same topographic region at an age of 20 weeks (panels 3 and 4). This process was found to further develop until Week 30 (panels 5 and 6), predominating in the subpleural regions (panels 3 and 5). At 40 weeks of age, enlarged alveolar ducts localized next to prominent septal walls (green and pink arrows) (panels 7 and 8); 10 weeks later, first fibrotic lesions (yellow arrows) appeared causing tensile stress of the surrounding lung parenchyma (panels 9 and 10). After 60 weeks, septal wall thickening progressed, whereas alveolar destabilization in sense of collapse induration continued (panels 11 and 12). Scale bars: 500 µm (left column) and 100 µm (right column). Age-dependent lung structure analysis of (*B*) volume density of alveolar space in parenchyma (Vv[alv/par]), (*C*) ductal airspace density (Vv[duct/par]), (*D*) mean linear intercept length, (*E*) mean volume-weighted mean volume (v_v[alv]), (*F*) absolute surface of the alveolar epithelium (S[alvepi]), and (*G*) septal wall thickness (µm) were quantified within the ventilated parenchyma (V[vent-par, lung]) with age. Mean ± SD, $n \geq 6$; horizontal black lines with an asterisk (*) represent a statistical difference $P < 0.05$ between SP-C KO versus healthy within age groups. Statistical differences over age are represented in blue for the SP-C KO group and in gray for the healthy controls. $^{+}P < 0.05$ versus 10 weeks; $^{\#}P < 0.05$ versus 20 weeks; $^{\S}P < 0.05$ versus 30 weeks; $^{<}P < 0.05$ versus 40 weeks.

chitinase-like-3 (*Ym1*) (Figure 5A). In contrast, slight changes in gene expression of BAL cells from healthy animals were observed (Figure E5A). *In vitro*, engulfment ability of macrophages from SP-C KO BAL was reduced when exposed to lipid, cholesterol-laden lipid, and SP-C–laden lipid vesicles compared with wild-type (WT) macrophages (Figure 5C). However, the addition of both cholesterol and SP-C to the lipid vesicles increased the uptake up to control conditions (SP-C KO macrophages exposed to lipid vesicles) and to their WT counterpart for this condition (WT macrophages exposed to cholesterol + SP-C–laden lipid vesicles). In addition, we analyzed the uptake of a mouse macrophage cell line, MHS-C, in its ability to uptake lipid vesicles with/without cholesterol and/or SP-C (Figure 5D) and changes in cholesterol metabolism and transport gene expression (Figures 5E–5G). Interestingly, the addition of SP-C to the cholesterol-laden vesicles increased not only the uptake, but also further activated genes for cholesterol metabolism and transport (such as *Pparg*, *SraI*, *Abca1*, *Abcg1*, *Lxrb*, and *Srebp2*).

Structure–Function Relationship in the Aging SP-C KO Lung

Peripheral arterial oxygen saturation (Sp_{O_2}) level was progressively reduced at older ages. Meanwhile, Sp_{O_2} in control mice remained unimpaired up to the age of 60 weeks (Figure 6A). In addition, the mixed-effect statistical analysis revealed that the

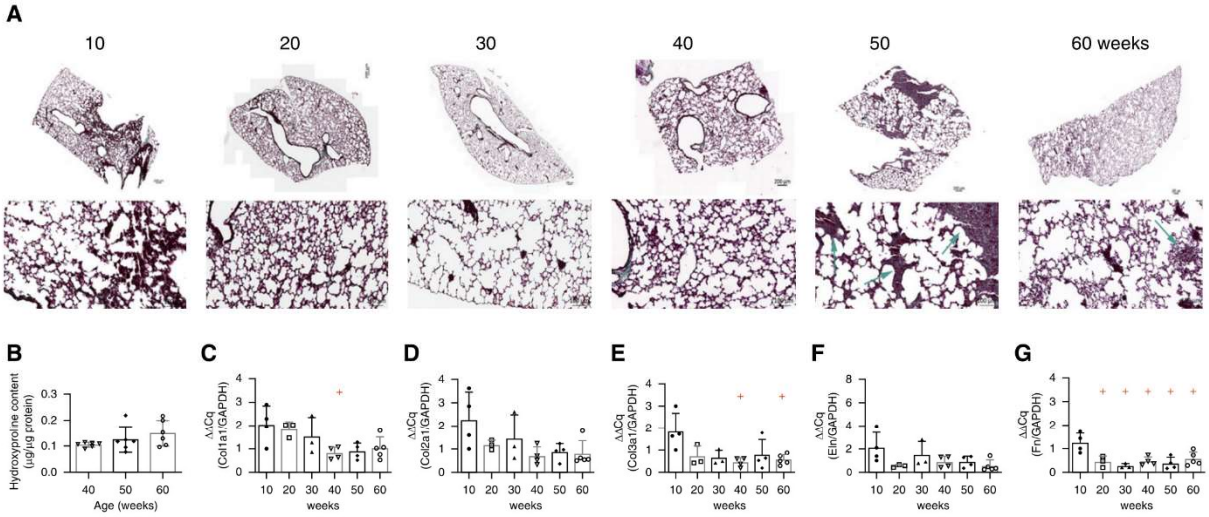

Figure 3. SP-C KO mice exhibit altered tissue composition and aberrant connective tissue protein gene expression. (*A*) Masson-Goldner trichrome staining over age showed the abundance of dense, nonventilated parenchyma areas at 10 and 50 weeks of age. At 50 weeks, these lesions (arrows) were interspersed with collagen (green interspersed areas are seen in the bottom images), whereas no collagen deposition was visible in lungs from 10-week-old mice (green arrows). Scale bars: 200 μm (top row) and 100 μm (bottom row). (*B*) Hydroxyproline level was quantified in representative tissue sections at 40, 50, and 60 weeks ($^{*}P < 0.05$, $n = 5$) and. (*C–G*) RT-PCR gene expression analysis of *Col1a1* (collagen 1a1), *Col2a1* (collagen 2a1), *Col3a1* (collagen 3a1), elastin, and *Fn* (fibronectin) in healthy and SP-C KO lungs at the ages of 10–60 weeks showed decreasing expression levels becoming significant for *Fn*, *Col1a1*, and *Col3a1*. Normalized by *Gapdh*; $^{+}P < 0.05$ versus 10 weeks, $n = 5$. Data are presented as mean ± SD.

genotype (group) was the main contributor to these changes (Table E3). microCT (μCT) imaging of a 60-week-old male SP-C KO mice showed multiple subpleural areas of consolidated lung tissue (Figure 6B). Similarly, an analogous thoracic HRCT image of a 75-year-old patient with IPF exhibited subpleural reticular septal thickening adjacent to cystic airspace enlargement (Figure 6C).

Over the whole study, increasing fractions of nonventilated parenchyma correlated with loss of alveolar surface at the light microscopic level ($r = -0.455$, $P = 0.001$; Figure 6D). Furthermore, absolute lung volume and surface density exhibited an inverse relationship ($r = -0.445$, $P = 0.001$; Figure 6G). Rising inspiratory capacity correlated significantly with an increase in Vv(duct/par) ($r = 0.292$, $P = 0.039$; Figure 6E). An increase in G was significantly proportional to rising septal thickness ($r = 0.290$, $P = 0.044$; Figure 6F), indicating pronounced tissue rigidity in thickened interalveolar septa. Simultaneously, a negative correlation was found between septal thickness and the fraction of ventilated parenchyma ($r = -0.532$, $P < 0.001$; Figure 6I). A summary of correlation statistics is provided in Table 2.

Discussion

Over a 60-week period, both adaptive and compensatory mechanisms may be activated to facilitate the main function of the lung—gas exchange—in SP-C–deficient mice. These mice suffered a mild decline in lung function, with reduced Sp_{O_2} values (Figure 6A) during reorganization of air spaces, but weeks before fibrotic wounds were detected. Similarly, it could be hypothesized that patients with IPF may undergo rearrangement of air spaces years before symptoms appear and they are diagnosed. This animal model was first developed and described by Glasser and colleagues (19). They demonstrated altered stability of lung surfactant activity from SP-$C^{-/-}$ mice compared with SP-$C^{+/+}$ mice, especially at low bubble volumes (*in vitro*) and low lung volumes (*in vivo*). It has already been described that SP-C is critical for the stability of the lipid surfactant film at the interface (17, 45); the lack of this protein may lead to collapse of small alveoli.

Interestingly, it has been reported that SP-C KO mice did not have any histological differences from their WT counterparts at the embryonal age of 18.5 and Postnatal Day 1 (40). However, we observed lungs of 10-week-old mice showing typically thickened septal walls and shortened alveolar septal tips, suggesting a delayed development, which seems to be normalized at the age of 20 weeks (Figure 2A). In addition, higher expression of the collagen genes in this group also points to an ongoing delayed development of the lung (Figures 3C and 3D). Interestingly, those 10-week-old lungs also contain a higher number of BAL cells (mainly macrophages; Figures 4A and 4B), pointing to an abnormal postnatal innate immune system. It is possible that SP-C does not play an important role during prenatal development, but that it does at the moment air enters the lung for the first time and during the first weeks of postnatal development. This suggests that, without SP-C, a newly air-breathing lung may suffer from alveolar instability and collapse (we could detect higher volume densities of nonventilated parenchyma in the KO mice at 10 weeks; Figure 1K) due to lung surfactant instability. This instability during compression (expiration) of the alveolar surface may lead to abnormal mechanical and physical forces (19, 23, 26). This may delay the normal postnatal development of the lung until the 10th week of life, when

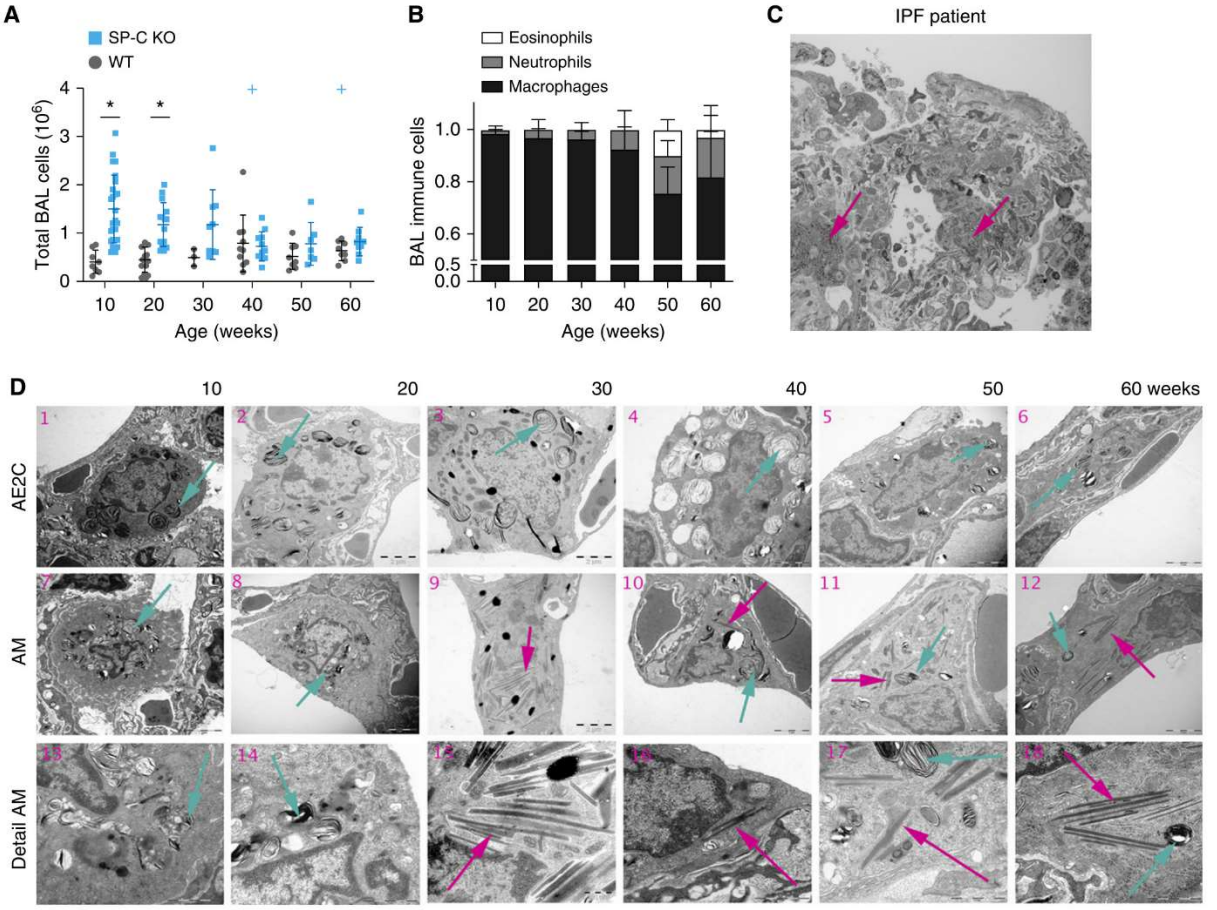

Figure 4. SP-C deficiency alters the innate immune system of the lung. (*A*) Total BAL fluid (BALF) cell count assessed in SP-C KO and healthy 129Sv mice. (*B*) Relative quantification of leukocyte subpopulations in BALF cells of SP-C KO mice. (*C*) Electron microscopic (EM) micrograph of an idiopathic pulmonary fibrosis (IPF) lung demonstrates the presence of intraparenchymal macrophages being loaded with electron-dense crystals (pink arrows). (*D*) Representative EM imaging of SP-C KO lungs over age demonstrates unaltered alveolar epithelial type 2 cell (AE2C) morphology with physiologically shaped lamellar bodies (green arrows) (panels 1–6) and electron-dense intracellular inclusions with cleft formation in lung macrophages (pink arrow) (panels 7–12). Onset of crystal formation starts at 30 weeks of age. Detailed structural morphology of the lamellar body–like inclusions and electron-dense clefts is provided on high-magnification micrographs (panels 13–18). Scale bars: 2 μm for pictures in the two top panels (AM and AE2C) and 500 nm in the Detail AM panels. Mean ± SD, $n \geq 6$; horizontal black lines with an asterisk represents a statistical difference $P < 0.05$ between SP-C KO and healthy within age groups. Statistical differences over age are represented in blue for the SP-C KO group and in gray for the healthy controls. $^{+}P < 0.05$ versus 10 weeks. AM = alveolar macrophage.

we analyzed our animals. In addition, other animal models, showing SP-C deficiency, have reported abnormal lung development (46, 47). However, because a complete analysis of pre- and postnatal lung development in these mice is missing, we could only speculate about the potential role of SP-C on these processes.

Alveoli seemed to be recruited with high pressure (such as PEEP of 6 cm H_2O) in normal healthy animals, but somehow recruitment was impaired in older SP-C KO mice (Figure 1E). Therefore, these results suggest that chronic alveolar instability seemed to lead to permanent derecruitability of alveoli in 50- and 60-week-old SP-C KO mice. This permanent derecruitment leads to changes in H and G with age, resulting in differences in η at the age of 60 weeks. Differences in H and G toward progressive loss of H and G have also been described in the elastase-induced emphysema mouse model (48) accompanied by an increase in η. Increases in η were also related to increased heterogeneity throughout the lung (49) in complex disease phenotypes. Therefore, the evidence from this study suggests a complex disease phenotype where overexpansion (emphysema-like phenotype) of air spaces and consolidated collapsed (derecruited alveoli) regions coexist within the lungs of SP-C KO mice. These results are supported by the lung micrographs in Figure 2A, and suggest that overdistension of ductal and alveolar spaces precedes the consolidation of lung tissue starting at 40 weeks of age. In addition, septal wall thickness tended to increase in the 40- to 60-week groups (Figure 2G). These changes were not statistically significant, mainly due to the increasing heterogeneity in the lungs (50). Moreover, although fibrotic alterations

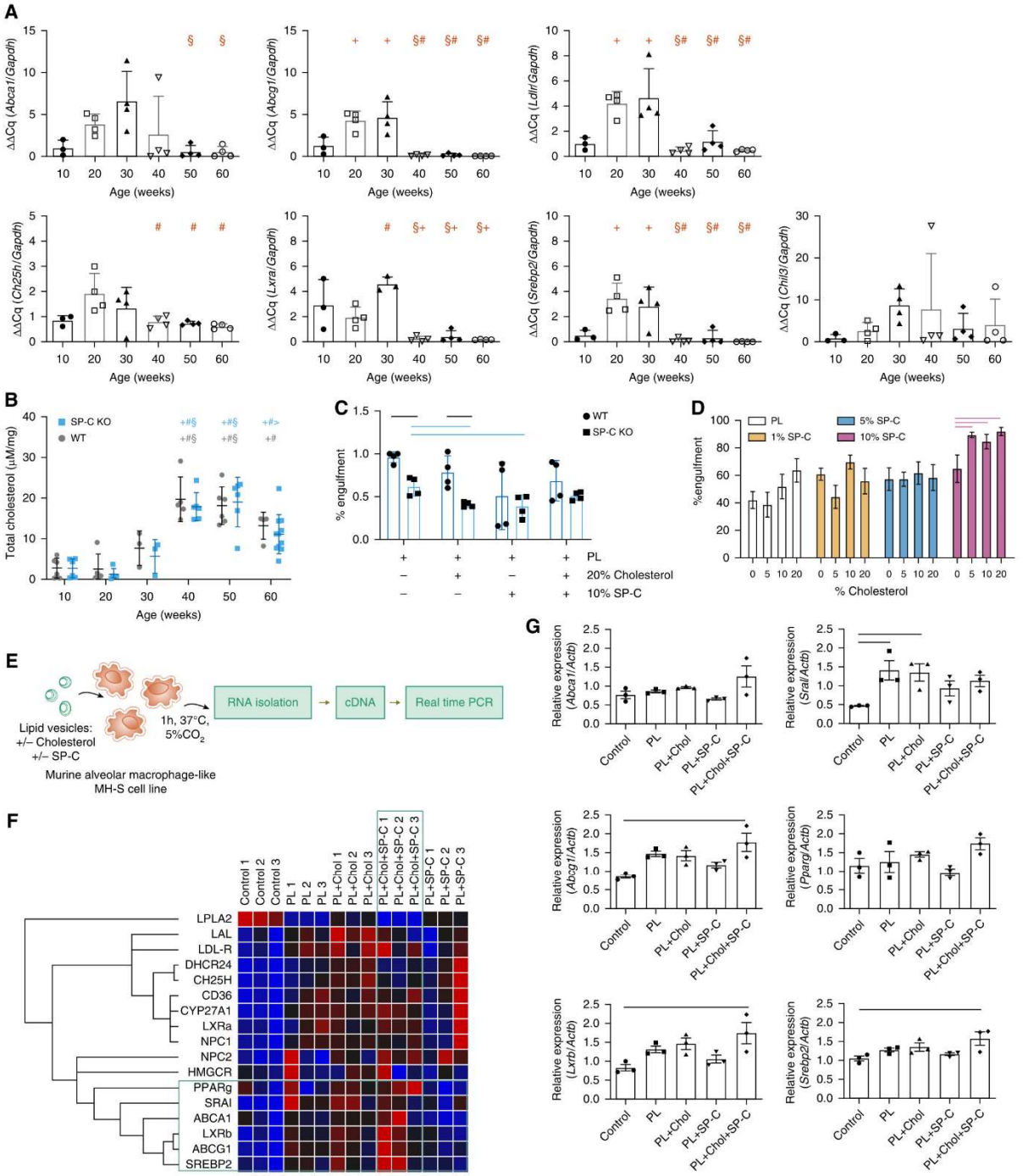

Figure 5. Absence of SP-C leads to impaired cholesterol metabolism in alveolar macrophages. (*A*) RT-PCR gene expression analysis of *Abca1* (ATP binding cassette A1), *Abcg1* (ATP binding cassette G1), *Ch25h* (cholesterol-25-hydroxylase), *Ldlr* (LDL receptor), *Lxra* (liver X receptor α), *Srebp2* (sterol response element binding protein 2), and *Chil3* (chitinase like 3 or Ym1) in BALF cells. Normalized by *Gapdh*. (*B*) Total cholesterol quantification in SP-C KO and healthy 129Sv lungs per microgram lung tissue at Weeks 10–60. (*C*) Fluorescent-lipid uptake by alveolar macrophages as percentage of

have been repeatedly linked to elevated lung stiffness, H in a pulmonary spring model only substantially increased once a certain percolation threshold was reached (51). Projected on the SP-C KO lung, these findings may explain why H showed only subtle increases at 60 weeks of age, despite the presence of multiple fibrotic lesions.

Further analysis of the septal wall composition confirmed the slight increase in collagen production at both the protein (Figure 3B) and mRNA (Figures 3C–3G) levels. As stated previously, pronounced phenotypic heterogeneity, with overdistended air spaces and aberrant wound healing, masks statistically significant differences. However, this heterogeneity itself is a common feature, and resembles human samples of patients suffering IPF, as shown in the HRCT scans in Figures 6B and 6C.

During the 60 weeks of the study, we did not observe any sign of edema or inflammation. In addition, the total number of BAL cells in aging SP-C KO mice decreased progressively, reaching the number of cells in healthy controls (Figure 4A). Analyzing the types of cells in BAL, we discovered some infiltrating cells in older lungs. At 40 weeks of age, neutrophils appeared in the BAL samples, but in a moderate proportion (<10%). This proportion increased further in the 50-week group, and eosinophils appeared, but again in a moderate proportion, not enough to suspect pulmonary inflammation or lung injury (Figure 4B). Therefore, the findings of this study suggest that these infiltrating cells may contribute to the remodeling of the tissue rather than a response to inflammation or infection. This assumption is supported by previous reports where both infiltrating cell types have been related to remodeling processes in the lung (47, 52–54). In addition, and noteworthy, are the changes in morphology of alveolar macrophages in the aging SP-C KO mice in accordance with findings in samples from patients with IPF (Figure 4C). As briefly described before (40), macrophages of SP-C KO mice contain electron-dense crystals in their cytoplasm (Figure 4D). Crystals were first detected in animals at 30 weeks of age. Although, in human patients, this may be a hallmark of an eosinophilic pneumonia, in some cases associated with pulmonary fibrosis (55) the appearance of crystals before the infiltration of eosinophils, or any other infiltrating cell as well as any sign of fibrotic remodeling in the SP-C KO lungs, leads to the rejection of the hypothesis. On the one hand, those crystals are similar to cholesterol crystals seen in macrophages throughout the literature in the presence of cholesterol (56–59). The 129Sv strain exhibits abnormal absorption of dietary cholesterol (60) and is widely used in the study of cholesterol metabolism. Besides, this macrophage phenotype has not been described in other SP-C KO strains with BALBc or B6N background. We observed a notable increase in cholesterol in the lung tissue of the SP-C KO mice from 30 weeks of age (Figure 5B). However, the same pattern was also observed for their healthy control counterparts (Figure 5B), but crystals were not found in alveolar macrophages. In this regard, Romero and colleagues (37) showed increased amounts of cholesterol in lung tissue of mice after bleomycin treatment, and attributed this to paracrine lipid cross-talk between AECs and alveolar macrophages. Thus, initial observations reported here suggest that this cross-talk may be impaired in the absence of SP-C in our model. Other lipid transporters have also been reported to be involved in development of fibrosis, including ApoE, ApoA1, and ABCG1 (61–64). Interestingly, gene expression of cholesterol metabolism and transport genes showed biphasic behavior as well as cholesterol content in the lung. When the genes under study were downregulated, cholesterol started accumulating in the lung, right at Week 30, where the first crystals appear under EM (Figures 4F, 5A, and 5B). In addition, *in vitro* experiments supplementing cholesterol-laden lipid vesicles with SP-C enhanced not only the uptake of those vesicles by MH-S, but also resulted in an increased expression of genes related to cholesterol metabolism and transport (such as *Pparg*, *SraI*, *Abca1*, *Abcg1*, *Lxrb*, and *Srebp2*). This supports the assumption that enhanced metabolism and mobilization of cholesterol in alveolar macrophages may be regulated by SP-C in alveolar macrophages.

Cholesterol metabolism has not been deeply studied in patients with lung fibrosis. Currently, there is growing evidence that lipid metabolism is impaired in lung fibrosis (36, 37, 65), but there are no data specific to cholesterol. Interestingly, it is not very surprising that, with the average age of patients with IPF being around 60 years, many of them suffer from comorbidities such as hypercholesterolemia. Kreuter and colleages (66–68) published some interesting analyses on the potential effect of the uptake of statins during the treatment of IPF with nintedanib. Although there is much controversy around it, they concluded that patients under treatment with statins and nintedanib showed a slower/delayed loss of forced expiratory volume, pointing to a potential beneficial effect of the lowering of cholesterol during treatment for IPF. No preclinical data as yet appear in the literature on this effect, so we could only speculate on the effect of cholesterol in the progression of the disease. Nevertheless, this opens up a new field of future research and new therapeutic strategies, which should first undergo preclinical studies.

In conclusion, the findings of this study suggest that overall loss of SP-C results in an age-dependent, complex, heterogeneous phenotype characterized by a combination of overdistended air spaces and fibrotic wounds

Figure 5. (Continued). engulfment, measured by FACS detection of fluorescent BAL cells from wild-type (WT) or SP-C KO mice. Macrophages were exposed to 0.25 μg of labeled phospholipid per 10^5 cells, with/without cholesterol and/or SP-C. Black horizontal lines represents $P < 0.05$ between WT and KO using a *t* test; light blue horizontal lines represents $P < 0.05$ when comparing different vesicle composition within the SP-C KO group using ANOVA. (*D*) MH-S cells, alveolar macrophage–like mouse cell line, were exposed to lipid vesicles laden with fluorescent cholesterol and/or SP-C, and lipid uptake was measured in FACS as explained previously here. (*E*) In another set of experiments, macrophages exposed to vesicles with different composition during 1 hour were collected for RNA isolation and RT-PCR analysis of expression of genes related to cholesterol metabolism and transport. (*F*) Representative heat map of relative expression of the different genes using clustering by targets (right) and samples ordered by type (top). The green rectangle shows different targets upregulated in the samples containing cholesterol and SP-C in comparison to samples containing only cholesterol or SP-C. (*G*) Relative gene expression (ΔΔCq, normalized by *Actb*) in the different samples ($n = 6$ per group) of the most interesting upregulated genes from the heat map: *Pparg*, *Sral*, *Abca1*, *Lxrb*, *Abcg1*, and *Srebp2*. Mean ± SD, $n \geq 6$; horizontal black lines with an asterisk (*) represent a statistical difference at $P < 0.05$ between SP-C KO and healthy within age groups. Statistical differences over age are represented in blue for the SP-C KO group and in gray for the healthy controls. $^{+}P < 0.05$ versus 10 weeks; $^{\#}P < 0.05$ versus 20 weeks; $^{\S}P < 0.05$ versus 30 weeks; $^{>}P < 0.05$ versus 40 weeks.

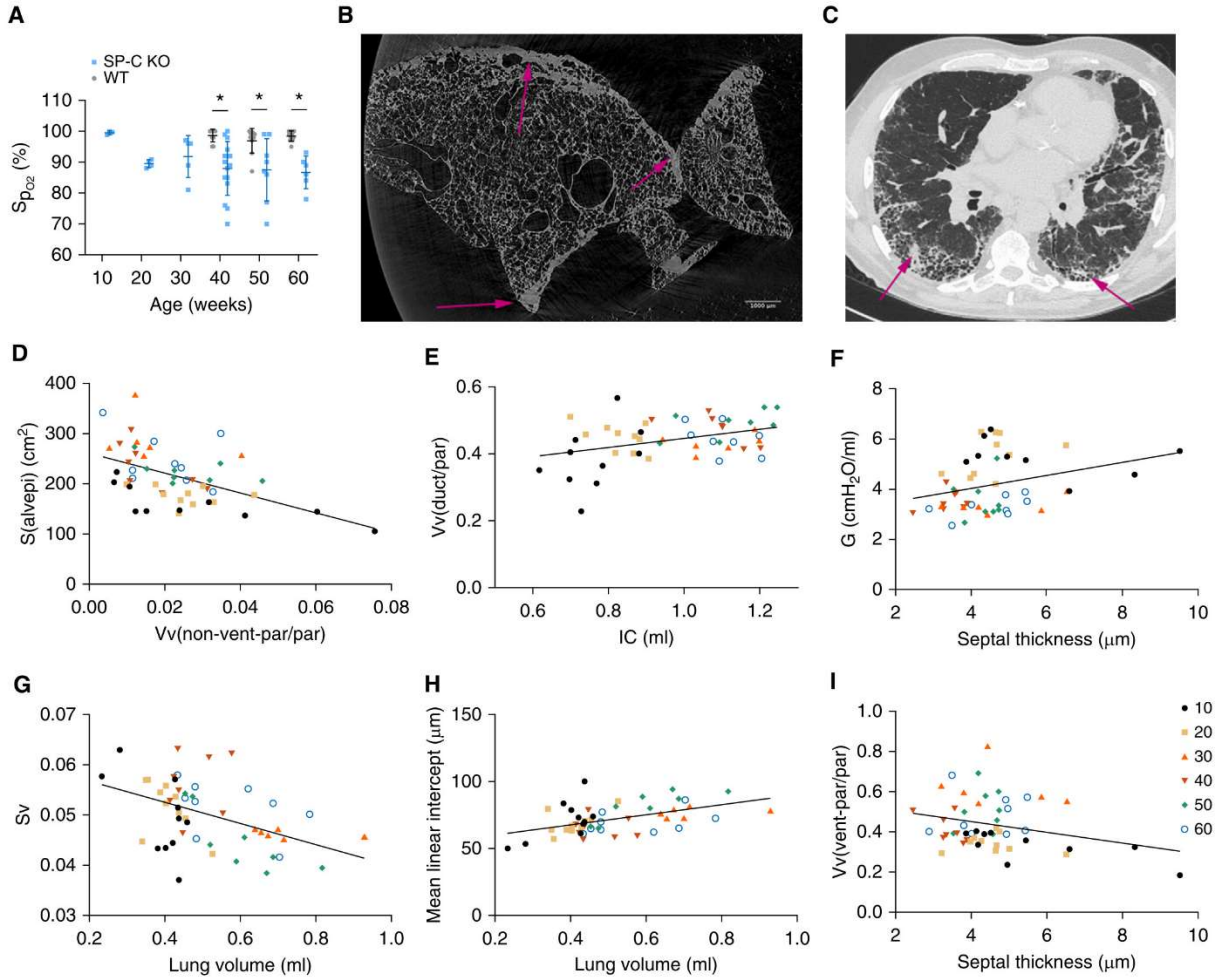

Figure 6. Structure–function relationship in the SP-C KO lung. (*A*) Peripheral arterial oxygen saturation (Sp_{O_2}) was measured at PEEP 3 cm H_2O before subsequent ventilation protocol was started in SP-C KO and healthy 129Sv mice. (*B*) microCT (computed tomography) imaging of a fixed SP-C KO lung shows distinct parenchymal lesions predominating in the subpleural compartments (pink arrows). Scale bar: 1,000 μm. (*C*) High-resolution computer tomography imaging of a 75-year-old patient with IPF. The pathology impresses with reticular septal thickening, honeycomb cysts, traction bronchiectasis, and tissue consolidation (pink arrows) in the means of usual interstitial pneumonia pattern. The pathology predominates in the subpleural regions and localizes in the direct neighborhood of overdistended lung parenchyma. Statistically significant correlation of structural and mechanical parameters over the whole study period (black circles, 10 wk; tan squares, 20 wk; brown triangles, 30 wk; inverted red triangles, 40 wk; green diamonds, 50 wk; open circles, 60 wk). (*D*) Negative correlations between alveolar surface and nonventilated parenchyma Vv by stereological analysis, and (*E*) surface density and absolute lung volume. (*F*) Proportional relationship of ductal Vv and inspiratory capacity acquired by FlexiVent. (*G*) Positive correlation of mean linear intercept and absolute lung volume as independently determined structural parameters. (*H*) G and septal thickness exhibit a positive structure–function relationship, whereas (*I*) ventilated parenchyma Vv and septal thickness correlate inversely. Mean ± SD, $n \geq 6$; horizontal black lines with an asterisk represents a statistical difference at $P < 0.05$ between SP-C KO and healthy within age groups. S(alvepi) = total surface of alveolar epithelium; Sv = surface density; Vv(vent-par/par) = volume density of ventilated parenchyma in parenchyma.

that resembles combined pulmonary fibrosis and emphysema in patients with IPF. Interestingly, this remarkable phenotype is unique to the 129Sv strain, which was previously shown to have an increased absorption of cholesterol, thus linking the accumulation of cholesterol and the absence of SP-C to a fibrotic remodeling process. Besides, addition of SP-C to cholesterol-laden lipid vesicles enhanced the expression of cholesterol metabolism and transport genes in alveolar macrophages, pointing toward a new lipid–protein axis involved in lung remodeling. ■

Author disclosures are available with the text of this article at www.atsjournals.org.

Acknowledgment: The authors are thankful for the excellent technical support of Carina Vogt and Andrea Herden (Hannover Medical School, Hannover, Germany).

References

1. Selman M, Thannickal VJ, Pardo A, Zisman DA, Martinez FJ, Lynch JP III. Idiopathic pulmonary fibrosis: pathogenesis and therapeutic approaches. *Drugs* 2004;64:405–430.
2. Raghu G, Remy-Jardin M, Myers JL, Richeldi L, Ryerson CJ, Lederer DJ, *et al*.; American Thoracic Society, European Respiratory Society, Japanese Respiratory Society, and Latin American Thoracic Society. Diagnosis of idiopathic pulmonary fibrosis: an official ATS/ERS/JRS/ALAT clinical practice guideline. *Am J Respir Crit Care Med* 2018;198:e44–e68.
3. Petroulia V, Funke M, Zumstein P, Berezowska S, Ebner L, Geiser T, *et al*. Increased expiratory computed tomography density reveals possible abnormalities in radiologically preserved lung parenchyma in idiopathic pulmonary fibrosis. *Invest Radiol* 2018;53:45–51.
4. Mai C, Verleden SE, McDonough JE, Willems S, De Wever W, Coolen J, *et al*. Thin-section CT features of idiopathic pulmonary fibrosis correlated with micro-CT and histologic analysis. *Radiology* 2017;283: 252–263.
5. García-Sancho C, Buendía-Roldán I, Fernández-Plata MR, Navarro C, Pérez-Padilla R, Vargas MH, *et al*. Familial pulmonary fibrosis is the strongest risk factor for idiopathic pulmonary fibrosis. *Respir Med* 2011;105:1902–1907.
6. Hodgson U, Laitinen T, Tukiainen P. Nationwide prevalence of sporadic and familial idiopathic pulmonary fibrosis: evidence of founder effect among multiplex families in Finland. *Thorax* 2002;57:338–342.
7. Sallese A, Suzuki T, McCarthy C, Bridges J, Filuta A, Arumugam P, *et al*. Targeting cholesterol homeostasis in lung diseases. *Sci Rep* 2017;7: 10211.
8. Marshall RP, Puddicombe A, Cookson WO, Laurent GJ. Adult familial cryptogenic fibrosing alveolitis in the United Kingdom. *Thorax* 2000; 55:143–146.
9. Allen RJ, Porte J, Braybrooke R, Flores C, Fingerlin TE, Oldham JM, *et al*. Genetic variants associated with susceptibility to idiopathic pulmonary fibrosis in people of European ancestry: a genome-wide association study. *Lancet Respir Med* 2017;5:869–880.
10. Fingerlin TE, Murphy E, Zhang W, Peljto AL, Brown KK, Steele MP, *et al*. Genome-wide association study identifies multiple susceptibility loci for pulmonary fibrosis. *Nat Genet* 2013;45: 613–620. [Published erratum appears in *Nat Genet* 45:1409.]
11. Armanios M. Telomerase and idiopathic pulmonary fibrosis. *Mutat Res* 2012;730:52–58.
12. Kropski JA, Blackwell TS. Progress in understanding and treating idiopathic pulmonary fibrosis. *Annu Rev Med* 2019;70:211–224.
13. Manolio TA, Collins FS, Cox NJ, Goldstein DB, Hindorff LA, Hunter DJ, *et al*. Finding the missing heritability of complex diseases. *Nature* 2009;461:747–753.
14. Borie R, Kannengiesser C, Nathan N, Tabèze L, Pradère P, Crestani B. Familial pulmonary fibrosis. *Rev Mal Respir* 2015;32:413–434.
15. McCarthy MI, Abecasis GR, Cardon LR, Goldstein DB, Little J, Ioannidis JPA, *et al*. Genome-wide association studies for complex traits: consensus, uncertainty and challenges. *Nat Rev Genet* 2008;9:356–369.
16. van Moorsel CHM, van Oosterhout MFM, Barlo NP, de Jong PA, van der Vis JJ, Ruven HJT, *et al*. Surfactant protein C mutations are the basis of a significant portion of adult familial pulmonary fibrosis in a Dutch cohort. *Am J Respir Crit Care Med* 2010;182:1419–1425.
17. Schürch D, Ospina OL, Cruz A, Pérez-Gil J. Combined and independent action of proteins SP-B and SP-C in the surface behavior and mechanical stability of pulmonary surfactant films. *Biophys J* 2010;99:3290–3299.
18. Han S, Mallampalli RK. The role of surfactant in lung disease and host defense against pulmonary infections. *Ann Am Thorac Soc* 2015;12: 765–774.
19. Glasser SW, Burhans MS, Korfhagen TR, Na C-L, Sly PD, Ross GF, *et al*. Altered stability of pulmonary surfactant in SP-C–deficient mice. *Proc Natl Acad Sci USA* 2001;98:6366–6371.
20. Gómez-Gil L, Schürch D, Goormaghtigh E, Pérez-Gil J. Pulmonary surfactant protein SP-C counteracts the deleterious effects of cholesterol on the activity of surfactant films under physiologically relevant compression-expansion dynamics. *Biophys J* 2009;97: 2736–2745.
21. Pérez-Gil J. Structure of pulmonary surfactant membranes and films: the role of proteins and lipid–protein interactions. *Biochim Biophys Acta* 2008;1778:1676–1695.
22. Whitsett JA, Wert SE, Weaver TE. Diseases of pulmonary surfactant homeostasis. *Annu Rev Pathol* 2015;10:371–393.
23. Mulugeta S, Nureki S, Beers MF. Lost after translation: insights from pulmonary surfactant for understanding the role of alveolar epithelial dysfunction and cellular quality control in fibrotic lung disease. *Am J Physiol Lung Cell Mol Physiol* 2015;309:L507–L525.
24. Kurland G, Deterding RR, Hagood JS, Young LR, Brody AS, Castile RG, *et al*.; American Thoracic Society Committee on Childhood Interstitial Lung Disease (chILD) and the chILD Research Network. An official American Thoracic Society clinical practice guideline: classification, evaluation, and management of childhood interstitial lung disease in infancy. *Am J Respir Crit Care Med* 2013;188:376–394.
25. Phelps DS, Floros J. Localization of pulmonary surfactant proteins using immunohistochemistry and tissue *in situ* hybridization. *Exp Lung Res* 1991;17:985–995.
26. Orgeig S, Bernhard W, Biswas SC, Daniels CB, Hall SB, Hetz SK, *et al*. The anatomy, physics, and physiology of gas exchange surfaces: is there a universal function for pulmonary surfactant in animal respiratory structures? *Integr Comp Biol* 2007;47:610–627.
27. Kipen HM, Lilis R, Suzuki Y, Valciukas JA, Selikoff IJ. Pulmonary fibrosis in asbestos insulation workers with lung cancer: a radiological and histopathological evaluation. *Br J Ind Med* 1987;44: 96–100.
28. Yoshida T, Tuder RM. Pathobiology of cigarette smoke-induced chronic obstructive pulmonary disease. *Physiol Rev* 2007;87: 1047–1082.
29. Cohen RAC, Patel A, Green FHY. Lung disease caused by exposure to coal mine and silica dust. *Semin Respir Crit Care Med* 2008;29: 651–661.
30. Knudsen L, Ochs M. The micromechanics of lung alveoli: structure and function of surfactant and tissue components. *Histochem Cell Biol* 2018;150:661–676.
31. Mead J, Takishima T, Leith D. Stress distribution in lungs: a model of pulmonary elasticity. *J Appl Physiol* 1970;28:596–608.
32. Lopez-Rodriguez E, Boden C, Echaide M, Perez-Gil J, Kolb M, Gauldie J, *et al*. Surfactant dysfunction during overexpression of TGF-β1 precedes profibrotic lung remodeling *in vivo*. *Am J Physiol Lung Cell Mol Physiol* 2016;310:L1260–L1271.
33. Chilosi M, Carloni A, Rossi A, Poletti V. Premature lung aging and cellular senescence in the pathogenesis of idiopathic pulmonary fibrosis and COPD/emphysema. *Transl Res* 2013;162:156–173.
34. Brandenberger C, Mühlfeld C. Mechanisms of lung aging. *Cell Tissue Res* 2017;367:469–480.
35. Janssens JP, Pache JC, Nicod LP. Physiological changes in respiratory function associated with ageing. *Eur Respir J* 1999;13:197–205.
36. Romero F, Hong X, Shah D, Kallen CB, Rosas I, Guo Z, *et al*. Lipid synthesis is required to resolve endoplasmic reticulum stress and limit fibrotic responses in the lung. *Am J Respir Cell Mol Biol* 2018;59:225–236.
37. Romero F, Shah D, Duong M, Penn RB, Fessler MB, Madenspacher J, *et al*. A pneumocyte-macrophage paracrine lipid axis drives the lung toward fibrosis. *Am J Respir Cell Mol Biol* 2015;53:74–86.
38. Lopez-Rodriguez E, Gay-Jordi G, Mucci A, Lachmann N, Serrano-Mollar A. Lung surfactant metabolism: early in life, early in disease and target in cell therapy. *Cell Tissue Res* 2017;367:721–735.
39. Chu SG, Villalba JA, Liang X, Xiong K, Tsoyi K, Ith B, *et al*. Palmitic acid-rich high-fat diet exacerbates experimental pulmonary fibrosis by modulating endoplasmic reticulum stress. *Am J Respir Cell Mol Biol* 2019;61:737–746.
40. Glasser SW, Detmer EA, Ikegami M, Na C-L, Stahlman MT, Whitsett JA. Pneumonitis and emphysema in sp-C gene targeted mice. *J Biol Chem* 2003;278:14291–14298.
41. Beike L, Wrede C, Hegermann J, Lopez-Rodriguez E, Kloth C, Gauldie J, *et al*. Surfactant dysfunction and alveolar collapse are linked with fibrotic septal wall remodeling in the TGF-β1–induced mouse model of pulmonary fibrosis. *Lab Invest* 2019;99:830–852.
42. Ochs M, Mühlfeld C. Quantitative microscopy of the lung: a problem-based approach. Part 1: basic principles of lung stereology. *Am J Physiol Lung Cell Mol Physiol* 2013;305:L15–L22.

43. Mühlfeld C, Ochs M. Quantitative microscopy of the lung: a problem-based approach. Part 2: stereological parameters and study designs in various diseases of the respiratory tract. *Am J Physiol Lung Cell Mol Physiol* 2013;305:L205–L221.
44. Reddy GK, Enwemeka CS. A simplified method for the analysis of hydroxyproline in biological tissues. *Clin Biochem* 1996;29:225–229.
45. Roldan N, Pérez-Gil J, Morrow MR, García-Álvarez B. Divide & conquer: surfactant protein SP-C and cholesterol modulate phase segregation in lung surfactant. *Biophys J* 2017;113:847–859.
46. Bridges JP, Wert SE, Nogee LM, Weaver TE. Expression of a human surfactant protein C mutation associated with interstitial lung disease disrupts lung development in transgenic mice. *J Biol Chem* 2003; 278:52739–52746.
47. Nureki S-I, Tomer Y, Venosa A, Katzen J, Russo SJ, Jamil S, *et al*. Expression of mutant Sftpc in murine alveolar epithelia drives spontaneous lung fibrosis. *J Clin Invest* 2018;128:4008–4024.
48. Ito S, Ingenito EP, Brewer KK, Black LD, Parameswaran H, Lutchen KR, *et al*. Mechanics, nonlinearity, and failure strength of lung tissue in a mouse model of emphysema: possible role of collagen remodeling. *J Appl Physiol (1985)* 2005;98:503–511.
49. Lundblad LK, Thompson-Figueroa J, Leclair T, Sullivan MJ, Poynter ME, Irvin CG, *et al*. Tumor necrosis factor-alpha overexpression in lung disease: a single cause behind a complex phenotype. *Am J Respir Crit Care Med* 2005;171:1363–1370.
50. Bates JHT, Davis GS, Majumdar A, Butnor KJ, Suki B. Linking parenchymal disease progression to changes in lung mechanical function by percolation. *Am J Respir Crit Care Med* 2007;176: 617–623.
51. Suki B, Bates JHT. Lung tissue mechanics as an emergent phenomenon. *J Appl Physiol (1985)* 2011;110:1111–1118.
52. Gregory AD, Kliment CR, Metz HE, Kim K-H, Kargl J, Agostini BA, *et al*. Neutrophil elastase promotes myofibroblast differentiation in lung fibrosis. *J Leukoc Biol* 2015;98:143–152.
53. Gieseck RL III, Wilson MS, Wynn TA. Type 2 immunity in tissue repair and fibrosis. *Nat Rev Immunol* 2018;18:62–76.
54. Katzen J, Wagner BD, Venosa A, Kopp M, Tomer Y, Russo SJ, *et al*. An SFTPC BRICHOS mutant links epithelial ER stress and spontaneous lung fibrosis. *JCI Insight* 2019;4:126125.
55. Allen JN, Davis WB. Eosinophilic lung diseases. *Am J Respir Crit Care Med* 1994;150:1423–1438.
56. Gilmore LB, Talley FA, Hook GE. Classification and morphometric quantitation of insoluble materials from the lungs of patients with alveolar proteinosis. *Am J Pathol* 1988;133:252–264.
57. Klinkner AM, Waites CR, Kerns WD, Bugelski PJ. Evidence of foam cell and cholesterol crystal formation in macrophages incubated with oxidized LDL by fluorescence and electron microscopy. *J Histochem Cytochem* 1995;43:1071–1078.
58. Tangirala RK, Jerome WG, Jones NL, Small DM, Johnson WJ, Glick JM, *et al*. Formation of cholesterol monohydrate crystals in macrophage-derived foam cells. *J Lipid Res* 1994;35:93–104.
59. de Aguiar Vallim TQ, Lee E, Merriott DJ, Goulbourne CN, Cheng J, Cheng A, *et al*. ABCG1 regulates pulmonary surfactant metabolism in mice and men. *J Lipid Res* 2017;58:941–954.
60. Jolley CD, Dietschy JM, Turley SD. Genetic differences in cholesterol absorption in 129/Sv and C57BL/6 mice: effect on cholesterol responsiveness. *Am J Physiol* 1999;276:G1117–G1124.
61. Gowdy KM, Fessler MB. Emerging roles for cholesterol and lipoproteins in lung disease. *Pulm Pharmacol Ther* 2013;26:430–437.
62. Samokhin AO, Bühling F, Theissig F, Brömme D. ApoE-deficient mice on cholate-containing high-fat diet reveal a pathology similar to lung sarcoidosis. *Am J Pathol* 2010;176:1148–1156.
63. Kim TH, Lee YH, Kim KH, Lee SH, Cha JY, Shin EK, *et al*. Role of lung apolipoprotein A-I in idiopathic pulmonary fibrosis: antiinflammatory and antifibrotic effect on experimental lung injury and fibrosis. *Am J Respir Crit Care Med* 2010;182:633–642.
64. Yao X, Gordon EM, Figueroa DM, Barochia AV, Levine SJ. Emerging roles of apolipoprotein E and apolipoprotein A-I in the pathogenesis and treatment of lung disease. *Am J Respir Cell Mol Biol* 2016;55: 159–169.
65. Fessler MB. A new frontier in immunometabolism: cholesterol in lung health and disease. *Ann Am Thorac Soc* 2017;14:S399–S405.
66. Kreuter M, Bonella F, Maher TM, Costabel U, Spagnolo P, Weycker D, *et al*. Effect of statins on disease-related outcomes in patients with idiopathic pulmonary fibrosis. *Thorax* 2017;72:148–153.
67. Kreuter M, Ehlers-Tenenbaum S, Palmowski K, Bruhwyler J, Oltmanns U, Muley T, *et al*. Impact of comorbidities on mortality in patients with idiopathic pulmonary fibrosis. *PLoS One* 2016;11:e0151425.
68. Kreuter M, Costabel U, Richeldi L, Cottin V, Wijsenbeek M, Bonella F, *et al*. Statin therapy and outcomes in trials of nintedanib in idiopathic pulmonary fibrosis. *Respiration* 2018;95:317–326.

Cite: Ruwisch J., Sehlmeyer K., Roldan N., Garcia-Alvarez B., Perez-Gil J., Weaver T.E., Ochs M., Knudsen L. & **Lopez-Rodriguez E**. *Air Space Distension Precedes Spontaneous Fibrotic Remodeling and Impaired Cholesterol Metabolism in the Absence of Surfactant Protein C.* American Journal of Respiratory Cell and Molecular Biology, 2020; 62(4): 466-478.
The American Journal of Respiratory Cell and Molecular Biology is an official journal of the American Thoracic Society.

RELEVANCE OF THIS WORK

In this paper, we concluded that the absence of SP-C in mice lungs leads to an early alveolar collapse followed by over-distension of ductal and alveolar spaces. The permanent de-recruitment of alveoli or collapse induration, together with the air re-organization into over distended ductal spaces may impose an aberrant mechanical stress into the lung tissue leading to the formation of fibrotic wounds at an age of approximate 50 weeks. The mouse model presented here represents a spontaneous model of fibrotic development, relevant to the human disease, as SP-C mutations and dysregulation has already been observed in patients with familial forms of IPF. In fact, the changes that we observed here may also represent an adaptive mechanism of the lung to compensate for malfunction. In comparison to other traditional induced animal models, where the disease development is faster and more acute, the presented animal model may represent a more relevant and more similar situation to the human disease, whose onset is around at an age of 65 years.

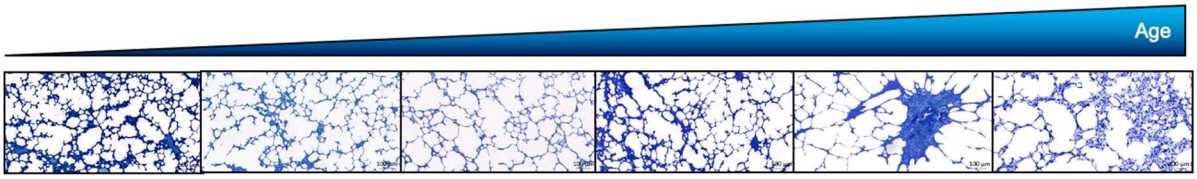

Figure 3: representative micrographs of the changes in alveolar parenchyma in SP-C deficient mice from 10 to 60 weeks of age. Modified from Ruwisch et al., 2020 (reprinted with permission of the American Thoracic Society).

Alveolar macrophages showed an interesting morphology with crystal accumulation in their cytoplasm. Even though this event has already been described in human samples and numerous animal models (91-93), there is a lack of further investigation and description on which molecular mechanisms may lead to this notable morphology. In this work, we could not characterize the molecular origin of those crystals, but morphologically they are very similar to cholesterol crystals and for that reason, we further investigated the cholesterol metabolism in BAL cells. Very interestingly, cholesterol metabolism was impaired in cells of mice deficient in SP-C and in vitro experiments demonstrated that SP-C increased the expression of important metabolic enzymes and transporters of cholesterol.

2.3 ALVEOLAR MACROPHAGES (ORIGINAL WORK 3)

Kloth C., Gruben N., Ochs M., Knudsen L. & **Lopez-Rodriguez E**. "*Flow cytometric analysis of the leukocyte landscape during bleomycin-induced lung injury and fibrosis in the rat*" American Journal of Physiology - Lung Cell and Molecular Physiology, 2019; 317(1): L109-L126.

As explained in the previous chapter, alveolar macrophages show many interesting changes during the development of lung fibrosis. This has been recently the focus of many reports, where the importance of these cells in alveolar homeostasis and disease (32, 94-98) are highlighted. However, the lung specific immune system is very complex and comprises multiple cells, cytokines and other signaling molecules.

The lung surface is under constant challenge to the environmental air components, especially airborne pathogens. For this purpose, the lung requires a fine-tuned and rapidly acting specific pulmonary immune system that recognizes and protects the gas exchange functional units, the alveoli (99-101). Resident and recruited cells and secreted innate immune proteins (such as mucins or collectins (SP-A and SP-D)) interplay in order to orchestrate host-pathogen (or particle) interactions (102). Epithelial cells (including AE2C), dendritic cells and alveolar macrophages (AM) are the sentinel system checking constantly for inhaled strange particles or microorganisms. They are also responsible to trigger the pro- or anti-inflammatory response as well as the recruitment of further immune cells. This process depends on chemo attractants, such as lipid mediators (prototypically eicosanoids/leukotrienes), complement factors, and chemokines (103-106). Some of the most important chemokines for the recruitment of leukocytes in the airway are the CXC family of chemokines, more specifically, CXCL1-8 and CXCL12, CCL2, CCL17 and CCL18. At the same time, the influence of these chemokines is dependent on the local immune status and the presence of different cytokines, such as IL-1α and IL-1β, IL-10, IL-17, IL-23, IL-25 and IL-33. Then, different immune cell populations are sequentially recruited into the alveolar space or parenchyma compartments. It has been well described (102), that after an acute inflammatory reaction, neutrophils are the first cells reaching the alveolar space and quickly engage in the activation of the immune response (107). For a more sustained/chronic immune system action, monocytes and lymphocytes come then into play.

In addition, lymphocytes may be organized in tertiary lymphoid organs within the lung tissue, called bronchus-associated lymphoid tissue (BALT) (108). Recent reports also highlight novel immune cells and signaling molecules, such as innate lymphoid cells (ILC), mucosal-associated invariant T cells (MAIT), chitinase-like proteins (CLP), and others (102) in the lung.

Alveolar macrophages play a central role in immunity, but also in tissue repair (34) and lung surfactant metabolism (109). These highly plastic cells respond rapidly to changes in their environment and molecular mediators, resulting in their differentiation into a classically (M1) or and alternatively (M2) activated phenotype (35, 110, 111). Classically activated macrophages produce pro-inflammatory cytokines (such as TNFα, IL-1, and IL-6) as response to LPS and IFNγ. In this way, these cells maintain tissue inflammation (112). On the other hand, alternatively activated macrophages produce pro-fibrotic and anti-inflammatory cytokines in response to their exposure to IL-4, IL-10, and IL-13. When the initial inflammation is not resolved but becomes chronic, the pro-inflammatory macrophages convert to a more anti-inflammatory (pro-fibrotic) phenotype, secreting mediators that promote wound healing (34). Therefore, anti-inflammatory/pro-fibrotic macrophages are often found in fibrotic wounds (35, 111). These macrophages secrete several growth factors, including TGF-β, platelet-derived growth factor-α (PDGF-α), fibroblast growth factor (FGF), vascular endothelial growth factor (VEGF), and insulin-like growth factor 1 (IGF1). In this way, pro-fibrotic macrophages contribute to the production and accumulation of extracellular matrix components, specifically to collagen synthesis through up-regulation of the L-arginine metabolism (112).

The bleomycin-induced lung injury and fibrosis in rodents is one of the most widely used animal models for the study of fibrotic development (113, 114). We have also described that surfactant dysfunction in this model in rats is an early event (115). While the fate of alveolar macrophages has been deeply studied in the mouse model, this was not shown in the rat model. As the rat model is often used to investigate potential therapeutic strategies, to complete this piece of knowledge is at this point of high relevance.

The aim of this work was to investigate the changes in the myeloid population in alveoli during the onset and progression of lung injury and fibrosis. For this purpose, we used the widely used animal model of bleomycin induced lung injury and fibrosis and analyzed the changes in the myeloid fraction of cells isolated in BAL every 3-4 days up to 21 days after bleomycin application. In this way, we could observe the changes in terms of recruitment of cells and activation and gene expression of different macrophage populations early in disease and before and during the onset of the fibrotic remodeling. We hypothesized that: 1) as shown previously in mice, bleomycin induces an early inflammatory response characterize by neutrophil recruitment and apoptosis of alveolar macrophages; 2) this is followed by monocyte recruitment and activation of macrophages to an anti-inflammatory phenotype; 3) monocytes are differentiated to mature macrophages, which are partly differentiated to pro-fibrotic phenotype in rats.

Am J Physiol Lung Cell Mol Physiol 317: L109–L126, 2019.
First published May 1, 2019; doi:10.1152/ajplung.00176.2018.

RESEARCH ARTICLE

Flow cytometric analysis of the leukocyte landscape during bleomycin-induced lung injury and fibrosis in the rat

Christina Kloth,[1,2,3,4] Nele Gruben,[1,2,3] Matthias Ochs,[1,2,3,5] Lars Knudsen,[1,2,3] and Elena Lopez-Rodriguez[1,2,3,5]

[1]*Institute of Functional and Applied Anatomy, Hannover Medical School, Hannover, Germany;* [2]*Biomedical Research in Endstage and Obstructive Lung Disease Hannover (BREATH), Member of the German Centre for Lung Research (DZL), Hannover, Germany;* [3]*Cluster of excellence REBIRTH (From Regenerative Biology to Reconstructive Therapy), Hannover, Germany;* [4]*Institute of Experimental Haematology, Hannover Medical School, Hannover, Germany; and* [5]*Institute of Vegetative Anatomy, Charité - Universitaetsmedizin Berlin, Berlin, Germany*

Submitted 12 April 2018; accepted in final form 28 April 2019

Kloth C, Gruben N, Ochs M, Knudsen L, Lopez-Rodriguez E. Flow cytometric analysis of the leukocyte landscape during bleomycin-induced lung injury and fibrosis in the rat. *Am J Physiol Lung Cell Mol Physiol* 317: L109–L126, 2019. First published May 1, 2019; doi:10.1152/ajplung.00176.2018.—Bleomycin-induced lung injury and fibrosis is a well-described model to investigate lung inflammatory and remodeling mechanisms. Rat models are clinically relevant and are also widely used, but rat bronchoalveolar lavage (BAL) cells are not fully characterized with flow cytometry due to the limited availability of antibodies for this species. We optimized a comprehensive time-dependent flow cytometric analysis of cells after bleomycin challenge, confirming previous studies in other species and correlating them to histological staining, cytokine profiling, and collagen accumulation analysis in rat lungs. For this purpose, we describe a novel panel of rat surface markers and a strategy to identify and follow BAL cells over time. By combining surface markers in rat alveolar cells ($CD45^+$), granulocytes and other myeloid cells, monocytes and macrophages can be identified by the expression of CD11b/c. Moreover, different activation states of macrophages ($CD163^+$) can be observed: steady state ($CD86^-$MHC-II^{low}), activation during inflammation ($CD86^+$,MHC-II^{high}), activation during remodeling ($CD86^+$MHC-II^{low}), and a population of newly recruited monocytes ($CD163^-\alpha$-$granulocyte^-$). Hydroxyproline measured as marker of collagen content in lung tissue showed positive correlation with the reparative phase ($CD163^-$ cells and tissue inhibitor of metalloproteinases (TIMP) and IL-10 increase). In conclusion, after a very early granulocytic recruitment, inflammation in rat lungs is observed by activated macrophages, and high release of IL-6 and fibrotic remodeling is characterized by recovery of the macrophage population together with TIMP, IL-10, and IL-18 production. Recruited monocytes and a second peak of granulocytes appear in the transitioning phase, correlating with immunostaining of arginase-1 in the tissue, revealing the importance of events leading the changes from injury to aberrant repair.

flow cytometry analysis; lung fibrosis in rats; macrophage activation; rat bronchoalveolar lavage

INTRODUCTION

Interest in the function of immune cells in the alveolar region of the lung, and specifically of alveolar macrophages during development of lung disease, is increasing exponentially nowadays (5, 38, 41). Besides the amount of data generated every year describing and characterizing the different subsets of cells involved in lung injury and repair, most of the studies focus on human (7, 51, 56, 59) or mouse material (40, 43, 45). Time-dependent studies regarding these cells during disease are difficult to perform in human material, and therefore the use of animal models comes into play. However, within animal models, rats have the size advantage in providing enough sample for correlative studies and are necessary to validate findings in mouse models (25) but are poorly studied in this regard. Although for different mouse models of lung injury and fibrosis a complete characterization and description of the cell subsets of interest by flow cytometry (FACS) can be easily found, the limited number of studies in rat models makes evident the lack of information and methodological limitations of this tool for this species. To date, no complete characterization of myeloid cells by means of flow cytometry exists for rat bronchoalveolar lavage (BAL) cells in the lung of the bleomycin-challenged model. Bleomycin-challenged lungs show an early phase of acute lung injury characterized by a neutrophilic inflammatory response followed by a phase of tissue remodeling, with a shift between them around day 9 (24, 37). Therefore, this model has been widely used to better understand the pathophysiological mechanisms and functional changes during inflammation and tissue remodeling (42), and it is also in use for testing different therapeutic approaches (10, 53, 57, 68, 71, 75). Misharin et al. (40) published a complete set of molecular markers to identify by flow cytometric analysis the changes and activation states of macrophages and dendritic cells in the lung after bleomycin challenge in mice. However, translation of this panel of mouse molecular markers to the rat model is limited due to the lack of known molecular markers in this species and the limited availability of commercially standardized antibodies for this subset of cells. On the one hand, a first approach on Fischer F344 rats was done by Garn et al. (16), who characterized alveolar macrophage subpopulations after NO_2 exposure mimicking chronic obstructive pulmonary disease *(COPD)* remodeling in the lung. They used flow cytom-

Address for reprint requests and other correspondence: E. Lopez-Rodriguez, Inst. of Functional and Applied Anatomy, Hannover Medical School, Carl-Neuberg-Str. 1, D-30625 Hannover, Germany (e-mail: lopez-rodriguez.elena@mh-hannover.de).

etry with nonconjugated antibodies, together with RT-PCR and cytokine quantitation. On the other hand, Venosa et al. (73) showed the characterization of alveolar macrophage subpopulations during nitrogen mustard-induced lung injury and fibrosis in rats. In this approach, they combined techniques such as RT-PCR after cell sorting and immunohistochemical analysis of lung sections. Therefore, we aim here to describe a panel of rat cellular markers to identify, during a time course of 21 days after bleomycin challenge, the different cell populations in BAL by flow cytometry and validate the model with different molecular markers to correlate the results with previously generated data on mice and humans. This tool allows fast analysis of different populations and activation states of the cells at the alveolar spaces, using membrane molecular markers, which also allows sorting of living cells, and a deeper understanding of the changes related to disease through time. We have selected commercially standardized antibodies, which can be used by others. In addition, to correlate our findings with the current knowledge on rat bleomycin-induced lung injury and fibrosis, we performed standard histological staining, cytokine profiling, and hydroxyproline quantification, proving the usefulness of our cytometric analysis in this model. For the first time, we have confirmed previous results, performed in mice and humans, regarding the activation of alveolar macrophages and recruitment of monocytes into the rat lung (7, 40, 43, 45, 51, 56, 59), providing a novel view of the rat as useful animal model in the study of lung injury and fibrosis.

MATERIALS AND METHODS

Rats. Sixty-five male Fischer F344 rats (10 wk old, 200–220 g, $n = 8$ per group) were obtained from Charles River Laboratories (Sulzfeld, Germany) and maintained in the animal facility of Hannover Medical School at 21 ± 2°C, 50% ± 5% humidity, and a 14-h:10-h light-dark cycle. They were supplied with autoclaved, acidulated water and fed ad libitum a standard diet. All animal procedures were approved by the Lower Saxony State Office for Consumer Protection and Food Safety (LAVES, 16/2126) and were carried out according to the guidelines of the German Regulations for Animal Protection.

Bleomycin-induced lung injury and fibrosis. Prior to instillation, rats were shortly anesthetized (4% isoflurane in a Plexiglas chamber), intubated orally, and instilled through the catheter with 4.5 U/kg bleomycin (Bleomedac, Wedel, Germany) dissolved in 0.9% NaCl. Samples were acquired before (*day 0*) and 2, 5, 7, 9, 12, 14, and 21 days after the instillation of bleomycin, $n = 8$ animals per experimental group. Animals exceeding the stress scoring (following the stress criteria of EU Directive 2010/63/EU) were excluded from the analysis and accounted for 10% of the total number of animals. Bronchoalveolar lavage (BAL) was performed using 3 × 4 ml PBS into the right lung. Individual lung lobes were isolated. The right lung was weighed and used for hydroxyproline assay, while the left lung was filled with PBS-octreotide (OCT; 1:1) and immediately frozen for cryosectioning and histological analysis. A second set of animals were used to perform BAL on the right lung and prepare single-cell suspensions after tissue digestion (collagenase type II), following the protocol described by Vanlandewijck et al. (71). The left lung was processed as explained before.

Isolation of mononuclear cells from blood. We used a density barrier with OptiPrep (StemCell Technologies, Vancouver, BC, Canada) to layer an enriched fraction of mononuclear rat cells from rat blood in a 1.077 g/ml density barrier. We collected blood by cardiac puncture into a syringe containing anticoagulant (EDTA) and diluted it with an equal volume of 50 mM Tricine and 0.9% NaCl. The gradient was created following the manufacturer's instructions and centrifuged at 700 *g* for 20 min at 20°C in a swinging-bucket rotor. After centrifugation, mononuclear cells form a sharp band between the plasma layer and the OptiPrep solution. A cytospot was differentially stained to determine the purity of the isolation, finding mostly lymphocytes and monocytes (Fig. 1*B*).

Flow cytometry analysis. BAL cells were pelleted at 300 *g*, and the remaining red blood cells were lysed. Viability of the cells in the BAL samples was measured with trypan blue, and cell numbers were obtained in an Automated Cell Counter (Bio-Rad Laboratories, Munich, Germany). BAL samples with a minimum of 80% viability were further processed for FACS analysis, and live/dead exclusion was performed by size in the first step of the gating strategy. BAL cells were used for flow cytometric analysis (FACS) using a MACSQuant Analyzer (Miltenyi Biotec, Bergisch Gladbach, Germany). Cells were incubated with FcBlock (Miltenyi Biotec), and stained with a mixture of fluorochrome-conjugated antibodies (table for a list of antibodies, clones, fluorochromes, and manufacturers is included in Table 1). Two parallel stainings were performed for identifying either the activation state of macrophages or the different recruited cells. For the activation state, BAL cells were incubated with cluster of differentiation 45 (CD45)-PE, CD11b/c-APC-Vio770, CD163-FITC, MHC-II-VioBlue, and CD86-APC antibodies; for identifying the recruited cells, BAL cells, we incubated with CD45-PE, CD11b/c-APC-Vio770, CD163-FITC, and α-granulocyte-APC antibodies. Data were acquired using MACSQuantify Software (Miltenyi Biotec). Specific cell populations were identified using a sequential gating strategy, and the percentage of cells in the living/singlets gate was multiplied by the number of live cells per lung to obtain an absolute live-cell count. Expression of activation markers is presented as mean fluorescence intensity (MFI). Antibodies included in Table 2 were tested in FACS or immunofluorescence but did not contribute to reliable results confirming the final analysis presented here. Single-cell suspensions were stained following the same protocol as with the first panel of antibodies.

After surface membrane labeling, as stated before, CD68 staining was performed after fixation and permeabilization of the cells. Briefly, cells were fixed with 4% paraformaldehyde in PBS at room temperature for 15 min. After a wash with PBS + 2% FBS, cells were permeabilized with 0.1% saponin in PBS + 10% FBS at room temperature for 15 min. Incubation with CD68 antibody was performed in the same saponin buffer for 30 min. Cells were washed three times before FACS analysis.

Apoptosis of CD163$^+$ cells. BAL cells were either analyzed directly after isolation from diseased animals at *day 1, 2*,or *3* after bleomycin challenge, or from healthy animals and plated with complete medium and different concentrations of bleomycin in triplicates and later pooled down into one experimental sample (Bleomedac). Cells were stained with annexin V-APC in Ca^{2+}-containing binding buffer (MabTag, Friesoythe, Germany), following the manufacturer's instructions, for 20 min, at 4°C, in the dark. Right before analysis of the cells in the flow cytometer, 10 μl of propidium iodide (PI; Miltenyi Biotec) were added to the cells. Cells CD163$^+$ and double-positive for annexin-V and PI were quantified as apoptotic cells.

Phagocytosis of CD163$^+$ cells. BAL cells were plated with Complete medium overnight. On the day of the assay, cells were incubated with pHrodo Red *E. coli* Bioparticles (Molecular Probes, Eugene, OR) for 3 h with Complete medium at 37°C in 5% CO_2, following the manufacturer's instructions. After a washing in the medium, cells were resuspended in MACS buffer for analysis by flow cytometry.

Cell sorting for differential staining and gene expression analysis. BAL cells were processed and stained using the same protocol as for flow cytometry. Sorting was performed in the Core Facility Cell Sorting (Hannover Medical School, Hannover, Germany) with a FACSAria (Becton-Dickinson, East Rutherford, NJ). The different cell populations were sorted, following the same gating strategy, combining the antibodies CD45-PE, CD11b/c-

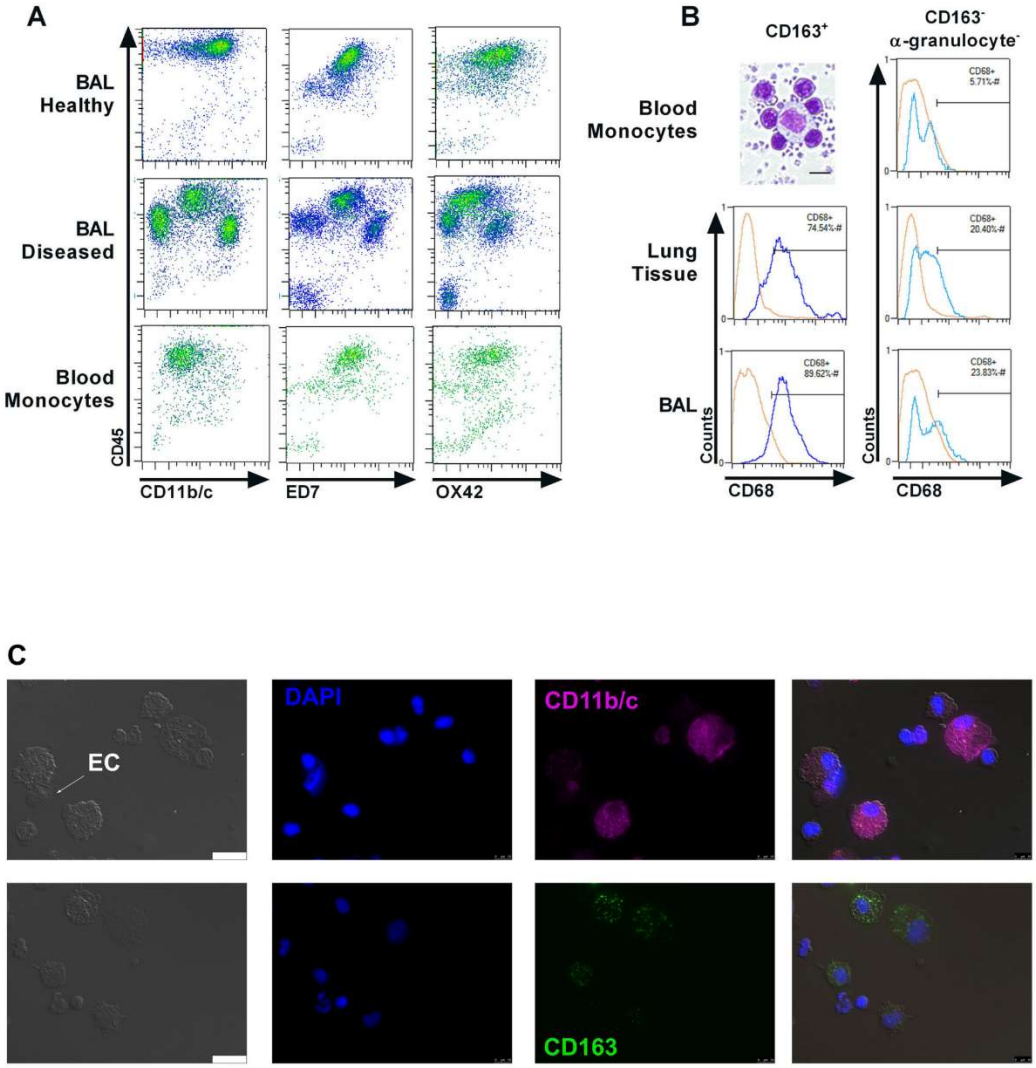

Fig. 1. Development of a complete immune cell panel in rat lung. *A*: representative density plots of bronchoalveolar lavage (BAL) from healthy or diseased animals as well as blood monocytes stained with CD45 and different CD11b/c antibodies (CD11b/c and clones ED7 and OX42). *B*: cytospot of isolated blood monocytes (and lymphocytes) after differential staining and staining of macrophages (CD11b/c$^+$, CD45$^+$, CD163$^+$) or monocytes (CD11b/c$^+$, CD45$^+$, CD163$^-$, α-granulocyte$^-$) with intracellular panmacrophage marker CD68 in BAL, lung tissue, and blood monocyte samples. *C*: representative fluorescence immune staining of BAL cells, showing positive ciliated epithelial cells (EC, arrow) in pink (*top*) and staining of macrophage-like cells with CD163 in green (*bottom*). Scale bar, 20 μm.

APC-Vio770, CD163-FITC, MHC-II-VioBlue, and α-granulocyte-APC, spun down into slides, and differentially stained using the Diff-Quick kit (Medion Diagnostics, Miami, FL) following the manufacturer's instructions. Cells for RNA isolation and gene expression were isolated, using the same panel of antibodies, during the days after bleomycin challenge when they peaked as follow: *1*) resident alveolar macrophages (AM) were gated as CD45$^+$, CD11b/c$^+$, CD163$^+$, and MHC-II^{low} at *day 0*; *2*) activated macrophages (aAM) as CD45$^+$, CD11b/c$^+$, CD163$^+$, and MHC-II^{high} at *day 9*; *3*) monocytes (Mo) as CD45$^+$, CD11b/c$^+$, CD163$^-$, and α-granulocyte$^-$ at *day 9*; and *4*) granulocytes (G) as CD45$^+$, CD11b/c$^+$, CD163$^-$, and α-granulocyte$^+$ at *day 2*.

Histological stainings. During the BAL procedure, the left lung was temporarily closed and then reopened for instillation of PBS-OCT (1:1) and permanently closed. The isolated left lung was then immediately frozen for later cryosectioning.

Masson-Goldner trichromic staining (Merck Millipore, Darmstadt, Germany) and hematoxylin-eosin (H&E; eosin Y-solution, 0.5% alcoholic, and hematoxylin solution, modified according to To Gill III, both Merck Millipore) staining were performed following the manufacturer's instructions. Stained slides were scanned in the AxioScan.Z1 (Zeiss, Jena, Germany) at ×20 magnification, and areas of interest were processed to images with the corresponding software (Zeiss lite 2012, Zeiss).

Table 1. *Membrane cell markers and antibodies used in rat bronchoalveolar lavage*

Marker	Conjugate	Source	Clone	Lymphocyte	Alveolar Macrophage	activated Macrophage	Granulocyte	Monocyte	Concentration, μg/ml
CD45	PE/VioBright-FITC	Miltenyi	REA504	+	+	+	+	+	0.15
CD11c/b	APC-Vio770	Miltenyi	REA325	−	+	++	+	+	0.3
MHC-II	FITC/VioBlue	Miltenyi	I-Ek	−	Low	High	−	−	0.3
CD86	APC	Miltenyi	24F	−	−	++	−	−	0.3
α-Granulocyte	APC	Miltenyi	REA535	−		−	+	−	0.3
CD163	FITC	Bio-Rad	ED2	−	+	+	−	−	1
CD3	VioBlue	Miltenyi	REA223	+	−	−	−	−	0.3
CD4	PerCP-Vio700	Miltenyi	REA489	+	+	+	−	+	0.3
CD68	APC	Miltenyi	REA237	−	+	+	−	−	0.3
CD90.1	APC	Miltenyi	His51	−	−	−	−	−	0.3

Arginase-1 immunostaining was performed using the anti-arginase-I antibody H-52 (Santa Cruz Biotechnology, Dallas, TX) at a concentration of 0.4 μg/ml with the ZytoChem Plus AP-Fast Red Kit (Zytomed Systems, Berlin, Germany).

Cleaved caspase-3 immunostaining was performed using the anti-cleaved caspase-3 Asp175 (Cell Signaling Technology, Frankfurt, Germany) at a dilution of 1:200 with the ZytoChem Plus AP Fast Red Kit (Zytomed Systems).

Hydroxyproline assay. Hydroxyproline assay was performed following a modified protocol from Reddy and Enwemeka (28). Briefly, we weighed and sampled the lavaged right lung in pieces. According to a smooth fractionator sampling protocol (20), 1/8 of the pieces was taken, corresponding to 1/8 of the total volume of the right lung. Determination of the amount of hydroxyproline in the sampled tissue, which was representative of the total organ, allowed calculation of the amount of hydroxyproline in the complete right lung. The tissue was then homogenized. After hydrolysis of the proteins in 6 N HCl, at 120°C for 24 h, neutralization of the sample was achieved by adding the same volume of 6 N NaOH; 20 μl of sample or standard per well was then used for the oxidation of hydroxyproline with chloramine-T (0.056 M) and further development of color with Ehrlich's reagent (1 M). The plate was read at 570 nm wavelength. Hydroxyproline values were then referred to the whole right lung.

Multiplex analysis of cytokines. Cytokine analysis was performed by using a multiplex kit (R&D Systems, Minneapolis, MN) customized for BAL from rats containing antibodies specific for C-X-C motif ligand 3 (CXCL3), interferon-γ (INF-γ), IL-4, IL-10, IL-18, tumor necrosis factor-α (TNFα), CXCL2, IL-1β, IL-6, IL-13, and tissue inhibitor matrix metalloproteinase-1 (TIMP-1), from which only CXCL3, IL-18, and TIMP-1 showed values within the sensitivity range of the assay. In addition, ELISA kits for rat IL-10 and IL-6 (BD Opt EIA, BD Bioscience, Heidelberg, Germany) were used.

Real-time-PCR. Total cell RNA was isolated from frozen sorted cells using an ISOLATE RNA Mini Kit (Bioline, Berlin, Germany) and quantified by spectrometry at 260 nm. Cells were sorted from five animals and pooled down to three to four samples to have enough RNA to analyze. Reverse transcription was performed using 1 μg of total RNA and the iScript cDNA Synthesis Kit (Bio-Rad Laboratories) in a thermocycler (MasterCycler, Eppendorf, Hamburg, Germany). Real-time PCR was performed using iTaq SYBR Green Supermix (Bio-Rad Laboratories) at a final primer concentration of 100 nm and 50 ng of cDNA. Antibody-mediated hot-start iTaq DNA polymerase was activated after an initial 3-min denaturation step at 95°C. Denaturation of DNA was performed by holding at 95°C for 10 s. Annealing and extension temperature was set to 60°C (30 s) for 40 cycles in a CFX96 RT-PCR system (Bio-Rad Laboratories). Primer design was performed using primer designing tool PrimerBLAST (https://www.ncbi.nlm.nih.gov/tools/primer-blast/index.cgi?LINK_LOC=BlastHome), and primer sequences are shown in Table 3. RT-PCR data are presented as normalized expression (ΔΔCq), which corresponds to the relative quantity of the target gene normalized to the quantity of the reference gene (L32).

Statistics. GraphPad Prism 7.0 (San Diego, CA) was used for calculation of means and standard deviation, representation, and statistical analysis. Statistical analysis was performed using one-way ANOVA throughout all data sets of the paper. Multiplicity-adjusted *P* values were reported using the Tukey multiple comparison test following one-way-ANOVA. An adjusted *P* value is an "exact *P* value" reported for each comparison, but its value depends on the number of comparisons. *P* values < 0.05 were considered statistically significant and are labeled in the figures with a straight line connecting the groups compared or with an asterisk in the tables.

RESULTS

Development of a complete immune cell panel in rat lung. When developing a strategy to identify and follow changes by flow cytometry in BAL cells from rats, one quickly realizes two important limitations that are interrelated. The first one is that the panels already described and standardized for BAL cells in mice cannot be easily translated into the rat, not only due to the difference in epitopes or clones but also in molecular markers. For example, widely used molecular markers for macrophages in mice, such as F4/80 or SiglecF, have not been described in rat macrophages; therefore, antibodies do not exist. Especially challenging are the rat antibodies against CD11b and CD11c, as well as the molecular markers for alveolar macrophages. We have tested different commercially available antibodies against CD11b or CD11b/c, since no provider could offer a specific antibody against rat CD11c. We found no differences in the populations labeled by the clone ED7 (CD11b), OX42 (CD11b/c), or REA325 (CD11b/c) in

Table 2. *Additional membrane cell markers and antibodies tested in rat bronchoalveolar lavage*

Marker	Conjugate	Source	Clone	Lymphocyte	Alveolar Macrophage	Activated Macrophage	Granulocyte	Monocyte
CD43	Alexa 647	BioLegend	W3/13	+	+	+	−/+	
CD80	PE	Ebioscience	B7-1	−	+	+	−	−
CCR7		Cell applications Inc		−	+	+	−	−
CD11b	Mouse anti-rat	Bio-Rad	ED7	−	+	+	+	+
CD11b/c	FITC	Serotec	Ox42	−	+	+	+	+

Table 3. *Primers used for RT-PCR*

Gene	Protein	Reference Sequence	Forward Primer	Reverse Primer
Fzz1	Resistin-like-α (Retnla)	NM_053333.1	TAAGGAAGACCCTCTCATGCA	TTCCCAAGATCCACAGGCAA
Ccl2	Chemokine ligand 2	NM_031530.1	TTCTGGGCCTGTTGTTCACA	TTGGGATCATCTTGCCAGTGA
Tgfb1	Transforming growth factor-β1	NM_021578.2	GACTCTCCACCTGCAAGACC	GGACTGGCGAGCCTTAGTTT
Arg1	Arginase-1	NM_017134.3	GGTGGATGCTCACACTGACA	AGAATCCTGGTACATCTGGGAA
Il13	Interleukin-13	NM_053828.1	AGATCCACATCTCCCCCTGT	GTCAGGTCCACGCTCCATAC
Il4	Interleukin-4	NM_201270.1	CGTGATGTACCTCCGTGCTT	GGTGCAGCTTCTCAGTGAGT
Il6	Interleukin-6	NM_012589.2	GCAAGAGACTTCCAGCCAGT	CTGGTCTGTTGTGGGTGGTA
Nos2	Inducible nitric oxide synthase	NM_012611.3	TTGCCACGGAAGAGACGCAC	CAGGCACACGCAATGATGGG
L32	Ribosomal protein L32	NM_013226.2	AAGCGAAACTGGCGGAAACC	CTGGCGTTGGGATTGGTGAC
Cox2	Cyclooxygenase-2	S67722.1	TCCATTTGTGAAGATTCCTGTGTTG	TCTCACTGGCTTATGCCGAA
Il12a	Interleukin-12A	NM_053390.1	GCGACAAAACCAGCACACTG	GCAGGCAGCTCCCTCTTATT
Mmp9	Matrix metallopeptidase-9	NM_031055.1	CTCTACACGGAGCATGGCAA	CACCAGCGATAACCATCCGA
Mmp10	Matrix metallopeptidase-10	NM_133514.1	GCGCATGAACTTGGTCACTC	AAAGGCGAATGTTGGCTTGG
ApoE	Apolipoprotein E	NM_001270681.1	CCGGAGGCTAAGGAGTTGTTT	CCCCACAGAGCCTTCATCTTCC
Ccn2	CTGF or communication network factor 2	NM_022266.2	CACCCGGGTTACCAATGACA	CGGATGCACTTTTTGCCCTT
Mki67	Marker of proliferation K_i-67	NM_001271366.1	GGTTTCCAGACACCAGACCAT	GGGTTCTAACTGGTCTTCCTGG

BAL cells of healthy or diseased rats, as well as in isolated blood monocytes (Fig. 1*A*). The last antibody is commercially available conjugated to plenty of different fluorophores, and therefore, it was the chosen antibody for this work. Details about the antibodies can be found in Tables 1 and 2. However, the lack of a specific antibody against CD11c implies that differentiation between monocytes ($CD11b^{high}$, $CD11c^{low}$) and resident macrophages ($CD11b^{low}$, $CD11b^{high}$) could not rely on the CD11b/c antibody used, as is normally done in mouse cells. On the other hand, the mouse panel available to label membrane molecular markers for alveolar macrophages is also challenging to translate to rat cells. Based on the work performed by Dijkstra and colleagues (3, 5, 12, 18, 56), CD163 (clone ED2) has been characterized to be present in alveolar rat macrophages; in addition, monocytes, dendritic cells, lymphocytes, and granulocytes are negative for this epitope (3). In contrast, ED1 is expressed in all subsets of rat monocytes, macrophages, and dendritic cells (12). Therefore, ED2 shows more advantages to be used in rat BAL cells and to discriminate between macrophages and other cells. In addition, CD163 has been described as a cell surface glycoprotein, member of the scavenger receptor group B. A specific CD68 antibody for rat cells exists, and our results showed differential expression between macrophages and monocytes from BAL, lung tissue, and blood (Fig. 1*B*), confirming the identity of the different subset of cells. However, for the staining of CD68, as a cytosolic protein, an additional step of fixing and permeabilizing cells is needed, and it is not suitable for analyzing living cells. Therefore, we chose CD163 to identify resident macrophages.

Cell populations in rat bronchoalveolar lavage after bleomycin challenge: gating strategy and validation of the identified populations. Identification of cell subpopulations during development of a disease is challenging, especially when cells change in morphology and expression profile, and new populations may appear. Therefore, to standardize a gating strategy for the entire time course study, we combined the gating strategies of healthy states, 7 and 14 days after bleomycin. As a result, Fig. 2 shows a simple gating strategy using the membrane cell markers in Table 1. After the exclusion of doublets and cell debris, CD45- and CD11b/c-positive cells were gated as myeloid cells for further analysis. $CD45^+$ cells but not $CD11b/c^-$ cells were identified as lymphocytes and further characterized as $CD3^+$ cells, whereas $CD11b/c^+$ cells with no myeloid origin ($CD45^-$) were considered contaminating epithelial cells (ECs) derived from damage of the epithelium during bronchoalveolar lavage (Fig. 1*C*). For differentiation of the cell subsets within myeloid cells ($CD45^+$, $CD11b/c^+$), resident alveolar macrophages could be readily identified as $CD163^+$ cells and also by higher autofluorescence; they were additionally identified as $CD68^+$ cells. A subpopulation of $CD163^-$ cells was also present. This latter population can be further characterized by the use of an α-granulocyte antibody, showing a positive population ($CD45^+$, $CD11b/c^+$, $CD163^-$ and α-granulocyte$^+$), indicating a clear population of granulocytes (mostly neutrophils, as shown in the sorted cytospot, and further characterized by expression of IL-1-3, IL-4, and IL-6 by RT-PCR, Fig. 2*B*), while a negative population of myeloid origin ($CD45^+$, $CD11b/c^+$) but negative for the macrophage or granulocyte marker ($CD163^-$ and α-granulocyte$^-$) points to a population of undifferentiated recruited monocytes (additionally characterized as $CD4^+$ cells). Within $CD163^+$ cells, other antibodies, such as MHC-II, shows two different populations, one with low MHC-II expression ($CD45^+$, $CD11b/c^+$, $CD163^+$, MHC-II^{low}), identified as resident alveolar macrophages, whereas the population showing high expression ($CD45^+$, $CD11b/c^+$, $CD163^+$, MHC-II^{high}) have been identified as activated macrophages. Corresponding isotype controls can be found in Fig. 2*C*.

Therefore, with this gating strategy, four distinct subpopulations of cells can be identified, changing through time and expression level in the rat lung alveolar spaces after bleomycin challenge. To validate our gating strategy, we also sorted the different cell populations following the same strategy and performed differential staining to show their corresponding morphologic features (microscopic pictures next to dot plots).

Overview and quantification of time-dependent changes in cell subset populations after bleomycin challenge. An overview of the changes in the different populations with time is presented in Fig. 3*A*. Representative images of the FACS dot plots are shown dividing the populations in either $CD45^-$ (ECs) or $CD11b/c^-$ (lymphocytes), $CD163^-$ containing recruited cells (both monocytes and granulocytes), and the $CD163^+$ cell population, containing resident alveolar macro-

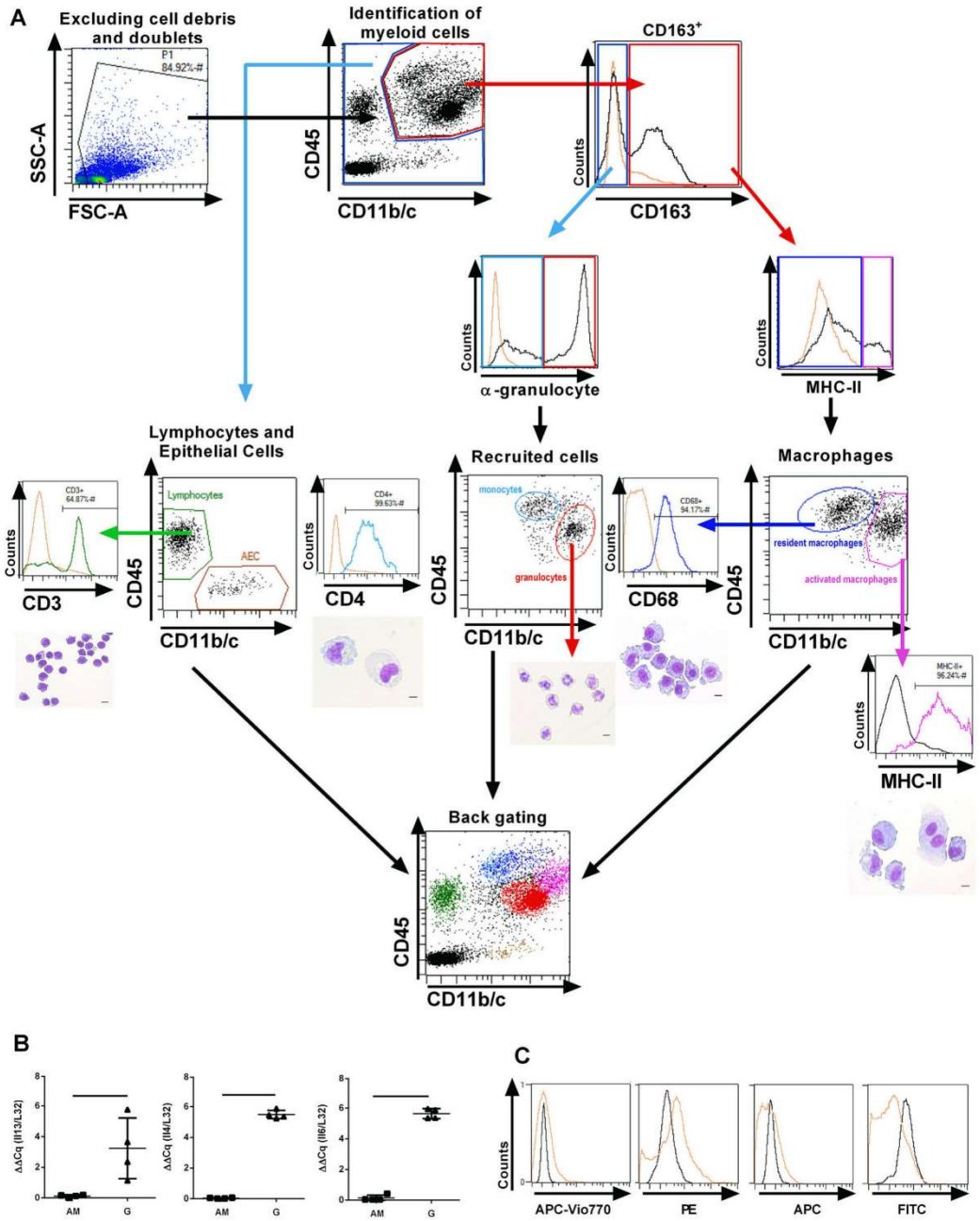

Fig. 2. Cell populations in rat bronchoalveolar lavage (BAL) after bleomycin challenge. Gating strategy and validation of the identified populations. *A*: after excluding doublets and cell debris, BAL myeloid cells were identified as CD11b/c$^+$ and CD45$^+$. Cells negative for CD11b/c but positive for CD45 are therefore identified as lymphocytes. Within myeloid cells, a third molecular marker, CD163, was used to identify the subset of resident alveolar macrophages (CD11b/c$^+$, CD45$^+$, CD163$^+$) or recruited cells (CD11b/c$^+$, CD45$^+$, CD163$^-$). Further characterization includes, on the one hand, use of markers for macrophage activation, such as MHC-II highly expressed in activated macrophages (CD11b/c$^+$, CD45$^+$, CD163$^+$, MHC-II^{high}); on the other hand, we used an α-granulocyte antibody to differentiate between granulocytes (CD11b/c$^+$, CD45$^+$, CD163$^-$, α-granulocyte$^+$) and monocytes (CD11b/c$^+$, CD45$^+$, CD163$^-$, α-granulocyte$^-$). Corresponding sorted cells can be visualized and morphologically identified next to the dot plots after quick-diff staining and additional specific staining for each population. Therefore, lymphocytes were also identified as CD3$^+$ cells, monocytes as CD4$^+$ cells, and macrophages as CD68$^+$ cells. *B*: RT-PCR gene expression analysis of IL-13, IL-6, and IL-4 of granulocytes (G) compared with a nonproducing cell (alveolar resident macrophages, AM). *C*: isotype controls (in orange) for APC-Vio770, FITC, PE, and APC directly conjugated antibodies compared to nonlabeled controls (in black).

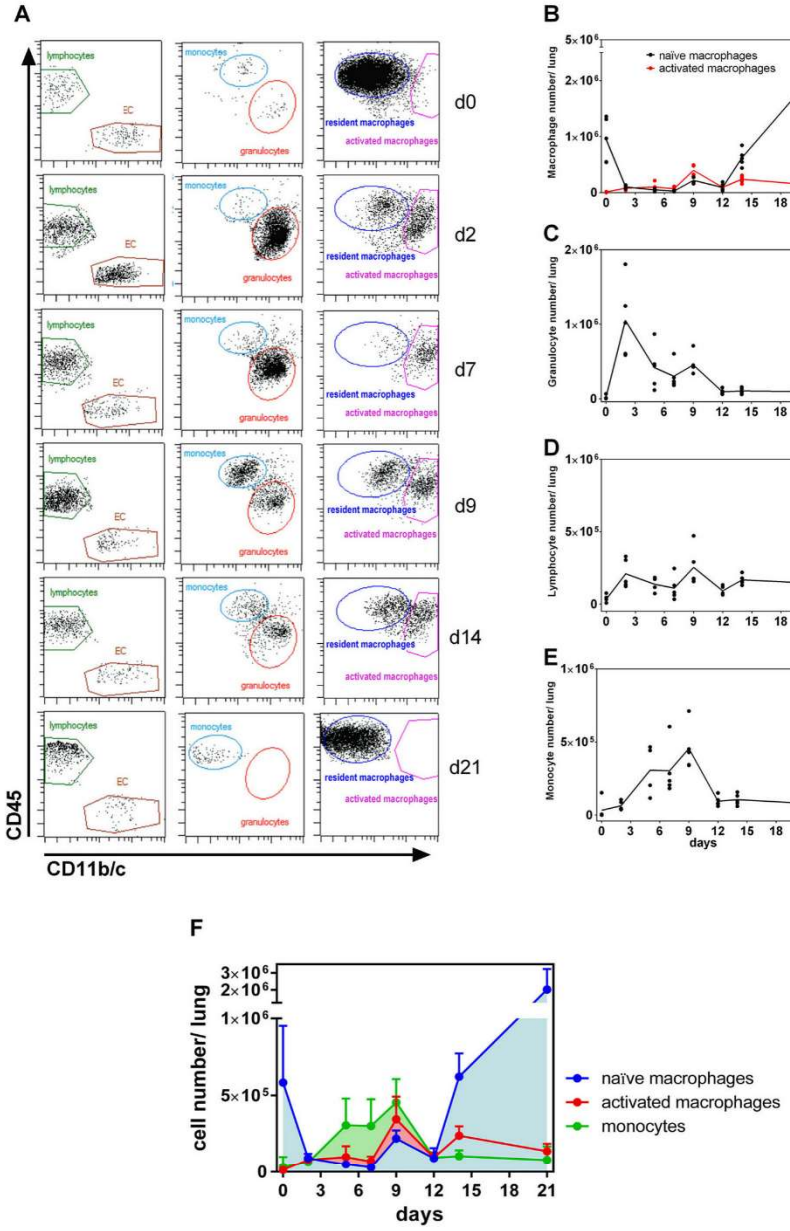

Fig. 3. Overview and quantification of time-dependent changes in cell subset populations after bleomycin challenge. *A*: representative dot plots from FACS analysis with different populations identified by our gating and molecular markers panel at different time points after bleomycin challenge. EC, epithelial cells; d, day. *B*: quantification of different macrophage populations (resident alveolar macrophages ($CD11b/c^+$, $CD45^+$, $CD163^+$, MHC-II^{low}) and activated macrophages ($CD11b/c^+$, $CD45^+$, $CD163^+$, MHC-II^{high}). Every dot represents an individual animal analyzed; line connects means of every group ($n = 5$) during time. *C*: changes in granulocytic population ($CD45^+$, $CD11b/c^+$, $CD163^-$, α-granulocyte$^+$) in time ($n = 5$). *D*: changes in lymphocyte ($CD45^+$, $CD11b/c^-$) numbers in time ($n = 5$). *E*: changes in population of recruited monocytes ($CD45^+$, $CD11b/c^+$, $CD163^-$, α-granulocyte$^-$) in time ($n = 5$). *F*: comparative plot with changes of macrophage and monocyte populations in time ($n = 5$ per group).

phages and activated macrophages. With a fast and simple gating strategy, the different populations were identified and monitored during time, allowing further quantification and characterization. Figure 3, *B–E*, shows changes in cell number of the different subpopulations with time, and the corresponding statistical analysis can be found in Table 4. As previously described, the resident alveolar macrophage population was notably reduced at very early stages after bleomycin challenge and increased rapidly again at the end of the time course from *day 12*, simultaneously with the disappearance of the monocyte population (Fig. 3, *B* and *E*), which peaked at *day 9* and disappeared at *day 12*. The granulocyte population peaked as early as 2 days after bleomycin as a result of the typical granulocyte inflammatory infiltration and a showed a second peak at *day 9* (Fig. 3*C*), while the lymphocyte population showed two small peaks at *day 2* and *9* (Fig. 3*D*), following the pattern of the granulocytic population. In Fig. 3*F* a comparative plot between macrophage and monocyte populations is

Table 4. *Statistical analysis of number of cells*

Group (day)	0	2	5	7	9	12	14	21
				Macrophage number/lung				
No. of samples	5	5	5	5	5	5	5	5
Mean	946,201	100,759	49,624	29,393	219,721	9,2261	622,658	2,024,000
SD	39,5591	25,273	19,831	10,322	53,215	67,199	151,015	1,198,000
Adj. *P* vs. *day 0*		0.0917	0.0616	0.0523	0.2112	0.0859	0.9436	0.0131*
Adj. *P* vs. *day 2*			>0.9999	>0.9999	0.9999	>0.9999	0.6037	<0.0001*
Adj. *P* vs. *day 5*				>0.9999	0.9987	>0.9999	0.4898	<0.0001*
Adj. *P* vs. *day 7*					0.9973	>0.9999	0.4463	<0.0001*
Adj. *P* vs. *day 9*						0.9998	0.8437	<0.0001*
Adj. *P* vs. *day 14*							0.5847	<0.0001*
Adj. *P* vs. *day 21*								0.0006*
				Activated macrophage number/lung				
No. of samples	5	5	5	5	5	5	5	5
Mean	12,430	80,578	100,208	69,941	398,330	932,63	239,428	137,928
SD	5,127	26,178	71,538	33,034	102,589	32,624	60,554	48,223
Adj. *P* vs. *day 0*		0.5731	0.2668	0.7535	<0.0001*	0.3193	<0.0001*	0.0305*
Adj. *P* vs. *day 2*			0.9990	>0.9999	<0.0001*	0.9998	0.0014*	0.6997
Adj. *P* vs. *day 5*				0.9851	<0.0001*	>0.9999	0.0066*	0.9508
Adj. *P* vs. *day 7*					<0.0001*	0.9935	0.0006*	0.5041
Adj. *P* vs. *day 9*						<0.0001*	0.0029*	<0.0001*
Adj. *P* vs. *day 14*							0.0049*	0.9192
Adj. *P* vs. *day 21*								0.0931
				Lymphocyte number/lung				
No. of samples	5	5	5	5	5	5	5	5
Mean	34,004	209,313	136,703	110,427	253,700	91,351	167,232	145,142
SD	28,442	99,134	51,472	83,360	132,995	31,380	33,664	115,736
Adj. *P* vs. *day 0*		0.0384*	0.5896	0.8198	0.0044*	0.9523	0.2117	0.4194
Adj. *P* vs. *day 2*			0.8875	0.5644	0.98883	0.3462	0.9915	0.9166
Adj. *P* vs. *day 5*				0.9997	0.4288	0.9906	0.9992	>0.9999
Adj. *P* vs. *day 7*					0.1469	>0.9999	0.9545	0.9974
Adj. *P* vs. *day 9*						0.0680	0.7134	0.4488
Adj. *P* vs. *day 14*							0.8249	0.9659
Adj. *P* vs. *day 21*								0.9999
				Granulocyte number/lung				
No. of samples	5	5	5	5	5	5	5	5
Mean	18,537	105,4000	41,9535	302,703	455,292	95,056	105,759	96,885
SD	27,421	505,361	293,009	17,3300	151,672	34,847	39,074	108,143
Adj. *P* vs. *day 0*		<0.0001*	0.1299	0.5063	0.0764	0.9994	0.9958	0.9992
Adj. *P* vs. *day 2*			0.0023*	0.0002*	0.0046*	<0.0001*	<0.0001*	<0.0001*
Adj. *P* vs. *day 5*				0.9909	>0.9999	0.3413	0.3822	0.3481
Adj. *P* vs. *day 7*					0.9593	0.8264	0.8611	0.8326
Adj. *P* vs. *day 9*					-	0.2244	0.2561	0.2296
Adj. *P* vs. *day 14*	-						>0.9999	>0.9999
Adj. *P* vs. *day 21*								>0.9999
				Monocyte number/lung				
No. of samples	5	5	5	5	5	5	5	5
Mean	32,855	63,528	307,073	302,703	455,292	95,056	105,759	80,759
SD	67,113	31,086	173,651	173,300	151,672	34,847	39,074	90,102
Adj. *P* vs. *day 0*		0.9998	0.0146*	0.0096*	<0.0001*	0.9836	0.9608	0.9965
Adj. *P* vs. *day 2*			0.0409*	0.0294*	<0.0001*	0.9998	0.9984	>0.9999
Adj. *P* vs. *day 5*				>0.9999	0.4805	0.1070	0.1442	0.0701
Adj. *P* vs. *day 7*					0.3709	0.0842	0.1169	0.0530
Adj. *P* vs. *day 9*						0.0003*	0.0004*	0.0002*
Adj. *P* vs. *day 14*							>0.9999	>0.9999
Adj. *P* vs. *day 21*								>0.9999

Adj., adjusted; SD, standard deviation. *$P < 0.05$.

shown in order to highlight the interrelation between them. As soon as *day 2*, the population of alveolar macrophages was drastically reduced, and 3 days later (*day 5*), a new population of recruited monocytes appeared, increasing up to *day 9*. At *day 12*, those monocytes seemed to disappear, and macrophage cell numbers recovered after 14 days. Activated macrophages appeared also as soon as *day 2* and peaked at *day 9* and *14*. However, the activation state of these cells is discussed in a later section of this paper. In addition, samples at *day 21* showed the recovery of the initial populations, but also an increased number of macrophages. Of note, even though these numbers point to a complete recovery of the diseased animals, we should clarify that 20% of the animals with the bleomycin concentration used (4.5 U/kg) showed an intermediate state

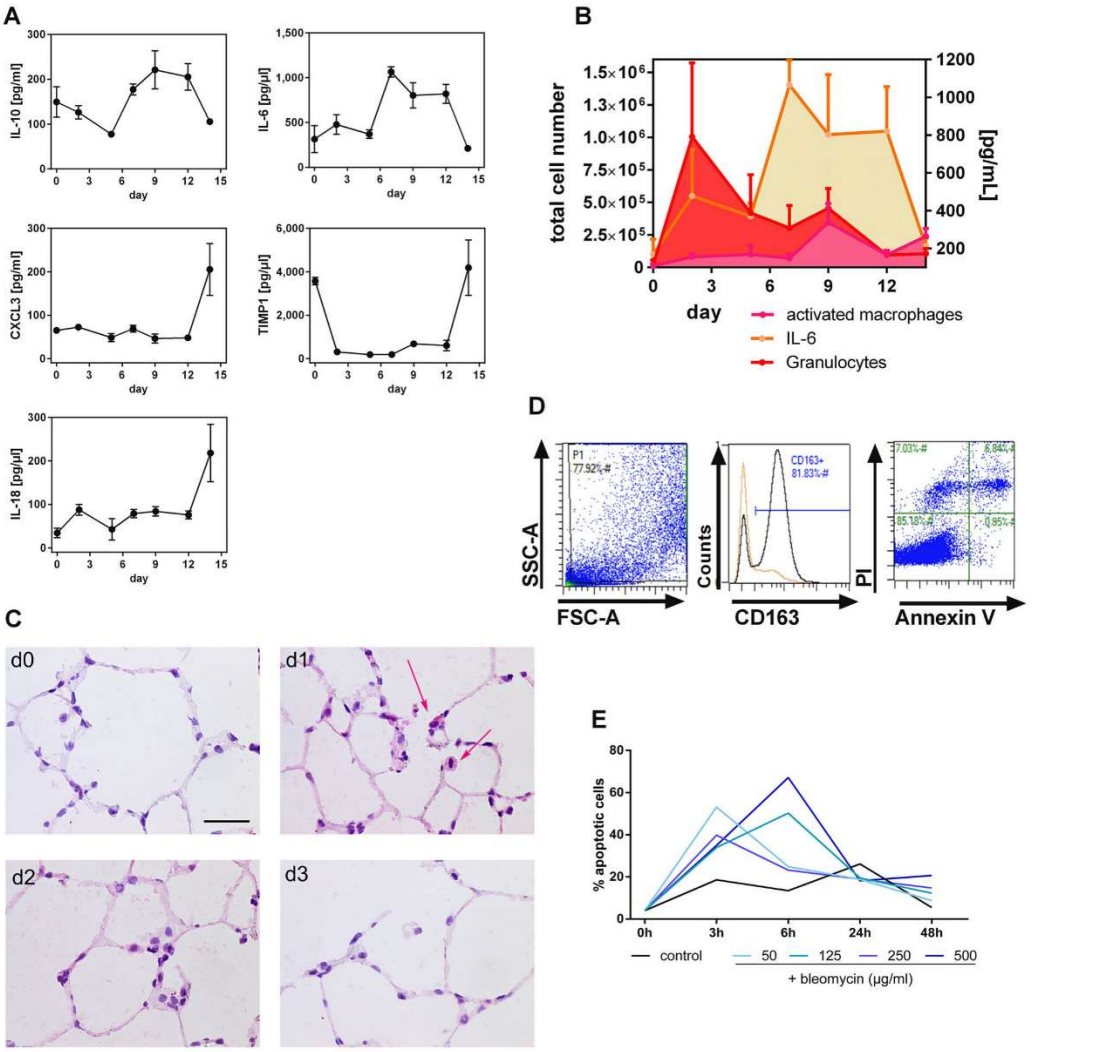

Fig. 4. Correlation of bleomycin-induced changes in bronchoalveolar lavage (BAL) cell populations with standard early acute lung injury. *A*: concentration of interleukin (IL)-10, IL-6, IL-18, C-X-C motif ligand 3 (CXCL3), and tissue inhibitor matrix metalloproteinase-1 (*TIMP-1*) in BAL fluid during time ($n = 5$ per group). *B*: comparative plot with changes in time of granulocytic ($CD45^+$, $CD11b/c^+$, $CD163^-$, α-$granulocyte^+$), activated macrophage ($CD11b/c^+$, $CD45^+$, $CD163^+$, $MHC\text{-}II^{high}$) population and IL-6 ($n = 5$ per group). *C*: representative micrographs of lung tissue sections ($n = 3$) stained with cleaved caspase-3 (pink, arrow) before and at *day* (d) *1*, 2, and *3* after bleomycin challenge. *D*: representative plots of analysis of BAL cells from diseased animals ($n = 3$) at *day 1* after bleomycin challenge. FSC, forward scatter; SSC, side scatter. *E*: apoptosis analysis of in vitro titration of bleomycin in healthy isolated BAL cells.

between *day 9* and *21*. However, this population of animals may represent either the survivors or the animals with the milder state of the disease phenotype.

Correlation of bleomycin-induced changes in BAL cell populations with standard early acute lung injury. A complete cytokine profile was measured in the BAL supernatants, and shown in Fig. 4*A* are the cytokine changes through the time course of the model, and the corresponding statistical analysis can be found in Table 5. The granulocyte peak (Fig. 4*B*) preceded the increase in IL-6 and IL-10 content in BAL during the early phase of inflammation. IL-6 was highly released to the alveolar spaces, with maximum at *day 7*, while it is maintained after *day 7*, as a second peak of granulocytes and a first peak of activated macrophages appeared (Fig. 4*B*). IL-6 content was reduced only between *day 12* and *14*, while other cytokines, such as TIMP-1, IL-18, and CXCL3 seemed to be increasing later, from *day 12*.

Figure 3*B* shows an early decrease of resident alveolar macrophage number, which in part could be explained as induction of apoptosis in these cells by bleomycin, as described before (21, 50, 79). Figure 4*C* shows immune staining with cleaved caspase-3 at 1, 2, and 3 days after bleomycin chal-

Table 5. *Statistical analysis of hydroxyproline and cytokine concentrations*

Group (day)	0	2	5	7	9	12	14
				Hydroxyproline, μg/mg			
No. of samples	5	5	5	5	5	5	5
Mean	1.662	1.670	1.378	1.674	1.898	2.560	2.912
SD	0.4531	0.3146	0.1638	0.2513	0.2436	0.5080	0.9081
Adj. *P* vs. *day 0*		>0.9999	0.9588	>0.9999	0.9834	0.0683	0.0039*
Adj. *P* vs. *day 2*			0.9530	>0.9999	0.0861	0.0724	0.0042*
Adj. *P* vs. *day 5*				0.9500	0.5871	0.0070*	0.0003*
Adj. *P* vs. *day 7*					0.9873	0.0745	0.0043*
Adj. *P* vs. *day 9*						0.3101	0.0281*
Adj. *P* vs. *day 12*							0.8928
				CXCL3, pg/ml			
No. of samples	4	5	2	5	5	5	5
Mean	64.94	72.66	48.43	69.03	46.37	47.99	205.6
SD	13.21	16.69	13.42	17.80	23.70	16.77	133.5
Adj. *P* vs. *day 0*		>0.9999	0.9999	>0.9999	0.9988	0.9993	0.0173*
Adj. *P* vs. *day 2*			0.9985	>0.9999	0.9892	0.9923	0.0170*
Adj. *P* vs. *day 5*				0.9994	>0.9999	>0.9999	0.0412*
Adj. *P* vs. *day 7*					0.9951	0.9967	0.0134*
Adj. *P* vs. *day 9*						>0.9999	0.0030*
Adj. *P* vs. *day 12*							0.0033*
				TIMP-1, pg/ml			
No. of samples	4	4	2	4	5	5	5
Mean	3572	309.3	186.5	188.2	681.0	605.6	4,190
SD	344.8	120.4	114.0	81.02	208.7	553.2	2,859
Adj. *P* vs. *day 0*		0.0189*	0.0636	0.0139*	0.0323*	0.0266*	0.9886
Adj. *P* vs. *day 2*			>0.9999	>0.9999	0.9993	0.9998	0.0022*
Adj. *P* vs. *day 5*				>0.9999	0.9990	0.9996	0.0139*
Adj. *P* vs. *day 7*					0.9966	0.9986	0.0016*
Adj. *P* vs. *day 9*						>0.9999	0.0034*
Adj. *P* vs. *day 12*							0.0027*
				IL-18, pg/ml			
No. of samples	5	5	4	5	5	5	5
Mean	34.14	87.62	42.43	78.85	83.65	75.74	218.3
SD	24.64	28.02	50.03	21.37	23.81	20.58	147.5
Adj. *P* vs. *day 0*		0.8221	>0.9999	0.9134	0.8678	0.9369	0.0014*
Adj. *P* vs. *day 2*			0.9298	>0.9999	>0.9999	>0.9999	0.0383*
Adj. *P* vs. *day 5*				0.9754	0.9538	0.9837	0.0044*
Adj. *P* vs. *day 7*					>0.9999	>0.9999	0.0229*
Adj. *P* vs. *day 9*						>0.9999	0.0304*
Adj. *P* vs. *day 12*							0.0190*
				IL-10, pg/ml			
No. of samples	4	5	2	5	5	5	5
Mean	149.6	126.5	77.55	177.4	221.0	205.3	105.7
SD	67.44	33.02	2.001	27.58	94.59	66.59	5.130
Adj. *P* vs. *day 0*		0.9956	0.7474	0.9881	0.4929	0.7485	0.8974
Adj. *P* vs. *day 2*			0.9369	0.7737	0.1466	0.3157	0.9965
Adj. *P* vs. *day 5*				0.3630	0.0668	0.1318	0.9961
Adj. *P* vs. *day 7*					0.8725	0.9838	0.4209
Adj. *P* vs. *day 9*						0.9993	0.0439*
Adj. *P* vs. *day 12*							0.1114
				IL-6, pg/ml			
No. of samples	4	5	2	5	5	5	5
Mean	315.9	477.9	370.7	1066	802.7	820.6	212.0
SD	302.1	245.8	67.68	130.7	317.4	235.7	45.25
Adj. *P* vs. *day 0*		0.9308	>0.9999	0.0008*	0.0494*	0.0382*	0.9922
Adj. *P* vs. *day 2*			0.9972	0.0061*	0.2949	0.2407	0.5216
Adj. *P* vs. *day 5*				0.0173*	0.2894	0.2482	0.9778
Adj. *P* vs. *day 7*					0.5321	0.6095	<0.0001*
Adj. *P* vs. *day 9*						>0.9999	0.0059*
Adj. *P* vs. *day 12*							0.0044*

Adj., adjusted; Il, interleukin; TIMP1, tissue inhibitor matrix metalloproteinase1; CXCL3, CXC motif ligand 3; SD, standard deviation. *$P < 0.05$.

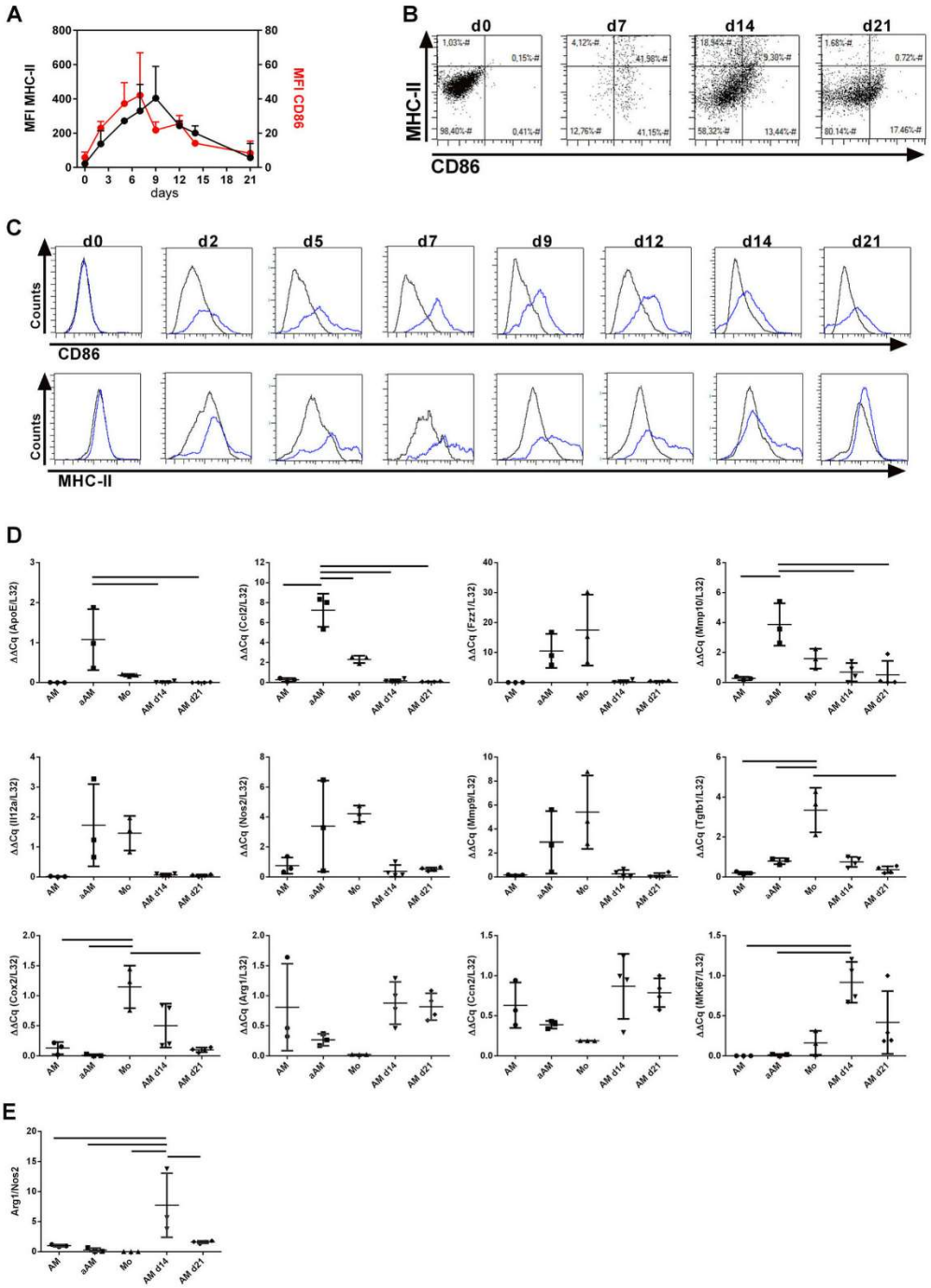

lenge. At *day 1*, it was already difficult to find alveolar macrophages, and they showed a slight upregulation of cleaved caspase-3. FACS analysis also showed a moderate increase in apoptosis at *day 1* in alveolar macrophages ($CD163^+$) (Fig. 4*D*). In addition, in vitro titration of bleomycin in isolated BAL cells showed a concentration-dependent increase of apoptosis in these $CD163^+$ cells as early as after 3 h of incubation (Fig. 4*E*). Samples incubated for 24 h showed reduced apoptosis due to the increased necrotic population. Therefore, it seems that bleomycin was able to induce apoptosis in less than 24 h, which may explain the slight increase observed in our in vivo data.

Activation of macrophages during bleomycin-induced lung injury and fibrosis. We also observed that, even when the number of alveolar macrophages was recovered after 21 days, those cells differed in expression of MHC-II and CD86 from resident alveolar or activated macrophages and may represent a different population from the initial one. The expression of CD86 (Fig. 5*A*) was rapidly induced at *day 2*, with a peak around *day 7* and was kept constant until the end of the time course, whereas the expression of MHC-II slowly increased up to *day 9*, decreasing to initial values at *day 21*. It seems therefore that the activation of macrophages during *day 7–9* was characterized by an increased expression of CD86 and MHC-II. We could not differentiate between classically or alternatively activated individual macrophages (Fig. 5*B*); it seemed that some cells differentially expressed one marker, the other or both at the same time, and this expression varied over time (Fig. 5*C*). Therefore, instead of identifying individual cells we could differentiate expression levels of the different molecular markers. A further detailed analysis of gene expression in the different populations of macrophages and monocytes showed differential expression of many genes (Fig. 5*D*). Activated macrophages and monocytes were sorted from animals 7 and 9 days after bleomycin, when those populations peaked, and the number of cells sorted allowed isolation of enough RNA to perform RT-PCR. Activated macrophages (aAM) showed a significant increase in gene expression of apolipoprotein E (*ApoE*), chemokine ligand 2 (*Ccl2*), and matrix metalloproteinase 10 (*Mmp10*) compared with resident alveolar macrophages (AM), monocytes (Mo), and macrophages from *day 14* (AM d14) and *day 21* (AM d21) after bleomycin challenge. In contrast, monocytes showed an interesting significant increase in the expression of transforming growth factor-β1 (*Tgfb1*) and cyclooxygenase-2 (*Cox2*) compared with resident alveolar (AM) and activated macrophages (aAM) as well as macrophages from *day 21* (AM d21). The proliferation marker Ki67 showed a significant increase in macrophages coming from *day 14* after bleomycin. Other genes, such as resistin like-α (*Fzz1*), interleukin 12A (*Il12a*), inducible nitric oxide synthase (*Nos2*), and matrix metalloproteinase 9 (*Mmp9*), showed no statistically significant increase in both activated macrophages and monocytes compared with the rest of the cells, while arginase 1 (*Arg1*) and CTGF or communication network factor 2 (*Ccn2*) seemed to be expressed mostly in resident alveolar macrophages coming from *day 14* and *21* after bleomycin. Thus, our described gating strategy seems to have identified between functionally differently activated cells in our model. Even though *Arg1* and *Nos2* showed no clear differential expression between samples, their expression ratio *Arg1*/*Nos2* pointed at alveolar macrophages to from *day 14* as alternatively activated or anti-inflammatory (Fig. 5*E*).

Fibrotic remodeling and changes in lung tissue. We tested the same panel of antibodies in single-cell suspensions from lungs after bleomycin challenge to elucidate whether the changes observed in the BAL cells were reflected in the tissue (gating strategy in Fig. 6*A*). In addition, we investigated the standard molecular markers of fibrotic remodeling. Identifying the cells in the lung tissue with our simple panel of antibodies was difficult due to the risk of confounding cell populations in the tissue. However, this may be an interesting starting point for further studies. Quantification of the different cell populations can be found in Fig. 6, *B* and *C*. Of note, recruited $CD163^-$ cells appeared between *day 3* and *5* and peaked between *day 5* and *9* (Fig. 6*C*), in accord with these cells traveling to the alveolar spaces, where we found them in BAL (Fig. 3, *C* and *D* and Fig. 4*B*). In addition, we added to this panel a molecular marker for fibroblast (CD90.1) to follow one of the most relevant cells involved in fibrotic remodeling. In Fig. 6*E*, it can be observed how changes in the $CD90.1^+$ population correlated with the increase in hydroxyproline, as a marker of collagen accumulation in the lung tissue.

To validate our approach, we also performed staining of lung sections to observe the time changes in the general lung structure and elastin and collagen distribution. In Fig. 6*D*, representative micrographs can be observed. In H&E-stained sections, heterogeneity of the pathophysiological changes was represented as normal, opened alveolar areas together with areas showing cell infiltration, edematous material, and fiber deposition. In addition, elastin (in pink, H&E) and collagen (in green, Masson-Goldner trichrome staining) were progressively accumulating up to *day 14* in the highly remodeled areas. Very interestingly, arginase-1 was immune detected well in advance, before the previously described changes. As soon as *day 7*, we could identify positive cells for arginase-1, not only in macrophages but also in other cells in the lung parenchyma, which may represent a necessary step before collagen deposition. Lungs at *day 21* after bleomycin showed a recovered normal lung structure; however, as stated before, this group may repre-

Fig. 5. Activation of macrophages ($CD11b/c^+$, $CD45^+$, $CD163^+$) during bleomycin-induced acute lung injury and fibrosis. *A*: mean fluorescence intensity (MFI) time course of MHC-II (black) and CD86 (red) in macrophages ($CD11b/c^+$, $CD45^+$, $CD163^+$) ($n = 5$ per time point). *B*: representative 2-dimensional plots showing expression of MHC-II and CD86 in the macrophage population at *day* (d) *0*, *7*, *14*, and *21*. *C*: representative histograms of CD86 and MHC-II (blue) compared with their respective negative controls (black) in alveolar macrophages during time. *D*: RT-PCR gene expression analysis of different sorted populations of AM ["naïve" (nonstimulated) alveolar macrophages; $CD11b/c^+$, $CD45^+$, $CD163^+$, MHC-II^{low} at *day 0*], aAM (activated macrophages; $CD11b/c^+$, $CD45^+$, $CD163^+$, MHC-II^{high} at *day 9*), Mo (monocytes; $CD45^+$, $CD11b/c^+$, $CD163^-$, α-granulocyte$^-$ at *day 9*), AM d14 (AM sorted at *day 14*; $CD11b/c^+$, $CD45^+$, $CD163^+$, MHC-II^{low}) and AM d21 (AM sorted at *day 21*; $CD11b/c^+$, $CD45^+$, $CD163^+$, MHC-II^{low}) after bleomycin challenge ($n = 3–4$ samples per group from $n = 5$ animals per group). *E*: arginase-1 to inducible nitric oxide synthase (Arg1/Nos2) ratio calculated from RT-PCR data.

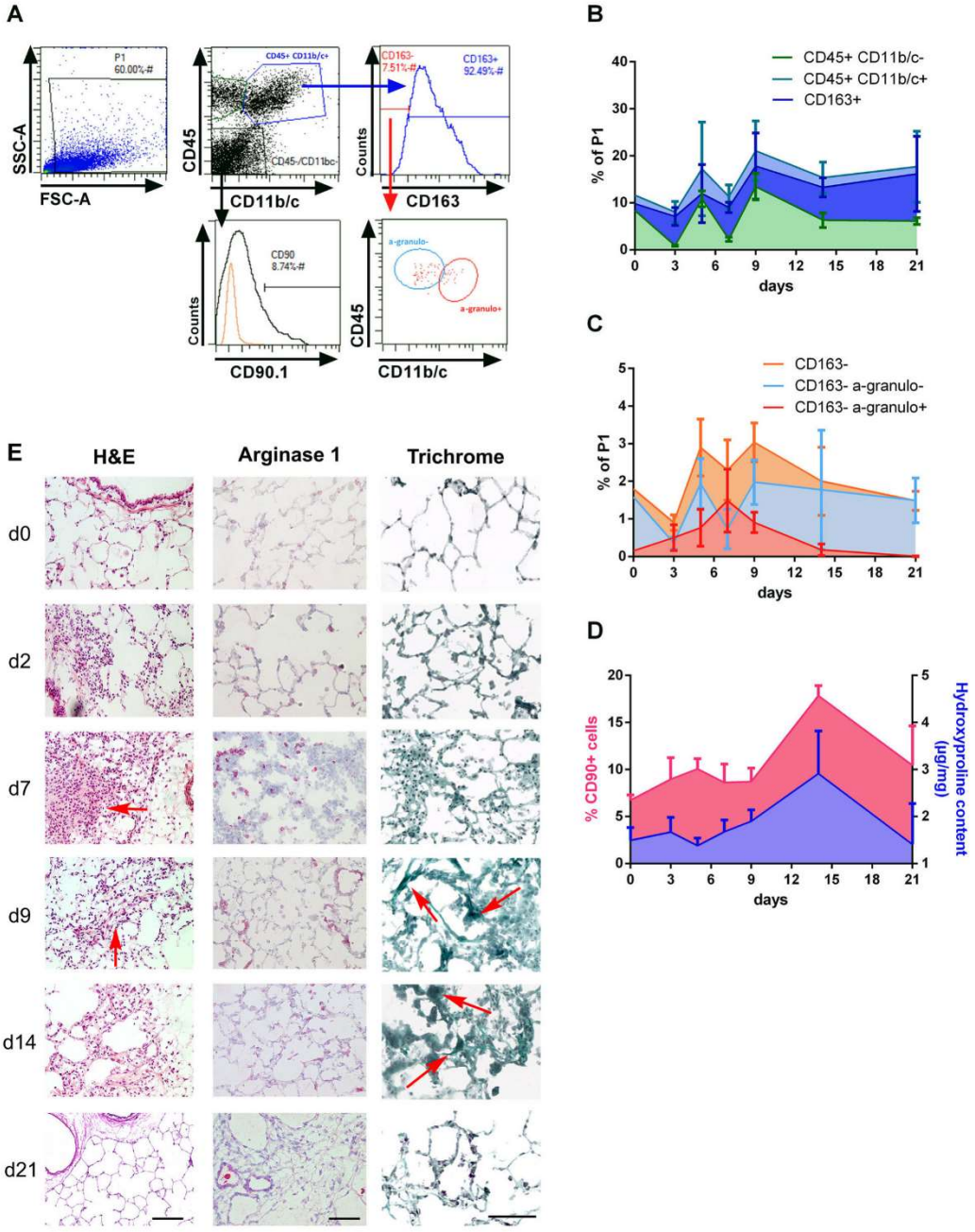

Fig. 6. Fibrotic remodeling and changes in lung tissue. *A*: representative plots of the gating strategy followed in lung tissue single cell suspensions. FSC, forward scatter; SSC, side scatter. *B*: quantification of $CD45^+$ cell populations, both CD11b/c-positive and -negative and $CD45^+$-, $CD11b/c^+$-, and $CD163^+$-positive cells as percentage of P1 ($n = 3$ per group). *C*: quantification of $CD45^+$, $CD11b/c^+$, and $CD163^-$ recruited cells, both antigranulocyte positive and negative ($n = 3$ per group). *D*: comparative plot with changes in time of the concentration of hydroxyproline ($n = 5$ per group) and appearance of CD90.1-positive cells in tissue ($n = 3$ per group). *E*: changes in lung tissue during bleomycin-induced acute lung injury and fibrosis, shown by overview pictures of hematoxylin-eosin (H&E) staining (scale bar, 100 µm), immunostaining of arginase-1 (scale bar, 100 µm), and trichrome staining (scale bar, 100 µm). Representative pictures show highly remodeled areas where elastin (in pink) and collagen (in green) accumulation can be observed; pink stained cells with arginase-1 can be seen in the *middle* panel. Red arrows indicate cell infiltration in H&E staining and fiber accumulation in Goldner trichrome staining.

sent the survivors and healthiest subjects. Therefore, it is difficult to conclude whether this group represents the milder form of the altered phenotype or the result of a repair phase.

DISCUSSION

The development of antibodies for rat is far behind the availability of antibodies for mouse. Connected to this is the lack of literature that can be consulted for studies such as this one. A quick search of literature in PubMed (https://www.ncbi.nlm.nih.gov/pubmed/) using the following terms: flow cytometry analysis AND BAL cells AND mouse (sorted by best match), gives a result of 91 publications available. When using the sequence: flow cytometry analysis AND BAL cells AND rat, the total number goes down to 23 available publications, of them, 10 from the 90s (vs. 20 of 91 for mouse literature). Even though the bleomycin model of lung injury and fibrosis in rats is widely used (10, 24, 30, 52, 53, 57, 67, 68, 71, 74), no complete analysis of BAL cell subsets using FACS exist. We have described here the first rat membrane marker panel for flow cytometry characterizing BAL myeloid cells during the inflammatory and remodeling phase of bleomycin-induced lung injury. Using commercially available antibodies (Table 1) and a simple gating strategy (Fig. 2), this method can be used by any researcher to isolate and functionally characterize the different cell subsets described here. For validation of our panel, we correlated the different cell subsets with molecular markers of the inflammatory or remodeling phase in this model (Figs. 3*F*, 4*B*, and 6*D*) and previously reported results in both species rat and mouse.

CD163 is a macrophage scavenger receptor from the family of cysteine-rich type I proteins characteristic of mature resident macrophages. Even though it has also been described to be characteristic of human-activated (18, 26) or multinucleated giant cell (MGC) (48) macrophages, the usefulness of this molecular marker in our approach is the ability to differentiate between resident macrophages and recruited monocytes (3). The evolution of these populations after bleomycin challenge shows the complexity of myeloid cells in the lung during disease progression. In accord with previous reports, the short-time effect of the intratracheal application of bleomycin is the reduced number of resident alveolar macrophages up to *day 2*. It has already been described that bleomycin causes apoptosis of resident alveolar macrophages (21, 50, 79) and our results confirm that the induction of apoptosis may take place during the first 24 h. In our model, this seems to be followed by increasing numbers of monocytes (from *day 2* to *9*). The role of this new population of monocytes ($CD45^+$, $cd11b/c^+$, $CD163^-$, and α-granulocyte$^-$) is not clear, but further functional analysis revealed that these cells may be the main origin of TGF-β1 and Cox2 expression (Fig. 5*D*). Elevated levels of both TGF-β1 (2, 4, 15, 33, 47) and prostaglandin E_2 (PGE_2) (49) (the product resulting from the enzymatic activity of Cox2), are directly related to lung remodeling (32). TGF-β1 has been described as regulating the demethylation of the Cox2 gene (11–13, 32, 78). Fibroblasts (55), injured epithelial cells (76), and alveolar macrophages (29, 64, 77) have been described as sources of TGF-β1 during the development of fibrosis; however our data point to recruited monocytes as another source of this profibrotic cytokine, as supported by other data (35, 41), and a potential target in therapy. It has recently been described that systemic depletion of monocytes (or immature macrophages) significantly improved the overall survival of a model of interstitial lung disease (SP-$C^{I73T/I73T}Flp^{+/-}$) in mice (72). Even though alveolar macrophages are thought to be long-lived resident and self-replenishing in the alveolar spaces, under certain conditions, this population of mature differentiated alveolar macrophages can be derived from bone marrow-recruited monocytes, too (31, 39–41). Very interestingly, the population of alveolar macrophages is recovered 14 days after bleomycin with different activation states, whereas the monocyte population disappears 12 days after bleomycin, pointing to monocytes as the possible origin of the new macrophages (6, 41, 59). The proliferation marker Ki67 was shown to be significantly upregulated in macrophages at *day 14*, pointing to both infiltration and differentiation of recruited monocytes as well as proliferation of resident alveolar macrophages as origins of the increased numbers found at *day 21*.

Right at *day 2*, the population of granulocytes started increasing according to the granulocytic inflammation of the lung after bleomycin (1, 9, 14), similarly to LPS-induced inflammation (3), and was followed by release of IL-6, as previously described (19, 42, 61). At *day 7*, activated macrophages ($CD45^+$, $CD11b/c^+$, $CD163^+$, MHC-II^{high}) come into play. Activation of macrophages is a complex field nowadays and more challenging to analyze with the limited availability of antibodies for certain species. We have approached here the activation state of macrophages with two molecular markers, MHC-II and CD86. MHC-II molecules are normally found only on antigen-presenting cells such as dendritic cells, mononuclear phagocytes, and B cells. These cells are important in initiating immune responses. An increase in expression of MHC-II in macrophages has been observed as part of the inflammatory response produced during lung injury by bleomycin in mice (54). And other animal models showed increased MHC-II expression in activated alveolar macrophages by different agents (8) as well as activated macrophages in human patients of asthma (17). Accordingly, we chose this molecule as a marker of activation during the acute lung injury phase. CD86, cluster of differentiation 86 also known as B7-2, together with CD80 (B7-1), work in tandem to activate T cells, characteristic of a type II or adaptive immune response and therefore chosen as a molecular marker of activation during the remodeling phase of the model. In addition, it has been shown that CD86 expression increases after bleomycin challenge, and it is maintained until *day 21* in mice (40). Taking into account the heterogeneity of the disease, we should carefully analyze the possibility that our described populations may reflect the fact that injury and fibrosis in this model are not homogeneously distributed all over the lung; rather, normal air spaces can be found coexisting with highly inflamed fibrotic sites or intermediate states (34). Therefore, even though we could not clearly differentiate populations of macrophages classically or alternatively activated, this may mean that both CD86 and MHC-II marker expressions are changing in cells, becoming activated at different lung sites. We approached the identification of four different activation states: MHC-$II^{low}CD86^-$, MHC-$II^{low}CD86^+$, MHC-$II^{high}CD86^-$, and, lately, MHC-$II^{high}CD86^+$, where evidence on changes from *day 0* to *day 21* can be seen (Fig. 5, *A–C*) but no clear individual populations can be

identified. Therefore, further membrane molecular markers for macrophage activation need to be developed to separate those populations and sort them in the future. Sorted activated macrophages (aAM) ($CD45^+$, $CD11b/c^+$, $CD163^+$, MHC-II^{high}) showed significant upregulation of *ApoE, Ccl2*, and *Mmp10* (Fig. 5*D*), which may be considered molecular markers of alternatively activated macrophages but, more importantly, which are related to lung remodeling (36, 58, 62, 65, 70, 73). Not significant, but anyway interesting is the upregulation in both monocytes ($CD45^+$, $CD11b/c^+$, $CD163^-$, α-granulocyte$^-$) and activated macrophages ($CD45^+$, $CD11b/c^+$, $CD163^+$, MHC-II^{high}) of *Fzz1, Il12a, Nos2*, and *Mmp9*, pointing to a mixed population of proinflammatory activated macrophages and intermediate monocytes. Most of these changes happened before *day 9*, preceding the appearance of molecular markers of lung fibrosis, such as accumulation of collagen or fibroblast, and therefore representing intermediate events needed and leading to fibrotic remodeling.

Arginase-1 could be immune detected from *day 5*, not only specifically in macrophages but also in epithelial cells (Fig. 6*E*, *middle*) according to previous studies (14). Arginase-1 is an enzyme involved in collagen metabolism, where L-proline (major amino acid present in this protein) is generated sequentially from L-ornithine and L-arginine. The result of the activity of arginase-1 is ornithine, therefore the supply of arginine is a necessary step previous to collagen synthesis and therefore fibrotic development (44, 75). Moreover, it has been described that alternatively activated macrophages, expressing high levels of mitochondrial arginase, are implicated in promoting cell division and deposition of collagen during ontogeny and wound repair (39). Even though arginase-1 expression was not statistically significant (Fig. 5*D*), the notable increase in the *Arg1* to *Nos2* ratio (Fig. 5*E*) at *day 14* is consistent with macrophages alternatively activated or anti-inflammatory (46, 66, 72). In addition, other cytokines associated with remodeling processes are found to be increased at *day 14*, such as IL-18 and CXCL3, at the same time that IL-6 and IL-10 are reduced to normal values. Changes in the secreted concentration of cytokines may also reflect the appearance/disappearance of their corresponding producing cells. In this sense, the first peak of IL-6 may be coming from the first granulocytic infiltration, while the second points to an additional cell source, such as damaged/stressed epithelial cells (9). In the case of IL-10, a first decline on the concentration of this cytokine in BAL can be observed, potentially due to the disappearance of the corresponding producing cell, such as alveolar macrophages (22), and a peak between *day 7* and *9*, where activated macrophages and monocytes come into the alveolar spaces. In addition, T, dendritic, and epithelial cells could also be producing IL-10 to finish the inflammatory phase (1, 69). TIMP-1 also shows a notable decrease early enough, following the drastic decrease in number of resident alveolar macrophages and a later increase from *day 12*, at the same time alveolar macrophages recovered their initial number. The changes in TIMP-1 may also reflect the changes in the macrophage population, as main origin of this factor (60, 63). Chemokine (C-X-C motif) ligand 3 (CXCL3), also known as macrophage inflammatory protein-2β (MIP2β), is thought to control migration and adhesion of monocytes. Furthermore, both CXCL2 and CXCL3 have already been correlated to hydroxyproline levels in bleomycin-induced fibrosis in mice (27). IL-18, also known as interferon-γ-inducing factor, is recognized as an important regulator of innate and acquired immune responses. Moreover, it has already been described that both IL-18 and IL-18 receptor (IL-18R) expression are enhanced in patients with bleomycin-induced lung injury. As well, mice lacking IL-18 or IL-18R developed attenuated bleomycin induced lung injury (23). Even though no specific literature was found for rat samples, our results confirm, for the first time, the use of these cytokines as molecular markers of fibrosis in the rat model of bleomycin-induced lung fibrosis. The limits of each phase are not clear, but rather overlapping, this approach seems to offer a comprehensive way to understand the different events going on for 21 days after bleomycin. At *day 14*, a clear fibrotic remodeling can be seen in amounts of hydroxyproline (Fig. 6*D*) and Massons-Goldner trichrome staining (Fig. 6*E*) with the associated changes in cytokine profile and activation state of the immune cells.

In our model, with the specific timing and bleomycin dose described, lungs from 21 days after bleomycin challenged showed an apparent recovery. However, due to regulations regarding animal experimentation, we had to avoid animals potentially suffering stress from either acute lung inflammation or acute breathing deficiency throughout the 21 days; thus, we were not able to analyze any of these acute situations leading to a biased group of animals showing a milder injury-related phenotype. However, we consider that this group may represent repair/resolution of the milder state of the previously described fibrotic phenotype at *day 14*. In general, the group at *day 21* shows recovery of the BAL cells to normal values, except from the increased number of resident alveolar macrophages, and the slight increase (compared with *day 0*) in percentage of $CD90.1^+$ cells and hydroxyproline content (Fig. 6*D*).

Previously published work (3, 16, 21, 31, 40, 43, 45, 50, 51, 59, 61, 74, 79) showed with more or less detail the same results that we can confirm now here: the population of macrophages disappearing from the lung after bleomycin injury, and then recruited monocytes reach the alveolar spaces, potentially giving rise to new alveolar macrophages (40, 41), which become activated. Interesting are all the intermediate processes leading to fibrotic remodeling, such as the appearance of recruited monocytes or the second peak of granulocytes, correlating with the increasing expression of enzymes critical for collagen synthesis, such as arginase-1. These processes are still not well understood but may potentially be important for therapeutic approaches stopping or reversing remodeling of the lung tissue.

For the future development and understanding of the mechanisms involved in lung injury and fibrosis at different time points, functional analysis as well as development of new antibodies should be achieved. This method can also be readily used in the study of the effect of potential therapies applied in bleomycin-induced fibrosis in rats targeted to the alveolar immune system. Another advantage of our approach is that it allows other researchers to sort the cells, since all the molecular markers are membrane markers, allowing the study of living cells. After sorting, the different subsets of cells can be further analyzed by RT-PCR or transcriptomics to characterize their expression profiles, as recently done by Mould et al. (45).

In conclusion, we performed a comprehensive time-dependent study on bleomycin-induced lung injury and fibrosis in

rat, which confirmed previous findings obtained in mice. With a simple strategy, time-dependent events are described and correlated in time, highlighting the importance of the not-well-described transitioning events from lung injury to fibrotic development in a rat model.

ACKNOWLEDGMENTS

The authors thank Carina Vogt, Susanne Fassbender, and Andrea Herden for excellent technical support.

GRANTS

This work was supported by Biomedical Research in Endstage and Obstructive Lung Disease Hannover (BREATH), Member of the German Centre for Lung Research (DZL), Cluster of Excellence REBIRTH (Regenerative Biology to Reconstructive Therapy), and the German Research Foundation (DFG KN 916 1-1).

DISCLOSURES

No conflicts of interest, financial or otherwise, are declared by the author(s).

AUTHOR CONTRIBUTIONS

C.K. and E.L.-R. conceived and designed research; C.K., N.G., and E.L.-R. performed experiments; C.K., N.G., and E.L.-R. analyzed data; C.K. and E.L.-R. interpreted results of experiments; C.K. and E.L.-R. prepared figures; C.K., M.O., L.K., and E.L.-R. drafted manuscript; C.K., N.G., M.O., L.K., and E.L.-R. edited and revised manuscript; C.K., N.G., M.O., L.K., and E.L.-R. approved final version of manuscript.

REFERENCES

1. **Akbari O, DeKruyff RH, Umetsu DT.** Pulmonary dendritic cells producing IL-10 mediate tolerance induced by respiratory exposure to antigen. *Nat Immunol* 2: 725–731, 2001. doi:10.1038/90667.
2. **Ask K, Bonniaud P, Maass K, Eickelberg O, Margetts PJ, Warburton D, Groffen J, Gauldie J, Kolb M.** Progressive pulmonary fibrosis is mediated by TGF-beta isoform 1 but not TGF-beta3. *Int J Biochem Cell Biol* 40: 484–495, 2008. doi:10.1016/j.biocel.2007.08.016.
3. **Barnett-Vanes A, Sharrock A, Birrell MA, Rankin S.** A single 9-colour flow cytometric method to characterise major leukocyte populations in the rat: validation in a model of LPS-induced pulmonary inflammation. *PLoS One* 11: e0142520, 2016. doi:10.1371/journal.pone.0142520.
4. **Bonniaud P, Kolb M, Galt T, Robertson J, Robbins C, Stampfli M, Lavery C, Margetts PJ, Roberts AB, Gauldie J.** Smad3 null mice develop airspace enlargement and are resistant to TGF-β-mediated pulmonary fibrosis. *J Immunol* 173: 2099–2108, 2004. doi:10.4049/jimmunol.173.3.2099.
5. **Bosurgi L, Cao YG, Cabeza-Cabrerizo M, Tucci A, Hughes LD, Kong Y, Weinstein JS, Licona-Limon P, Schmid ET, Pelorosso F, Gagliani N, Craft JE, Flavell RA, Ghosh S, Rothlin CV.** Macrophage function in tissue repair and remodeling requires IL-4 or IL-13 with apoptotic cells. *Science* 356: 1072–1076, 2017. doi:10.1126/science.aai8132.
6. **Byrne AJ, Maher TM, Lloyd CM.** Pulmonary macrophages: a new therapeutic pathway in fibrosing lung disease? *Trends Mol Med* 22: 303–316, 2016. doi:10.1016/j.molmed.2016.02.004.
7. **Carré PC, Mortenson RL, King TE Jr, Noble PW, Sable CL, Riches DW.** Increased expression of the interleukin-8 gene by alveolar macrophages in idiopathic pulmonary fibrosis. A potential mechanism for the recruitment and activation of neutrophils in lung fibrosis. *J Clin Invest* 88: 1802–1810, 1991. doi:10.1172/JCI115501.
8. **Chavez-Santoscoy AV, Roychoudhury R, Pohl NLB, Wannemuehler MJ, Narasimhan B, Ramer-Tait AE.** Tailoring the immune response by targeting C-type lectin receptors on alveolar macrophages using "pathogen-like" amphiphilic polyanhydride nanoparticles. *Biomaterials* 33: 4762–4772, 2012. doi:10.1016/j.biomaterials.2012.03.027.
9. **Crestani B, Cornillet P, Dehoux M, Rolland C, Guenounou M, Aubier M.** Alveolar type II epithelial cells produce interleukin-6 in vitro and in vivo. Regulation by alveolar macrophage secretory products. *J Clin Invest* 94: 731–740, 1994. doi:10.1172/JCI117392.
10. **Dik WA, McAnulty RJ, Versnel MA, Naber BAE, Zimmermann LJI, Laurent GJ, Mutsaers SE.** Short course dexamethasone treatment following injury inhibits bleomycin induced fibrosis in rats. *Thorax* 58: 765–771, 2003. doi:10.1136/thorax.58.9.765.
11. **Domingo-Gonzalez R, Huang SK, Laouar Y, Wilke CA, Moore BB.** COX-2 expression is upregulated by DNA hypomethylation after hematopoietic stem cell transplantation. *J Immunol* 189: 4528–4536, 2012. doi:10.4049/jimmunol.1201116.
12. **Domingo-Gonzalez R, Katz S, Serezani CH, Moore TA, Levine AM, Moore BB.** Prostaglandin E2-induced changes in alveolar macrophage scavenger receptor profiles differentially alter phagocytosis of *Pseudomonas aeruginosa* and *Staphylococcus aureus* post-bone marrow transplant. *J Immunol* 190: 5809–5817, 2013. doi:10.4049/jimmunol.1203274.
13. **Domingo-Gonzalez R, Moore BB.** Defective pulmonary innate immune responses post-stem cell transplantation; review and results from one model system. *Front Immunol* 4: 126, 2013. doi:10.3389/fimmu.2013.00126.
14. **Endo M, Oyadomari S, Terasaki Y, Takeya M, Suga M, Mori M, Gotoh T.** Induction of arginase I and II in bleomycin-induced fibrosis of mouse lung. *Am J Physiol Lung Cell Mol Physiol* 285: L313–L321, 2003. doi:10.1152/ajplung.00434.2002.
15. **Fernandez IE, Eickelberg O.** The impact of TGF-β on lung fibrosis: from targeting to biomarkers. *Proc Am Thorac Soc* 9: 111–116, 2012. doi:10.1513/pats.201203-023AW.
16. **Garn H, Siese A, Stumpf S, Wensing A, Renz H, Gemsa D.** Phenotypical and functional characterization of alveolar macrophage subpopulations in the lungs of NO_2-exposed rats. *Respir Res* 7: 4, 2006. doi:10.1186/1465-9921-7-4.
17. **Girodet P-O, Nguyen D, Mancini JD, Hundal M, Zhou X, Israel E, Cernadas M.** Alternative macrophage activation is increased in asthma. *Am J Respir Cell Mol Biol* 55: 467–475, 2016. doi:10.1165/rcmb.2015-0295OC.
18. **Gordon S, Taylor PR.** Monocyte and macrophage heterogeneity. *Nat Rev Immunol* 5: 953–964, 2005. doi:10.1038/nri1733.
19. **Grommes J, Soehnlein O.** Contribution of neutrophils to acute lung injury. *Mol Med* 17: 293–307, 2011. doi:10.2119/molmed.2010.00138.
20. **Gundersen HJG.** The smooth fractionator. *J Microsc* 207: 191–210, 2002. doi:10.1046/j.1365-2818.2002.01054.x.
21. **Hamilton RF Jr, Li L, Felder TB, Holian A.** Bleomycin induces apoptosis in human alveolar macrophages. *Am J Physiol Lung Cell Mol Physiol* 269: L318–L325, 1995. doi:10.1152/ajplung.1995.269.3.L318.
22. **Hedrich CM, Bream JH.** Cell type-specific regulation of IL-10 expression in inflammation and disease. *Immunol Res* 47: 185–206, 2010. doi:10.1007/s12026-009-8150-5.
23. **Hoshino T, Okamoto M, Sakazaki Y, Kato S, Young HA, Aizawa H.** Role of proinflammatory cytokines IL-18 and IL-1β in bleomycin-induced lung injury in humans and mice. *Am J Respir Cell Mol Biol* 41: 661–670, 2009. doi:10.1165/rcmb.2008-0182OC.
24. **Izbicki G, Segel MJ, Christensen TG, Conner MW, Breuer R.** Time course of bleomycin-induced lung fibrosis. *Int J Exp Pathol* 83: 111–119, 2002. doi:10.1046/j.1365-2613.2002.00220.x.
25. **Jenkins RG, Moore BB, Chambers RC, Eickelberg O, Königshoff M, Kolb M, Laurent GJ, Nanthakumar CB, Olman MA, Pardo A, Selman M, Sheppard D, Sime PJ, Tager AM, Tatler AL, Thannickal VJ, White ES; ATS Assembly on Respiratory Cell and Molecular Biology.** An Official American Thoracic Society Workshop Report: Use of animal models for the preclinical assessment of potential therapies for pulmonary fibrosis. *Am J Respir Cell Mol Biol* 56: 667–679, 2017. doi:10.1165/rcmb.2017-0096ST.
26. **Kaku Y, Imaoka H, Morimatsu Y, Komohara Y, Ohnishi K, Oda H, Takenaka S, Matsuoka M, Kawayama T, Takeya M, Hoshino T.** Overexpression of CD163, CD204 and CD206 on alveolar macrophages in the lungs of patients with severe chronic obstructive pulmonary disease. *PLoS One* 9: e87400, 2014. doi:10.1371/journal.pone.0087400.
27. **Keane MP, Belperio JA, Moore TA, Moore BB, Arenberg DA, Smith RE, Burdick MD, Kunkel SL, Strieter RM.** Neutralization of the CXC chemokine, macrophage inflammatory protein-2, attenuates bleomycin-induced pulmonary fibrosis. *J Immunol* 162: 5511–5518, 1999.
28. **Reddy GK, Enwemeka CS.** A simplified method for the analysis of hydroxyproline in biological tissues. *Clin Biochem* 29: 225–229, 1996. doi:10.1016/0009-9120(96)00003-6.
29. **Khalil N, Parekh TV, O'Connor R, Antman N, Kepron W, Yehaualaeshet T, Xu YD, Gold LI.** Regulation of the effects of TGF-β1 by activation of latent TGF-β1 and differential expression of TGF-β receptors (TβR-I and TβR-II) in idiopathic pulmonary fibrosis. *Thorax* 56: 907–915, 2001. doi:10.1136/thorax.56.12.907.

30. **Knudsen L, Lopez-Rodriguez E, Berndt L, Steffen L, Ruppert C, Bates JHT, Ochs M, Smith BJ.** Alveolar micromechanics in bleomycin-induced lung injury. *Am J Respir Cell Mol Biol* 59: 757–769, 2018. doi:10.1165/rcmb.2018-0044OC.
31. **Landsman L, Jung S.** Lung macrophages serve as obligatory intermediate between blood monocytes and alveolar macrophages. *J Immunol* 179: 3488–3494, 2007. doi:10.4049/jimmunol.179.6.3488.
32. **Lappi-Blanco E, Kaarteenaho-Wiik R, Maasilta PK, Anttila S, Pääkkö P, Wolff HJ.** COX-2 is widely expressed in metaplastic epithelium in pulmonary fibrous disorders. *Am J Clin Pathol* 126: 717–724, 2006. doi:10.1309/PFGXCLNG2N17PJX9.
33. **Lopez-Rodriguez E, Boden C, Echaide M, Perez-Gil J, Kolb M, Gauldie J, Maus UA, Ochs M, Knudsen L.** Surfactant dysfunction during overexpression of TGF-β1 precedes profibrotic lung remodeling in vivo. *Am J Physiol Lung Cell Mol Physiol* 310: L1260–L1271, 2016. doi:10.1152/ajplung.00065.2016.
34. **Lutz D, Gazdhar A, Lopez-Rodriguez E, Ruppert C, Mahavadi P, Günther A, Klepetko W, Bates JH, Smith B, Geiser T, Ochs M, Knudsen L.** Alveolar derecruitment and collapse induration as crucial mechanisms in lung injury and fibrosis. *Am J Respir Cell Mol Biol* 52: 232–243, 2015. doi:10.1165/rcmb.2014-0078OC.
35. **Mathai SK, Gulati M, Peng X, Russell TR, Shaw AC, Rubinowitz AN, Murray LA, Siner JM, Antin-Ozerkis DE, Montgomery RR, Reilkoff RA, Bucala RJ, Herzog EL.** Circulating monocytes from systemic sclerosis patients with interstitial lung disease show an enhanced profibrotic phenotype. *Lab Invest* 90: 812–823, 2010. doi:10.1038/labinvest.2010.73.
36. **Mercer PF, Johns RH, Scotton CJ, Krupiczojc MA, Königshoff M, Howell DCJ, McAnulty RJ, Das A, Thorley AJ, Tetley TD, Eickelberg O, Chambers RC.** Pulmonary epithelium is a prominent source of proteinase-activated receptor-1-inducible CCL2 in pulmonary fibrosis. *Am J Respir Crit Care Med* 179: 414–425, 2009. doi:10.1164/rccm.200712-1827OC.
37. **Mestas J, Hughes CCW.** Of mice and not men: differences between mouse and human immunology. *J Immunol* 172: 2731–2738, 2004. doi:10.4049/jimmunol.172.5.2731.
38. **Minutti CM, Jackson-Jones LH, García-Fojeda B, Knipper JA, Sutherland TE, Logan N, Ringqvist E, Guillamat-Prats R, Ferenbach DA, Artigas A, Stamme C, Chroneos ZC, Zaiss DM, Casals C, Allen JE.** Local amplifiers of IL-4Rα-mediated macrophage activation promote repair in lung and liver. *Science* 356: 1076–1080, 2017. doi:10.1126/science.aaj2067.
39. **Minutti CM, Knipper JA, Allen JE, Zaiss DMW.** Tissue-specific contribution of macrophages to wound healing. *Semin Cell Dev Biol* 61: 3–11, 2017. doi:10.1016/j.semcdb.2016.08.006.
40. **Misharin AV, Morales-Nebreda L, Mutlu GM, Budinger GRS, Perlman H.** Flow cytometric analysis of macrophages and dendritic cell subsets in the mouse lung. *Am J Respir Cell Mol Biol* 49: 503–510, 2013. doi:10.1165/rcmb.2013-0086MA.
41. **Misharin AV, Morales-Nebreda L, Reyfman PA, Cuda CM, Walter JM, McQuattie-Pimentel AC, Chen C-I, Anekalla KR, Joshi N, Williams KJN, Abdala-Valencia H, Yacoub TJ, Chi M, Chiu S, Gonzalez-Gonzalez FJ, Gates K, Lam AP, Nicholson TT, Homan PJ, Soberanes S, Dominguez S, Morgan VK, Saber R, Shaffer A, Hinchcliff M, Marshall SA, Bharat A, Berdnikovs S, Bhorade SM, Bartom ET, Morimoto RI, Balch WE, Sznajder JI, Chandel NS, Mutlu GM, Jain M, Gottardi CJ, Singer BD, Ridge KM, Bagheri N, Shilatifard A, Budinger GRS, Perlman H.** Monocyte-derived alveolar macrophages drive lung fibrosis and persist in the lung over the life span. *J Exp Med* 214: 2387–2404, 2017. doi:10.1084/jem.20162152.
42. **Moeller A, Ask K, Warburton D, Gauldie J, Kolb M.** The bleomycin animal model: a useful tool to investigate treatment options for idiopathic pulmonary fibrosis? *Int J Biochem Cell Biol* 40: 362–382, 2008. doi:10.1016/j.biocel.2007.08.011.
43. **Mora AL, Torres-González E, Rojas M, Corredor C, Ritzenthaler J, Xu J, Roman J, Brigham K, Stecenko A.** Activation of alveolar macrophages via the alternative pathway in herpesvirus-induced lung fibrosis. *Am J Respir Cell Mol Biol* 35: 466–473, 2006. doi:10.1165/rcmb.2006-0121OC.
44. **Morris SM Jr.** Arginine: beyond protein. *Am J Clin Nutr* 83: 508S–512S, 2006. doi:10.1093/ajcn/83.2.508S.
45. **Mould KJ, Barthel L, Mohning MP, Thomas SM, McCubbrey AL, Danhorn T, Leach SM, Fingerlin TE, O'Connor BP, Reisz JA, D'Alessandro A, Bratton DL, Jakubzick CV, Janssen WJ.** Cell origin dictates programming of resident vs.recruited macrophages during acute lung injury. *Am J Respir Cell Mol Biol* 57: 294–306, 2017. doi:10.1165/rcmb.2017-0061OC.
46. **Munder M, Eichmann K, Morán JM, Centeno F, Soler G, Modolell M.** Th1/Th2-regulated expression of arginase isoforms in murine macrophages and dendritic cells. *J Immunol* 163: 3771–3777, 1999.
47. **Munger JS, Huang X, Kawakatsu H, Griffiths MJ, Dalton SL, Wu J, Pittet J-F, Kaminski N, Garat C, Matthay MA, Rifkin DB, Sheppard D.** A mechanism for regulating pulmonary inflammation and fibrosis: the integrin αvβ6 binds and activates latent TGF β1. *Cell* 96: 319–328, 1999. doi:10.1016/S0092-8674(00)80545-0.
48. **Murray PJ, Allen JE, Biswas SK, Fisher EA, Gilroy DW, Goerdt S, Gordon S, Hamilton JA, Ivashkiv LB, Lawrence T, Locati M, Mantovani A, Martinez FO, Mege J-L, Mosser DM, Natoli G, Saeij JP, Schultze JL, Shirey KA, Sica A, Suttles J, Udalova I, van Ginderachter JA, Vogel SN, Wynn TA.** Macrophage activation and polarization: nomenclature and experimental guidelines. *Immunity* 41: 14–20, 2014. doi:10.1016/j.immuni.2014.06.008.
49. **Ogushi F, Endo T, Tani K, Asada K, Kawano T, Tada H, Maniwa K, Sone S.** Decreased prostaglandin E2 synthesis by lung fibroblasts isolated from rats with bleomycin-induced lung fibrosis. *Int J Exp Pathol* 80: 41–49, 1999. doi:10.1046/j.1365-2613.1999.00096.x.
50. **Ortiz LA, Moroz K, Liu J-Y, Hoyle GW, Hammond T, Hamilton RF, Holian A, Banks W, Brody AR, Friedman M.** Alveolar macrophage apoptosis and TNF-α, but not p53, expression correlate with murine response to bleomycin. *Am J Physiol Lung Cell Mol Physiol* 275: L1208–L1218, 1998. doi:10.1152/ajplung.1998.275.6.L1208.
51. **Pechkovsky DV, Prasse A, Kollert F, Engel KMY, Dentler J, Luttmann W, Friedrich K, Müller-Quernheim J, Zissel G.** Alternatively activated alveolar macrophages in pulmonary fibrosis-mediator production and intracellular signal transduction. *Clin Immunol* 137: 89–101, 2010. doi:10.1016/j.clim.2010.06.017.
52. **Phan SH, Thrall RS, Ward PA.** Bleomycin-induced pulmonary fibrosis in rats: biochemical demonstration of increased rate of collagen synthesis. *Am Rev Respir Dis* 121: 501–506, 1980. doi:10.1164/arrd.1980.121.3.501.
53. **Pilling D, Roife D, Wang M, Ronkainen SD, Crawford JR, Travis EL, Gomer RH.** Reduction of bleomycin-induced pulmonary fibrosis by serum amyloid P. *J Immunol* 179: 4035–4044, 2007. doi:10.4049/jimmunol.179.6.4035.
54. **Pittet J-F, Griffiths MJD, Geiser T, Kaminski N, Dalton SL, Huang X, Brown LAS, Gotwals PJ, Koteliansky VE, Matthay MA, Sheppard D.** TGF-β is a critical mediator of acute lung injury. *J Clin Invest* 107: 1537–1544, 2001. doi:10.1172/JCI11963.
55. **Popova AP, Bozyk PD, Goldsmith AM, Linn MJ, Lei J, Bentley JK, Hershenson MB.** Autocrine production of TGF-β1 promotes myofibroblastic differentiation of neonatal lung mesenchymal stem cells. *Am J Physiol Lung Cell Mol Physiol* 298: L735–L743, 2010. doi:10.1152/ajplung.00347.2009.
56. **Prasse A, Pechkovsky DV, Toews GB, Jungraithmayr W, Kollert F, Goldmann T, Vollmer E, Müller-Quernheim J, Zissel G.** A vicious circle of alveolar macrophages and fibroblasts perpetuates pulmonary fibrosis via CCL18. *Am J Respir Crit Care Med* 173: 781–792, 2006. doi:10.1164/rccm.200509-1518OC.
57. **Punithavathi D, Venkatesan N, Babu M.** Curcumin inhibition of bleomycin-induced pulmonary fibrosis in rats. *Br J Pharmacol* 131: 169–172, 2000. doi:10.1038/sj.bjp.0703578.
58. **Rohani MG, McMahan RS, Razumova MV, Hertz AL, Cieslewicz M, Pun SH, Regnier M, Wang Y, Birkland TP, Parks WC.** MMP-10 regulates collagenolytic activity of alternatively activated resident macrophages. *J Invest Dermatol* 135: 2377–2384, 2015. doi:10.1038/jid.2015.167.
59. **Rosseau S, Hammerl P, Maus U, Walmrath H-D, Schütte H, Grimminger F, Seeger W, Lohmeyer J.** Phenotypic characterization of alveolar monocyte recruitment in acute respiratory distress syndrome. *Am J Physiol Lung Cell Mol Physiol* 279: L25–L35, 2000. doi:10.1152/ajplung.2000.279.1.L25.
60. **Russell REK, Culpitt SV, DeMatos C, Donnelly L, Smith M, Wiggins J, Barnes PJ.** Release and activity of matrix metalloproteinase-9 and tissue inhibitor of metalloproteinase-1 by alveolar macrophages from patients with chronic obstructive pulmonary disease. *Am J Respir Cell Mol Biol* 26: 602–609, 2002. doi:10.1165/ajrcmb.26.5.4685.
61. **Saito F, Tasaka S, Inoue K, Miyamoto K, Nakano Y, Ogawa Y, Yamada W, Shiraishi Y, Hasegawa N, Fujishima S, Takano H, Ishizaka A.** Role of interleukin-6 in bleomycin-induced lung inflamma-

tory changes in mice. *Am J Respir Cell Mol Biol* 38: 566–571, 2008. doi:10.1165/rcmb.2007-0299OC.

62. **Samokhin AO, Bühling F, Theissig F, Brömme D.** ApoE-deficient mice on cholate-containing high-fat diet reveal a pathology similar to lung sarcoidosis. *Am J Pathol* 176: 1148–1156, 2010. doi:10.2353/ajpath.2010.090857.
63. **Selman M, Ruiz V, Cabrera S, Segura L, Ramírez R, Barrios R, Pardo A.** TIMP-1, -2, -3, and -4 in idiopathic pulmonary fibrosis. A prevailing nondegradative lung microenvironment? *Am J Physiol Lung Cell Mol Physiol* 279: L562–L574, 2000. doi:10.1152/ajplung.2000.279.3.L562.
64. **Sheppard D.** Transforming growth factor beta: a central modulator of pulmonary and airway inflammation and fibrosis. *Proc Am Thorac Soc* 3: 413–417, 2006. doi:10.1513/pats.200601-008AW.
65. **Sokai A, Handa T, Tanizawa K, Oga T, Uno K, Tsuruyama T, Kubo T, Ikezoe K, Nakatsuka Y, Tanimura K, Muro S, Hirai T, Nagai S, Chin K, Mishima M.** Matrix metalloproteinase-10: a novel biomarker for idiopathic pulmonary fibrosis. *Respir Res* 16: 120, 2015. doi:10.1186/s12931-015-0280-9.
66. **Shi JD, Golden T, Guo CJ, Tu SP, Scott P, Lee MJ, Yang CS, Gow AJ.** Tocopherol supplementation reduces NO production and pulmonary inflammatory response to bleomycin. *Nitric Oxide* 34: 27–36, 2013. doi:10.1016/j.niox.2013.04.006.
67. **Steffen L, Ruppert C, Hoymann H-G, Funke M, Ebener S, Kloth C, Mühlfeld C, Ochs M, Knudsen L, Lopez-Rodriguez E.** Surfactant replacement therapy reduces acute lung injury and collapse induration-related lung remodeling in the bleomycin model. *Am J Physiol Lung Cell Mol Physiol* 313: L313–L327, 2017. doi:10.1152/ajplung.00033.2017.
68. **Sugahara K, Iyama K, Kuroda MJ, Sano K.** Double intratracheal instillation of keratinocyte growth factor prevents bleomycin-induced lung fibrosis in rats. *J Pathol* 186: 90–98, 1998. doi:10.1002/(SICI)1096-9896(199809)186:1<90:AID-PATH137>3.0.CO;2-X.
69. **Sun J, Cardani A, Sharma AK, Laubach VE, Jack RS, Müller W, Braciale TJ.** Autocrine regulation of pulmonary inflammation by effector T-cell derived IL-10 during infection with respiratory syncytial virus. *PLoS Pathog* 7: e1002173, 2011. doi:10.1371/journal.ppat.1002173.
70. **Sun L, Louie MC, Vannella KM, Wilke CA, LeVine AM, Moore BB, Shanley TP.** New concepts of IL-10-induced lung fibrosis: fibrocyte recruitment and M2 activation in a CCL2/CCR2 axis. *Am J Physiol Lung Cell Mol Physiol* 300: L341–L353, 2011. doi:10.1152/ajplung.00122.2010.
71. **Thrall RS, McCormick JR, Jack RM, McReynolds RA, Ward PA.** Bleomycin-induced pulmonary fibrosis in the rat: inhibition by indomethacin. *Am J Pathol* 95: 117–130, 1979.
72. **Venosa A, Katzen J, Tomer Y, Kopp M, Jamil S, Russo SJ, Mulugeta S, Beers MF.** Epithelial expression of an interstitial lung disease-associated mutation in surfactant protein-C modulates recruitment and activation of key myeloid cell populations in mice. *J Immunol* 202: 2760–2771, 2019. doi:10.4049/jimmunol.1900039.
73. **Venosa A, Malaviya R, Choi H, Gow AJ, Laskin JD, Laskin DL.** Characterization of distinct macrophage subpopulations during nitrogen mustard-induced lung injury and fibrosis. *Am J Respir Cell Mol Biol* 54: 436–446, 2016. doi:10.1165/rcmb.2015-0120OC.
74. **Wang H-D, Yamaya M, Okinaga S, Jia Y-X, Kamanaka M, Takahashi H, Guo L-Y, Ohrui T, Sasaki H.** Bilirubin ameliorates bleomycin-induced pulmonary fibrosis in rats. *Am J Respir Crit Care Med* 165: 406–411, 2002. doi:10.1164/ajrccm.165.3.2003149.
75. **Wu G, Morris SM Jr.** Arginine metabolism: nitric oxide and beyond. *Biochem J* 336: 1–17, 1998. doi:10.1042/bj3360001.
76. **Xu YD, Hua J, Mui A, O'Connor R, Grotendorst G, Khalil N.** Release of biologically active TGF-β1 by alveolar epithelial cells results in pulmonary fibrosis. *Am J Physiol Lung Cell Mol Physiol* 285: L527–L539, 2003. doi:10.1152/ajplung.00298.2002.
77. **Yehualaeshet T, O'Connor R, Green-Johnson J, Mai S, Silverstein R, Murphy-Ullrich JE, Khalil N.** Activation of rat alveolar macrophage-derived latent transforming growth factor β-1 by plasmin requires interaction with thrombospondin-1 and its cell surface receptor, CD36. *Am J Pathol* 155: 841–851, 1999. doi:10.1016/S0002-9440(10)65183-8.
78. **Zasłona Z, Okunishi K, Bourdonnay E, Domingo-Gonzalez R, Moore BB, Lukacs NW, Aronoff DM, Peters-Golden M.** Prostaglandin E_2 suppresses allergic sensitization and lung inflammation by targeting the E prostanoid 2 receptor on T cells. *J Allergy Clin Immunol* 133: 379–387.e1, 2014. doi:10.1016/j.jaci.2013.07.037.
79. **Zhao HW, Hu SY, Barger MW, Ma JKH, Castranova V, Ma JYC.** Time-dependent apoptosis of alveolar macrophages from rats exposed to bleomycin: involvement of tnf receptor 2. *J Toxicol Environ Health A* 67: 1391–1406, 2004. doi:10.1080/15287390490471569.

Reprinted with permission

RELEVANCE OF THIS WORK

In this paper, we concluded that before the onset of lung fibrosis myeloid cells may play an important role as first response to an injury and remodeling stimuli. We could observe many changes in the myeloid cell population before collagen deposition and CD90⁺ cells (fibroblast) recruitment. Within myeloid cells, we focused on alveolar macrophages, which are in addition to important players in the innate immune system, also responsible of the alveolar homeostasis, including lung surfactant metabolism (degradation and recycling).

Monocyte recruitment may be important as precursors of alveolar macrophages. In addition, fibrocytes are derived from monocytes and these are precursors of fibroblasts, which are responsible of producing collagen. Very interestingly, we found that recruited monocytes are a source of pro-fibrotic markers, such as TGF-b1 and Cox2, directly related to the stimulation of collagen deposition by fibroblasts and tissue remodeling. These results point at alveolar macrophages and recruited monocytes as new therapeutic targets for the treatment of lung fibrosis.

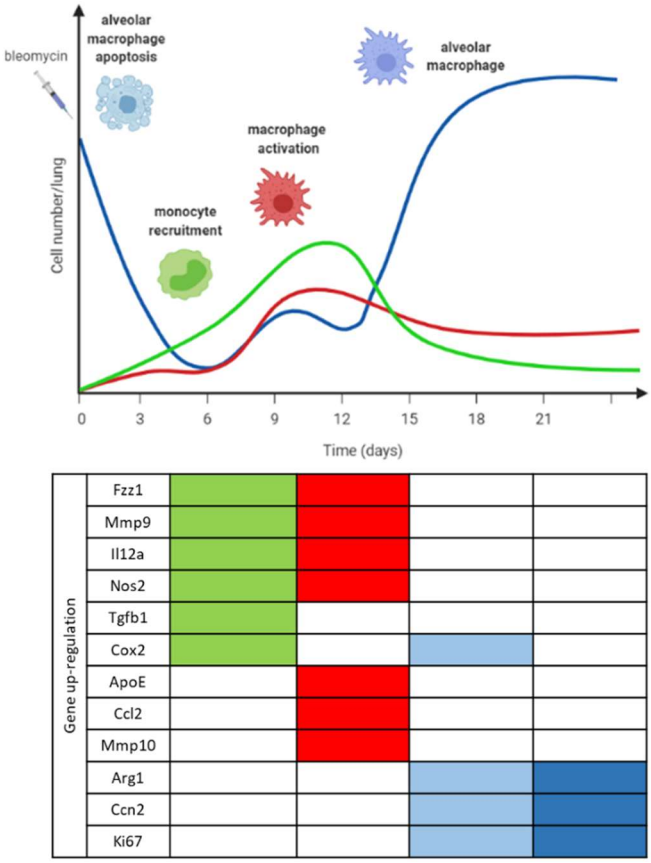

Figure 4: Top panel: overview of the changes of monocyte and macrophage populations after bleomycin application (Created with BioRender.com). Bottom panel: genes upregulated in the different populations (monocytes, activated macrophages and macrophages at day 14 or 21 after bleomycin application compared to naïve alveolar macrophages) related to lung fibrotic remodeling and macrophage activation state.

3 LUNG SURFACTANT AS TREATMENT FOR LUNG FIBROSIS

3.1 SURFACTANT REPLACEMENT THERAPY (ORIGINAL WORK 4)

Steffen L., Ruppert C., Hoymann H.G., Funke M., Ebener S., Kloth C., Mühlfeld C., Ochs M., Knudsen L*. & Lopez-Rodriguez E*. *"Surfactant replacement therapy reduces acute lung injury and collapse induration-related lung remodeling in the bleomycin model"* American Journal of Physiology - Lung Cell and Molecular Physiology. 2017; 313(2): L313-L327.

The important role of lung surfactant in helping to regulate some of the physical forces in the lung has become clearer in the last chapters. In addition, already in 1988, the role of alveolar collapse in the development of fibrotic remodeling in the lung has been already described by Myers and Katzenstein (116). The connection between high surface tension and alveolar collapse is also well described in the acute respiratory distress syndrome (ARDS) and acute lung injury (ALI) (117, 118). In this field, many studies already showed increased surface tension, and the associated alveolar instability, in ARDS (119, 120) leading to an acute respiratory pathology with a high mortality. In addition, patients recovering from ARDS are at higher risk to develop lung fibrosis after recovery, leading to the hypothesis that both diseases may have underlying similar mechanisms (6, 121). These mechanisms, alveolar collapse, respiratory distress, and disease in-homogeneities through the lung have been demonstrated in patients from both diseases (119, 122, 123).

Repetitive alveolar collapse (or atelectrauma) caused by lung surfactant inactivation has been directly linked to alveolar wall stretching and ductal air space over-distension (124). During expiration, the alveolar surface area is reduced by alveolar septal wall folding. In the presence of an active surfactant, surface tension is theoretically low enough to prevent both walls to glue to each other permanently. In the absence of an active surfactant, the fluid lining the alveoli will tend to minimize the area exposed to the air closing the alveolus.

During inspiration, the transpulmonary pressure gradient is normally sufficient to inflate or open (recruit (R)) the closed alveoli (de-recruited (D)), also called alveolar R/D. Some physiological alveolar R/D exists in every breathing cycle (125), however it imposes some mechanical stress in the alveolar epithelium (126). The mechanical axial shear forces needed to re-open the alveoli may lead to injurious deformation of AE2C. It has been already described that these cell-damaging forces strongly increase with higher surface tension at the interface of the lining fluid (127, 128). In addition, AE2C injury reduces epithelial integrity, which may result in leaking and formation of edematous material at the alveolar spaces, which in turn, inactivates surfactant. This may trigger a vicious chronic cycle of AE2C injury and surfactant

dysfunction preceding fibrotic remodeling (129-131). On the other hand, if the maximal generated transpulmonary pressure fails to exceed the intra-alveolar pressure, the alveolus remains collapsed and its alveolar walls stay adjacent to each other. This may trigger the permanent closing of the alveolus, permanent de-recruitment or collapse induration. These atelectatic areas also impose stretching forces on the surrounding alveolar walls, which may experience further mechanical stress and may over-distend (as seen in Chapter 2.2). These atelectatic areas, where the alveolar surface is lost are not functional in the gas exchange and as two alveolar walls are "glued" together, this contributes to the septal wall thickening (Figure 5), which in turn may stimulate the production of pro-fibrotic cytokines and collagen.

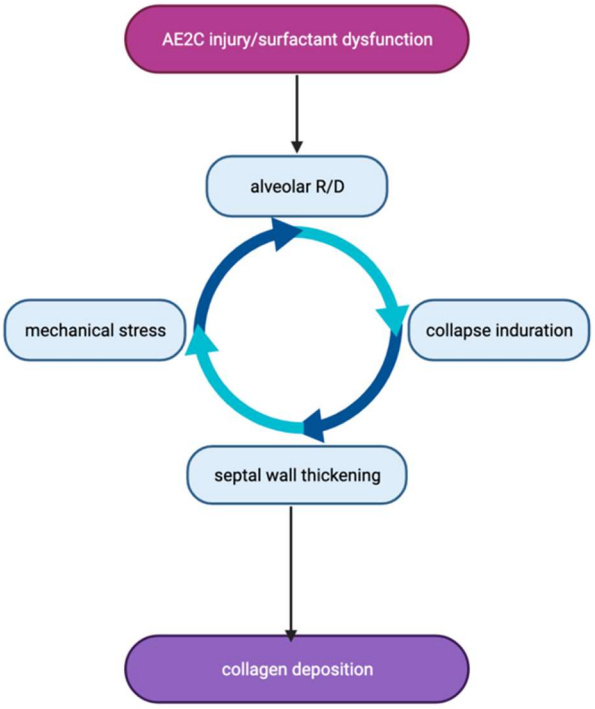

Figure 5: "mechanical injuries" due to lung surfactant dysfunction leading to fibrotic development (Created in BioRender.com).

As shown before, lung surfactant dysfunction and dysregulation occur in early stages of lung injury and precedes lung fibrotic remodeling in the bleomycin induced lung injury and fibrosis animal model (115). Therefore, it seems reasonable to replace surfactant as soon as possible in the development of the disease, as preventive treatment therapeutic strategy, and later during the onset of the fibrotic remodeling, in order to understand if the "treatment of the mechanical injuries" may decrease or slow down the development of fibrosis, as supportive therapeutic strategy.

The aim of this work was to investigate whether a surfactant replacement therapy may be beneficial to stop or slow down the development of fibrotic remodeling. For this purpose, we used the bleomycin induced lung injury and fibrosis rat model. We performed SRT early in the lung injury phase of the model and analyzed early events (day 3), including inflammation, and later on the onset of fibrosis (day 7) to analyze fibrotic molecular and structural markers. We hypothesized that: SRT may stabilize alveoli preventing mechanical injuries during lung injury and fibrotic development in the bleomycin rat model. To test this hypothesis, we investigated if: 1) preventing alveolar collapse early in the lung injury phase of the model may decrease the alveolar R/D and mechanical stress leading to a reduced inflammatory response; and 2) preventing collapse induration during the onset of lung fibrosis may decrease the septal wall thickening and collagen deposition delaying the development of a fibrotic phenotype.

Am J Physiol Lung Cell Mol Physiol 313: L313–L327, 2017.
First published April 27, 2017; doi:10.1152/ajplung.00033.2017.

RESEARCH ARTICLE | *Translational Research in Acute Lung Injury and Pulmonary Fibrosis*

Surfactant replacement therapy reduces acute lung injury and collapse induration-related lung remodeling in the bleomycin model

Lilian Steffen,[1] Clemens Ruppert,[2] Heinz-Gerd Hoymann,[3] Manuela Funke,[4,5] Simone Ebener,[4,5] Christina Kloth,[1] Christian Mühlfeld,[1,6] Matthias Ochs,[1,6] Lars Knudsen,[1,6]* and Elena Lopez-Rodriguez[1,6]*

[1]*Institute of Functional and Applied Anatomy, Hannover Medical School, Germany and Biomedical Research in Endstage and Obstructive Lung Disease Hannover, Member of the German Center for Lung Research, Hannover, Germany;* [2]*Department of Internal Medicine, Justus-Liebig-University Giessen, Germany, and Universities of Giessen and Marburg Lung Center, Member of the German Center for Lung Research (DZL), Giessen, Germany;* [3]*Fraunhofer Institute of Toxicology and Experimental Medicine, Hannover, Germany;* [4]*Department of Pulmonary Medicine, Bern University Hospital, University of Bern, Bern, Switzerland;* [5]*Department of Clinical Research, University of Bern, Bern, Switzerland; and* [6]*Cluster of Excellence Regenerative Biology to Reconstructive Therapy, Hannover, Germany*

Submitted 26 January 2017; accepted in final form 22 April 2017

Steffen L, Ruppert C, Hoymann H, Funke M, Ebener S, Kloth C, Mühlfeld C, Ochs M, Knudsen L, Lopez-Rodriguez E. Surfactant replacement therapy reduces acute lung injury and collapse induration-related lung remodeling in the bleomycin model. *Am J Physiol Lung Cell Mol Physiol* 313: L313–L327, 2017. First published April 27, 2017; doi:10.1152/ajplung.00033.2017.—Bleomycin-induced lung injury leads to surfactant dysfunction and permanent loss of alveoli due to a remodeling process called collapse induration. Collapse induration also occurs in acute interstitial lung disease and idiopathic pulmonary fibrosis in humans. We hypothesized that surfactant dysfunction aggravates lung injury and early remodeling resulting in collapse induration within 7 days after lung injury. Rats received bleomycin to induce lung injury and either repetitive surfactant replacement therapy (SRT: 100 mg Curosurf/kg BW = surf group) or saline (0.9% NaCl = saline group). After 3 (D3) or 7 (D7) days, invasive pulmonary function tests were performed to determine tissue elastance (H) and static compliance (Cst). Bronchoalveolar lavage (BAL) was taken for surfactant function, inflammatory markers, and protein measurements. Lungs were fixed by vascular perfusion for design-based stereology and electron microscopic analyses. SRT significantly improved minimum surface tension of alveolar surfactant as well as H and Cst at D3 and D7. At D3 decreased inflammatory markers including neutrophilic granulocytes, IL-1β, and IL-6 correlated with reduced BAL-protein levels after SRT. Numbers of open alveoli were significantly increased at D3 and D7 in SRT groups whereas at D7 there was also a significant reduction in septal wall thickness and parenchymal tissue volume. Septal wall thickness and numbers of open alveoli highly correlated with improved lung mechanics after SRT. In conclusion, reduction in surface tension was effective to stabilize alveoli linked with an attenuation of parameters of acute lung injury at D3 and collapse induration at D7. Hence, SRT modifies disease progression to collapse induration.

surfactant; collapse induration; lung injury and fibrosis; stereology; bleomycin

MECHANICAL STRESS is well accepted to contribute to the pathogenesis of acute lung injury in particular in the context of ventilator-induced lung injury where mechanical ventilation can aggravate preexisting early stages of lung injury (11, 50). Harmful stresses operating on lung parenchyma result from atelectrauma and volutrauma (63). Atelectrauma is a consequence of instability of distal airspaces with intratidal alveolar recruitment/derecruitment (alveolar R/D) (59), whereas heterogeneous ventilation with dynamic overstretching of some distal airspaces during ventilation is the basic concept behind volutrauma (43). A key mechanism resulting in alveolar R/D and therefore atelectrauma in acute lung injury is surfactant dysfunction which fails to stabilize alveoli at low lung volumes during ventilation (4, 50). Surfactant dysfunction has not only been linked with acute lung injury but also with diseases resulting from repetitive or ongoing injury of the alveolar epithelium such as idiopathic pulmonary fibrosis (IPF) (19). Although the impact of high surface tension for disease progression in IPF is currently not clear, animal models suggest a relevant causal relationship between alveolar epithelial type II (AE2) cell dysfunction, surfactant dysfunction, high surface tension with mechanical stress, and profibrotic remodeling (36, 40, 72). Recent studies provided evidence that mechanical stress in IPF lung tissue results in excessive release of profibrotic factors such as TGF-β1 (13). However, it is not clear if mechanical stress due to surfactant dysfunction during spontaneous breathing is also an independent trigger of ongoing lung injury and remodeling. The typical distribution of pathological lesions, however, suggests a role of mechanical stress as an aggravating factor for tissue remodeling in the IPF lungs (9). The effects of IPF on lung structure are complex since it involves interstitial fibrosis (31, 32) but also alveolar collapse most likely resulting from high surface tension (32, 35, 46). Alveolar collapse as such has been shown to contribute to

* L. Knudsen and E. Lopez-Rodriguez contributed equally to this work.
Address for reprint requests and other correspondence: L. Knudsen, Inst. of Functional and Applied Anatomy, Hannover Medical School, Carl-Neuberg Str. 1, 30625 Hannover, Germany (e-mail: Knudsen.lars@mh-hannover.de).

septal wall thickening, mimicking interstitial remodeling in acute idiopathic interstitial pneumonia (24). Similar findings could be reproduced in animal models of lung injury and fibrosis induced by amiodarone (6) or by bleomycin as early as 7 days after injury (39). Since the alveolar epithelial basal lamina was absorbed in interstitial tissue, pathologists referred to the term "collapse induration" or "collapse cirrhosis" meaning that alveoli which are injured and remain collapsed throughout a longer period will not be able to be reopened due to remodeling. This remodeling includes overgrowth of the entrances of collapsed alveoli by alveolar epithelial cells and an obliteration of their former lumen: opposing denuded basal laminae are glued together so that the collapsed airspace is integrated into the thickened septal wall becoming part of the interstitial tissue (8, 29). Coxson and coworkers performed a quantitative morphological study in IPF lungs and observed that the main consequence of IPF on lung structure is a dramatic decline in surface area of the alveolar epithelium (12) so that it has been discussed very comprehensively that alveolar collapse and collapse induration are extremely important pathological events in fibrosing lung diseases (35, 46, 67). Also, micro-CT studies from human IPF suggest that alveolar collapse takes place at a very early stage of the disease in the absence of severe fibrotic remodeling so that it obviously predates collagen deposition in IPF (41). Structure-function relationships in the bleomycin model of lung injury and fibrosis showed that the number of open alveoli per lung was highly correlated with lung mechanical impairment (39). During the first 3 days after bleomycin instillation alveoli could be opened with increasing positive end-expiratory pressure (PEEP) ventilation whereas this was not the case at *day 7*, where collapse induration-related remodeling was seen (28). Similar structural findings were found in biopsies of patients suffering from acute interstitial pneumonia (24) or usual interstitial pneumonia (46). In the bleomycin model the decrease in alveolar number per lung which ends at *day 7* in collapse induration was associated with severe surfactant dysfunction (39, 60, 66). In this model, the fate of injured alveoli can be characterized by initial intratidal alveolar R/D (*day 1*), permanent alveolar derecruitment [not yet remodeled but collapsed at physiological pressures (*day 3*)], and persistent alveolar derecruitment due to remodeling [collapse induration (*day 7*)]. These events occur during the first week in this model and during the same period lung mechanical properties decline to the worst values. During fibroproliferation including collagen deposition there is no further loss of alveoli and most importantly lung function in this model (39). Hence, alveolar collapse and collapse induration occurs before collagen deposition and are highly linked with lung mechanical degradation. The present study was designed to test the hypothesis that surfactant dysfunction triggers acute lung injury with alveolar derecruitment as well as early lung remodeling resulting in collapse induration. For this purpose, bleomycin-challenged lungs were intratracheally treated with exogenous surfactant of porcine origin (Curosurf), to prevent high surface tension due to endogenous surfactant dysfunction, or saline. Structural and functional data were used as primary read-out parameters.

MATERIALS AND METHODS

Animal model. All animal experiments were approved by the authorities of Lower Saxony, Germany (LAVES: Niedersächsisches Landesamt für Verbraucherschutz und Lebensmittelsicherheit), which house the German equivalent of an institutional animal care and use committee, according to the European Animal Welfare Regulations (Approval No.: 12/1022). The rat model of bleomycin-induced lung injury and fibrosis was used in this study as described elsewhere (39). Male Wistar WU rats ($N = 70$) at the age of 10 wk were obtained from Charles River, Sulzfeld, Germany. Animals were anesthetized using an inhalation narcosis with 4% isoflurane at room air in a Plexiglas chamber. Animals were intubated with an 18G plastic catheter, and 1 U of bleomycin dissolved in 330 μl 0.9% NaCl was instilled into the lungs using a Microsprayer aerosolizer (PennCentury). Body weight and a clinical score were documented daily. Another group of animals randomized into the healthy control (= control) group did not receive bleomycin instillation.

Therapeutic interventions. For surfactant replacement therapy (SRT), the porcine-derived natural surfactant preparation Curosurf was used. Curosurf was supplied for research purposes within the scope of an in-kind donation by Chiesi Pharmaceutics, Parma, Italy. Animals were anesthetized, intubated, and instilled using a MicroSprayer Aerosolizer-Model IA-1B (PennCentury, Wyndmoor, PA) (mass median diameter of the droplet of 25–30 μm) with either prewarmed (37°C) Curosurf in a dosage of 100 mg/kg body wt (= surf groups) or an equivalent volume of 0.9% NaCl solution representing the vehicle/solvent of Curosurf (= saline groups). Provided no differences between bleomycin alone and bleomycin + NaCl treatment (data not shown), NaCl controls here serve as therapy controls with the same number of instrumentations of the animals, by means of intubation and intratracheal instillation of a volume of liquid into the lungs (37). Treatments were performed on *days 1* and *2* after bleomycin challenge for evaluations on *day 3* ($N = 33$) or *days 1, 2, 4*, and *5* for animals analyzed at *day 7* ($N = 26$). The control group did not receive any treatment.

Lung mechanical measurements. All animals were anesthetized with isoflurane, orotracheally intubated, and subjected to invasive pulmonary function tests during spontaneous respiration to calculate dynamic compliance from dynamic pressure-volume loops according to published methodology (21). Afterwards 5–7 of the animals of each group underwent BAL. In all other animals the depth of anesthesia was increased to perform invasive pulmonary function tests during mechanical ventilation followed by fixation of the lung for structural analyses. Procedures related to measurements of lung mechanics during invasive ventilation are described in detail in the online supplement of reference (39). In brief, animals were anesthetized using 80 mg/kg ketamine and 5 mg/kg xylazine solution in 0.9% NaCl, tracheostomized, and volume controlled mechanically ventilated by means of a FlexiVent rodent ventilator (Scireq, Montreal, Canada) with a tidal volume of 10 ml/kg body wt, PEEP of 3 or 6 cmH_2O, and an inspiratory to expiratory (I:E) ratio of 0.67. A muscle relaxation with pancuronium bromide was attained by intraperitoneal application. Following a run in phase of at least 5 min, a script was started, and the following perturbations and measurements were recorded: 2 recruitment maneuvers consisting of total lung capacity perturbation for measurement of inspiratory capacity (IC) followed by repetitive measurements of tissue elastance (H) by means of forced oscillation perturbation (FOT) every 30 s for 5 min. Tissue elastance (H) as performed by FOT (forced oscillation technique) and calculated by fitting to the CPM (constant phase model) is interpreted as elastic rigidity/stiffness of the lung tissue or the energy conservation in the alveoli. At the end, three pressure-controlled pressure-volume loops were performed, and quasi-static compliance was calculated. H measurements were carried out after recruitment maneuvers (= total lung capacity perturbation) during ventilation with both PEEP of 3 cmH_2O and PEEP of 6 cmH_2O using the same PEEP pressure during

the FOT of 3 or 6 cmH_2O. Hence, even during FOT the airway opening pressure did not fall below 3 or 6 cmH_2O.

Perfusion fixation and tissue processing for design-based stereology. After analysis of lung mechanics, a median laparotomy was performed followed by the preparation of the caudal vena cava and abdominal aorta. The abdominal aorta was opened for exsanguination. The lungs were slowly inflated to a maximum pressure of 30 cmH_2O over a period of 6 s; maximum pressure of 30 cmH_2O was kept stable for 3 s before the lung was slowly deflated to a positive end-expiratory airway opening pressure of 5 cmH_2O. This maneuver mimicked the total lung capacity recruitment maneuver. At fixed positive end-expiratory airway opening pressure of 5 cmH_2O, the trachea was ligated. A perfusion fixation was carried out via the caudal vena cava after opening of the abdominal aorta applying a hydrostatic pressure of 40 cmH_2O. Initially, the pulmonary vasculature was rinsed with 0.9% NaCl until the fluid coming out of the opened aorta cleared. Afterwards, the fixative consisting of 1.5% glutaraldehyde, 1.5% paraformaldehyde in 0.15 M HEPES buffer was perfused through the lung. Finally, the lung was dissected and placed in the fixative for at least 2 days at 4°C temperature. After fixation of the lung, structures not belonging to the lung such as the heart were carefully removed and the volume of the lung [V(lung)] was determined by means of fluid displacement, which produces comparable results when compared with the Cavalieri principle (57). Tissue sampling and embedding in hydroxyethylmethacrylate (Technovit 8100, Haerus Kulzer, Wehrheim, Germany) were performed as described elsewhere (61, 68). Six to nine tissue blocks per lung were sampled and included in this study. Plastic embedded tissue was cut in 1.5-μm-thick sections, and the first and the fourth of a consecutive row of sections were mounted on a glass slide and stained with toluidine blue.

Design-based stereology. Design-based stereology is the gold standard of image-based morphometry. It results in unbiased quantitative information on three-dimensional (3D) structures based on measurements on two-dimensional (2D) sections (7, 70).

The stereological analysis was performed with an Axioskop light microscope DM6000B (Leica, Wetzlar, Germany) equipped with a digital camera DP72 (Olympus, Hamburg, Germany), a slide scanner Axio Scan.Z1 (Zeiss, Göttingen, Germany), and a computer equipped with newCAST stereology software (Visiopharm, Horsholm, Denmark).

For volume estimation point probes on single thin sections were analyzed. The test system design was adjusted with the aim of 100–200 counting events per parameter of interest per animal using 6–9 sections and ~100 fields of view in total. This usually results in a sufficient precision of the stereological parameter (16, 17). A counting event is defined as a "hit" on the structure of interest. In the first step (10× magnification) the parameters parenchyma [V(par, lung)] and nonparenchyma [V(nonpar,lung)] were determined. Parenchyma was defined as all structures taking part in the process of gas exchange, non-parenchyma as conducting airways, pleura, larger vessels and associated connective tissue (54). Following a cascade sampling design, the parenchyma was differentiated into alveolar space [V(alvair,lung)], ductal space [V(ductair,lung)], alveolar septal tissue [V(sep,lung)], and alveolar edema [V(alved,lung)] in the second step (20× magnification). Also, the surface area of alveolar walls covered by air [S(alvair,lung)] or alveolar edema [S(alved,lung)] were estimated. All parameters of interest were determined according to current recommendations for structural quantification of lung injury and fibrosis (48).

Volume fractions, e.g., V_v(par/lung), could be calculated by dividing points hitting lung parenchyma and the total number of points hitting the reference space corresponding to the total lung (52).

$$V_v(\text{par/lung}) = \frac{\sum P(\text{par})}{\sum P(\text{total})}$$

By multiplying the volume fraction (V_v) with the total lung volume [V(lung) = the reference space], the absolute volume of each structure of interest could be determined.

$$V_v(\text{par/lung}) \cdot V(\text{lung})(\text{ml}) = V(\text{par,lung})(\text{ml})$$

Equivalent formulas were used to differentiate the structures of the parenchyma, e.g., alveolar space:

$$V_v(\text{alvair/par}) = \frac{\sum P(\text{alvair})}{\sum P(\text{par})}$$

$$V_v(\text{alvair/par}) \cdot V(\text{par,lung})(\text{ml}) = V(\text{alvair,lung})(\text{ml}).$$

Second, line probes were used and intersections between the test line and the interface of alveolar wall and alveolar airspace or alveolar edema were used to determine the surface density (S_v) of alveolar walls covered by air or alveolar edema (cm^{-1}), respectively. The surface density represents the area of an interface within a reference volume: in this case the functional (air-covered) or nonfunctional (edematous) area of gas exchange surface. By multiplying S_v with the reference volume we calculated the surface area (cm^2), an absolute parameter for the total lung.

$$S_v(\text{alvair/par})(\text{cm}^{-1}) = \frac{2 \cdot \sum I(\text{epiair})}{\left(\frac{\ell}{p}\right) \cdot \sum P(\text{line par})}$$

$$S(\text{alvair,lung})(\text{cm}^2) = S_v(\text{alvair/par})(\text{cm}^{-1}) \cdot V(\text{par,lung})(\text{cm}^3).$$

Here, I(epiair) corresponds to the intersections of the test line with alveolar epithelium covered by air, P(line par) is the number of test lines hitting lung parenchyma, and l/p is the length of one test line. Thereupon the septal wall thickness could be calculated:

$$\tau(\text{sep}) = \frac{V_v(\text{sep/par})}{S_v(\text{alvair/par})} \cdot 2(\mu\text{m}).$$

The number of ventilated alveoli per lung [*N*(alv,lung)] was determined with a physical disector at the light microscopic level (5, 10) and the number-weighted mean alveolar volume [ν_n(alv)] was calculated as a ratio of total volume of alveolar airspaces and number of open alveoli. The disector pair consisted of sections from the same area of the lung, and the distance from the top of one section to the top of the other section was 4.5 μm (= disector height). Using a counting frame with a size of 45,042 μm^2 a volume was generated in which the numbers of open alveoli could be counted. A counting event was defined as an alveolus which was open (connected to alveolar duct) on the one section but closed on the other section. Within the defined test volume [disector height multiplied by size of the counting frame and total number of counting frames], the density of alveolar openings per unit reference space was determined. By multiplication of the numerical density of alveolar openings with the reference space, absolute numbers per organ were calculated.

BAL fluid and tissue analyses. Six separate animals for each group were included in this study for analyses of bronchoalveolar lavage (BAL) fluid and tissue. Animals were tracheostomized, the chest opened, and the pulmonary vasculature rinsed free of blood cells using a 0.9% NaCl solution after euthanizing by exsanguination. Afterwards, lungs were washed with 3 aliquots of 5 ml 0.9% NaCl, and ~13 ml of BAL fluid per lung was recovered. BAL fluid was centrifuged; the supernatant was frozen in liquid nitrogen for further assessments of surfactant function, measurements of cytokine/chemokines, as well as protein levels while the cells were directly subjected to FACS analyses. Briefly, BAL cells were analyzed by flow cytometry using antibodies recognizing CD45 and CD11b/c (Miltenyi Biotec, Bergisch Gladbach, Germany) to identify the lymphocytes and the macrophages/granulocytes population (M/G-population). Additionally M/G-population was than first differentiated via α-CD163 (Bio-Rad, Puchheim, Germany) into activated macrophages (CD163+ cells) and

granulocytes/monocytes (CD163− cells) and finally CD163− cells were divided into granulocytes and monocytes using the α-granulocytes antibody from Miltenyi Biotec (clone REA535). At *day 3*, MCP-1, IL1-β, IL-4, IL-6, and Il-10 were determined using the BioPlex magnetic beat-based multiplex immunoassay according to the manufacturer's instructions (BioPlex Pro, Bio-Rad, Germany). Biophysical properties of BAL derived alveolar surfactant were evaluated using a pulsating bubble surfactometer as described in detail previously (5). In brief, BAL-derived large surfactant aggregates (LSA) were isolated by high-speed centrifugation (48,000 *g*, 1 h, 4°C, Sorvall centrifuge), resuspended in saline containing 2 mM Ca^{2+}, and adjusted to a constant phospholipid concentration of 2 mg/ml. The surface activity of samples was assessed using the oscillating bubble technique (Electronetics, Amherst, MA). Following a static measurement of film adsorption over an initial 12-s period (referred to as γads), bubble pulsation was started by sinusoidally oscillating the bubble radius between 0.4 and 0.55 mm at a rate of 20 times/min. The γmin value given here refers to the minimal surface tension value obtained after 5 min of pulsation.

Similar to previous publications (10) we evaluated effects of lung injury from bleomycin with or without SRT by measurement of total protein concentration in BAL. Protein concentration was determined according to the method from Lowry (38) using the commercially available DC Protein Assay Kit, from Bio-Rad (USA) according to the manufacturer's protocol. Albumin concentrations in BAL fluid were assessed with the rat albumin ELISA kit (Bethyl Laboratories, Montgomery, AL) according to the manufacturer's instructions. Protein and albumin concentrations in BAL fluid served as indicators of vascular leak.

Statistical analyses. The loss of body weight with time in surf D7 and saline D7 as well as the derecruitability tests measuring H as a function of time after recruitment maneuver and treatment were subjected to a 2-way ANOVA on ranks followed by Bonferroni correction. According to the hypotheses, data were analyzed for statistically significant differences at *day 3* and *day 7* separately since at *day 3* the effects on acute lung injury and at *day 7* effects on collapse induration were in focus. For this purpose, a parametric *t*-test was used to compare saline and surf groups at either *day 3* or *day 7*. Statistically significant differences are indicated in the figures for surf vs. saline groups with a P level of ≤ 0.05. A P level between 0.05 and 0.10 was defined as a statistical trend. For structure-function relationships pooled data from all study groups were used and a Spearman's test for significant correlations applied to determine the P level and the correlation coefficient. All statistical analyses were performed using GraphPad PRISM Version 7.

RESULTS

Surfactant replacement therapy improves surfactant function. At light and electron microscopy level, assessment of the intra-alveolar surfactant at a qualitative level in perfusion-fixed lung tissue was performed. In addition, BAL-derived alveolar surfactant was functionally assessed (Fig. 1). At light microscopic level intra-alveolar surfactant forms could not be detected in controls (Fig. 1*A*) or saline-treated groups at *day 3* (Fig. 1*B*) or *day 7* (Fig. 1*E*). After SRT, however, alveolar surfactant was seen in diseased and nondiseased areas of the lung at *day 3* (Fig. 1*C*) and *day 7* (Fig. 1*F*). At electron microscopic level, active intra-alveolar surfactant subtypes such as lamellar body-like structures (lbl) and multilamellated vesicles (mlv) in surfactant-treated lungs could be observed after SRT (Fig. 1*J*). This finding reproduces previous observations in animal models of acute lung injury or meconium aspiration syndrome, which also used Curosurf as therapeutic agent (27, 47, 55). Along with tubular myelin, multilamellated vesicles and lamellar body-like structures belong to the active surfactant components within alveolar space (44). Tubular myelin was a typical representative of intra-alveolar surfactant in control lungs (Fig. 1*H*: tm) whereas lamellar body-like structures were virtually absent. In saline-treated lungs, neither tubular myelin nor lamellar body-like surfactant formations were representative findings whereas unilamellated vesicles (Fig. 1*I*: ulv) dominated the intra-alveolar surfactant pool, being in line with previous quantitative assessments (39). Using a pulsating bubble surfactometer, the surface tension adsorption properties (Fig. 1*D*) as well as the minimum surface tension after 1 (Fig. 1*G*) and 5 min (Fig. 1*K*) of cyclic pulsations was also determined. BAL-derived intra-alveolar surfactant demonstrated a significant reduction in minimum surface tension at *day 3* and a trend toward reduction at *day 7* ($P = 0.06$). During the observational period of 5 min the repetitively measured minimum surface tension declined faster in BAL derived from surfactant-treated groups compared with saline-treated groups. On the one hand, a significant decrease of surface tension after adsorption comparing SRT groups with their corresponding saline controls could be observed. On the other hand, even though the equilibrium surface tension (~25 mN/m) after adsorption was not reached in the SRT groups, surfactant could lower minimum surface tension during compression to values comparable to controls.

Surfactant replacement therapy decreases lung deaeration by stabilization of alveoli at day 3. In general, perfusion fixation was successfully performed since in control lungs distal airspaces were open and capillaries within septal walls were nearly free of blood cells and well recruited (Fig. 2*A*). At a qualitative level, however, it was not possible to definitely detect beneficial effects of SRT on lung structure at *day 3* in all animals. The bleomycin groups were characterized by collapsed alveoli as indicated by aggregation of piled up interalveolar septal walls in both the saline D3 group (Fig. 2, *B* and *B1*) and surf D3 (Fig. 2, *C* and *C1*). In addition, small amounts of alveolar edema fluid were observed, in general as a very thin leaflet interposing between piled up septal walls (Fig. 2, *B1* and *C1*), but also as a thin leaflet covering alveolar epithelium in some open alveoli (Fig. 2*D*). Moreover, inflammatory cells were occasionally seen in edema-filled alveolar spaces, and this was in particular true regarding accumulations of AM in the surfactant-treated groups (Fig. 1, *A* and *B*).

In total, four lungs had to be excluded from stereological evaluation since air leakage and partial lung collapse occurred during dissection of the lung (control and saline D3, 1 lung each; and in surf D3, 2 lungs). Design-based stereology at the light microscopic level was used to quantify volumes of alveolar and ductal airspaces (Fig. 2, *E–G*). The saline group at *day 3* was characterized by decreased volumes of acinar airspaces which were significantly lower compared with the surf D3 group (Fig. 2*E*). Although there was virtually no difference regarding the volume of ductal airspaces (Fig. 2*F*), a significant increase in the volume of alveolar airspaces was found (Fig. 2*G*). In line with this finding, the SRT lungs had a larger surface area for gas exchange compared with the saline group, since the total surface area of alveoli covered by air (without edema) was significantly increased reaching similar values as the control group (Fig. 2*H*). Nevertheless, this increase in surface area per lung correlated with an increase in the total number of open alveoli per lung which was significantly

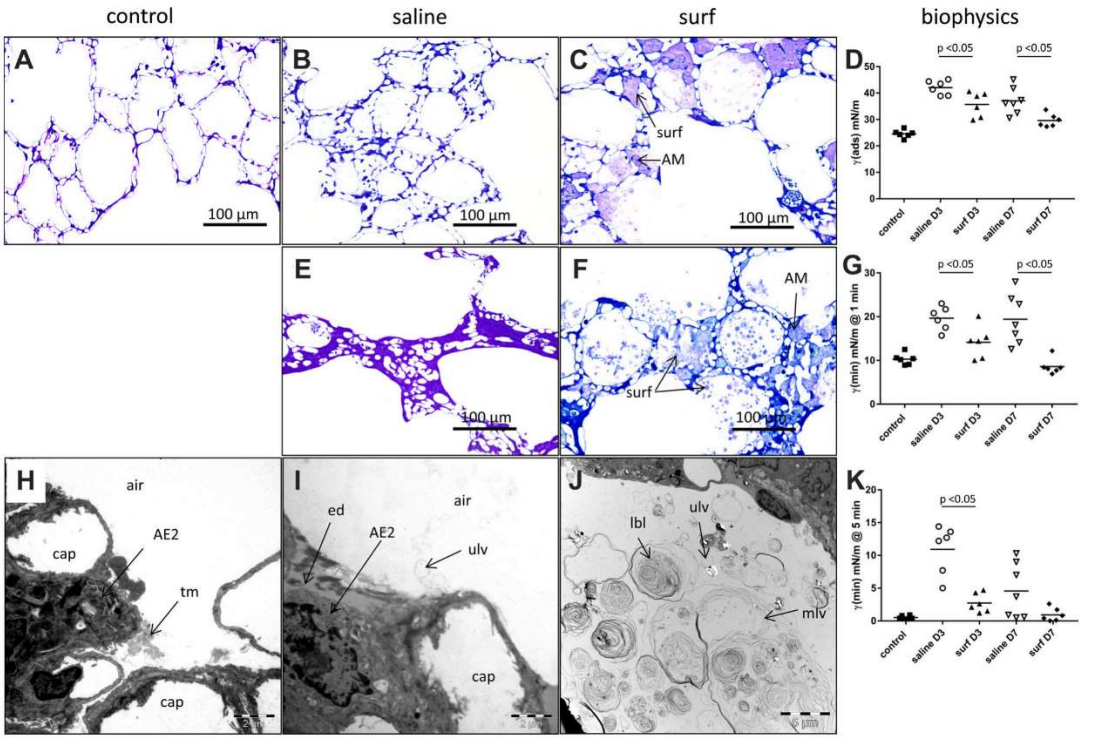

Fig. 1. Structure and function of alveolar surfactant. Three (*C*) and 7 (*F*) days after bleomycin instillation followed by repetitive SRT, intra-alveolar surfactant (surf) can be seen in distal airspaces at light microscopic level. Foamy appearing alveolar macrophages (AM) can be seen in close neighborhood of intra-alveolar surfactant following SRT. No surfactant is visible at light microscopic level in control (*A*) and saline-treated groups 3 (*B*) or 7 (*E*) days after bleomycin challenge. At ultrastructural level, tubular myelin (tm) was the most abundant intra-alveolar surfactant component in control (*H*). Bleomycin-injured and saline-treated lungs show unilamellated vesicles (ulv) as the dominant intra-alveolar surfactant component (*I*). After SRT, however, intra-alveolar surfactant is dominated by lamellar body like (lbl) and multi-lamellated vesicles (mlv) at electron microscopic level. Small amounts of unilamellated vesicles (ulv) are also present (*J*). BAL-derived surfactant was used for biophysical assessments. Both initial adsorption surface tension [*D*: γ(ads)] and minimum surface tension [γ(min)] after 1 (*G*) and 5 min (*K*) of cyclic expansion and compression was improved due to SRT at *day 3* and *day 7*. AE2, alveolar epithelial type II cell; cap, capillary lumen, ed, alveolar edema.

increased in the surf D3 group compared with the saline D3 group but did not reach values found in the control (Fig. 2*I*). The number-weighted volume of alveoli was increased in both bleomycin groups but SRT showed a trend ($P = 0.06$) regarding a reduction of this parameter compared with the saline-treated lungs (Fig. 2*J*).

Invasive pulmonary function tests were used to assess lung mechanics in those lungs which were also subjected to design-based stereological evaluation, and results are given in Fig. 3, *A–C*. In line with the structural parameters, lung mechanical properties were improved, and compared with the saline D3 group, the surf D3 group demonstrated a significant increase in quasi-static lung compliance (Fig. 3*A*) as well as inspiratory capacity (Fig. 3*B*). Tissue elastance H after recruitment maneuver during ventilation with PEEP of 3 cmH_2O and PEEP of 6 cmH_2O did not show any significant time-dependent effects on H in either of the study groups. However, although no statistically significant effect of treatment (saline vs. surf) could be observed during ventilation with PEEP of 3 cmH_2O, there was a significant treatment effect during ventilation with PEEP of 6 cmH_2O showing a decrease in tissue elastance H in the surf D3 group compared with the saline D3 group (Fig. 3*C*). Dynamic pressure-volume loops were used to determine the dynamic compliance of the respiratory system during spontaneous breathing. At *day 3* no significant differences in Cdyn could be observed between control, saline D3 and surf D3 (Fig. 3*D*).

Surfactant replacement therapy reduces inflammatory markers and edema formation. Surfactant is cleared from alveolar space by recycling or degradation via AE2 cells but also by degradation involving alveolar macrophages (56). In some regions after SRT, accumulations of alveolar macrophages containing large amounts of lamellar body-like structures (Figs. 1 and 4*A*) were observed, indicating that exogenous surfactant is taken up and accumulated in alveolar macrophages, which might modify their inflammatory state. Also, based on ex vivo experiments, exogenous surfactant therapy has been suggested to augment biotrauma and thus increases proinflammatory cytokines (65). Hence, effects of SRT on inflammatory markers in the distal airspaces were assessed. Total numbers of cells in BAL fluid were reduced after bleomycin challenge. Differentiation of BAL-derived cells by means of FACS analyses revealed an increase in neutrophilic granulocytes in bleomycin-injured lungs. SRT was associated with a relative and absolute reduction of neutrophilic granulo-

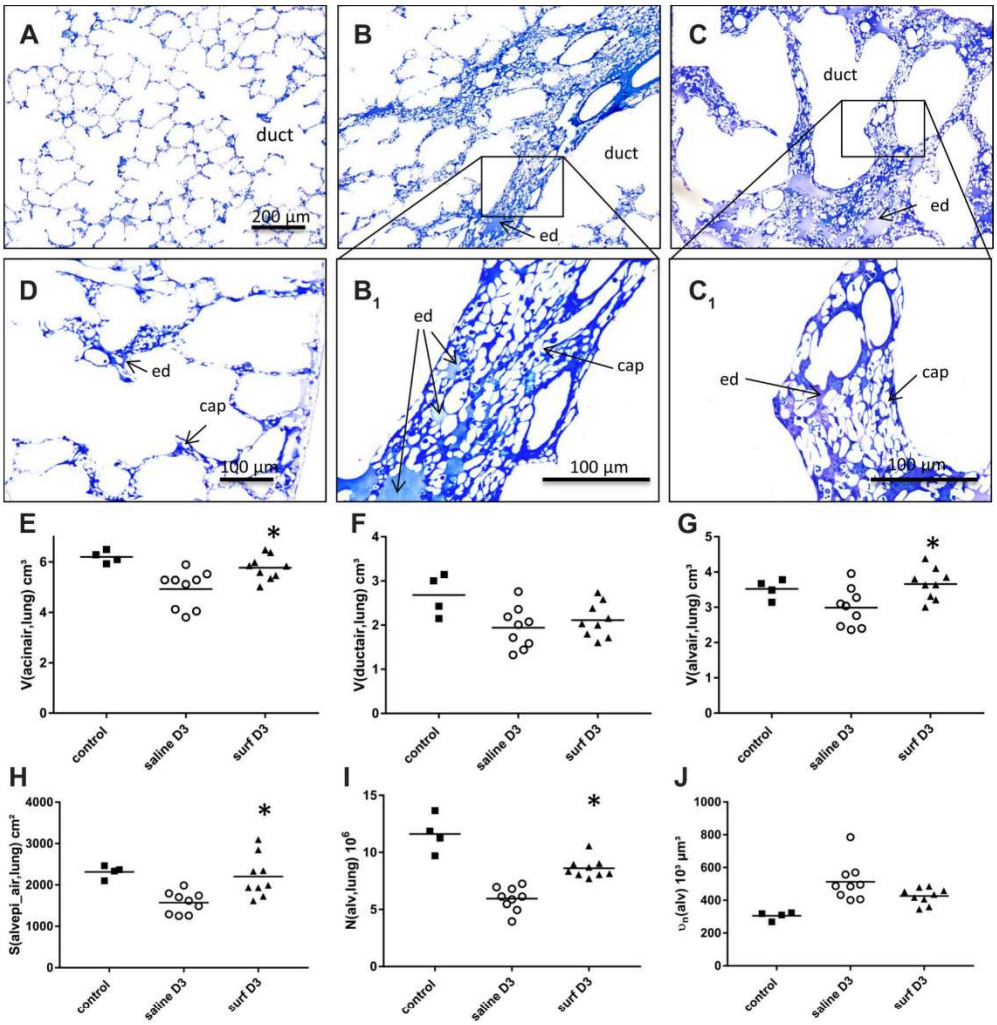

Fig. 2. Effects of SRT on lung architecture at D3. Representative findings at light microscopic level from control (*A*) as well as bleomycin-injured lungs at *day 3* treated with saline (*B* and *B1*) or surfactant (*C* and *C1*). Collapsed distal airspaces are characterized by enlarged alveolar ducts (duct) and septal walls which are piled up and contain their typical capillary network (cap). Small leaflets of alveolar edema (ed) can be seen distinguishing opposing septal walls. In *D*, small leaflets of alveolar edema can also be observed in aerated areas with open alveoli, covering the alveolar epithelium 3 days after bleomycin challenge. Stereological data of total volume of acinar airspace (*E*), ductal airspace (*F*), alveolar airspace (*G*), surface area of air-covered alveolar epithelium (*H*), total number of open alveoli (*I*), and number-weighted mean volume of alveoli (*J*). Primary magnification in overview images 5× (*A, B, C*) or 10× (*D*). Primary magnification for *B1* and *C1*, 20×. *$P < 0.05$ vs. saline D3.

cytes in the airspaces whereas the proportion of activated macrophages was increased toward values found in controls (Fig. 4*B*). Using BioPlex measurement of cytokines/chemokines in BAL fluid, a significant reduction in IL-1β, IL-6, and IL-10 was found whereas IL-4 was increased toward levels observed in controls after SRT treatment (Fig. 4, *D–G*). With respect to MCP-1, surf D3 demonstrated a trend for a reduction compared with saline D3 ($P = 0.06$).

Since lungs were fixed by vascular perfusion, quantification of the volume of the alveolar edema per lung as well as the surface area of alveolar epithelium covered by edema fluid was possible. Figure 2, *B–D*, illustrates examples of edema fluid in collapsed and noncollapsed areas which were present in both the surf D3 and the saline D3 group without obvious differences between these groups. The mean volume fraction of alveolar edema fluid within lung parenchyma was 3.6% and 6.0% in surf D3 and saline D3 groups, respectively. Hence, in both study groups alveolar edema fluid corresponded to a minor fraction within lung parenchyma. Regarding the total volumes of alveolar edema fluid per lung, there was a trend toward reduction in the surf D3 group compared with the saline D3 group (Fig. 5*A*, $P = 0.07$). The total surface area of the

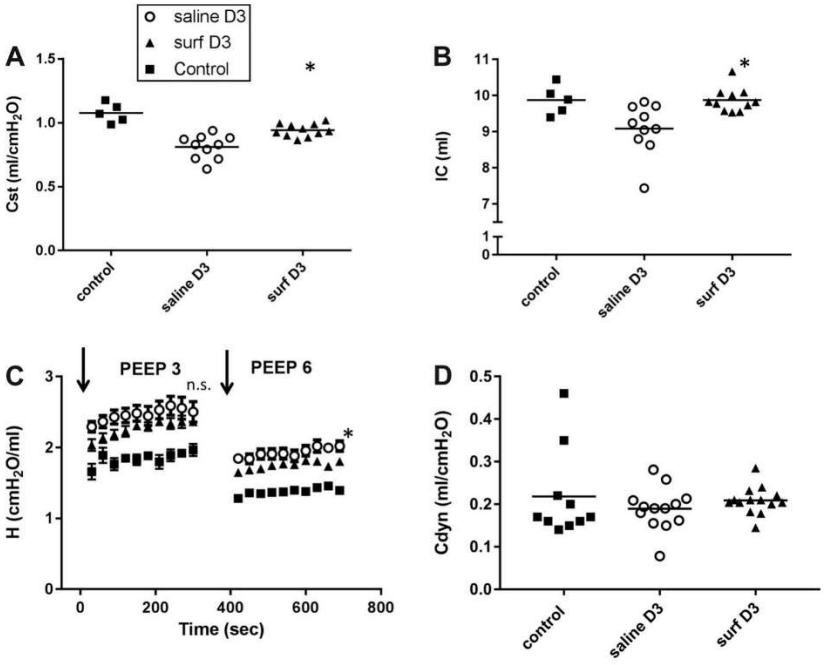

Fig. 3. Lung mechanical properties at D3. Static compliance (Cst) calculated from pressure-controlled pressure-volume loops (*A*), inspiratory capacity (IC; *B*), and tissue elastance (H) during positive end-expiratory pressure (PEEP) ventilation with 3 and 6 cmH_2O after recruitment maneuver (arrow) (*C*). In addition, dynamic compliance (Cdyn) from dynamic pressure-volume loops during spontaneous breathing is given in *D*. $^*P < 0.05$ vs. saline D3.

alveolar epithelium per lung covered with edema fluid was, however, not significantly reduced (Fig. 5*B*). In line with these observations, a reduced protein concentration in BAL fluid obtained from the surf D3 group compared with the saline D3 group was observed (Fig. 5*C*). The albumin level in BAL fluid demonstrated a trend for reduction due to SRT but failed to reach statistical significance as a consequence of one outlier (Fig. 5*D*).

Surfactant replacement therapy modulates collapse induration-related remodeling at day 7. Having demonstrated that SRT is efficient to recruit alveoli at *day 3*, the effects of SRT

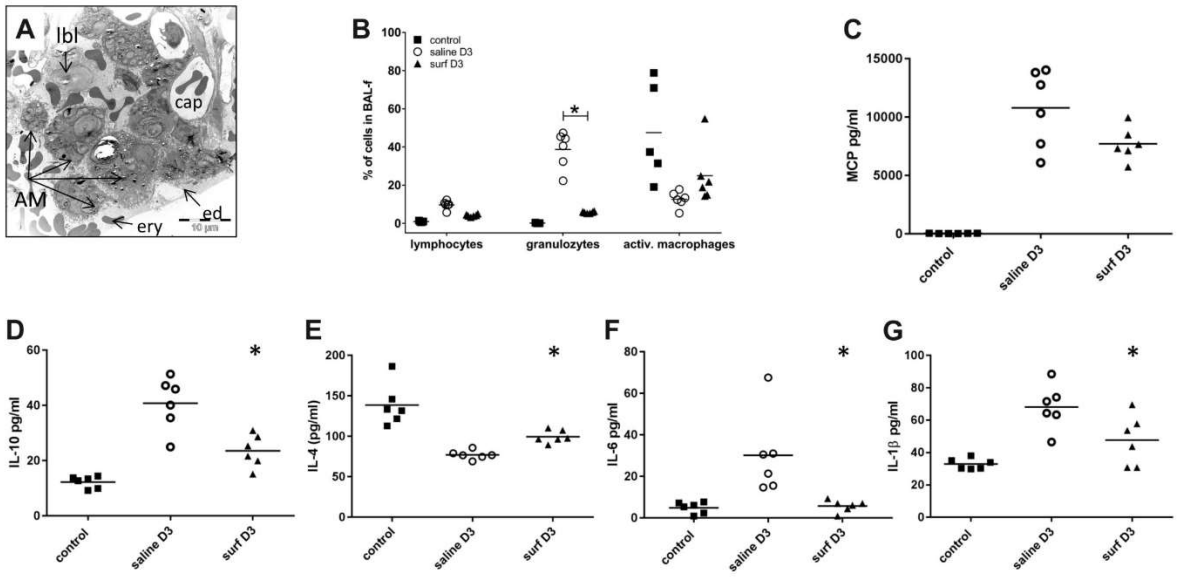

Fig. 4. SRT and markers of inflammation. At *day 3*, inflammatory markers in controls (= healthy) and saline- or surfactant-treated bleomycin challenged lungs were assessed. At electron microscopic level, foamy appearing alveolar macrophages (AM) were observed in D3 surf (*A*). In this example, AM were found in neighborhood to alveolar edema (ed), some erythrocytes (ery) and lamellar body like structures (lbl). Differential cell counts (*B*), and levels of cytokines/chemokines (*C–G*) demonstrated a shift toward healthy situation due to SRT in the surf D3 group. $^*P < 0.05$ vs. saline D3.

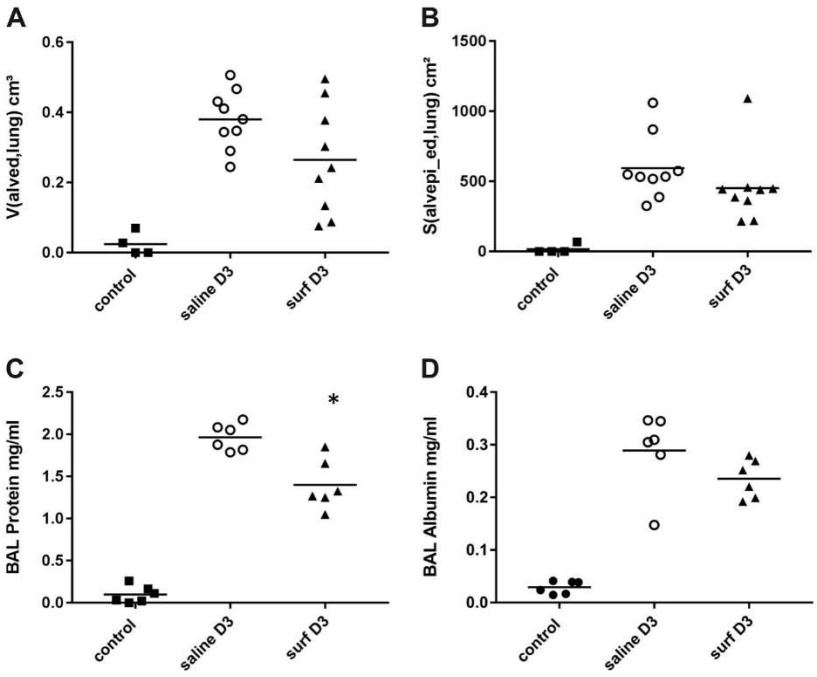

Fig. 5. Alveolar edema at D3. Markers of alveolar edema formation were measured including the total volume of alveolar edema per lung (*A*), the surface area of alveolar epithelium covered by alveolar edema (*B*), the total protein (*C*) and albumin (*D*) concentration in BAL. *$P < 0.05$ vs. saline D3

on collapse induration and related remodeling were studied. Compared with the saline group, a significant deceleration in body weight loss in SRT group was found (Fig. 6*A*). On a qualitative basis, no obvious differences in lung structure could be detected at the light microscopic level between the bleomycin-challenged study groups. In line with a previous study (39) a beginning remodeling process in particular in areas which were characterized by microatelectases or alveolar collapse in both the surf D7 (Fig. 6*B*) and the saline D7 (Fig. 6*C*) group could be observed. Interposing the capillaries of the piled up alveolar septal walls in collapsed areas, cell-rich consolidations were observed (Fig. 6, *B* and *C*). In addition, little amounts of alveolar edema and inflammatory cells were seen. On a quantitative level, no significant differences in volumes of acinar airspaces and surface area of alveolar epithelium covered with air or volume of alveolar edema fluid per lung were found. Compared with the time point D3 the total volume of alveolar edema as well as the total surface area covered by alveolar edema was at time point D7 not progressive. In line with these stereological data were the data from BAL showing mean protein concentration of 1.25 mg/ml (SD: 0.15 mg/ml) and 1.35 mg/ml (SD: 0.20 mg/ml) in surf D7 and saline D7 groups, respectively, which did not differ significantly from each other. Also, albumin concentration in BAL did not differ between these two study groups at *day 7* [surf D7 0.177 (0.04) vs. saline D7 0.173 (0.033) mg/ml]. However, in both bleomycin groups there was an increase in the total volume of septal wall tissue per lung which was significantly less pronounced in the surf D7 group compared with the saline D7 group (Fig. 6*D*). Moreover, the arithmetic mean thickness of parenchymatous/septal wall tissue was significantly decreased in the surf D7 group in comparison to the saline D7 group (Fig. 6*E*). Although no significant differences with respect to the total volumes of acinar airspaces or surface area of air covered alveolar epithelium were observed, a significant increase in the number of open alveoli per lung in the surf D7 group compared with the corresponding saline group was detected (Fig. 6*F*). The mean difference between the study groups amounted to ~900,000 alveoli. In line with the structural data, the lung mechanical properties revealed slight but significant increases in static compliance (Fig. 7*A*), inspiratory capacity (Fig. 7*B*), and a clear decrease in tissue elastance H both during PEEP of 3 cmH_2O and PEEP of 6 cmH_2O ventilation (Fig. 7*C*) in the surf D7 group compared with the saline D7 group. However, during spontaneous respiration the dynamic compliance showed only a trend ($P = 0.075$) for improvement in surf D7 at this time point (Fig. 7*D*). Hence, during mechanical ventilation, the lung was more compliant (= higher Cst) and less stiff (= reduced H) in the surf D7 group which could not convincingly be confirmed during spontaneous respiration.

Structure-function relationships: which structural changes correlate with lung mechanical improvement in this model? At the structural level SRT led to a decrease in alveolar edema and an increase in alveolar number per lung at *day 3*, whereas at *day 7* there was, aside from an increase in alveolar number, also a decrease in septal wall thickness without any effects on alveolar edema volume. Alveolar derecruitment (loss of open alveoli), septal wall thickening, fibrosis, and alveolar edema are structural parameters leading to an increase in tissue elastance (26, 39). To better understand by which structural improvement SRT leads to an attenuation of lung mechanical properties, correlation analyses of lung functional parameters static compliance (Cst) and tissue elastance (H) during PEEP of 6 cmH_2O ventilation with structural data were performed

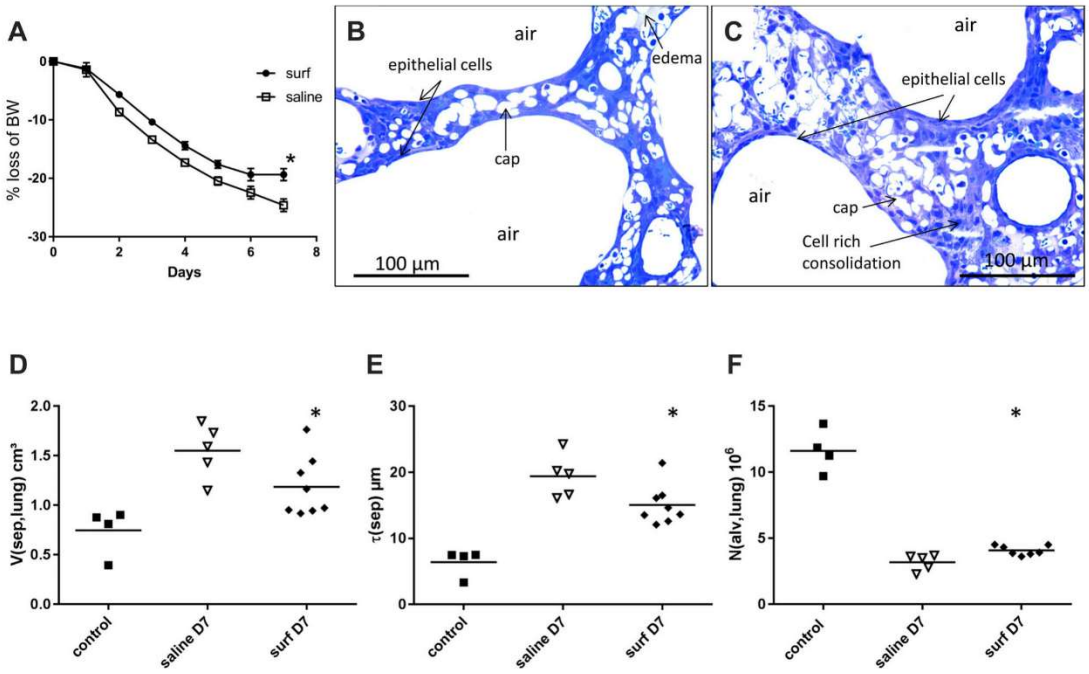

Fig. 6. SRT reduces body weight loss and modifies tissue remodeling at D7. After bleomycin challenge (*day 0*), body weight was determined daily. *A* illustrates changes of body weight (BW) in percent (%) from baseline (*day 0*) (mean and SD) of $n = 12$ in saline D7 and $n = 15$ in surf D7. Characteristic findings at *day 7* from surf D7 group (*B*) and saline D7 group (*C*). There are piled septal walls in both groups characterized by the densities of the septal wall-associated capillary network (cap). As a typical feature of collapse induration, epithelial cells covering these piled septal walls can be observed. Moreover, between the capillaries, cell rich consolidations can be found. All these structures are underneath the epithelium. For quantification, total volume of septal walls per lung which corresponded to the total volume of parenchymatous tissue (*D*), arithmetic mean thickness of septal walls/parenchymatous tissue (*E*), and total number of open alveoli (*F*) are illustrated.*$P <$ 0.05 vs. saline D7.

(Fig. 8). Among the structural data, the number of open alveoli in fixed lungs correlated best with both static compliance and tissue elastance (Fig. 8*A*). Second, also a good correlation between septal wall thickness and lung mechanical parameters could be established (Fig. 8*B*). Alveolar edema volume per lung (Fig. 8*C*), however, did hardly show a correlation with lung functional parameters using pooled data from all study groups until *day 7*.

DISCUSSION

Alveolar instability resulting in alveolar R/D, permanent alveolar derecruitment, and collapse induration with corresponding tissue remodeling has been shown to be of relevance in both acute and chronic human lung diseases (14, 24, 31, 46, 67) and in animal models mimicking lung injury and subsequent fibrotic remodeling (6, 39). Moreover, quantitative data of lung microarchitecture from patients diagnosed with IPF are suggestive for alveolar collapse as an important pathomechanism, since the primary effect of IPF on lung structure is loss of alveolar surface area without a relevant increase in tissue volume (12, 41). IPF is considered to be the consequence of repetitive minor injuries of the alveolar epithelium, impaired regeneration capacity, and at the end a fibrotic remodeling (2, 15). Injurious events also hit the alveolar epithelial type II (AE2) cells which are in charge of regeneration of the alveolar epithelium as well as surfactant homeostasis. Functional surfactant reduces surface tension and thereby prevents alveolar collapse at low lung volumes as well as the development of alveolar edema (49, 53). It has been shown that in IPF, AE2 cells are subject of apoptosis, endoplasmic reticulum, and lysosomal stress (18) in line with the demonstrated impaired activity of lung surfactant (19). In this regard it has been demonstrated in animal models that an isolated injury of AE2 cells or disruption of the surfactant system is either sufficient to induce a fibrotic lung remodeling (40, 51, 62, 71, 72) or results in a higher susceptibility for injury and fibrotic remodeling (69). Although the role of mechanical stress resulting from alveolar R/D and volutrauma is appreciated as an aggravating factor of lung injury in the context of ventilator-induced lung injury (11, 50, 63), the relevance for disease progression from acute lung injury to tissue remodeling and fibrosis during spontaneous breathing is less clear and therefore represents a gap of knowledge in the context of human diseases characterized by high surface tension, ongoing lung injury, and remodeling (20). In the present study we tested the hypothesis whether surfactant dysfunction is involved in aggravating/triggering lung injury and remodeling processes such as collapse induration during the time course of disease progression. The bleomycin model represents a useful approach regarding this question since during the course of the disease surfactant dysfunction is initially associated with intratidal alveolar R/D (*days 1–3*) which progresses to permanent derecruitment at *day*

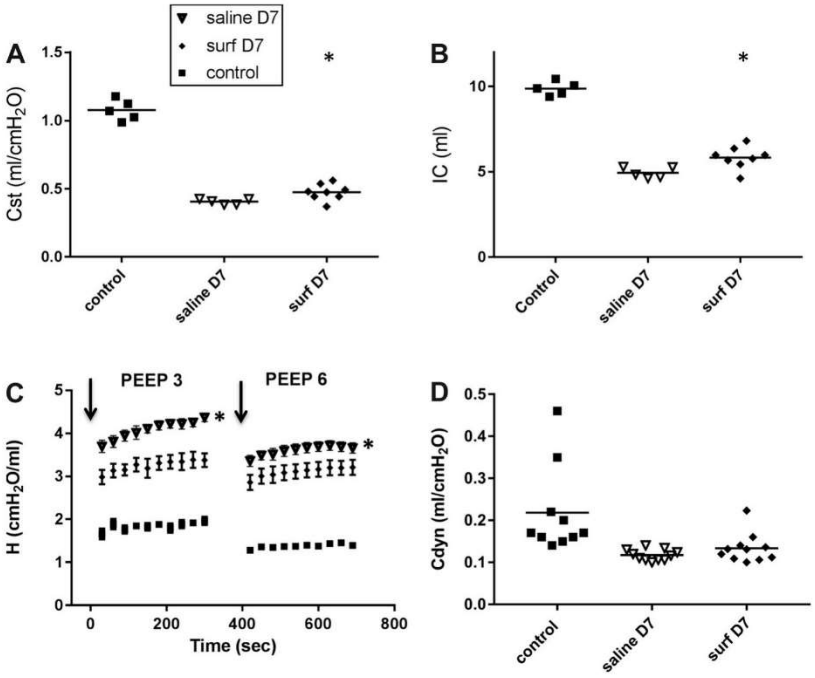

Fig. 7. Lung mechanical properties at D7. Static compliance (Cst) calculated from pressure-controlled pressure-volume loops (*A*), inspiratory capacity (*B*), and tissue elastance during positive end-expiratory pressure (PEEP) ventilation with 3 and 6 cmH_2O after recruitment maneuver (arrow) (*C*). In addition, dynamic compliance (Cdyn) from dynamic pressure-volume loops during spontaneous breathing is given in *D*. n.s., Not significant. *$P < 0.05$ between saline D7 and surf D7.

3, meaning that alveoli cannot be opened by physiological pressures (28). At *day 7* tissue remodeling starts and collapsed alveoli are subjected to collapse induration meaning that their opposing, denuded basal laminae are glued together and their former entrance is overgrown by epithelial cells. This contributes to septal wall thickening, before deposition of collagen can be observed (8, 39). Hence surfactant dysfunction, high surface tension, and impairment in alveolar micromechanics predate the development of lung remodeling and are rather the cause than the consequence. In an attempt to reduce high surface tension-related remodeling we started SRT already at *day 1* after bleomycin challenge and continued treatment until *day* 3 (effect on permanent derecruitment) or *day 7* (effect on collapse induration). Early treatment with exogenous surfactant was efficient to improve function of intra-alveolar surfactant until *day 7* as demonstrated by ultrastructural appearance and surface tension (Fig. 1). During the early phase of progressive acute lung injury SRT led to a significant reduction of inflammatory markers such as numbers of neutrophilic granulocytes as well as cytokines levels in BAL including IL-1β and IL-10, both of which have also been shown to be profibrotic (Fig. 4) (22, 30). These reduced levels of inflammatory markers were linked with slight anti-edematous effects as shown by reduced protein concentration in BAL (Fig. 5*C*). As BAL protein can also be increased by vascular leak, we analyzed albumin, which is more specific for vascular leak. The increased albumin levels in BAL fluid provide clear evidence for vascular leak following bleomycin challenge (Fig. 5*D*). However, the albumin assay could not convincingly confirm that SRT reduces vascular leak. Although a strong trend for a reduction of albumin at *day 3* was observed, the difference was not statistically significant. Taken together the data demonstrate that SRT attenuates highly relevant markers of acute lung injury at this early stage of the model (42).

Of note, alveolar edema was predominantly observed in areas where alveoli were not inflated. The surfactant-treated lungs contained more air in distal airspaces, in particular in the alveolar compartment at a defined end-expiratory positive airway pressure of 5 cmH_2O. This increase in alveolar airspace was a result of an increase in the total number of open alveoli which was escorted by a near normalization of the surface area of alveolar epithelium and therefore surface area available for gas exchange (Fig. 2, *H–J*). These findings were in line with lung mechanical properties demonstrating normalization of the inspiratory capacity and attenuation of the loss of static lung compliance. The improvements in lung functional data reproduced previous observations in the bleomycin-induced lung injury model using an SP-C analog containing synthetic surfactant preparation for dry powder inhalation leading to normalization in blood oxygenation within a short period of <1 h (58). Also, instead of an anti-inflammatory environment, previous studies have suggested an increase in biotrauma characterized by pro-inflammatory markers in an ex vivo model of ventilator-induced lung injury due to SRT (65), findings which were not reproduced in our experimental setup showing a decrease in, e.g., IL-1β and IL-6. Although more profiles of alveolar macrophages could be observed after SRT in our study (Fig. 4*A*), there was no increase in MCP-1 (Fig. 4*C*) and cell numbers in BAL (Fig. 4*B*), arguing against a more pronounced attracting microenvironment for inflammatory cells in the context of SRT. In other words, although we observed in areas with increased surfactant deposition aberrant, foamy appearing alveolar macrophages full with surfactant material, we did not find an aggravation of the inflammatory response—both cyto-

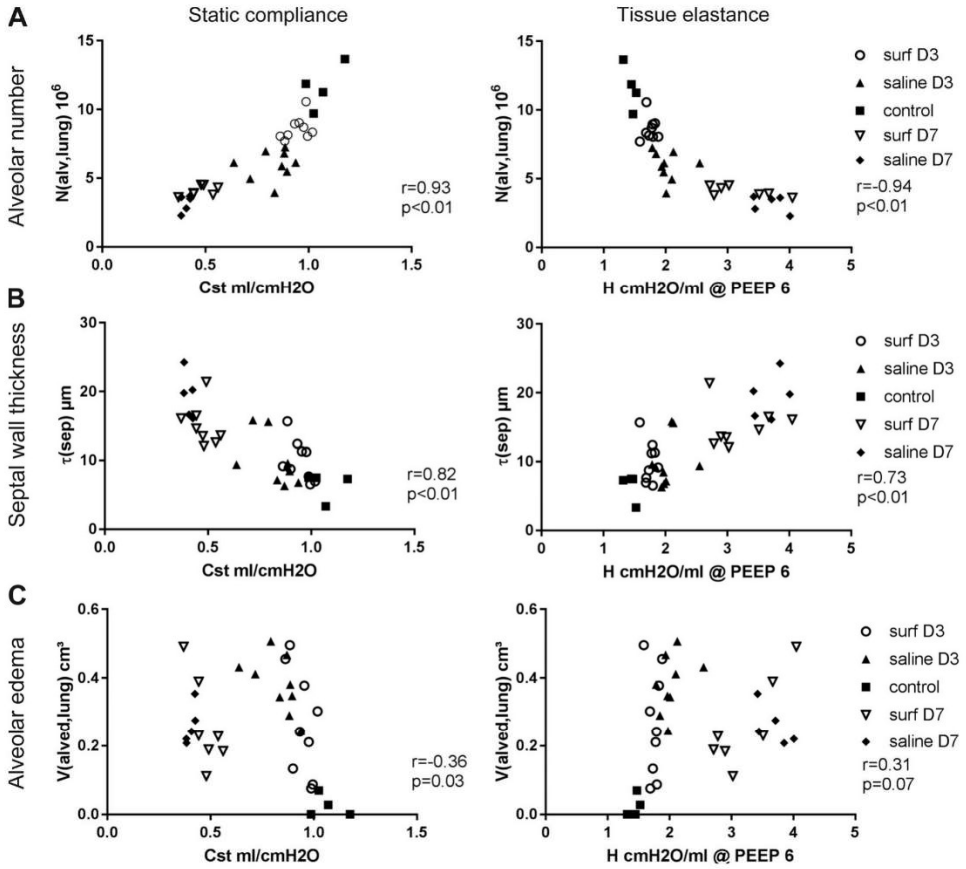

Fig. 8. Structure-function relationships. Pooled data were used for correlation studies between functional parameter static compliance/tissue elastance and structural parameters including total number of open alveoli (*A*), arithmetic mean thickness of septal wall/parenchymatous tissue thickness (*B*), and total volume of alveolar edema (*C*).

kines linked with inflammation (classical activation: e.g., IL-1β) and reparative (alternative activation: e.g., IL-4, IL-10) polarization of macrophages (33) were either unchanged or shifted toward normal values in the BAL of surfactant-treated animals.

The "anti-inflammatory" action of surfactant seems to be related to reduction of mechanical stress and as a consequence amelioration of lung injury, since stabilization of alveoli after early SRT treatment is associated with reduced inflammatory markers. The increased number of open alveoli per lung suggests decreased dynamic mechanical stress due to atelectrauma (Fig. 2*I*). This correlates with the finding that mere high surface tension was sufficient to induce inflammation in a conditional surfactant protein B knockout mouse model (23). In addition, it is well known that high surface tension as such has edematous effects in the lung (49). Thus SRT is expected to normalize surface tension and reduce the accumulation of edematous material. The SRT model proved direct anti-edematous effects in concert with a reduction in mechanical stress due to less alveolar derecruitment and less stress forces attributable to the normalization of biophysical properties. Although natural surfactant preparations like the one used in the present study do not contain the strongest immunomodulatory components known to be present in surfactant, namely hydrophilic surfactant proteins A and D, it might be possible that unknown or less known immunomodulatory factors in the phospholipid fraction also contributed to reduction in acute lung injury via reduction of lung inflammation (25, 45).

A very convincing effect of SRT in the context of acute lung injury is the increase in the total number of open alveoli per lung which was associated with a concomitant improvement in lung functional parameters, in particular static compliance and inspiratory capacity. Opposed to tissue elastance during PEEP of 6 cmH_2O ventilation, tissue elastance during PEEP of 3 cmH_2O ventilation did not show significant differences at *day 3* (Fig. 3). It has been shown for acute lung injury that increase in aeration of the lung, e.g., by alveolar recruitment, is responsible for the decrease of elastance at the organ scale with increasing PEEP ventilation (3, 64). The treatment effect during ventilation with PEEP of 6 cmH_2O in concert with the missing effect during PEEP of 3 cmH_2O suggests that in the surf group ventilation with increasing PEEP values is able to recruit alveoli more efficiently compared with the saline D3 group. Therefore, surfactant-treated lungs compared with sa-

line-treated lungs showed significantly reduced stiffness by more efficient stabilization of alveoli. Hence, the recruitability of alveoli is increased as a consequence of higher PEEP ventilation and SRT. Anti-edematous effects of SRT were present, but all together limited or even absent at *day 7*. Alveoli remained collapsed in some areas where small amounts of edema could be detected between opposing septal walls of collapsed alveoli indicating that such alveoli are glued together by edema fluid. Therefore, some lung areas are still prone to derecruitment and finally collapse induration even if SRT is performed. In addition alveolar lipoproteinosis has also been shown to be associated with an increase in tissue elastance in animal models and in our study, we occasionally observed alveoli which were filled with alveolar surfactant due to SRT. The viscoelastic properties of surfactant itself might, in concert with edema formation, mask the positive impact on lung functional parameters such as tissue elastance in particular at PEEP of 3 cmH_2O.

At *day 7* beneficial effects of SRT in comparison to saline treatment in lung mechanical and structural parameters were observed, although the effects can at best be characterized as modest. At *day 7* we could convincingly find remodeling processes in areas with collapsed alveoli; epithelial cells now covered areas of aggregated septal walls belonging to collapsed distal airspaces with infiltrating cells, likely fibroblasts between capillaries (Fig. 6, *B–C*) (34). Invading fibroblasts have been shown to be attracted into provisory matrix very effectively by diverse mediators as early as at *day 7* after bleomycin challenge (1). Regarding stereological counting, these regions of collapsed alveoli covered by epithelial cells and invaded by cells such as fibroblasts were now counted as one "septal wall" since all structures were engulfed in the tissue underneath an epithelium. The fact that in the SRT group both the total volume of parenchymatous tissue (= remodeled alveolar septal walls) as well as the mean thickness of such septal walls were reduced compared with the saline-treated group demonstrates that SRT modifies these remodeling processes (Fig. 6, *D* and *E*). Alveolar number was significantly improved suggesting that stabilization of alveoli by SRT reduces collapse induration and interferes with the remodeling process at least in part (Fig. 6*F*). However, compared with the data obtained at *day 3*, there was a considerable decline of lung functional properties and alveolar number per lung in both study groups at *day 7* so that SRT is able to decelerate but not to abrogate degradation of lung structural and mechanical parameters in this model. Of note, the described remodeling process appears before collagen deposition can be detected, e.g., by hydroxyproline level, and is therefore independent of collagen deposition. Accordingly, the hydroxyproline levels were not statistically different between saline D7 and surf D7 (data not shown) so that the differences in the thickness of septal walls cannot be explained by excessive collagen deposition but rather by collapse induration. Observations from human material support the existence and relevance of remodeling processes involving alveolar collapse and collapse induration in the absence of noticeable collagen deposition, which is usually used to define fibrotic remodeling (24, 41). In an ultrastructural study of human lung tissue from patients with idiopathic interstitial pneumonia, Katzenstein (24) described collapsed alveoli which were overgrown by alveolar epithelial cells and discussed this mechanism as the cause for septal wall thickening questioning the relevance of interstitial fibrosis in this context. Such observations were reproduced in the animal model used in the current study and SRT had a clear impact on this mechanism: septal wall thickening was reduced and the number of open alveoli increased even before an increase in hydroxyproline levels can be expected. Also, Mai and coworkers used IPF explants for correlative imaging studies (41). Since IPF is characterized by temporal heterogeneity, different stages of disease progression from initiation to end-stage remodeling can be observed in the same lung. The authors also found convincing evidence for alveolar collapse which could be detected in regions which were obviously not (yet) subject to fibrotic remodeling. Hence, Mai and coworkers discuss alveolar collapse as a trigger of fibrotic remodeling. These observations provide evidence for alveolar collapse and collapse induration as early events in human diseases but also in the bleomycin model predating collagen deposition. These events can at least in the animal model be modified by reducing surface tension. SRT is able to stabilize alveoli at *day 3*, but it can save only a minor fraction of alveoli from collapse induration at *day 7* as demonstrated by the pronounced decline in alveolar number between *day 3* (Fig. 2*J*) and *day 7* (Fig. 6*F*). The reason for this might be a limited effect on alveolar edema formation (Fig. 5, *A* and *B*) in this model so that at the end the septal walls of collapsed alveoli are glued together independent of surfactant substitution. According to correlation analyses the effects on alveolar number were nevertheless highly correlated to the observed beneficial effects on lung mechanical properties (Fig. 8), indicating that the therapeutic goal in diseases resulting in ongoing lung injury should be the stabilization of alveoli. The relevance of these findings in the context of human diseases is, however, debatable since the bleomycin model has several limitations. Also, it is not entirely clear which protocol serves best as control for surfactant replacement therapies. We decided to use a saline-treated group which was subjected to the same procedures and volume challenge as the surfactant-treated group. This decision was based on previous findings that saline challenge after bleomycin instillation did not further aggravate lung mechanical impairment (38).

In summary, SRT seems to stabilize alveoli, by reducing acute lung injury, and demonstrates beneficial effects on mechanical and structural parameters related to collapse induration and tissue remodeling in the bleomycin model. Hence, surfactant dysfunction seems to be partially responsible or contributing to tissue remodeling resulting in the functionally relevant loss of alveoli. The beneficial effects of SRT on lung mechanical properties are linked with an increase in the number of open alveoli and a reduction in the thickness of parenchymatous (septal wall) tissue. Although the so-called open lung concept has been followed for treatment of acute lung injury by means of mechanical ventilation already for a long time, we pursued this concept for the first time in a more chronic model of ongoing lung injury during spontaneous breathing by means of SRT. The data provide evidence that the open lung concept might also be of relevance for tissue remodeling in diseases resulting from ongoing lung injury with a more subacute or chronic time course.

ACKNOWLEDGMENTS

We thank C. Vogt and K. Westermann for excellent technical support.

GRANTS

This work was supported by a grant of the German Research Foundation (DFG KN 916 1-1) to C. Ruppert, H.-G. Hoymann, and L. Knudsen.

DISCLOSURES

No conflicts of interest, financial or otherwise are declared by the authors.

AUTHOR CONTRIBUTIONS

L.S., C.R., H.-G.H., L.K., and E.L.-R. conceived and designed research; L.S., C.R., H.-G.H., M.F., S.E., C.K., L.K., and E.L.-R. performed experiments; L.S., C.R., H.-G.H., M.F., S.E., C.K., C.M., M.O., L.K., and E.L.-R. analyzed data; L.S., C.R., H.-G.H., M.F., S.E., C.K., C.M., M.O., L.K., and E.L.-R. interpreted results of experiments; L.S., C.R., C.K., L.K., and E.L.-R. prepared figures; L.S., L.K., and E.L.-R. drafted manuscript; L.S., C.R., H.-G.H., M.F., S.E., C.K., C.M., M.O., L.K., and E.L.-R. edited and revised manuscript; L.S., C.R., H.-G.H., M.F., S.E., C.K., C.M., M.O., L.K., and E.L.-R. approved final version of manuscript.

REFERENCES

1. **Ahluwalia N, Grasberger PE, Mugo BM, Feghali-Bostwick C, Pardo A, Selman M, Lagares D, Tager AM.** Fibrogenic lung injury induces non-cell-autonomous fibroblast invasion. *Am J Respir Cell Mol Biol* 54: 831–842, 2016. doi:10.1165/rcmb.2015-0040OC.
2. **Ahluwalia N, Shea BS, Tager AM.** New therapeutic targets in idiopathic pulmonary fibrosis. Aiming to rein in runaway wound-healing responses. *Am J Respir Crit Care Med* 190: 867–878, 2014. doi:10.1164/rccm.201403-0509PP.
3. **Allen GB, Pavone LA, DiRocco JD, Bates JH, Nieman GF.** Pulmonary impedance and alveolar instability during injurious ventilation in rats. *J Appl Physiol (1985)* 99: 723–730, 2005. doi:10.1152/japplphysiol.01339.2004.
4. **Bachofen H, Schürch S.** Alveolar surface forces and lung architecture. *Comp Biochem Physiol A Mol Integr Physiol* 129: 183–193, 2001. doi:10.1016/S1095-6433(01)00315-4.
5. **Beck-Broichsitter M, Ruppert C, Schmehl T, Günther A, Seeger W.** Biophysical inhibition of pulmonary surfactant function by polymeric nanoparticles: role of surfactant protein B and C. *Acta Biomater* 10: 4678–4684, 2014. doi:10.1016/j.actbio.2014.07.026.
6. **Birkelbach B, Lutz D, Ruppert C, Henneke I, Lopez-Rodriguez E, Günther A, Ochs M, Mahavadi P, Knudsen L.** Linking progression of fibrotic lung remodeling and ultrastructural alterations of alveolar epithelial type II cells in the amiodarone mouse model. *Am J Physiol Lung Cell Mol Physiol* 309: L63–L75, 2015. doi:10.1152/ajplung.00279.2014.
7. **Brandenberger C, Ochs M, Mühlfeld C.** Assessing particle and fiber toxicology in the respiratory system: the stereology toolbox. *Part Fibre Toxicol* 12: 35, 2015. doi:10.1186/s12989-015-0110-8.
8. **Burkhardt A.** Alveolitis and collapse in the pathogenesis of pulmonary fibrosis. *Am Rev Respir Dis* 140: 513–524, 1989. doi:10.1164/ajrccm/140.2.513.
9. **Carloni A, Poletti V, Fermo L, Bellomo N, Chilosi M.** Heterogeneous distribution of mechanical stress in human lung: a mathematical approach to evaluate abnormal remodeling in IPF. *J Theor Biol* 332: 136–140, 2013. doi:10.1016/j.jtbi.2013.04.038.
10. **Casey J, Kaplan J, Atochina-Vasserman EN, Gow AJ, Kadire H, Tomer Y, Fisher JH, Hawgood S, Savani RC, Beers MF.** Alveolar surfactant protein D content modulates bleomycin-induced lung injury. *Am J Respir Crit Care Med* 172: 869–877, 2005. doi:10.1164/rccm.200505-767OC.
11. **Cong X, Hubmayr RD, Li C, Zhao X.** Plasma membrane wounding and repair in pulmonary diseases. *Am J Physiol Lung Cell Mol Physiol* 312: L371–L391, 2017. doi:10.1152/ajplung.00486.2016.
12. **Coxson HO, Hogg JC, Mayo JR, Behzad H, Whittall KP, Schwartz DA, Hartley PG, Galvin JR, Wilson JS, Hunninghake GW.** Quantification of idiopathic pulmonary fibrosis using computed tomography and histology. *Am J Respir Crit Care Med* 155: 1649–1656, 1997. doi:10.1164/ajrccm.155.5.9154871.
13. **Froese AR, Shimbori C, Bellaye PS, Ask K, Inman M, Obex S, Fatima S, Jenkins G, Gauldie J, Kolb M.** Stretch Induced Activation of transforming growth factor-β1 in Pulmonary Fibrosis. *Am J Respir Crit Care Med* 194: 84–96, 2016. doi:10.1164/rccm.201508-1638OC.
14. **Galvin JR, Frazier AA, Franks TJ.** Collaborative radiologic and histopathologic assessment of fibrotic lung disease. *Radiology* 255: 692–706, 2010. doi:10.1148/radiol.10090717.
15. **Geiser T.** Idiopathic pulmonary fibrosis–a disorder of alveolar wound repair? *Swiss Med Wkly* 133: 405–411, 2003. 2003/29/smw-09986.
16. **Gundersen HJ, Jensen EB.** The efficiency of systematic sampling in stereology and its prediction. *J Microsc* 147: 229–263, 1987. doi:10.1111/j.1365-2818.1987.tb02837.x.
17. **Gundersen HJ, Osterby R.** Optimizing sampling efficiency of stereological studies in biology: or 'do more less well!'. *J Microsc* 121: 65–73, 1981. doi:10.1111/j.1365-2818.1981.tb01199.x.
18. **Günther A, Korfei M, Mahavadi P, von der Beck D, Ruppert C, Markart P.** Unravelling the progressive pathophysiology of idiopathic pulmonary fibrosis. *Eur Respir Rev* 21: 152–160, 2012. doi:10.1183/09059180.00001012.
19. **Günther A, Schmidt R, Nix F, Yabut-Perez M, Guth C, Rosseau S, Siebert C, Grimminger F, Morr H, Velcovsky HG, Seeger W.** Surfactant abnormalities in idiopathic pulmonary fibrosis, hypersensitivity pneumonitis and sarcoidosis. *Eur Respir J* 14: 565–573, 1999. doi:10.1034/j.1399-3003.1999.14c14.x.
20. **Hinz B, Suki B.** Does breathing amplify fibrosis? *Am J Respir Crit Care Med* 194: 9–11, 2016. doi:10.1164/rccm.201601-0149ED.
21. **Hoymann HG.** Invasive and noninvasive lung function measurements in rodents. *J Pharmacol Toxicol Methods* 55: 16–26, 2007. doi:10.1016/j.vascn.2006.04.006.
22. **Huaux F, Louahed J, Hudspith B, Meredith C, Delos M, Renauld JC, Lison D.** Role of interleukin-10 in the lung response to silica in mice. *Am J Respir Cell Mol Biol* 18: 51–59, 1998. doi:10.1165/ajrcmb.18.1.2911.
23. **Ikegami M, Whitsett JA, Martis PC, Weaver TE.** Reversibility of lung inflammation caused by SP-B deficiency. *Am J Physiol Lung Cell Mol Physiol* 289: L962–L970, 2005. doi:10.1152/ajplung.00214.2005.
24. **Katzenstein AL.** Pathogenesis of "fibrosis" in interstitial pneumonia: an electron microscopic study. *Hum Pathol* 16: 1015–1024, 1985. doi:10.1016/S0046-8177(85)80279-3.
25. **Kerecman J, Mustafa SB, Vasquez MM, Dixon PS, Castro R.** Immunosuppressive properties of surfactant in alveolar macrophage NR8383. *Inflamm Res* 57: 118–125, 2008. doi:10.1007/s00011-007-7212-1.
26. **Knudsen L, Atochina-Vasserman EN, Massa CB, Birkelbach B, Guo CJ, Scott P, Haenni B, Beers MF, Ochs M, Gow AJ.** The role of inducible nitric oxide synthase for interstitial remodeling of alveolar septa in surfactant protein D-deficient mice. *Am J Physiol Lung Cell Mol Physiol* 309: L959–L969, 2015. doi:10.1152/ajplung.00017.2015.
27. **Knudsen L, Boxler L, Mühlfeld C, Schaefer I-M, Becker L, Bussinger C, von Stietencron I, Madershahian N, Richter J, Wahlers T, Wittwer T, Ochs M.** Lung preservation in experimental ischemia/reperfusion injury and lung transplantation: a comparison of natural and synthetic surfactants. *J Heart Lung Transplant* 31: 85–93, 2012. doi:10.1016/j.healun.2011.10.002.
28. **Knudsen L, Lopez-Rodriguez E, Berndt L, Boden C, Bates J, Smith B.** Pressure dependent alveolar derecruitment is linked with surfactant dysfunction in bleomycin-induced acute lung injury. *Am J Respir Crit Care Med* 193: A4813, 2016.
29. **Knudsen L, Ruppert C, Ochs M.** Tissue remodelling in pulmonary fibrosis. *Cell Tissue Res* 367: 607–626, 2017. doi:10.1007/s00441-016-2543-2.
30. **Kolb M, Margetts PJ, Anthony DC, Pitossi F, Gauldie J.** Transient expression of IL-1beta induces acute lung injury and chronic repair leading to pulmonary fibrosis. *J Clin Invest* 107: 1529–1536, 2001. doi:10.1172/JCI12568.
31. **Kuhn C III, Boldt J, King TE Jr, Crouch E, Vartio T, McDonald JA.** An immunohistochemical study of architectural remodeling and connective tissue synthesis in pulmonary fibrosis. *Am Rev Respir Dis* 140: 1693–1703, 1989. doi:10.1164/ajrccm/140.6.1693.
32. **Kuhn C, McDonald JA.** The roles of the myofibroblast in idiopathic pulmonary fibrosis. Ultrastructural and immunohistochemical features of sites of active extracellular matrix synthesis. *Am J Pathol* 138: 1257–1265, 1991.
33. **Laskin DL, Sunil VR, Gardner CR, Laskin JD.** Macrophages and tissue injury: agents of defense or destruction? *Annu Rev Pharmacol Toxicol* 51: 267–288, 2011. doi:10.1146/annurev.pharmtox.010909.105812.
34. **Lazenby AJ, Crouch EC, McDonald JA, Kuhn C III.** Remodeling of the lung in bleomycin-induced pulmonary fibrosis in the rat. An immunohistochemical study of laminin, type IV collagen, and fibronectin. *Am Rev Respir Dis* 142: 206–214, 1990. doi:10.1164/ajrccm/142.1.206.
35. **Leslie KO.** Idiopathic pulmonary fibrosis may be a disease of recurrent, tractional injury to the periphery of the aging lung: a unifying hypothesis

regarding etiology and pathogenesis. *Arch Pathol Lab Med* 136: 591–600, 2012. doi:10.5858/arpa.2011-0511-OA.

36. **Lopez-Rodriguez E, Boden C, Echaide M, Perez-Gil J, Kolb M, Gauldie J, Maus UA, Ochs M, Knudsen L.** Surfactant dysfunction during overexpression of TGF-β1 precedes profibrotic lung remodeling in vivo. *Am J Physiol Lung Cell Mol Physiol* 310: L1260–L1271, 2016. doi:10.1152/ajplung.00065.2016.
37. **Lopez-Rodriguez E, Laucamp C, Hidalgo A, Cruz A, Perez-Gil J, Ochs MLK.** Using pulmonary surfactant as Pirfenidone vehicle to target lung epithelium in bleoycin-induced lung fibrosis. *Am J Respir Crit Care Med* 193: A2378, 2016.
38. **Lowry OH, Rosebrough NJ, Farr AL, Randall RJ.** Protein measurement with the Folin phenol reagent. *J Biol Chem* 193: 265–275, 1951.
39. **Lutz D, Gazdhar A, Lopez-Rodriguez E, Ruppert C, Mahavadi P, Günther A, Klepetko W, Bates JH, Smith B, Geiser T, Ochs M, Knudsen L.** Alveolar derecruitment and collapse induration as crucial mechanisms in lung injury and fibrosis. *Am J Respir Cell Mol Biol* 52: 232–243, 2015. doi:10.1165/rcmb.2014-0078OC.
40. **Mahavadi P, Korfei M, Henneke I, Liebisch G, Schmitz G, Gochuico BR, Markart P, Bellusci S, Seeger W, Ruppert C, Guenther A.** Epithelial stress and apoptosis underlie Hermansky-Pudlak syndrome-associated interstitial pneumonia. *Am J Respir Crit Care Med* 182: 207–219, 2010. doi:10.1164/rccm.200909-1414OC.
41. **Mai C, Verleden SE, McDonough JE, Willems S, De Wever W, Coolen J, Dubbeldam A, Van Raemdonck DE, Verbeken EK, Verleden GM, Hogg JC, Vanaudenaerde BM, Wuyts WA, Verschakelen JA.** Thin-section CT features of idiopathic pulmonary fibrosis correlated with micro-CT and histologic analysis. *Radiology* 283: 252–263, 2017. doi:10.1148/radiol.2016152362.
42. **Matute-Bello G, Downey G, Moore BB, Groshong SD, Matthay MA, Slutsky AS, Kuebler WM; Acute Lung Injury in Animals Study Group.** An official American Thoracic Society workshop report: features and measurements of experimental acute lung injury in animals. *Am J Respir Cell Mol Biol* 44: 725–738, 2011. doi:10.1165/rcmb.2009-0210ST.
43. **Mertens M, Tabuchi A, Meissner S, Krueger A, Schirrmann K, Kertzscher U, Pries AR, Slutsky AS, Koch E, Kuebler WM.** Alveolar dynamics in acute lung injury: heterogeneous distension rather than cyclic opening and collapse. *Crit Care Med* 37: 2604–2611, 2009. doi:10.1097/CCM.0b013e3181a5544d.
44. **Mühlfeld C, Becker L, Bussinger C, Vollroth M, Nagib R, Schaefer I-M, Knudsen L, Richter J, Madershahian N, Wahlers T, Wittwer T, Ochs M.** Exogenous surfactant in ischemia/reperfusion: effects on endogenous surfactant pools. *J Heart Lung Transplant* 29: 327–334, 2010. doi:10.1016/j.healun.2009.07.019.
45. **Mulugeta S, Nureki S, Beers MF.** Lost after translation: insights from pulmonary surfactant for understanding the role of alveolar epithelial dysfunction and cellular quality control in fibrotic lung disease. *Am J Physiol Lung Cell Mol Physiol* 309: L507–L525, 2015. doi:10.1152/ajplung.00139.2015.
46. **Myers JL, Katzenstein AL.** Epithelial necrosis and alveolar collapse in the pathogenesis of usual interstitial pneumonia. *Chest* 94: 1309–1311, 1988. doi:10.1378/chest.94.6.1309.
47. **Mühlfeld C, Becker L, Bussinger C, Vollroth M, Nagib R, Schaefer IM, Knudsen L, Richter J, Madershahian N, Wahlers T, Wittwer T, Ochs M.** Exogenous surfactant in ischemia/reperfusion: effects on endogenous surfactant pools. *J Heart Lung Transplant* 29: 327–334, 2010. doi:10.1016/j.healun.2009.07.019.
48. **Mühlfeld C, Ochs M.** Quantitative microscopy of the lung: a problem-based approach. Part 2: stereological parameters and study designs in various diseases of the respiratory tract. *Am J Physiol Lung Cell Mol Physiol* 305: L205–L221, 2013. doi:10.1152/ajplung.00427.2012.
49. **Nieman GF, Bredenberg CE.** High surface tension pulmonary edema induced by detergent aerosol. *J Appl Physiol (1985)* 58: 129–136, 1985.
50. **Nieman GF, Gatto LA, Habashi NM.** Impact of mechanical ventilation on the pathophysiology of progressive acute lung injury. *J Appl Physiol (1985)* 119: 1245–1261, 2015. doi:10.1152/japplphysiol.00659.2015.
51. **Nogee LM, Dunbar AE III, Wert SE, Askin F, Hamvas A, Whitsett JA.** A mutation in the surfactant protein C gene associated with familial interstitial lung disease. *N Engl J Med* 344: 573–579, 2001. doi:10.1056/NEJM200102223440805.
52. **Ochs M.** A brief update on lung stereology. *J Microsc* 222: 188–200, 2006. doi:10.1111/j.1365-2818.2006.01587.x.
53. **Ochs M.** The closer we look the more we see? Quantitative microscopic analysis of the pulmonary surfactant system. *Cell Physiol Biochem* 25: 27–40, 2010. doi:10.1159/000272061.
54. **Ochs M, Mühlfeld C.** Quantitative microscopy of the lung: a problem-based approach. Part 1: basic principles of lung stereology. *Am J Physiol Lung Cell Mol Physiol* 305: L15–L22, 2013. doi:10.1152/ajplung.00429.2012.
55. **Ochs M, Schüttler M, Stichtenoth G, Herting E.** Morphological alterations of exogenous surfactant inhibited by meconium can be prevented by dextran. *Respir Res* 7: 86, 2006. doi:10.1186/1465-9921-7-86.
56. **Perez-Gil J, Weaver TE.** Pulmonary surfactant pathophysiology: current models and open questions. *Physiology (Bethesda)* 25: 132–141, 2010. doi:10.1152/physiol.00006.2010.
57. **Pozarska A, Rodríguez-Castillo JA, Surate Solaligue DE, Ntokou A, Rath P, Mižíková I, Madurga A, Mayer K, Vadász I, Herold S, Ahlbrecht K, Seeger W, Morty RE.** Stereological monitoring of mouse lung alveolarization from the early postnatal period to adulthood. *Am J Physiol Lung Cell Mol Physiol* 312: L882–L895, 2017. doi:10.1152/ajplung.00492.2016.
58. **Ruppert C, Kuchenbuch T, Boensch M, Schmidt S, Mathes U, Hillebrand V, Henneke I, Markart P, Reiss I, Schermuly RT, Seeger W, Günther A.** Dry powder aerosolization of a recombinant surfactant protein-C-based surfactant for inhalative treatment of the acutely inflamed lung. *Crit Care Med* 38: 1584–1591, 2010. doi:10.1097/CCM.0b013e3181dfcb3b.
59. **Schiller HJ, McCann UG II, Carney DE, Gatto LA, Steinberg JM, Nieman GF.** Altered alveolar mechanics in the acutely injured lung. *Crit Care Med* 29: 1049–1055, 2001. doi:10.1097/00003246-200105000-00036.
60. **Schmidt R, Ruppert C, Markart P, Lübke N, Ermert L, Weissmann N, Breithecker A, Ermert M, Seeger W, Günther A.** Changes in pulmonary surfactant function and composition in bleomycin-induced pneumonitis and fibrosis. *Toxicol Appl Pharmacol* 195: 218–231, 2004. doi:10.1016/j.taap.2003.11.011.
61. **Schneider JP, Ochs M.** Alterations of mouse lung tissue dimensions during processing for morphometry: a comparison of methods. *Am J Physiol Lung Cell Mol Physiol* 306: L341–L350, 2014. doi:10.1152/ajplung.00329.2013.
62. **Sisson TH, Mendez M, Choi K, Subbotina N, Courey A, Cunningham A, Dave A, Engelhardt JF, Liu X, White ES, Thannickal VJ, Moore BB, Christensen PJ, Simon RH.** Targeted injury of type II alveolar epithelial cells induces pulmonary fibrosis. *Am J Respir Crit Care Med* 181: 254–263, 2010. doi:10.1164/rccm.200810-1615OC.
63. **Slutsky AS, Ranieri VM.** Ventilator-induced lung injury. *N Engl J Med* 369: 2126–2136, 2013. doi:10.1056/NEJMra1208707.
64. **Smith BJ, Grant KA, Bates JH.** Linking the development of ventilator-induced injury to mechanical function in the lung. *Ann Biomed Eng* 41: 527–536, 2013. doi:10.1007/s10439-012-0693-2.
65. **Stamme C, Brasch F, von Bethmann A, Uhlig S.** Effect of surfactant on ventilation-induced mediator release in isolated perfused mouse lungs. *Pulm Pharmacol Ther* 15: 455–461, 2002. doi:10.1006/pupt.2002.0383.
66. **Thrall RS, Swendsen CL, Shannon TH, Kennedy CA, Frederick DS, Grunze MF, Sulavik SB.** Correlation of changes in pulmonary surfactant phospholipids with compliance in bleomycin-induced pulmonary fibrosis in the rat. *Am Rev Respir Dis* 136: 113–118, 1987. doi:10.1164/ajrccm/136.1.113.
67. **Todd NW, Atamas SP, Luzina IG, Galvin JR.** Permanent alveolar collapse is the predominant mechanism in idiopathic pulmonary fibrosis. *Expert Rev Respir Med* 9: 411–418, 2015. doi:10.1586/17476348.2015.1067609.
68. **Tschanz S, Schneider JP, Knudsen L.** Design-based stereology: Planning, volumetry and sampling are crucial steps for a successful study. *Ann Anat* 196: 3–11, 2014. doi:10.1016/j.aanat.2013.04.011.
69. **Wang K, Qin S, Liang Z, Zhang Y, Xu Y, Chen A, Guo X, Cheng H, Zhang X, Ke Y.** Epithelial disruption of Gab1 perturbs surfactant homeostasis and predisposes mice to lung injuries. *Am J Physiol Lung Cell Mol Physiol* 311: L1149–L1159, 2016. doi:10.1152/ajplung.00107.2016.
70. **Weibel ER, Hsia CC, Ochs M.** How much is there really? Why stereology is essential in lung morphometry. *J Appl Physiol (1985)* 102: 459–467, 2007. doi:10.1152/japplphysiol.00808.2006.

71. **Young LR, Gulleman PM, Bridges JP, Weaver TE, Deutsch GH, Blackwell TS, McCormack FX.** The alveolar epithelium determines susceptibility to lung fibrosis in Hermansky-Pudlak syndrome. *Am J Respir Crit Care Med* 186: 1014–1024, 2012. doi:10.1164/rccm.201207-1206OC.

72. **Zhang X, Zhang Y, Tao B, Teng L, Li Y, Cao R, Gui Q, Ye M, Mou X, Cheng H, Hu H, Zhou R, Wu X, Xie Q, Ning W, Lai M, Shen H, Feng GS, Ke Y.** Loss of Shp2 in alveoli epithelia induces deregulated surfactant homeostasis, resulting in spontaneous pulmonary fibrosis. *FASEB J* 26: 2338–2350, 2012. doi:10.1096/fj.11-200139.

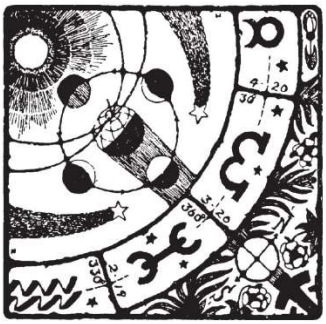

Reprinted with permission

RELEVANCE OF THIS WORK

In this paper, we concluded that the SRT beneficial effect probably relies on the stabilization of alveoli, thus the prevention of alveolar collapse and mechanical stress in the alveolar epithelium. Firstly, SRT improved surfactant biophysical function by means of decreased surface tension in vitro. Normalized surface tension seemed to help in maintaining alveoli opened, avoiding alveolar collapse and the associated mechanical stress in the alveolar epithelium. Interestingly the stabilization of alveoli had a positive effect in not only the mechanical properties of the lung but also "anti-inflammatory" properties. In summary SRT before day 3, increased the structural markers of stabilized opened alveoli (volume of acinar air spaces, alveolar air spaces, alveolar surface and number of opened alveoli) as well as improved mechanical parameters, such as static compliance, inspiratory capacity and elastance. In addition, most of the inflammatory cellular and biochemical markers were notably decreased (such as number of granulocytes and activated macrophages, as well as IL4, IL-6, IL10 and IL-1β). This demonstrated that SRT could prevent alveolar collapse and the associated inflammation response, resulting from the mechanical stress in the alveolar epithelium. Applying repetitive SRT before the onset of fibrosis led to a reduction of the septal wall volume and thickness, increased number of opened alveoli and improved mechanical parameters. Taking all together, SRT may help slowing down the progression of fibrotic remodeling in the lung, serving as a supportive treatment for lung fibrosis.

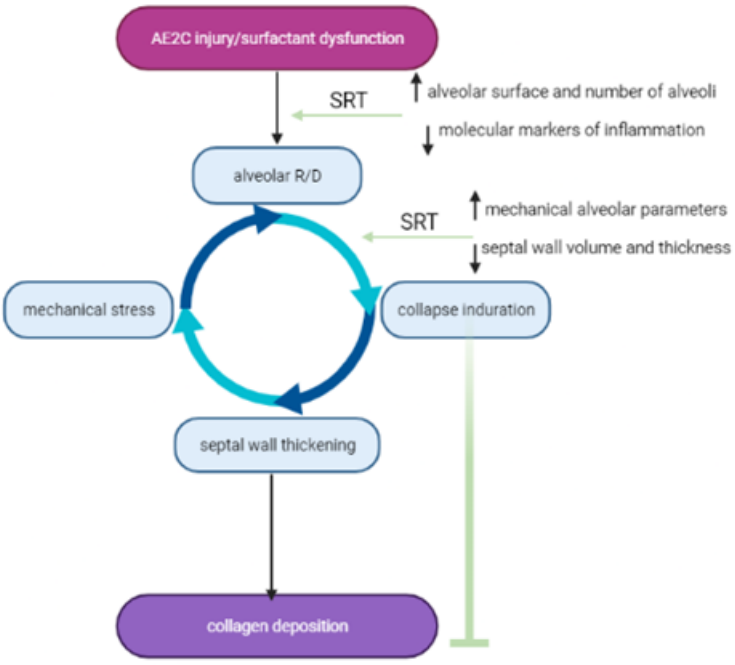

Figure 6: effects of SRT at the application points and beneficial effects in the rat model of bleomycin induced lung injury and fibrosis (Created in BioRender.com).

3.2 ALVEOLAR EPITHELIAL TYPE II CELL TRANSPLANTATION (ORIGINAL WORK 5)

Lopez-Rodriguez E.*, Guy-Jordi G.*, Knudsen L., Ochs M. & Serrano-Mollar A. "*Improved alveolar dynamics and structure after alveolar epithelial type II cell transplantation in bleomycin induced lung fibrosis"* Frontiers in Medicine 2021; 8: 640020

As seen in the previous chapter the application of one dose of surfactant as preventive or supportive treatment seems to be very promising in delaying the fibrotic remodeling onset and reducing the inflammation. Another interesting therapeutic strategy may be to replace not only surfactant but also the injured AE2C, which may act as the source of new freshly secreted surfactant.

AE2C injury during fibrotic remodeling has already been involved in the development of lung fibrosis. AE2C are subjected to apoptosis, endoplasmic reticulum stress and lysosomal damage during the development of lung fibrosis (131-134). As explained before, changes in the mechanical forces in the lung parenchyma lead to epithelial stress and alveolar epithelial cell (AEC) injury. It has been demonstrated, that strain forces induced by pressure over 40cmH2O are enough to cause membrane blebbing and induce cellular apoptosis (135). Plasma membrane injury of AEC is seen under normal healthy conditions. In fact, AEC are able to repair their membrane to prevent cellular damage in a Ca^{2+}- and lysosome-dependent mechanism. However, if the mechanical stress induce a membrane defect larger than 1µm, aberrant wound healing mechanisms are activated (136). In addition, lysosomal stress may also impair cellular repair, as seen in Hermansky-Pudlack Syndrome (HPS) patients. This leads to aberrant wound repair and release of profibrotic cytokines ending in the development of unusual interstitial pneumonia (UIP) (137, 138).

In addition, AEC response to mechanical stress activates the signaling of a number of mechano-transduction pathways, which includes the TGF-β1, Wnt β-catenin, sonic hedgehog (Shh) and the Notch-midkine pathways. Moreover, mechanical injury also induces endoplasmic reticulum (ER) stress. All of these pathways have been related to aberrant wound healing and the activation of profibrotic genes, epithelial-to-mesenchymal transition (EMT) and increased ECM deposition. In addition, ER stress has been shown to impair the secretory function of the AE2C, impairing surfactant secretion and metabolism, therefore initiating a vicious cycle that contribute to alveolar instability and mechanical stress (136). In a murine model of surfactant depletion, induced by hydrochloric acid (HCl) intratracheal application, the lung mechanics was notably impaired, showing an increase in tissue elastance (or increased stiffening of the lung tissue). This was accompanied by an increase in mesenchymal markers, such as α-smooth muscle actin (α-SMA) and vimentin in AE2C. At the same time, AE2C markers, such as proSP-B, were notably decreased (56, 139). Therefore, EMT seems to contribute to fibrotic

remodeling by impairing AE2C 2 most important functions, surfactant metabolism and regeneration of AEC.

On the one hand, both AECs as well as resident inflammatory cells like AM (45) express TGF-β1. On the other hand, the increase in epithelial injury results in increased expression of epithelial αVβ6-integrins, which further stimulate the production of TGF-β1 by mechano-transduction (140). In this regard, the increased expression and release of TGF-β1 in IPF fibrotic lungs have been already described, along with parenchymal stiffening (141). Nevertheless, the role of collapse-induced parenchymal stiffening in the context of extracellular TGF-β1 release to date has not been clarified. As shown in Chapter 2.1, TGF-β1 treated mice have been shown to develop surfactant dysfunction and high surface tension (40) including down-regulation of SP-C expression, by interfering with its transcription factor activity.

As explained in the previous chapter, lung surfactant dysfunction is an early event in the development of the lung fibrosis in the bleomycin induced lung fibrosis rat model. More specifically surfactant dysfunction has been seen to happen 3 days after bleomycin application (115). Therefore, we can hypothesize that mechanical stress in this model may be initiated as soon as surfactant function is impaired. In addition, in this model, TGF-β1 is elevated in alveolar macrophages, epithelial cells, endothelial cells and interstitial fibroblasts (142), which will further contribute to collagen deposition changing the elastic properties of the tissue and thus, the mechanics and alveolar dynamics.

The aim of this work was to investigate whether a pulmonary AE2C transplantation therapy may be beneficial to stop or slow down the development of fibrotic remodeling. For this purpose, we used the bleomycin induced lung injury and fibrosis rat model, as before. We performed pulmonary AE2C transplantation early in the lung injury phase of the model (at day3) and analyzed early events (at day 7). In addition, we performed the transplantation of AE2C later during the onset of fibrosis (at day 7) and analyze fibrotic remodeling (at day 14). We hypothesized that replacing injured AE2C in the bleomycin rat model by healthy AE2C may lead to a reduced lung injury and fibrosis, partly through the production of new surfactant. To test this hypothesis, we assessed if: 1) after transplantation in the injury phase the healthy AE2C are able to reduce inflammation, normalizing the alveolar dynamics, including tissue elastance and structural parameters, such as edema; 2) after transplantation in the fibrotic remodeling phase, healthy AE2C are able to reduce the fibrotic remodeling, normalizing structural, such as septal wall thickness, and alveolar dynamics of the lung parenchyma, and; 3) the potential beneficial effect may be due to the secretion of fresh surfactant, thus replacing the endogenous surfactant.

frontiers in Medicine

ORIGINAL RESEARCH
published: 17 February 2021
doi: 10.3389/fmed.2021.640020

Improved Alveolar Dynamics and Structure After Alveolar Epithelial Type II Cell Transplantation in Bleomycin Induced Lung Fibrosis

Elena Lopez-Rodriguez[1,2†], *Gemma Gay-Jordi*[3,4†], *Lars Knudsen*[1,5], *Matthias Ochs*[1,2,6*] and *Anna Serrano-Mollar*[3,4*]

[1] Institute of Functional Anatomy, Charité - Universitaetsmedizin Berlin, Berlin, Germany, [2] Institute of Functional and Applied Anatomy, Hannover Medical School, Hannover, Germany, [3] Experimental Pathology Department, Institut d'Investigacions Biomèdiques de Barcelona, Consejo Superior de Investigaciones Cientificas (IIBB-CSIC) Barcelona, Institut d'Investigacions Biomédiques August Pi i Sunyer (IDIBAPS), Barcelona, Spain, [4] Centro de Investigaciones Biomédicas en Red de Enfermedades Respiratorias (CIBERES), Madrid, Spain, [5] Biomedical Research in Endstage and Obstructive Lung Disease Hannover (BREATH), Member of the German Center for Lung Research (DZL), Hannover, Germany, [6] German Center for Lung Research (DZL), Berlin, Germany

OPEN ACCESS

Edited by:
Mehdi Mirsaeidi, University of Miami, United States

Reviewed by:
Michael Roth, University Hospital of Basel, Switzerland
Jesus Perez-Gil, Complutense University of Madrid, Spain

***Correspondence:**
Anna Serrano-Mollar
anna.serranomollar@iibb.csic.es
Matthias Ochs
matthias.ochs@charite.de

[†]*These authors have contributed equally to the work*

Specialty section:
This article was submitted to Pulmonary Medicine, a section of the journal Frontiers in Medicine

Received: *10 December 2020*
Accepted: *25 January 2021*
Published: *17 February 2021*

Citation:
Lopez-Rodriguez E, Gay-Jordi G, Knudsen L, Ochs M and Serrano-Mollar A (2021) Improved Alveolar Dynamics and Structure After Alveolar Epithelial Type II Cell Transplantation in Bleomycin Induced Lung Fibrosis. Front. Med. 8:640020. doi: 10.3389/fmed.2021.640020

Idiopathic pulmonary fibrosis (IPF) is a progressively and ultimately fatal lung disease. Previously it has been shown that intratracheal administration of alveolar epithelial type II cells (AE2C) in the animal model of bleomycin-induced pulmonary fibrosis is able to reverse fibrosis and restore surfactant protein levels. However, to date, it has not been evaluated whether these changes involve any improvement in alveolar dynamics. Consequently, the aim of the present work was to study lung physiology after AE2C transplantation at different time points during the development of injury and fibrosis. Lung fibrosis was induced by intratracheal instillation of bleomycin (4U/kg) in rat lungs. The animals were transplanted with AE2C (2.5×10^6 cells/animal) 3 or 7 days after bleomycin instillation. Assessments were done at day 7 and 14 after the induction of fibrosis to plot time dependent changes in lung physiology and mechanics. To assess the pressures and rates at which closed alveoli reopens invasive pulmonary tests using a small-animal mechanical ventilator (Flexivent®, Scireq, Canada) including de-recruitability tests and forced oscillation technique as well as quasi-static pressure volume loops were performed. Afterwards lungs were fixed by vascular perfusion and subjected to design-based stereological evaluation at light and electron microscopy level. AE2C delivered during the lung injury phase (3 days) of the disease are only able to slightly recover the volume of AE2C and volume fraction of LB in AE2C. However, it did not show either positive effects regarding ventilated alveolar surface nor any increase of lung compliance. On the other hand, when AE2C are delivered at the beginning of the fibrotic phase (7 days after bleomycin instillation), an increased ventilated alveolar surface to control levels and reduced septal wall thickness can be observed. Moreover, transplanted animals showed better lung performance, with increased inspiratory capacity and compliance. In addition, a detailed analysis of surfactant active forms [mainly tubular myelin, lamellar body (LB)-like structures and multilamellar vesicles (MLV)], showed an effective recovery during the pro-fibrotic phase

due to the healthy AE2C transplantation. In conclusion, AE2C transplantation during fibrogenic phases of the disease improves lung performance, structure and surfactant ultrastructure in bleomycin-induced lung fibrosis.

Keywords: lung fibrosis, alveolar epithelial type 2 cells, lung surfactant, cell therapy, bleomycin, alveolar dynamics, lung structure

INTRODUCTION

Idiopathic pulmonary fibrosis (IPF) is a progressive and severe disease with no known cause and with a limited response to currently available therapies, ultimately IPF is a fatal lung disease (1–3). The median survival time is 3–5 years from the time of diagnosis (1). The classic features of the disorder include progressive dyspnea and a non-productive cough. Pulmonary function tests usually reveal decreased lung volumes (especially decreased forced vital capacity, total lung capacity, and functional residual capacity) and diminished carbon monoxide diffusing capacity. During the course of the disease patients show a progressive decline in pulmonary function leading to respiratory failure and death.

The pathogenesis of IPF is characterized primarily by epithelial cell damage and inadequate regeneration. In normal physiological conditions, the renewal of alveolar epithelial cells occurs through the specific proliferation and differentiation of alveolar epithelial type 2 cells (AE2C) into alveolar type 1 cells. However, IPF is characterized by the loss of both alveolar cell types leading over time to epithelial necrosis, the appearance of fibroblast foci and persistent alveolar collapse (4, 5). In addition to AE2C dysfunction (5–7), IPF is also characterized by impaired surfactant function (8). In this sense, it is important to note that AE2C are also the cells responsible for synthesizing, storing, secreting and recycling the components of surfactant (9, 10) and therefore also play a crucial role in pulmonary mechanics by stabilizing alveolar dimensions and surface throughout the respiratory cycle (11, 12). During fibrosis development the surfactant dysfunction and edema increase the degree of alveolar recruitment and de-recruitment (alveolar R/D). The localized mechanical stresses imparted on the alveolar epithelium during R/D aggravate lung injury (13) leading to fibrotic remodeling (14, 15). The surface tension in some collapsed alveoli may become so high that recruitment is impossible. Eventually, collapse induration can occur whereby chronically collapsed alveoli effectively disappear by being reabsorbed into the surrounding interstitial tissue increasing the damage (5, 16, 17).

Since AE2C seem to be key cells in the fibrotic development, it has been proposed that re-generation or replacement of AE2C may be an alternative for the therapy of lung fibrosis patients (18–20). In this context, transplanting healthy donor AE2C in fibrotic lungs is a promising tool to explore. Previously, our research group has shown that intratracheal administration of AE2C in the animal model of bleomycin-induced pulmonary fibrosis was able to reverse fibrosis and restores surfactant protein levels (18, 19). Although our research group pioneered the development of this cell therapy, our results have also been corroborated by other research groups. They have also observed that both AE2C and stem cells derived to AE2C have also been able to reverse pulmonary fibrosis (20–24). Moreover, in a clinical study performed with IPF patients, the intratracheal administration of heterologous AE2C was safe, well-tolerated, with no relevant side effects, and was able to stabilize disease progression, improving health-related quality of life throughout a 1-year clinical follow-up (25). Those astonishing results obtained in humans were assessed by means of non-invasive pulmonary function tests, however to date it has not been evaluated whether these changes are related to any improvement in lung dynamics and structure. Consequently, the aim of the present work was to study lung physiology after AE2C transplantation at different time points during the development of fibrosis.

METHODS

Animals

Fischer 344 rats, weighting 200–225 g at the beginning of the experiment, were used, in accordance with the European Community (Directive 2010/63/EU) for experimental animals and it was approved by the local authorities of Lower Saxony (Niedersächsisches Landesamt für Verbraucherschutz und Lebensmittelsicherheit, LAVES, Lower Saxony, Germany) with number TVA 15/1890.

Bleomycin-Induced Lung Fibrosis

Lung fibrosis was induced by intratracheal instillation of a single dose of BLM (4U/kg) (Sigma, USA) dissolved in 200 μl of sterile saline under isoflurane anesthesia. Control animals received the same volume of saline. The animal body weights were recorded every day during the course of the experiment.

Isolation of Alveolar Epithelial Type II Cells

Fresh alveolar epithelial type II cells (AE2C) were isolated from healthy donor animals. The protocol for purification has been described by Richards RJ group (26). Briefly, to isolate AE2C, the lungs were removed from the animal and lavaged with 5 × 10 ml saline. The lungs were digested by filling with 0.25% trypsin dissolved in saline (100 ml) (T8003, Sigma, Missouri, USA) and suspended in 0.9% NaCl at 37°C for 30 min, with the trypsin constantly topped up to expand the parenchyma for 30 min, suspended in a saline solution at 37°C. Following digestion, the lungs were chopped into 1–2 mm^2 cubes, treated with 75 U/ ml DNase dissolved in saline and filtered through nylon meshes ranging from 150 to 30 μm. The resulting cell suspension was centrifuged (250 × *g*, 20 min at 10°C) through a sterile Percoll gradient and the AE2C rich band was removed. A second DNase treatment of 20 U/ml was administered, and the cells were recovered as a pellet by centrifugation at 250 × *g* for

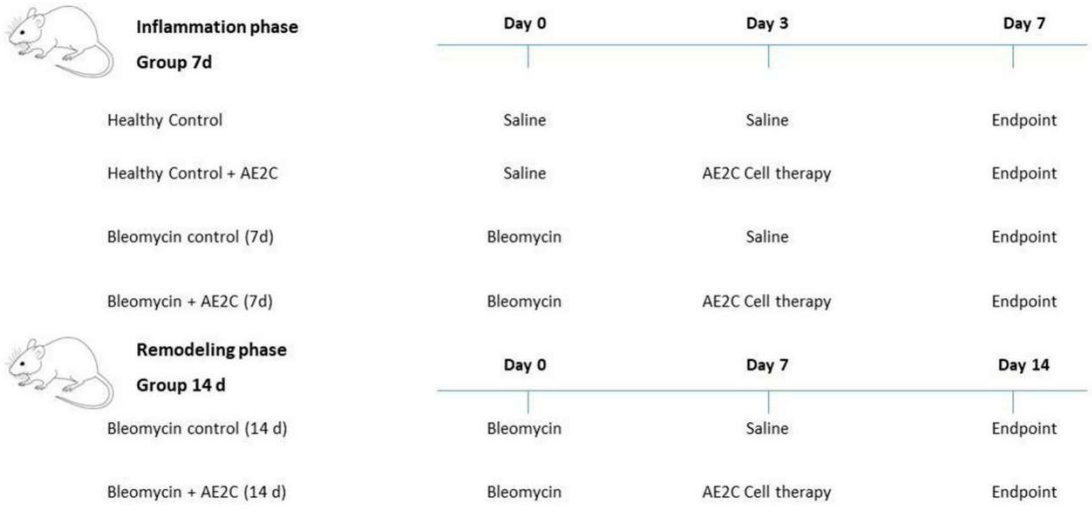

FIGURE 1 | Scheme of the experimental design. The animals were randomly distributed into four experimental groups and two different time points during the inflammatory phase (Group 7d) and fibrotic phase (Group 14 d) (n = 5–8 in each group).

20 min. These cells were resuspended in 5 ml DCCM 1 (Biological Industries, Kibbutz Beit Haemek, Israel) completed with a 2% (w/v) L- Glutamine and subjected to differential attachment on a plastic Petri dish. Non-adherent AE2C were collected after 2 h and counted to establish the final cell yield of freshly purified cells.

The AE2C viability was assessed by Trypan Blue (Sigma, Missouri, USA), showing >95% viability. Cell yield, purity and characterization of freshly isolated AE2C were established by the presence of intracellular alkaline phosphatase (Sigma, USA).

Transplantation Procedure

At day 3 or 7 after intratracheal BLM, recipient animals were transplanted with AE2C by intratracheal instillation (2.5×10^6 cells/animal suspended in 400 µl of sterile saline) under isoflurane anesthesia. The control group received the same dose of cells 3 or 7 days after saline instillation. The animals were sacrificed at day 7 and 14 after the induction of lung fibrosis to plot time dependent changes in lung physiology and functionality.

Experimental Groups

The animals were randomly distributed into four experimental groups and we studied two different time points (n = 5–8 in each group): Healthy Control: Saline instillation; Healthy Control + AE2C (3 days after saline instillation); Bleomycin control: Bleomycin instillation + saline (3 or 7 days after bleomycin instillation); Bleomycin + AE2C: Bleomycin instillation + alveolar type II cell transplantation (3 or 7 days after bleomycin instillation). **Figure 1** shows a scheme of the experimental design.

Invasive Pulmonary Function Test

To assess the pressures and rates at which alveoli in the injured lungs closed, de-recruitability tests at different PEEP (positive end-expiratory pressures) as well as quasi-static pressure volume-loops using a Flexivent ventilator (SCIREQ, Canada) were performed (27). The de-recruitability tests consist of two recruitment maneuvers (up to 30 cmH_2O followed) followed by 5 min of low-tidal volume ventilation (10 ml/kg body weight) interspersed with 8 s multi-frequency forced oscillation perturbations at 30 s intervals. Tissue elastance (H), tissue damping (G) and tissue hysteresivity (G/H) were calculated by fitting the constant phase model to impedance spectra. After each de-recruitability test, 3 quasi-static PV loops were recorded, and quasi-static compliance was calculated according to the Salazar-Knowles equation.

Perfusion-Fixation of Lungs and Sampling Procedures for Light and Electron Microscopy

Fixation and sampling were conducted according to standards on quantitative morphology of the lung (28). The lungs were fixed by vascular perfusion at an airway pressure of 13 cm H_2O on expiration. The volume of the lungs was determined and followed by a systematic uniform random sampling. Seven to 9 tissue slices per lung were randomized for light microscopy and 5–6 tissue blocks per lung for electron microscopic evaluation. Slices for light microscopy were embedded in Technovite resin and stained with toluidine blue. Lung blocks for electron microscopy were embedded in Epon resin and contrasted with uranyl acetate and lead citrate.

Design-Based Stereology

At the light microscopic level, a newCAST-system (Visiopharm A/S, Denmark) was used to perform systematic uniform random area sampling and to superimpose an appropriate test system on the fields of view. A transmission electron microscope (FEI Morgagni, Netherlands) equipped with a digital camera (Olympus Soft Imaging Systems, Germany) was used to obtain representative fields of view. The parameters useful to characterize the pathology of fibrotic development were volume of lungs, volume of parenchyma, volume of ventilated parenchyma, thickness of the septal wall, volume fraction of AE2C cells, volume of lamellar bodies per AE2C cell, volume of intra-alveolar surfactant, lamellar body like structures, multilamellar vesicles, tubular myelin, and unilamellar vesicles. A stereology tool (STEPanizer®, Bern, Switzerland) was employed for definitive stereological morphometry. A point grid was chosen as a test system for volume estimation. Securing sufficient stereological precision, the number of test points was adjusted to a minimum of 200 to 300 counting events per parameter per lung (29). A counting event was defined as a match of a structure of interest (SOI) with the test probe. At 5x magnification, volume fractions of parenchyma [Vv(par/lung)] and non-parenchyma [Vv(non-par/lung)] were obtained. Parenchyma was defined as lung tissue enabling gas exchange, comprising septa and airspaces, and was differentiated in ventilated [Vv(ventpar/par)] and non-ventilated parenchyma [Vv(non-vent/par)]. Pleura, conducting airways and large vessels with the surrounding connective tissue were defined as non-parenchyma. Volume densities of ductal airspaces [Vv(duct/par), alveolar airspaces (Vv(alv/par) and alveolar septa (Vv(sept/par)] were determined at 20x magnification within ventilated parenchyma. Herein, an additional test system consisting of 4 line-pairs was utilized for counting intersections of test probes and alveolar surface. All analyzed parameters for lung structure regarding fibrosis were chosen according to recommendations from Ochs and Mühlfeld (29) for stereology in pulmonary fibrosis and (30) for stereology in bleomycin induced lung injury and fibrosis.

Volume fractions [e.g., Vv(par/lung)] were calculated by dividing the number of points (P) hitting the SOI (structure of interest) by the number of points hitting the reference space, e.g., total lung.

$$\mathrm{Vv(par/lung)} = \sum[\mathrm{Ppar}]/\sum[\mathrm{Ppar} + \mathrm{Pnon{-}par}]$$

Multiplication of the volume fraction with total lung volume provided total volumes of each SOI [e.g., V(par,lung)]: V(par,lung) = Vv(par/lung)*V(lung),

Analogous calculations were performed for parenchymal components, e.g., alveolar airspaces, LB in AE2C and TM fraction in total intra-alveolar surfactant:

$$\mathrm{Vv(alv/ven{-}par)} = \sum[\mathrm{Palv}]/\sum[\mathrm{Pvent{-}par}]$$
$$\mathrm{V(alv, vent{-}par)} = \mathrm{Vv(alv/vent{-}par)}^{*}\mathrm{V(vent{-}par, lung)},$$

Intersection (I) countings were utilized in combination with the length per point of the test system (l(p)) to estimate the alveolar surface density of ventilated parenchyma. The calculated absolute volume describes the alveolar surface contributing to pulmonary gas exchange:

$$\mathrm{Sv(alv/vent{-}par)} = (2^{*}\sum[\mathrm{I}])/(\mathrm{l(p)}^{*}\sum[\mathrm{Pvent{-}par}]$$
$$\mathrm{Salv} = \mathrm{Sv(alv/(vent{-}par))}^{*}\mathrm{V(vent{-}par, lung)},$$

Septal thickness was computed as follows: τ (sep) = Vv(sept/par)/Sv(alv/par)*2.

Statistical Analysis

Data are expressed as mean values for each subject, horizontal bars represent the mean of the group. In bar graphs, data is represented as mean and SD in error bars. Statistical analysis was carried out by a non-parametric analysis (Kruskal-Wallis test) followed by appropriate *post hoc* tests, Dunn's multiple comparisons test when differences were significant (GraphPad Software Inc, USA). A $p < 0.05$ was considered significant.

RESULTS

Alveolar Dynamics of Bleomycin Induced Lung Injury (d7) and Fibrosis (d14) After AE2C Transplantation

After isolation of healthy AE2C, the purity of the cells measured by positive staining with alkaline phosphatase was 87 ± 2%. After transplantation of AE2C, we performed a complete alveolar dynamics analysis by means of Forced Oscillation Technique (FOT) in a small animal ventilator. **Figures 2A,B** shows the elastance (H) of the lungs 7 days after bleomycin application and 4 days after AE2C transplantation in the corresponding treatment and control groups. As already described, elastance is significantly increased after bleomycin application at both PEEP of 3 (**Figure 2A**) and 6 cmH2O (**Figure 2B**) compared to healthy controls. In addition, after AE2C transplantation, no changes in elastance could be observed compared to bleomycin control. In accordance, the application of bleomycin reduced static compliance (**Figure 2C**) and AE2C showed no improvement of this value. Tissue hysteresivity (G/H) was also significantly reduced in the groups with application of bleomycin with no changes after AE2C transplantation (**Figure 2D**).

When analyzing the alveolar dynamics 14 days after bleomycin application, and 7 days after AE2C transplantation, an improvement on elastance (**Figures 2E,F**) and compliance (**Figure 2G**) could be observed. The group that received an AE2C transplantation after bleomycin application showed significantly lower elastance values than the bleomycin control group, between those of the bleomycin control group and the healthy groups. This could be related to a beneficial effect of the newly transplanted AE2C in the mechanical properties of the lung. Accordingly, static compliance was also significantly higher in the disease group that received the AE2C transplantation than the bleomycin control group. Tissue hysteresivity was also affected by AE2C transplantation, showing a significant reduction (**Figure 2H**).

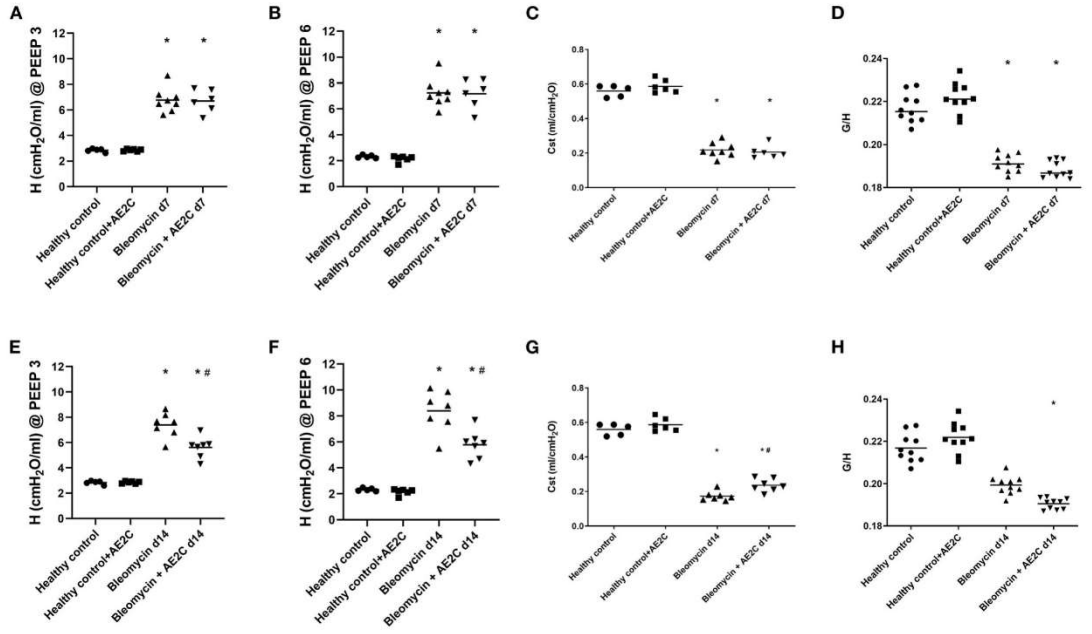

FIGURE 2 | Alveolar dynamics of bleomycin induced lung injury (d7) and fibrosis (d14) after AE2C transplantation. **(A–D)** Alveolar dynamics of bleomycin induced lung injury (7 days after bleomycin application) and AE2C transplantation (3 days after bleomycin application). **(A)** Tissue elastance (H) at a positive end-expiratory pressure (PEEP) of 3cmH2O over the 5 min forced oscillation technique (FOT) at day 7 after bleomycin application. **(B)** Tissue elastance (H) at a PEEP of 6cmH2O at day 7 after bleomycin application. **(C)** Static compliance (ml/cmH2O) at day 7 after bleomycin application. **(D)** Tissue histeresivity **(G,H)** at day 7 after bleomycin application. **(E–H)** Alveolar dynamics of bleomycin induced lung fibrosis (14 days after bleomycin application) and AE2C transplantation (7 days after bleomycin application). **(E)** Tissue elastance **(H)** at a positive end-expiratory pressure (PEEP) of 3cmH2O over the 5 min forced oscillation technique (FOT) at day 14 after bleomycin application. **(F)** Tissue elastance **(H)** at a PEEP of 6cmH2O at day 14 after bleomycin application. **(G)** Static compliance (ml/cmH2O) at day 14 after bleomycin application. **(H)** Tissue histeresivity **(G,H)** at day 14 after bleomycin application. *$p < 0.05$ vs. healthy controls, #$p < 0.05$ vs. bleomycin control.

Lung Structure of Bleomycin Induced Lung Injury (d7) and Fibrosis (d14) After AE2C Transplantation

In order to understand if the mechanical parameters are a reflection of changes in lung structure, we immediately inflated and fixed the lungs of the animals after performing the alveolar dynamics in the small animal mechanical ventilator. **Figure 3** shows representative micrographs of the lungs from the animals at light (two upper panels, micrographs 1–12) and electron microscopy (two bottom panels, micrographs 13–24) level to illustrate the quantitative results shown in the following figures. As expected from stiffer and less compliant injured lungs (d7), the lung volume measured by fluid displacement and the volume of air used for inflation at constant pressure, is reduced in the bleomycin groups with and without AE2C transplantation (**Supplementary Figures 1A,B**). Looking closely at the parenchymal tissue, we also observed a significant decrease in ventilated (**Figure 4A**) and an increase of non-ventilated (**Figure 4B**) parenchyma total volume (**Figure 3**, micrographs 3 and 9). In addition, we also observed a significant increase in septal wall thickness (**Figure 4C**) and a decrease in total alveolar surface (**Figure 4D**) in the bleomycin treated with and without AE2C transplantation (**Figure 3**, micrographs 3-4 and 9-10). Within ventilated parenchyma, the alveolar spaces seemed to be the most affected by bleomycin application (**Figure 4E** and **Supplementary Figures 2A–C**). While there was a trend to increase in ductal volume density (**Figure 4E**), the total volume of ductal spaces remained unchanged (**Supplementary Figure 2B**), leading us to think that the air lost in the alveolar side is due to collapse and is not over-distending alveolar ducts.

On the other hand, the AE2C transplantation in lungs undergoing fibrotic remodeling showed more promising results (**Figure 3**, micrographs 5-6 and 11-12). According to the mechanical parameters presented above, the decrease in elastance and the increase in compliance in the transplanted group compared to the bleomycin group, was accompanied by an increase in ventilated parenchyma (**Figure 4F**) and a decrease in non-ventilated parenchyma (**Figure 4G**). In addition, there was a significant reduction of the septal wall thickness (**Figure 4H**) and increased alveolar surface (**Figure 4I**).

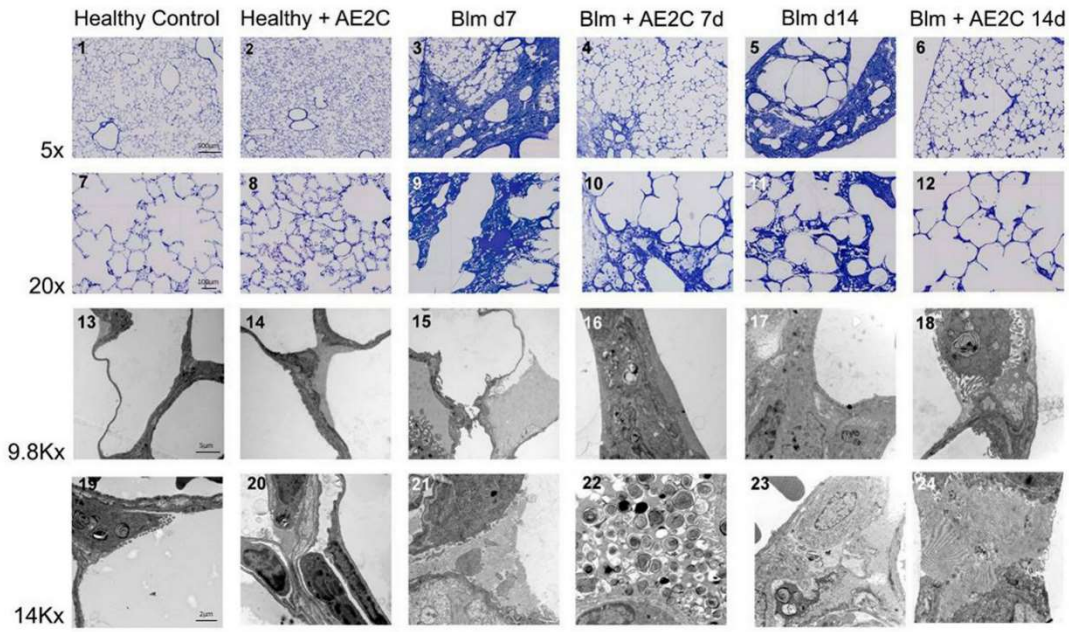

FIGURE 3 | Representative light and electron microscopy pictures of bleomycin induced lung injury (d7) and fibrosis (d14) after AE2C transplantation. Upper panels (micrographs 1-12): toluidine blue stained tissue at 5 and 20X magnification of the different experimental groups. Bottom panels (micrographs 13-24): electron microscopy pictures at 9.8 and 14Kx magnification of the different experimental groups.

As for the treatment during lung injury, within ventilated parenchyma, the alveolar spaces seemed to be the most affected ones by the bleomycin application and the transplantation treatment (**Figure 4J** and **Supplementary Figures 2D–F**). In this case, a significant increase in total volume of alveolar spaces (**Supplementary Figure 2D**) was observed in the bleomycin treated and transplanted lung compared to the bleomycin control.

Taking all together, the improved mechanics shown by the fibrotic lung treated with AE2C seemed to be supported by an improved lung structure by means of increased opened alveolar spaces and surface with thinner septal walls.

Lung Surfactant Ultrastructure of Bleomycin Induced Lung Injury (d7) and Fibrosis (d14) After AE2C Transplantation

In order to dissect the fine structure and composition of the alveolar parenchyma, we further analyzed the lung ultrastructure by means of quantification using electron microscopy micrographs (**Figure 3**, micrographs 13-24). This analysis allowed us to look closely at AE2C total volume in the alveolar parenchyma, as well as the total volume of edema and extracellular matrix. In addition, we have quantified the volume fraction of lamellar bodies (LB) in AE2C, to understand if surfactant synthesis is influenced by the AE2C transplantation.

As described before (30), the application of bleomycin reduces the volume of AE2C and the transplantation of AE2C slightly changed this (**Figure 5A**). However, the volume fraction of LB inside AE2C showed a trend to increase (non-statistically significant) in the transplanted injured group compared to the bleomycin group (**Figure 5B**). Also according to previous reports, bleomycin induced the formation of alveolar edema and its volume was unchanged after transplantation (**Figure 3**, micrograph 15 and 21, **Figure 5C**). Since the volume of ECM was not changed in any group (**Figure 5D**), the increase in septal wall thickness reported above (**Figure 4C**) is likely due to the alveolar edema and not to a remodeling process in the ECM.

When looking at fibrotic lungs (d14), the decrease in volume of AE2C after bleomycin was not significant compared to control groups, but the AE2C transplantation resulted in an increased total volume of these cells over the values of the controls (**Figure 5E**). The volume fraction of LB in AE2C also showed the same pattern, non-statistically significant against the bleomycin control (**Figure 5F**). Even when the volume of edema in bleomycin treated lungs was still significantly higher than in controls (**Figure 5G**), the values are much lower than the lung injured (d7) groups (**Figure 5C**). However, the volume of

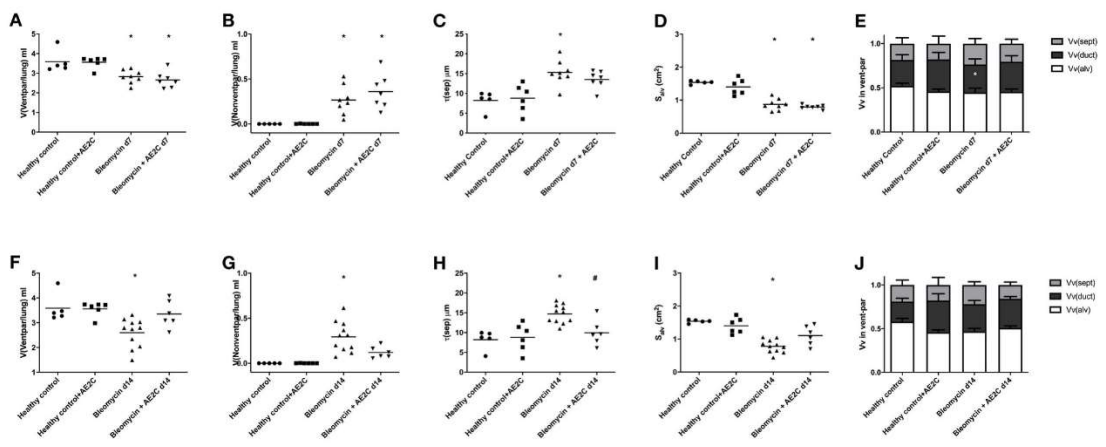

FIGURE 4 | Lung structure of bleomycin induced lung injury (d7) and fibrosis (d14) after AE2C transplantation. **(A–E)** Lung structure of bleomycin induced lung injury (7 days after bleomycin application) and AE2C transplantation (3 days after bleomycin application). **(A)** Total volume of ventilated parenchyma per lung (ml) at day 7 after bleomycin application. **(B)** Total volume of non-ventilated parenchyma per lung (ml) at day 7 after bleomycin application. **(C)** Thickness of septal wall (τ) at day 7 after bleomycin application. **(D)** Total alveolar surface per lung (S_{alv}). **(E)** Volume fractions of alveolar spaces (white bar), ductal spaces (dark gray bar) and septal wall (light gray bar) per ventilated parenchyma at day 7 after bleomycin application. **(F–J)** Lung structure of bleomycin induced lung fibrosis (14 days after bleomycin application) and AE2C transplantation (7 days after bleomycin application). **(F)** Total volume of ventilated parenchyma per lung (ml) at day 14 after bleomycin application. **(G)** Total volume of non-ventilated parenchyma per lung (ml) at day 14 after bleomycin application. **(H)** Thickness of septal wall (τ) at day 14 after bleomycin application. **(I)** Total alveolar surface per lung (S_{alv}). **(J)** Volume fractions of alveolar spaces (white bar), ductal spaces (dark gray bar) and septal wall (light gray bar) per ventilated parenchyma at day 14 after bleomycin application. $^*p < 0.05$ vs. healthy controls, $\#p < 0.05$ vs. bleomycin control.

ECM was notably increased in the bleomycin group 14 days after application, and significantly reduced after transplantation (**Figure 5H**). Therefore, the increase in septal wall thickness described above (**Figure 4H**) could be mainly related to aberrant accumulation of ECM components.

As AE2C are responsible for surfactant synthesis and secretion, we investigated whether the volume fraction of surfactant in alveolar spaces was affected by the AE2C transplantation. In addition, we were also interested in describing if the surfactant present in the alveolar spaces presented different fractions of active (tubular myelin (TM), lamellar body-like (LBL) and multilamellar vesicles (MLV) or inactive (unilamellar vesicles (ULV)) forms (9, 31) within the different disease stages or treatments.

For both experimental settings, the application of bleomycin significantly reduced the volume fraction of intra-alveolar surfactant and its active forms (**Figure 6**). AE2C transplantation during lung injury resulted in a non-significant increase of volume fraction of intra-alveolar surfactant (**Figure 6A**) compared to the bleomycin group. In addition, the transplantation did not change the reduction of TM and LBL induced by bleomycin, and inversely the increase on ULV (**Figure 6B**). On the other hand, AE2C transplantation in the lungs undergoing fibrotic remodeling showed a promising, but not significant, increase of volume fraction of intra-alveolar surfactant, accompanied by a statistically significant increase in TM and LBL active forms of surfactant (**Figure 3**, micrograph 24, **Figures 6C,D**).

Lung Structure-Mechanics Relationships of Bleomycin Induced Lung Injury (d7) and Fibrosis (d14) After AE2C Transplantation

Lastly, in order to investigate which structural parameters may impact the mechanical properties of the lungs after the different treatments and potential causal relationships, we systematically correlated the mechanical and structural data. In **Figure 7**, the most interesting correlations are presented for either the bleomycin induced lung injury (**Figures 7A–D**) and fibrosis (**Figures 7E–H**) after transplantation. Even though we found a significant correlation between tissue elastance and thickness of the septal wall (**Figure 7A**) and elastance and volume fraction of intra-alveolar surfactant (**Figure 7B**), there is no effect of the therapy in the bleomycin induced lung injury model (d7). In addition, the increase in septal wall thickness previously described here is not significantly correlated with the total volume of extracellular matrix (**Figure 7C**), but with the volume fraction of edema (**Figure 7D**). Therefore, it seems that edema is the main structural change induced in this model and preventing the transplantation treatment to have a positive effect. On the other hand, when the treatment is performed during the fibrotic remodeling phase, the correlation of tissue elastance and septal wall thickness (**Figure 7E**) and tissue elastance and volume fraction of intra-alveolar surfactant (**Figure 7F**) were statistically significant and showed the transplanted group to be between the control and disease groups. In addition, in this experimental setting, the main structural component change in the septal walls was the increase in total volume of extracellular matrix

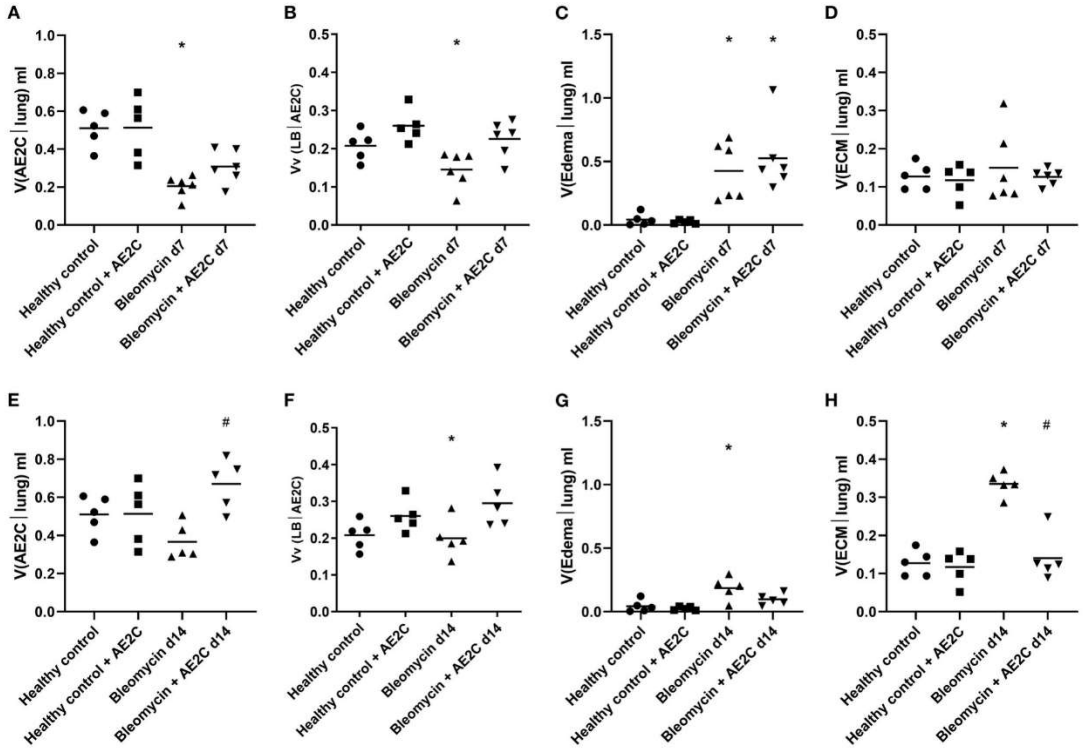

FIGURE 5 | Lung ultrastructure of bleomycin induced lung injury (d7) and fibrosis (d14) after AE2C transplantation. **(A–D)** Lung ultrastructure of bleomycin induced lung injury (7 days after bleomycin application) and AE2C transplantation (3 days after bleomycin application). **(A)** Total volume of AE2C in alveolar parenchyma at day 7 after bleomycin application. **(B)** Volume fraction of lamellar bodies (LB) in AE2C at day 7 after bleomycin application. **(C)** Total volume of edema in alveolar parenchyma at day 7 after bleomycin application. **(D)** Total volume of extracellular matrix (ECM) in alveolar parenchyma at day 7 after bleomycin application. **(E–H)** Lung ultrastructure of bleomycin induced lung injury (14 days after bleomycin application) and AE2C transplantation (7 days after bleomycin application). **(E)** Total volume of AE2C in alveolar parenchyma at day 14 after bleomycin application. **(F)** Volume fraction of LB in AE2C at day 14 after bleomycin application. **(G)** Total volume of edema in alveolar parenchyma at day 14 after bleomycin application. **(H)** Total volume of ECM in alveolar parenchyma at day 14 after bleomycin application. *$p < 0.05$ vs. healthy controls, #$p < 0.05$ vs. bleomycin control.

(**Figure 7G**). Edema was not statistically significantly correlated to septal wall thickness (**Figure 7H**). Therefore, remodeling and aberrant accumulation of extracellular matrix seemed to be the main component of the increase of septal wall thickness. Very interestingly, the transplantation with AE2C seemed to prevent this aberrant accumulation of extracellular matrix and consequently the septal wall thickness was not increased.

DISCUSSION

Damage/injury and apoptosis of AE2C (32–34) is a well-described process contributing to lung remodeling. AE2C are essential cells for the proper functioning of the lung and surfactant homeostasis (8, 35). Therefore, a therapeutic strategy to replace the injured AE2C may help to improve the disease outcome. Previously, Serrano-Mollar et al. demonstrated, in preclinical studies, that AE2C intratracheal transplantation was able to reduce fibrosis and restore pulmonary surfactant proteins levels (18, 19). They also observed that the induced pluripotent stem cells (iPSCs) derived AE2C reduce fibrosis by inhibiting TGF-β and α-SMA expression (23). Furthermore, in a clinical study performed with IPF patients, the intratracheal administration of heterologous AE2C was safe, well-tolerated and with no relevant side effects. Furthermore, this cell therapy was able to stabilize disease progression and improve health-related quality of life throughout a 1-year clinical follow-up (25). The functionality tests evaluated in that clinical study were DLCo and FVC (25), although these results provide information regarding lung capacity and performance, to date it has not been assessed whether these changes involve any improvement in lung structure functionality. Here, we studied the mechanical and structural changes induced by bleomycin and changed by the AE2C transplantation in order to contribute to understanding the effect of the replacement of injured AE2C as a therapeutic

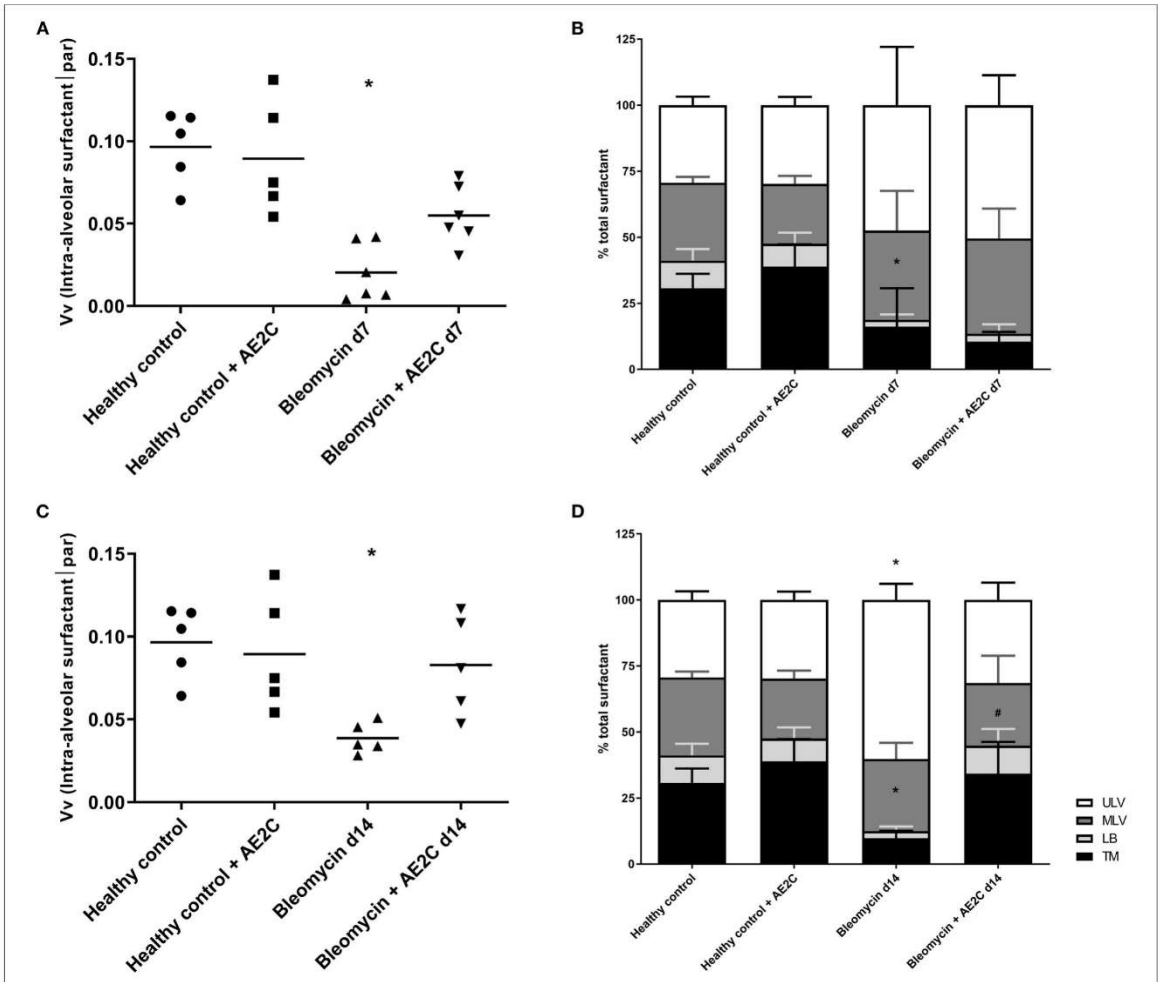

FIGURE 6 | Lung surfactant ultrastructure of bleomycin induced lung injury (d7) and fibrosis (d14) after AE2C transplantation. **(A,B)** surfactant ultrastructure of bleomycin induced lung injury (7 days after bleomycin application) and AE2C transplantation (3 days after bleomycin application). **(A)** Volume fraction of intra-alveolar surfactant in alveolar parenchyma at day 7 after bleomycin application. **(B)** Proportion of different surfactant ultrastructures, tubular myelin (TM, black bars), lamellar body-like (LBL, light gray bars), multilamellar vesicles (MLV, dark gray bars) and unilamellar vesicles (ULV, white bars) at day 7 after bleomycin application. **(C,D)** Surfactant ultrastructure of bleomycin induced lung fibrosis (14 days after bleomycin application) and AE2C transplantation (7 days after bleomycin application). **(A)** Volume fraction of intra-alveolar surfactant in alveolar parenchyma at day 14 after bleomycin application. **(B)** Proportion of different surfactant ultrastructures, tubular myelin (TM, black bars), lamellar body-like (LBL, light gray bars), multilamellar vesicles (MLV, dark gray bars) and unilamellar vesicles (ULV, white bars) at day 14 after bleomycin application. $^{*}p < 0.05$ vs. healthy controls, $\#p < 0.05$ vs. bleomycin control.

approach. Interestingly, we can conclude that when performing the treatment early during the lung injury phase of the bleomycin model, mainly edema and edematous material seem to impose a barrier to the potential beneficial effect of the transplanted cells. As already described (36), the formation of alveolar edema is one of the earliest events induced by the intratracheal application of bleomycin. Lutz and colleagues (30) also showed that already at day 3 after bleomycin application, the presence of edema and inactivation of surfactant, showing abnormally high surface tension, lead to a decreased number of opened alveoli. Accordingly, we found that 7 days after bleomycin application, the volume of ventilated parenchyma (**Figure 4A**) as well as total alveolar surface (**Figure 4D**) was reduced. In addition, there was an increase in septal wall thickness, mainly due to the formation of alveolar edema (**Figures 4C**, **5C**, **7D**), rather than a remodeling process with ECM accumulation (**Figure 7C**).

We found a non-statistical significant increase in the volume fraction of intra-alveolar surfactant in the transplanted group

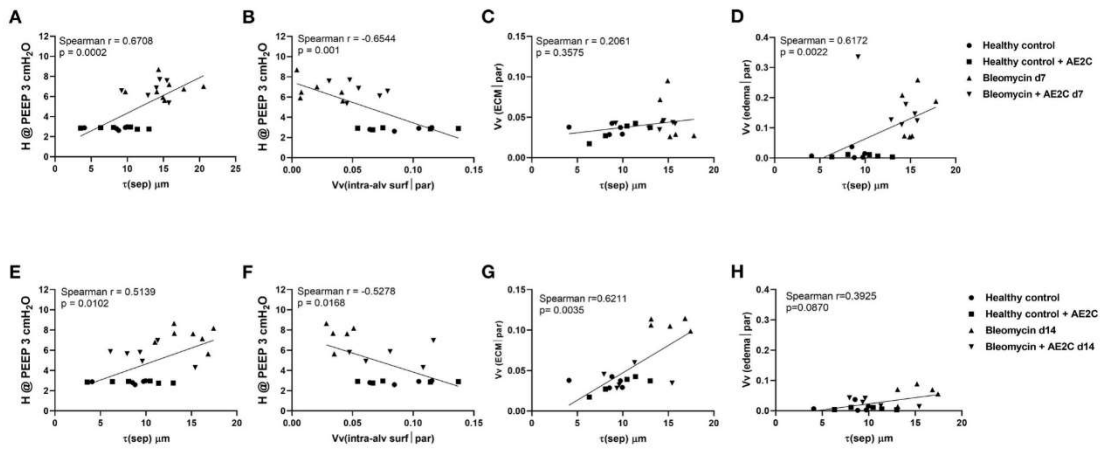

FIGURE 7 | Alveolar dynamics and structure correlations in bleomycin induced lung injury (d7) and fibrosis (d14) after AE2C transplantation. **(A–D)** Alveolar dynamics and structure correlation of bleomycin induced lung injury (7 days after bleomycin application) and AE2C transplantation (3 days after bleomycin application). **(A)** Correlation between tissue elastance at PEEP 3 cmH2O and septal wall thickness (τ) at day 7 after bleomycin application. **(B)** Correlation between tissue elastance at PEEP 3 cmH2O and volume fraction of intra-alveolar surfactant in alveolar parenchyma at day 7 after bleomycin application. **(C)** Correlation between volume fraction of ECM and septal wall thickness at day 7 after bleomycin application. **(D)** Correlation between alveolar edema and septal wall thickness at day 7 after bleomycin application. **(E–H)** Alveolar dynamics and structure correlation of bleomycin induced lung injury (14 days after bleomycin application) and AE2C transplantation (7 days after bleomycin application). **(A)** Correlation between tissue elastance at PEEP 3cmH2O and septal wall thickness (τ) at day 14 after bleomycin application. **(B)** Correlation between tissue elastance at PEEP 3cmH2O and volume fraction of intra-alveolar surfactant in alveolar parenchyma at day 14 after bleomycin application. **(C)** Correlation between volume fraction of ECM and septal wall thickness at day 14 after bleomycin application. **(D)** Correlation between alveolar edema and septal wall thickness at day 14 after bleomycin application. $^{*}p < 0.05$ vs. healthy controls, $\#p < 0.05$ vs. bleomycin control.

compared to the bleomycin diseased group (**Figure 6A**) in accordance with the increased volume fraction of LB in AE2C (**Figure 5B**). However, when analyzing the ultrastructure of this surfactant, we found an increased amount of ULV, as in the bleomycin control group, which seems to be the result of an inactivating process of surfactant by the edematous material, as previously reported (37–41). As surfactant remained inactivated, and edema was still present, we could not observe any improvement in alveolar dynamics. Therefore, freshly isolated and transplanted AE2C could not help in resolving edema and/or activating/replacing surfactant.

On the other hand, when transplanting the AE2C during the fibrotic remodeling phase, we can observe a promising beneficial effect of the therapy in improving alveolar dynamics and lung structure. At day 14 after bleomycin application, tissue elastance is further increased (**Figures 2E,F**) as a consequence of a statistically significant reduced volume of ventilated parenchyma and total alveolar surface, with the associated increase in non-ventilated parenchyma and septal wall thickness (**Figures 4A–I**). Interestingly, at this stage the total volume of edema is minimally increased (**Figure 5G**) compared to d7 (**Figure 5C**), whereas the volume of ECM is statistically significantly increased (**Figure 5H**), as previously described (30, 36). Therefore, in this case, the increase in septal wall thickness may be mainly due to the aberrant accumulation of ECM (**Figure 7G**), rather than alveolar edema (**Figure 7H**). In addition, bleomycin application also impacted the volume fraction of intra-alveolar surfactant (**Figure 6C**) and induced the conversion of active to inactive structures of lung surfactant (**Figure 6D**), as previously shown (30). The transplantation of AE2C at day 7, prevented the accumulation of ECM (**Figure 5H**), and therefore the increase in septal wall thickness (**Figure 4H**), resulting in a statistically significant reduction of elastance and an increase in compliance in alveolar dynamics (**Figures 2E–H**). A higher PEEP during forced oscillation perturbation was linked with a reduced tissue elastance in healthy controls but an increase in untreated bleomycin challenged lungs at day 14. The AE2C transplantation could convert this PEEP-dependent behavior of tissue elastance to normal – a higher PEEP resulted in a reduction in tissue elastance. In healthy lungs, the increase in the PEEP level from 3 to 6 cmH_2O results in a recruitment of folds in the alveolar walls and probably also alveolar shape changes without overdistension which would place ventilated airspaces to the upper non-linear portion of their pressure volume relationship. In bleomycin challenged lungs with their heterogeneous ventilation due to higher fraction of non-ventilated lung parenchyma and thickened septa those distal airspaces which are still ventilated become overstretched between PEEP 3 and 6 cmH_2O so that tissue elastance increases. Such an overdistension of lung parenchyma which occurs already at quite low airway opening pressures might represent an additional trigger for fibrotic remodeling even during spontaneous breathing e.g., by release of active TGF-β1 as demonstrated by (14). AE2C transplantation at day 7 results in a more homogenous ventilation of the lung

as indicated by the reduced fraction of non-ventilated lung parenchyma, reduced septal wall thickness and improved alveolar surface area so that the reduction in tissue elastance at PEEP 6 compared to PEEP 3 cmH_2O can be interpreted by recruitment of folding or even complete alveoli without overdistension of distal airspaces so that at the organ scale the pressure-volume relationship does not reach the upper non-linear portion. Hence, in this range of airway opening pressures there is no hint for overdistension and therefore pro-fibrotic mechanical stress. The improvement in homogeneity of ventilation within the lung after AE2C transplantation might be a consequence of improved regeneration and/or reduction in surface tension.

Of note, the transplantation of freshly isolated healthy AE2C at day 7, induced the increase in total volume of AE2C and volume fraction of LB in AE2C, which persisted 7 days later (day 14) compared to the bleomycin control group. This seems to be related to the secretion of functional surfactant, as the volume fraction of intra-alveolar surfactant recovered to healthy levels (**Figure 6C**) and the most active structures of surfactant (mainly TM and LBL) were also similar to the controls (**Figure 6D**). Therefore, we can conclude that the transplantation of AE2C showed to be very effective in recovering the healthy status of lung surfactant, contributing to prevent ECM accumulation and septal wall thickening, resulting in softer lung tissue.

Taking all together, even though the treatment with AE2C shows no effect in the treatment of lung injury, this treatment is able to prevent the main features of lung fibrotic remodeling, mainly aberrant accumulation of ECM and thickening of the septal wall. Whether this effect is a direct consequence to the newly secreted active surfactant deserves further research. However, it has already been described that mechanical stress, for example, due to surfactant dysfunction and increased surface tension, may contribute to the fibrotic remodeling (42). Preventing this mechanical stress by the production and secretion of active surfactant may be one of the mechanisms of action in this therapeutic model.

DATA AVAILABILITY STATEMENT

The raw data supporting the conclusions of this article will be made available by the authors, without undue reservation.

ETHICS STATEMENT

The animal study was reviewed and approved by Lower Saxony (Nidersächsisches Landesamt für Verbraucherschutz und Lebensmittelsicherheit, LAVES, Lower Saxony, Germany) with number TVA 15/1890.

AUTHOR CONTRIBUTIONS

EL-R, GG-J, LK, MO, and AS-M: conception and design of the work, interpretation of the data, revision of the manuscript, and approval of the submitted version of the manuscript. EL-R, GG-J, and AS-M: drafting of the manuscript. EL-R and GG-J: acquisition and analysis of the data. All authors contributed to the article and approved the submitted version.

FUNDING

GG-J was supported by the European respiratory Society/Sociedad Española de Neumología y Cirugía Torácica, ERS/SEPAR Short-Term Research Training Fellowship (STRTF 2014-6502). This work was supported by grants from Ministerio de Economía y Competitividad, Instituto de Salud Carlos III (PI13/00282), Cofinanciado por el Fondo Europeo de Desarrollo Regional (FEDER), Unión Europea, Una manera de hacer Europa, Fundació la Marató de TV3 (MTV3 122410). Biomedical Research in Endstage and Obstructive Lung Disease Hannover (BREATH), Member of the German Center for Lung Research (DZL), Cluster of Excellence REBIRTH (Regenerative Biology to Reconstructive Therapy), and the German Research Foundation (DFG KN 916 1-1).

ACKNOWLEDGMENTS

The authors thank Carina Vogt, Susanne Fassbender, and Andrea Herden for excellent technical support at Hannover Medical School.

SUPPLEMENTARY MATERIAL

The Supplementary Material for this article can be found online at: https://www.frontiersin.org/articles/10.3389/fmed.2021.640020/full#supplementary-material

REFERENCES

1. Raghu G, Collard HR, Egan JJ, Martinez FJ, Behr J, Brown KK, et al. ATS/ERS/JRS/ALAT committee on idiopathic pulmonary fibrosis. An official ATS/ERS/JRS/ALAT statement: idiopathic pulmonary fibrosis: evidence-based guidelines for diagnosis and management. *Am J Respir Crit Care Med.* (2011) 183:788–824. doi: 10.1164/rccm.2009-040GL
2. Noble PW, Albera C, Bradford WZ, Costabel U, Glassberg MK, Kardatzke D, et al. Pirfenidone in patients with idiopathic pulmonary fibrosis (CAPACITY): two randomised trials. *Lancet.* (2011) 377:1760–9. doi: 10.1016/S0140-6736(11)60405-4
3. Richeldi L, Costabel U, Selman M, Kim DS, Hansell DM, Nicholson AG, et al. Efficacy of a tyrosine kinase inhibitor in idiopathic pulmonary fibrosis. *N Engl J Med.* (2011) 365:1079–87. doi: 10.1056/NEJMoa1103690
4. Bishop AE. Pulmonary epithelial stem cells. *Cell Prolif.* (2004) 37:89–96. doi: 10.1111/j.1365-2184.2004.00302.x
5. Myers JL, Katzenstein AL. Epithelial necrosis and alveolar collapse in the pathogenesis of usual interstitial pneumonia. *Chest.* (1988) 94:1309–11. doi: 10.1378/chest.94.6.1309
6. Uhal BD, Joshi I, Hughes WF, Ramos C, Pardo A, Selman M. Alveolar epithelial cell death adjacent to underlying myofibroblasts in advanced fibrotic human lung. *Am J Physiol.* (1998) 275:L1192–9. doi: 10.1152/ajplung.1998.275.6.L1192
7. Selman M, Pardo A. Role of epithelial cells in idiopathic pulmonary fibrosis: from innocent targets to serial killers. *Proc Am Thorac Soc.* (2006) 3:364–72. doi: 10.1513/pats.200601-003TK
8. Günther A, Schmidt R, Nix F, Yabut-Perez M, Guth C, Rosseau S, et al. Surfactant abnormalities in idiopathic pulmonary fibrosis,

hypersensitivity pneumonitis and sarcoidosis. *Eur Respir J.* (1999) 14:565–73. doi: 10.1034/j.1399-3003.1999.14c14.x
9. Ochs M. The closer we look the more we see? Quantitative microscopic analysis of the pulmonary surfactant system. *Cell Physiol Biochem.* (2010) 25:27–40. doi: 10.1159/000272061
10. Perez-Gil J, Weaver TE. Pulmonary surfactant pathophysiology: current models and open questions. *Physiology.* (2010) 25:132–41. doi: 10.1152/physiol.00006.2010
11. Bachofen H, Gehr P, Weibel ER. Alterations of mechanical properties and morphology in excised rabbit lungs rinsed with a detergent. *J Appl Physiol.* (1979) 47:1002–10. doi: 10.1152/jappl.1979.47.5.1002
12. Sera T, Yokota H, Tanaka G, Uesugi K, Yagi N, Schroter RC. Murine pulmonary acinar mechanics during quasi-static inflation using synchrotron refraction-enhanced computed tomography. *J Appl Physiol.* (2013) 115:219–28. doi: 10.1152/japplphysiol.01105.2012
13. Mead J, Takishima T, Leith D. Stress distribution in lungs: a model of pulmonary elasticity. *J Appl Physiol.* (1970) 28:596–608. doi: 10.1152/jappl.1970.28.5.596
14. Froese AR., Shimbori C, Bellaye PR, Inman M, Obex S, Fatima S, et al. Stretch-induced activation of transforming growth factor-β1 in pulmonary fibrosis. *Am J Resp Crit Care Med.* (2016) 194:84–96. doi: 10.1164/rccm.201508-1638OC
15. Cabrera-Benítez NE, Parotto M, Post M, Han B, Spieth PM, Cheng WE, et al. Mechanical stress induces lung fibrosis by epithelial-mesenchymal transition. *Crit Care Med.* (2012) 40:510–7. doi: 10.1097/CCM.0b013e31822f09d7
16. Sisson TH, Mendez M, Choi K, Subbotina N, Courey A, Cunningham A, et al. Targeted injury of type II alveolar epithelial cells induces pulmonary fibrosis. *Am J Respir Crit Care Med.* (2010) 181:254–63. doi: 10.1164/rccm.200810-1615OC
17. Burkhardt A. Alveolitis and collapse in the pathogenesis of pulmonary fibrosis. *Am Rev Respir Dis.* (1989) 140:513–24. doi: 10.1164/ajrccm/140.2.513
18. Serrano-Mollar A, Nacher M, Gay-Jordi G, Closa D, Xaubet A, Bulbena O. Intratracheal transplantation of alveolar type II cells reverses bleomycin-induced lung fibrosis. *Am J Respir Crit Care Med.* (2007) 176:1261–8. doi: 10.1164/rccm.200610-1491OC
19. Guillamat-Prats R, Gay-Jordi G, Xaubet A, Peinado VI, Serrano-Mollar A. Alveolar type II cell transplantation restores pulmonary surfactant protein levels in lung fibrosis. *J Heart Lung Transplant.* (2014) 33:758–65. doi: 10.1016/j.healun.2014.03.008
20. Banerjee ER, Laflamme MA, Papayannopoulou T, Kahn M, Murry CE, Henderson WR Jr. Human embryonic stem cells differentiated to lung lineage-specific cells ameliorate pulmonary fibrosis in a xenograft transplant mouse model. *PLoS ONE.* (2012) 7:e33165. doi: 10.1371/journal.pone.0033165
21. How CK, Chien Y, Yang KY, Shih HC, Juan CC, Yang YP, et al. Induced pluripotent stem cells mediate the release of interferon gamma-induced protein 10 and alleviate bleomycin induced lung inflammation and fibrosis. *Shock.* (2013) 39:261–70. doi: 10.1097/SHK.0b013e318285f2e2
22. Huang K, Kang X, Wang X, et al. Conversion of bone marrow mesenchymal stem cells into type II alveolar epithelial cells reduces pulmonary fibrosis by decreasing oxidative stress in rats. *Mol Med Rep.* (2015) 11:1685. doi: 10.3892/mmr.2014.2981
23. Alvarez-Palomo B, Sanchez-Lopez LI, Moodley Y, Edel MJ, Serrano-Mollar A. Induced pluripotent stem cell-derived lung alveolar epithelial type II cells reduce damage in bleomycin-induced lung fibrosis. *Stem Cell Res Ther.* (2020) 11:213. doi: 10.1186/s13287-020-01726-3
24. Serrano-Mollar A. Cell therapy in idiopathic pulmonary fibrosis†. *Med Sci.* (2018) 6:64. doi: 10.3390/medsci6030064
25. Serrano-Mollar A, Gay-Jordi G, Guillamat-Prats R, Closa D, Hernandez-Gonzalez F, Marin P, et al. Safety and tolerability of alveolar type II cell transplantation in idiopathic pulmonary fibrosis. *Chest.* (2016) 150:533–43. doi: 10.1016/j.chest.2016.03.021
26. Richards RJ, Davies N, Atkins J, Oreffo VI. Isolation, biochemical characterisation, and culture of lung type II cells of the rat. *Lung.* (1987) 165:143–58. doi: 10.1007/BF02714430
27. Knudsen L, Lopez-Rodriguez E, Berndt L, Steffen L, Ruppert C, Bates JHT, et al. Alveolar micromechanics in bleomycin-induced lung injury. *Am J Resp Cell Mol Biol.* (2018) 59:757–69. doi: 10.1165/rcmb.2018-0044OC
28. Hsia CW, Hyde DM, Ochs M, Weibel ER. An official research policy statement of the american thoracic society/european respiratory society: standards for quantitative assessment of lung structure. *Am J Resp Crit Care Med.* (2010) 181:394–418. doi: 10.1164/rccm.200809-1522ST
29. Ochs M, and Mühlfeld C. Quantitative microscopy of the lung: a problem-based approach. Part 1: basic principles of lung stereology. *Am J Physiol-Lung Cell Mol Physiol.* (2013) 305:L15–22. doi: 10.1152/ajplung.00429.2012
30. Lutz D, Gazdhar A, Lopez-Rodriguez E, Ruppert C, Mahavadi P, Günther A, et al. Alveolar derecruitment and collapse induration as crucial mechanisms in lung injury and fibrosis. *Am J Resp Cell Mol Biol.* (2015) 52:232–43. doi: 10.1165/rcmb.2014-0078OC
31. Ochs M, Nenadic I, Fehrenbach A, Albes JM, Wahlers T, Richter J, et al. Ultrastructural alterations in intraalveolar surfactant subtypes after experimental ischemia and reperfusion. *Am J Resp Crit Care Med.* (1999) 160:718–24. doi: 10.1164/ajrccm.160.2.9809060
32. Parimon T, Yao C, Stripp BR, Noble PW, Chen P. Alveolar epithelial type II cells as drivers of lung fibrosis in idiopathic pulmonary fibrosis. *Int J Mol Sci.* (2020) 21:2269. doi: 10.3390/ijms21072269
33. Mahavadi P, Henneke I, Ruppert C, Knudsen L, Venkatesan S, Liebisch G, et al. Altered surfactant homeostasis and alveolar epithelial cell stress in amiodarone-induced lung fibrosis. *Tox Sci.* (2014) 142:285–97. doi: 10.1093/toxsci/kfu177
34. Korfei M, Ruppert C, Mahavadi P, Henneke I, Markart P, Koch M, et al. Epithelial endoplasmic reticulum stress and apoptosis in sporadic idiopathic pulmonary fibrosis. *Am J Resp Crit Care Med.* (2008) 178:838–46. doi: 10.1164/rccm.200802-313OC
35. Lopez-Rodriguez E, Gay-Jordi G, Mucci A, Lachmann N, Serrano-Mollar A. Lung surfactant metabolism: early in life, early in disease and target in cell therapy. *Cell Tissue Res.* (2017) 367:721–35. doi: 10.1007/s00441-016-2520-9
36. Moeller A, Ask K, Warburton D, Gauldie J, Kolb M. The bleomycin animal model: a useful tool to investigate treatment options for idiopathic pulmonary fibrosis? *Int J Biochem Cell B.* (2008) 40:362–82. doi: 10.1016/j.biocel.2007.08.011
37. Kobayashi T, Nitta K, Ganzuka M, Inui S, Grossmann G, Robertson B. Inactivation of exogenous surfactant by pulmonary edema fluid. *Pediatr Res.* (1991) 29:353–6. doi: 10.1203/00006450-199104000-00005
38. Nitta K, Kobayashi T. Impairment of surfactant activity and ventilation by proteins in lung edema fluid. *Respir Physiol.* (1994) 95:43–51. doi: 10.1016/0034-5687(94)90046-9
39. Zasadzinski A, Alig TF, Alonso C, Bernardino de la Serna J, Perez-Gil J, Taeusch HW. Inhibition of pulmonary surfactant adsorption by serum and the mechanisms of reversal by hydrophilic polymers: theory. *Biophys J.* (2005) 89:1621–9. doi: 10.1529/biophysj.105.062646
40. Gunasekara L, Schoel WM, Schürch S, Amrein MW. A comparative study of mechanisms of surfactant inhibition. *Biochim Biophys Acta-Biomembranes.* (2008) 1778:433–44. doi: 10.1016/j.bbamem.2007.10.027
41. Lopez-Rodriguez E, Ospina OL, Echaide M, Taeusch HW, Pérez-Gil J. Exposure to polymers reverses inhibition of pulmonary surfactant by serum, meconium, or cholesterol in the captive bubble surfactometer. *Biophys J.* (2012) 103:1451–9. doi: 10.1016/j.bpj.2012.08.024
42. Lopez-Rodriguez E, Boden C, Echaide M, Perez-Gil J, Kolb M, Gauldie J, et al. Surfactant dysfunction during overexpression of TGF-β1 precedes profibrotic lung remodeling *in vivo*. *Am J Physio-Lung Cell Mol Physiol.* (2016) 310:L1260–71. doi: 10.1152/ajplung.00065.2016

Conflict of Interest: The authors declare that the research was conducted in the absence of any commercial or financial relationships that could be construed as a potential conflict of interest.

RELEVANCE OF THIS WORK

In this paper, we concluded that the pulmonary transplantation of AE2C showed a beneficial effect during the lung remodeling phase. Whereas, during the lung injury phase, the AE2C transplantation was only able to normalize the volume of secreted surfactant, this surfactant seemed to be inactivated, most probably by the protein components of the edema resulting after epithelial damage. Surfactant inactivation by edematous components has been previously well described and includes molecules such as albumin, fibrinogen, C-reactive protein, hemoglobin, and immunoglobulins (143-154).

However, during fibrotic remodeling, this intervention was able to not only normalize surfactant and AE2C volumes in the treated lungs, but also prevent the accumulation of collagen and the thickening of septal walls. This is also reflected in the reduced tissue elastance at both PEEP of 3 and 6 cmH_2O, indicating improvement in the structure and dynamics of the alveolar spaces after the treatment. In addition, we also observed an increase in the volume of AE2C, potentially coming from the engrafting of the healthy transplanted cells or induction of epithelial proliferation, and higher volumes of not only alveolar surfactant, but also the most active forms of surfactant, TM, LB and MLV, also potentially newly secreted and functional. These findings may represent the beneficial effect of newly secreted surfactant in normalizing mechanical forces, preventing mechanical stress and further fibrotic remodeling of the lung tissue.

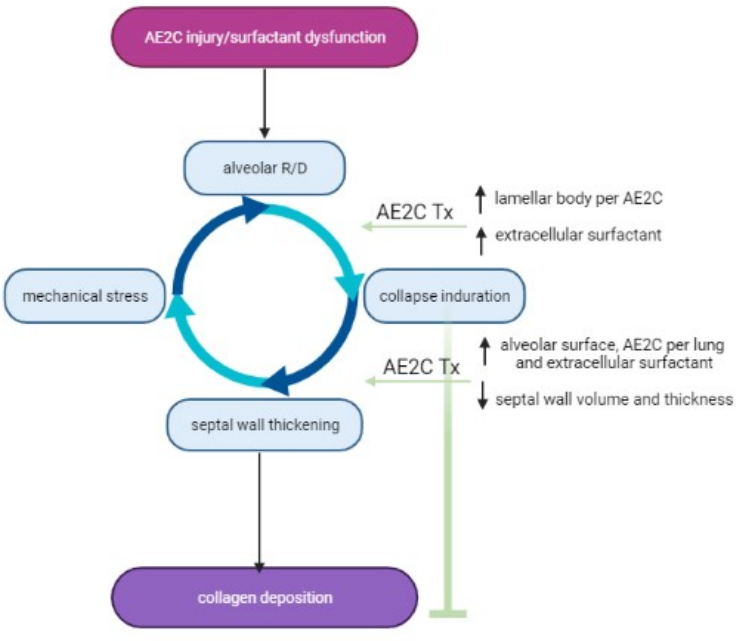

Figure 7: AE2C transplantation (Tx) experimental schema with beneficial effects (Created in BioRender.com).

4 DISCUSSION AND OUTLOOK

Lung surfactant discovery was considered a scientific breakthrough in bioscience (155), when the development of SRT helped to cut down neonatal mortality (156-158). Lung surfactant importance is highlighted in the neonatal respiratory distress syndrome (NRDS), where premature babies are born before surfactant synthesis or secretion has started in the developing lung. Therefore, these premature babies are born with a lack of surfactant that leads to failure in stabilizing the lung and collapse of alveoli. NRDS mortality was calculated to be around the 80% by the 80-90´s (159, 160).

The death of the second child of the US president, JF Kennedy due to NRDS (at that time known as hyaline membrane disease, HMD) in 1963 awaked the interest and research investment in the field, not only to understand the origin of the disease, but also to look for potential treatments. Already in 1959, Avery and Mead described for the first time the relation between NRDS and surfactant deficiency, by measuring the surface tension of lung extracts, as Clemens described in the very first experiments where surface tension was measured in a handmade surface balance (161). Soon enough, Fujiwara in US (162) and Robertson and Curstedt (163) in Europe, isolated surfactant from animal lungs and tested it in animal models of RDS. In the early 90´s the first commercial surfactant formulations where tested and available for the treatment of NRDS, reducing notably the mortality of premature babies (158).

The pathophysiology of NRDS is characterized by an acute surfactant deficiency, which leads to: alveolar collapse, lung injury, edema formation and surfactant inactivation/dysfunction (164). In the same direction, acute dysfunction/deficiency of surfactant due to lung injury and edema formation contributes to the pathophysiology of ARDS (acute respiratory distress syndrome). As well as for the NRDS, many clinical trials tested SRT for the treatment of ARDS in adult patients. However, it is hypothesized that surfactant inactivation of the exogenously applied surfactant in the SRT led to the failure of those clinical trials (165-167).

These two acute respiratory syndromes highlight the importance of lung surfactant in the normal or healthy physiology and the stabilization of the opened lung. However, one can imagine that surfactant dysfunction/deficiency in a mild but chronic modality, may also influence lung health and function.

4.1 LUNG SURFACTANT METABOLISM IN ALVEOLI DURING FIBROTIC REMODELING

Surfactant down-regulation has previously been shown in patients suffering lung fibrosis (37-39), as well as dysfunction/alteration in AE2C (133, 168). Therefore, it seems reasonable to hypothesize about the influence and contribution of lung surfactant in the development of

lung fibrosis. Through Chapters 2.1-2.3, we have described that surfactant dysfunction is an early event contributing to fibrotic remodeling of the lung tissue. Stablished either as genetic deficiency (such as in the SP-C deficient mouse model) or resulting from lung injury, edema formation and inactivation (such as in the bleomycin-induced rat model), lung surfactant seemed to play an important role in keeping the alveoli open and preventing collapse and the associated mechanical stress in alveolar epithelial cells.

Even though the lung is not considered as a lipid metabolic organ, it does sustain an active lipid metabolism that is key for the proper lung surfactant homeostasis and function of the alveolar space and ultimately gas exchange. In this regard, not only the synthesis and release of surfactant, uniquely performed by the AE2C is important, but also the recycling and degrading of surfactant should be taken into account. Lipid recycling and catabolism is thought to happen not only in the AE2C but also in the AM. Traditionally, it was thought that lipid catabolism only takes up to 20-30% in AM (169-171) and most of the clearance may take place by recycling in AE2C (172). However, it is important to understand not only what happens in healthy conditions, where the AE2C may predominantly be in place to be in charge of the lipid homeostasis, but also under pathological conditions, where either AE2C or AM may be impaired, dysfunctional or no longer active. Recent advances in the study of AM in pulmonary alveolar proteinosis (PAP) have been decisive in elucidating the involvement of AM in lipid catabolism. Many genes have been found to be impaired in AM in PAP, leading to accumulation of lung surfactant and protein complexes in the alveoli, impairing alveolar dynamics. Mutation or deficiency in ABC transporters A1 (ABCA1), G1 (ABCG1) and peroxisome proliferator-activated receptor gamma (PPARγ) are related to inefficient surfactant catabolism in AM, which leads to the PAP phenotype (173-175). Very interestingly, ABCG1 deficient mice showed crystal accumulation in their cytoplasm, described as cholesterol crystals (91, 92) very similar to the crystals present in the AM of SP-C deficient mice presented here. Altogether, this highlights the importance of healthy AM in surfactant metabolism regulation. Therefore, the question is what would happen with surfactant proper homeostasis if AM are impaired or activated with the purpose to actively participate in the immune response.

The amount of surfactant in the alveolar spaces is tightly regulated. Interestingly, the pool size of surfactant does not change through life (176), except during the perinatal period, where on average the surfactant pool is 5 to 10 fold higher (177). It has already been described that de novo synthesis of PC is rather slow (178), so the recycling and re-use of surfactant components in AE2C and AM may play an important role in the regulation of the surfactant pools. Therefore, it seems that regulation mechanisms may exist in order to adapt surfactant pools to changes in the environment or pathological conditions. However, very little is known about these regulatory mechanisms or how both AE2C and AM may sense the amount of surfactant in the alveolar spaces in order to meet the requirements of either synthesizing, degrading or recycling the components.

In order to understand recycling mechanisms of lung surfactant components in the lung, we may need to have a look at the common pathways shared between AE2C and AM. For example, both cells express ABC transporters for lipid transport, such as ABCA1 and ABCG1, transporters responsible of the inverse cholesterol transport from the alveolar spaces back to the circulation (179-181). This may represent a mechanism of cholesterol recycling. SP-A has been reported to enhance surfactant recycling. On the one hand, SP-A is able to bind to phospholipids from surfactant. On the other hand, both AE2C and AM express a high affinity receptor for SP-A (182, 183). SP-A is endocytosed in a clathrin-dependent mechanism by AE2C (184, 185). Lipids endocytosed this way seem to be recycled and not degraded, whereas in the absence of SP-A they are degraded, comprising therefore a specific potential recycling mechanism (170). AM are also able to endocytose SP-A (186), but whether this is part of a recycling or degrading pathway is still unknown. Lastly, since TGF-β1- and ITG-β6-deficient mice showed impaired phospholipid catabolism in AM (187, 188), it has been proposed that both TGF-β1 and β6-integrin play a key role in maintaining surfactant pool levels and macrophage function (189).

The interesting finding in the SP-C deficient mice model also points at AM playing an important role not only in surfactant metabolism but at the same time in the development of lung fibrosis. The finding of cytosolic crystal accumulation leads to think that in the absence of SP-C these AM have some metabolic problems (41), which in turn may convert them in a more pro-fibrotic phenotype contributing to the development of the disease. This is still a gap of knowledge to fill in and probably, more factors and signaling molecules are involved in surfactant recycling and lung homeostasis.

Even though, lung fibrosis is to date considered an interstitial lung disease and the fibroblast has been for long in the center of the pathophysiology, this may be of relevance when analyzing end-stage fibrotic lungs. However, in this work we focused on the early events, which may trigger or contribute to develop fibrotic remodeling, before recruiting and activation of fibroblasts and deposition of collagen. One should consider that with such a big surface exposed to the environment, most of the challenges that may trigger disease would come from the environment and affect the alveolar side and alveolar epithelium in the first line. This is clear in case of lung infection induced diseases (such as pneumonias or infections of the lower respiratory tract, (190-192), smoking related obstructive disease (193, 194) or other diseases triggered by aspiration of particles such as silica or asbestos (195-198). We can conclude, from our animal models, that epithelial damage, both acute and chronic, may lead to an aberrant wound healing in the epithelium, triggering a fibrotic remodeling response in the interstitium. Therefore, lung fibrosis may be initiated by factors impairing proper lung mechanics, including proper lung surfactant function, in the alveolar side of the lung parenchyma.

Even though, animal models have a number of limitations, regarding similarities or disparities in the induction and progression of the disease in comparison to the human disease, they also contribute with important advantages. In the case of lung diseases, more specifically in lung

fibrosis, with the possibility to analyze time dependent changes, especially at very early stages. In this way, animal models allow us to understand what may have happened before the onset of and during fibrotic remodeling, in order to understand how and why an end-stage lung looks like it is. The bleomycin-induced lung injury and fibrosis animal model is very widely used to investigate molecular mechanisms and potential therapeutic strategies. However, this model shows a lung injury phase that is not properly resolved resulting in an aberrant lung remodeling. Whether patients suffering lung fibrosis underwent a phase of lung injury and inflammation has been intensively discussed and is still unknown. The most important scientific evidence against this is the failure of the clinical trials, which tested anti-inflammatory (corticosteroids) drugs for the treatment of lung fibrosis (199, 200). However, new findings related to higher risk of developing lung fibrosis after ARDS (201, 202) or Covid-19 (203, 204) recovery might point at inflammation as another early event triggering aberrant wound healing. This will also mean that potential anti-inflammatory treatments should be given with the right timing, meaning early in the development of the disease, before the onset of the fibrotic wounds.

In conclusion, as shown in Chapter 2.1-2.3, both AE2C and AM change during lung fibrosis development, impairing surfactant function and metabolism. Therefore, lung surfactant dysfunction may be considered as an important pathophysiologic event, which seems to happen early in the disease, contributing to the development of lung fibrosis. Taking this into consideration, it may be reasonable to propose to replace the dysfunctional surfactant by fresh functional surfactant as a therapeutic strategy. In addition, AE2C and AM should be considered of high importance in the development of targeted therapies since they are key players in the regulation of surfactant homeostasis and development of lung fibrosis.

4.2 LUNG SURFACTANT AS THERAPEUTIC STRATEGY FOR THE TREATMENT OF LUNG FIBROSIS

In order to treat lung surfactant dysfunction, two options come into play. On the one hand, there is the option of directly replacing the dysfunctional surfactant by an exogenous functional one, as in the treatment of NRDS. On the other hand, the source of surfactant, the AE2C, may also be replaced in order to aim for a long-term effect of the newly secreted surfactant by the healthy transplanted cells. In both cases, the timing of the application is key in order to understand what changes are expected to be seen.

On the one hand, in chapter 3.1 we have shown that surfactant may have anti-inflammatory activity by means of preventing the inflammatory response resulting from epithelial mechanical stress. The anti-inflammatory properties of surfactant have been already studied and related to some of its phospholipid components (205). However, in chapter 3.2, the inflammation caused by bleomycin lung injury and the consequent edema formation

prevented transplanted AE2C to show a beneficial effect. This discrepancy between treatments may be explained by the fact that in an edema filled alveoli the exogenous surfactant (applied as SRT) may be placed on top of the albumin layer occupying the interface, there surfactant may exclude albumin and lower down surface tension. However, in the AE2C treatment, we observed individual cells surrounded by edematous material, if they are able to secrete surfactant, this surface active material has to travel all the way up to the interface and exclude the albumin from there. This means that surfactant has to compete with albumin for a place at the interface. This has been shown to be the most efficient inhibitory mechanism of albumin, preventing surfactant to reach the alveolar interface (206).

In order to counteract this inhibitory effect, the possibility to enrich or pre-treat surfactant with fortifying agents or increase its resistance to inhibition has already been proposed and studied. For example, the mixing of surfactant with different polymers, such as hyaluronan (207, 208), dextran (209) or PEG (210) resulted in a surfactant able to overcome the inhibitory effect of albumin in vitro. The pre-treatment of surfactant with HA (207) showed that conformational and compositional changes may convert surfactant into a highly active state, able to overcome inhibition in vitro. These strategies may be useful to counteract the inhibition of surfactant in the presence of edematous material in vivo, increasing the anti-inflammatory efficacy of surfactant at this stage of the disease development.

Very interestingly, the SRT showed to be beneficial lowering down the production of ECM and collagen in both the bleomycin-induced (43) and TGF-β1 overexpression-induced lung fibrosis models (211).This points at surfactant stabilizing the alveoli, preventing mechanical stress and as a consequence, slowing down the progression of the disease.

In addition, in can also be proposed to use lung surfactant to target those important cells for surfactant function and metabolism, mainly AE2C and AM. In this way, negative effects may also be prevented. In a step further, one may think about using SRT not only to treat surfactant dysfunction but also as carrier to deliver different molecules to targeted cells. Nowadays SRT has been proposed and is under investigation for the treatment of lung infection, alone or in combination with antibiotics (212-214) or the treatment of bronchopulmonary dysplasia (BPD) in combination with glucocorticosteroids (215, 216). In addition, recently many authors proposed, and some clinical trials already started, the use of SRT in the treatment or as supportive therapy for Covid-19 patients (217). However, the non-invasive application of lung surfactant in adults probably constitutes the biggest challenge for current medicine to adopt SRT for the treatment of adult lung diseases. For this purpose, many researchers and companies are trying to aerosolize surfactant with the hope to bring surfactant in the alveolar spaces without the need of an intratracheal intubation (218, 219).

On the other hand, in chapter 3.2 we showed the beneficial effect of AE2C transplantation in the alveolar dynamics and recovery of active surfactant. Previously, this therapeutic strategy

was proposed as approach to treat IPF (220-222), initially in an animal model, and later in 16 patients with moderate and progressive IPF (221). Results from this clinical study suggested that the beneficial effects observed might be related to the replacement of surfactant by the transplanted AE2C. The treatment in the IPF patients consisted in 4 intratracheal administrations of halogenic AE2C by a fiber-optic bronchoscopy with 15 days between cell instillations. After 12 months, 13 IPF patients did not show any progression of the disease, by means of stabilization of functional pulmonary test, high-resolution computed tomography, increased distance in the 6-min walking test and improvement on health related quality of life parameters. The authors stated that during the first 2 months, all patients remained stable, even the three non-responders. Given that these 2 months correspond to the period when patients were receiving AE2C, the authors speculated that this observation could be related to the capacity of AE2C to restore pulmonary surfactant. Surfactant from transplanted AE2C could help to open up collapsed but still functional alveoli, thereby enhancing breathing capacity (109, 221). Our animal experiments confirmed this hypothesis, as we were able to measure higher fractions of intra-alveolar surfactant and comprising highly active forms, such as TM and LB in the treated groups. Alternatively, other options have also been proposed, such as iPSC-derived AE2C (223) or MSC-derived AE2C (224-226) as the availability of pure isolated AE2C from healthy donor lungs may be limited and difficult to standardize.

However, the most noteworthy result of both therapeutic strategies presented in here (chapter 3.1 and 3.2) is the reduction of fibrosis or delay of the fibrosis onset in the animal models. Either by replacing surfactant or the cellular source of surfactant, it seems that the restoration of surfactant levels is influencing fibrotic remodeling. This could only be explained by surfactant normalizing the aberrant physical and mechanical forces acting in the diseased alveoli.

In conclusion, understanding the pathophysiological changes preceding fibrotic development will help understand many of the mechanisms triggering and contributing to the disease. An important patho-mechanism seems to be the dysfunction of lung surfactant, with the associated induced mechanical stress due to abnormally high surface tension. This can be potentially treated by either SRT or AE2C transplantation as therapeutic strategies. The transplantation of AE2C or SRT (alone or in combination with other drugs as drug delivery system), open the concept of targeted and directed therapy, versus systemic application, to the alveolar spaces. This will contribute to a new field of research and potential advance of pulmonary medicine, where SRT could be used beyond neonatal/perinatal medicine.

5 REFERENCES

1. Ochs M, Weibel ER. Chapter 2: Functional design of the human lung for gas exchange. In: Grippi MA, Elias JA, Fishman JA, Kotloff RM, Pack AI, Senior RM, et al., editors. Fishman's Pulmonary Diseases and Disorders. 5th ed. United States of America: McGraw-Hill Education; 2015. p. 20-62.
2. Altose MD. Chapter 10: Pulmonary mechanics. In: Grippi MA, Elias JA, Fishman JA, Kotloff RM, Pack AI, Senior RM, et al., editors. Fishman's Pulmonary Diseases and Disorders. 5th ed. United States of America: McGraw-Hill Education; 2015. p. 137-47.
3. Whitsett JA, Weaver TE. Chapter 5: Pulmonary surfactant and disorders of surfactant homeostasis. In: Grippi MA, Elias JA, Fishman JA, Kotloff RM, Pack AI, Senior RM, et al., editors. Fishman's Pulmonary Diseases and Disorders. 5th ed. United States of America: McGraw-Hill Education; 2015. p. 83-92.
4. Nkadi PO, Merritt TA, Pillers D-AM. An overview of pulmonary surfactant in the neonate: Genetics, metabolism, and the role of surfactant in health and disease. Molecular Genetics and Metabolism. 2009;97(2):95-101.
5. Fulmer JD, Bienkowski RS, Cowan MJ, Breul SD, Bradley KM, Ferrans VJ, et al. Collagen Concentration and Rates of Synthesis in Idiopathic Pulmonary Fibrosis. American Review of Respiratory Disease. 1980;122(2):289-301.
6. Snijder J, Peraza J, Padilla M, Capaccione K, Salvatore MM. Pulmonary fibrosis: a disease of alveolar collapse and collagen deposition. 2019. p. 615-9.
7. Herzog EL, Brody AR, Colby TV, Mason R, Williams MC. Knowns and Unknowns of the Alveolus. Proceedings of the American Thoracic Society. 2008;5(7):778-82.
8. West JB. Distribution of mechanical stress in the lung, a possible factor in localisation of pulmonary disease. The Lancet. 1971;297(7704):839-41.
9. Weaver TE. Synthesis, processing and secretion of surfactant proteins B and C. Biochimica et Biophysica Acta (BBA) - Molecular Basis of Disease. 1998;1408(2–3):173-9.
10. Haller T, Ortmayr J, Friedrich F, Volkl H, Dietl P. Dynamics of surfactant release in alveolar type II cells. Proceedings of the National Academy of Sciences. 1998;95(4):1579-84.
11. Voyno-Yasenetskaya TA, Dobbs LG, Williams MC. Regulation of ATP-dependent surfactant secretion and activation of second-messenger systems in alveolar type II cells. American Journal of Physiology - Lung Cellular and Molecular Physiology. 1991;261(4):105-9.
12. Haller T, Dietl P, Pfaller K, Frick M, Mair N, Paulmichl M, et al. Fusion pore expansion is a slow, discontinuous, and Ca2+-dependent process regulating secretion from alveolar type II cells. The Journal of cell biology. 2001;155(2):279-89.
13. Patel AS, Reigada D, Mitchell CH, Bates SR, Margulies SS, Koval M. Paracrine stimulation of surfactant secretion by extracellular ATP in response to mechanical deformation. American journal of physiology Lung cellular and molecular physiology. 2005;289(3):L489-L96.
14. Nag K, Munro JG, Hearn SA, Rasmusson J, Petersen NO, Possmayer F. Correlated atomic force and transmission electron microscopy of nanotubular structures in pulmonary surfactant. Journal of Structural Biology. 1999;126(1):1-15.
15. Perez-Gil J, Weaver TE. Pulmonary surfactant pathophysiology: current models and open questions. Physiology. 2010;25(3):132-41.
16. Chapter 2: Introduction to surface tension and surfactants. In: Notter RH, editor. Lung surfactants: basic science and clinical applications. 149. 5th ed. New York: CRC Press; 2000. p. 16-31.
17. Raghu G, Collard HR, Egan JJ, Martinez FJ, Behr J, Brown KK, et al. An Official ATS/ERS/JRS/ALAT Statement: Idiopathic Pulmonary Fibrosis: Evidence-based Guidelines for Diagnosis and Management. American Journal of Respiratory and Critical Care Medicine. 2011;183(6):788-824.
18. Raghu G, Rochwerg B, Zhang Y, Garcia CAC, Azuma A, Behr J, et al. An Official ATS/ERS/JRS/ALAT Clinical Practice Guideline: Treatment of Idiopathic Pulmonary Fibrosis. An Update of the 2011 Clinical Practice Guideline. American Journal of Respiratory and Critical Care Medicine. 2015;192(2):e3-e19.

19. Sauleda J, Núñez B, Sala E, Soriano JB. Idiopathic Pulmonary Fibrosis: Epidemiology, Natural History, Phenotypes. Medical Sciences. 2018;6(4):110.
20. Richeldi L, du Bois RM, Raghu G, Azuma A, Brown KK, Costabel U, et al. Efficacy and Safety of Nintedanib in Idiopathic Pulmonary Fibrosis. New England Journal of Medicine. 2014;370(22):2071-82.
21. King TE, Bradford WZ, Castro-Bernardini S, Fagan EA, Glaspole I, Glassberg MK, et al. A Phase 3 Trial of Pirfenidone in Patients with Idiopathic Pulmonary Fibrosis. New England Journal of Medicine. 2014;370(22):2083-92.
22. Cottin V, Maher T. Long-term clinical and real-world experience with pirfenidone in the treatment of idiopathic pulmonary fibrosis. European Respiratory Review. 2015;24(135):58-64.
23. Richeldi L, Cottin V, du Bois RM, Selman M, Kimura T, Bailes Z, et al. Nintedanib in patients with idiopathic pulmonary fibrosis: Combined evidence from the TOMORROW and INPULSIS trials. Respiratory Medicine. 2016;113:74-9.
24. Nathan SD, Albera C, Bradford WZ, Costabel U, du Bois RM, Fagan EA, et al. Effect of continued treatment with pirfenidone following clinically meaningful declines in forced vital capacity: analysis of data from three phase 3 trials in patients with idiopathic pulmonary fibrosis. Thorax. 2016;71(5):429-35.
25. Fernandez IE, Eickelberg O. New cellular and molecular mechanisms of lung injury and fibrosis in idiopathic pulmonary fibrosis. The Lancet. 2012;380(9842):680-8.
26. Wynn TA. Integrating mechanisms of pulmonary fibrosis. Journal of Experimental Medicine. 2011;208(7):1339-50.
27. Okano T, Kobayashi T, Yasuma T, D'Alessandro-Gabazza CN, Toda M, Fujimoto H, et al. Low-Dose of Intrapulmonary Pirfenidone Improves Human Transforming Growth Factorβ1-Driven Lung Fibrosis. Frontiers in Pharmacology. 2020;11(1948):593620.
28. Shin J-M, Park J-H, Park I-H, Lee H-M. Pirfenidone Inhibits Transforming Growth Factor β1-induced Extracellular Matrix Production in Nasal Polyp-derived Fibroblasts. American Journal of Rhinology & Allergy. 2015;29(6):408-13.
29. Tian XL, Yao W, Guo ZJ, Gu L, Zhu YJ. Low dose pirfenidone suppresses transforming growth factor beta-1 and tissue inhibitor of metalloproteinase-1, and protects rats from lung fibrosis induced by bleomycina. Chin Med Sci J. 2006;21(3):145-51.
30. Fernandez IE, Eickelberg O. The Impact of TGF-beta on Lung Fibrosis. Proceedings of the American Thoracic Society. 2012;9(3):111-6.
31. Border WA, Noble NA. Transforming Growth Factor β in Tissue Fibrosis. New England Journal of Medicine. 1994;331(19):1286-92.
32. Romero F, Shah D, Duong M, Penn RB, Fessler MB, Madenspacher J, et al. A Pneumocyte–Macrophage Paracrine Lipid Axis Drives the Lung toward Fibrosis. American Journal of Respiratory Cell and Molecular Biology. 2014;53(1):74-86.
33. Romero F, Hong X, Shah D, Kallen CB, Rosas I, Guo Z, et al. Lipid synthesis is required to resolve endoplasmic reticulum stress and limit fibrotic responses in the lung. American Journal of Respiratory Cell and Molecular Biology. 2018;59(2):225-36.
34. Heukels P, Moor CC, von der Thüsen JH, Wijsenbeek MS, Kool M. Inflammation and immunity in IPF pathogenesis and treatment. Respiratory Medicine. 2019;147:79-91.
35. Wynn TA, Chawla A, Pollard JW. Macrophage biology in development, homeostasis and disease. 2013. p. 445-55.
36. Wynn TA, Barron L. Macrophages: master regulators of inflammation and fibrosis. Seminars in liver disease. 2010;30(3):245-57.
37. Guenther A, Schmidt R, Nix F, Yabut-Perez M, Guth C, Rosseau S, et al. Surfactant abnormalities in idiopathic pulmonary fibrosis, hypersensitivity pneumonitis and sarcoidosis. European Respiratory Journal. 1999;14(3):565-73.
38. Schmidt R, Meier U, Markart P, Grimminger F, Velcovsky HG, Morr H, et al. Altered fatty acid composition of lung surfactant phospholipids in interstitial lung disease. American Journal of Physiology - Lung Cellular and Molecular Physiology. 2002;283(5):L1079-L85.

39. Schmidt R, Meier U, Yabut-Perez M, Walmrath D, Grimminger F, Seeger W, et al. Alteration of Fatty Acid Profiles in Different Pulmonary Surfactant Phospholipids in Acute Respiratory Distress Syndrome and Severe Pneumonia. American Journal of Respiratory and Critical Care Medicine. 2001;163(1):95-100.
40. Lopez-Rodriguez E, Boden C, Echaide M, Perez-Gil J, Kolb M, Gauldie J, et al. Surfactant dysfunction during overexpression of TGF-beta1 precedes profibrotic lung remodeling in vivo. American journal of physiology Lung cellular and molecular physiology. 2016;310(11):L1260-L71.
41. Ruwisch J, Sehlmeyer K, Roldan N, Garcia-Alvarez B, Perez-Gil J, Weaver TE, Ochs M, Knudsen L, Lopez-Rodriguez E. Air Space Distension Precedes Spontaneous Fibrotic Remodeling and Impaired Cholesterol Metabolism in the Absence of Surfactant Protein C. American Journal of Respiratory Cell and Molecular Biology. 2020;62(4):466-78.
42. Kloth C, Gruben N, Ochs M, Knudsen L, Lopez-Rodriguez E. Flow cytometric analysis of the leukocyte landscape during bleomycin-induced lung injury and fibrosis in the rat. Am J Physiol Lung Cell Mol Physiol. 2019:L109-L26.
43. Steffen L, Ruppert C, Hoymann H-G, Funke M, Ebener S, Kloth C, Muehfeld C, Ochs M, Knudsen L, Lopez-Rodriguez E. Surfactant replacement therapy reduces acute lung injury and collapse induration related lung remodeling in the bleomycin model. Am J Physiol Lung Cell Mol Physiol. 2017;313:L313-L27.
44. Lopez-Rodriguez E, Gay-Jordi G, Knudsen L, Ochs M, Serrano-Mollar A. Improved Alveolar Dynamics and Structure After Alveolar Epithelial Type II Cell Transplantation in Bleomycin Induced Lung Fibrosis. Frontiers in Medicine. 2021;8(127):640020.
45. Saito A, Horie M, Nagase T. TGF-β Signaling in Lung Health and Disease. International Journal of Molecular Sciences. 2018;19(8):2460.
46. Aschner Y, Downey GP. Transforming Growth Factor-β: Master Regulator of the Respiratory System in Health and Disease. American Journal of Respiratory Cell and Molecular Biology. 2016;54(5):647-55.
47. Roberts AB, Sporn MB. The Transforming Growth Factor-βs. In: Sporn MB, Roberts AB, editors. Peptide Growth Factors and Their Receptors I. Berlin, Heidelberg: Springer Berlin Heidelberg; 1990. p. 419-72.
48. Derynck R, Jarrett JA, Chen EY, Eaton DH, Bell JR, Assoian RK, et al. Human transforming growth factor-β complementary DNA sequence and expression in normal and transformed cells. Nature. 1985;316(6030):701-5.
49. Franzén P, ten Dijke P, Ichijo H, Yamashita H, Schulz P, Heldin CH, et al. Cloning of a TGF beta type I receptor that forms a heteromeric complex with the TGF beta type II receptor. Cell. 1993;75(4):681-92.
50. Morikawa M, Derynck R, Miyazono K. TGF-β and the TGF-β Family: Context-Dependent Roles in Cell and Tissue Physiology. Cold Spring Harbor Perspectives in Biology. 2016;8(5):a021873.
51. Stetler-Stevenson WG, Aznavoorian S, Liotta LA. Tumor Cell Interactions with the Extracellular Matrix During Invasion and Metastasis. Annual Review of Cell Biology. 1993;9(1):541-73.
52. Barcellos-Hoff MH, Dix TA. Redox-mediated activation of latent transforming growth factor-beta 1. Molecular Endocrinology. 1996;10(9):1077-83.
53. Wipff P-J, Hinz B. Integrins and the activation of latent transforming growth factor β1 – An intimate relationship. European Journal of Cell Biology. 2008;87(8):601-15.
54. Horbelt D, Denkis A, Knaus P. A portrait of Transforming Growth Factor β superfamily signalling: Background matters. The International Journal of Biochemistry & Cell Biology. 2012;44(3):469-74.
55. Border WA, Ruoslahti E. Transforming growth factor-beta in disease: the dark side of tissue repair. The Journal of Clinical Investigation. 1992;90(1):1-7.
56. Cabrera-Benitez NE, Parotto M, Post M, Han B, Spieth PM, Cheng W-E, et al. Mechanical stress induces lung fibrosis by epithelial–mesenchymal transition. Critical Care Medicine. 2012;40(2):510-7.
57. Yang J, Pan X, Wang L, Yu G. Alveolar cells under mechanical stressed niche: critical contributors to pulmonary fibrosis. Molecular Medicine. 2020;26(1):95.

58. Wu H, Yu Y, Huang H, Hu Y, Fu S, Wang Z, et al. Progressive Pulmonary Fibrosis Is Caused by Elevated Mechanical Tension on Alveolar Stem Cells. Cell. 2020;180(1):107-21.e17.
59. Tschumperlin DJ, Shively JD, Kikuchi T, Drazen JM. Mechanical Stress Triggers Selective Release of Fibrotic Mediators from Bronchial Epithelium. American Journal of Respiratory Cell and Molecular Biology. 2003;28(2):142-9.
60. Zhou BaZQaMPaLCaADKaFBaMEEaCEDaBZ. Foxp2 Inhibits Nkx2.1-Mediated Transcription of SP-C via Interactions with the Nkx2.1 Homeodomain. American Journal of Respiratory Cell and Molecular Biology. 2008;38(6):750-8.
61. Potter S, Orgeig S, Donnellan S, Daniels CB. Purifying selection drives the evolution of surfactant protein C (SP-C) independently of body temperature regulation in mammals. Comparative Biochemistry and Physiology Part D: Genomics and Proteomics. 2007;2(2):165-76.
62. Korfhagen TR, Glasser SW, Wert SE, Bruno MD, Daugherty CC, McNeish JD, et al. Cis-acting sequences from a human surfactant protein gene confer pulmonary-specific gene expression in transgenic mice. Proceedings of the National Academy of Sciences. 1990;87(16):6122-6.
63. Johansson J. Membrane properties and amyloid fibril formation of lung surfactant protein C. Biochemical Society Transactions. 2001;29(4):601-6.
64. Johansson J, Weaver TE, Tjernberg LO. Proteolytic generation and aggregation of peptides from transmembrane regions: lung surfactant protein C and amyloid β-peptide. Cellular and Molecular Life Sciences CMLS. 2004;61(3):326-35.
65. Plasencia I, Cruz A, Casals C, Pérez-Gil J. Superficial disposition of the N-terminal region of the surfactant protein SP-C and the absence of specific SP-B–SP-C interactions in phospholipid bilayers. Biochemical Journal. 2001;359(3):651-9.
66. Lukovic D, Cruz A, Gonzalez-Horta A, Almlen A, Curstedt T, Mingarro I, et al. Interfacial Behavior of Recombinant Forms of Human Pulmonary Surfactant Protein SP-C. Langmuir. 2012;28(20):7811-25.
67. Morrow MR, Taneva S, Simatos GA, Allwood LA, Keough KM. 2H NMR studies of the effect of pulmonary surfactant SP-C on the 1,2-dipalmitoyl-sn-glycero-3-phosphocholine headgroup: a model for transbilayer peptides in surfactant and biological membranes. Biochemistry. 1993;32(42):11338-44.
68. Dico AS, Taneva S, Morrow MR, Keough KM. Effect of calcium on phospholipid interaction with pulmonary surfactant protein C. Biophysical journal. 1997;73(5):2595-602.
69. Plasencia I, Rivas L, Keough KMW, Marsh D, Pérez-Gil J. The N-terminal segment of pulmonary surfactant lipopeptide SP-C has intrinsic propensity to interact with and perturb phospholipid bilayers. Biochem J. 2004;377(Pt 1):183-93.
70. Parra E, Moleiro Lara H, López-Montero I, Cruz A, Monroy F, Pérez-Gil J. A combined action of pulmonary surfactant proteins SP-B and SP-C modulates permeability and dynamics of phospholipid membranes. Biochemical Journal. 2011;438(3):555-64.
71. Parra E, Alcaraz A, Cruz A, Aguilella Vicente M, Pérez-Gil J. Hydrophobic Pulmonary Surfactant Proteins SP-B and SP-C Induce Pore Formation in Planar Lipid Membranes: Evidence for Proteolipid Pores. Biophysical Journal. 2013;104(1):146-55.
72. Possmayer F, Nag K, Rodriguez K, Qanbar R, Schürch S. Surface activity in vitro: role of surfactant proteins. Comparative Biochemistry and Physiology Part A: Molecular & Integrative Physiology. 2001;129(1):209-20.
73. Wang L, Cai P, Galla H-J, He H, Flach CR, Mendelsohn R. Monolayer–multilayer transitions in a lung surfactant model: IR reflection–absorption spectroscopy and atomic force microscopy. European Biophysics Journal. 2005;34(3):243-54.
74. Creuwels LA, Demel RA, van Golde LM, Benson BJ, Haagsman HP. Effect of acylation on structure and function of surfactant protein C at the air-liquid interface. Journal of Biological Chemistry. 1993;268(35):26752-8.
75. Amrein M, von Nahmen A, Sieber M. A scanning force- and fluorescence light microscopy study of the structure and function of a model pulmonary surfactant. European Biophysics Journal. 1997;26(5):349-57.

76. Glasser SW, Burhans MS, Korfhagen TR, Na CLL, Sly PD, Ross GF, et al. Altered stability of pulmonary surfactant in SP-C-deficient mice. Proceedings of the National Academy of Sciences. 2001;98(11):6366-71.
77. Sehlmeyer K, Ruwisch J, Roldan N, Lopez-Rodriguez E. Alveolar Dynamics and Beyond – The Importance of Surfactant Protein C and Cholesterol in Lung Homeostasis and Fibrosis. Frontiers in Physiology. 2020;11(386).
78. Thomas AQ, Lane K, Phillips J, Prince M, Markin C, Speer M, et al. Heterozygosity for a Surfactant Protein C Gene Mutation Associated with Usual Interstitial Pneumonitis and Cellular Nonspecific Interstitial Pneumonitis in One Kindred. American Journal of Respiratory and Critical Care Medicine. 2002;165(9):1322-8.
79. Tredano M, Griese M, Brasch F, Schumacher S, Blic Jd, Marque S, et al. Mutation of SFTPC in infantile pulmonary alveolar proteinosis with or without fibrosing lung disease. American Journal of Medical Genetics Part A. 2004;126A(1):18-26.
80. Abou Taam R, Jaubert F, Emond S, Le Bourgeois M, Epaud R, Karila C, et al. Familial interstitial disease with I73T mutation: A mid- and long-term study. Pediatric Pulmonology. 2009;44(2):167-75.
81. Thouvenin G, Taam RA, Flamein F, Guillot L. Characteristics of disorders associated with genetic mutations of surfactant protein C. Archives of Disease in Childhood. 2010;95(6):449-54.
82. Cottin V, Reix P, Khouatra C, Thivolet-Bjui F, Feldmann D, Cordier J-F. Combined pulmonary fibrosis and emphysema syndrome associated with familial SFTPC mutation. Thorax. 2011;66(10):918-9.
83. Avital A, Hevroni A, Godfrey S, Cohen S, Maayan C, Nusair S, et al. Natural history of five children with surfactant protein C mutations and interstitial lung disease. Pediatric pulmonology. 2014;49(11):1097-105.
84. Hevroni A, Goldman A, Springer C. Infant pulmonary function testing in chronic pneumonitis of infancy due to surfactant protein C mutation. Pediatric Pulmonology. 2015;50(6):E17-E23.
85. Salerno T, Peca D, Menchini L, Schiavino A, Boldrini R, Esposito F, et al. Surfactant Protein C-associated interstitial lung disease; three different phenotypes of the same SFTPC mutation. Italian Journal of Pediatrics. 2016;42(1):23.
86. Ono S, Tanaka T, Ishida M, Kinoshita A, Fukuoka J, Takaki M, et al. Surfactant protein C G100S mutation causes familial pulmonary fibrosis in Japanese kindred. The European respiratory journal. 2011;38(4):861-9.
87. Kuse N, Abe S, Hayashi H, Kamio K, Saito Y, Azuma A, et al. Familial interstitial pneumonia in an adolescent boy with surfactant protein C gene (Y104H) mutation. Sarcoidosis, vasculitis, and diffuse lung diseases : official journal of WASOG. 2013;30(1):73-7.
88. van Hoorn J, Brouwers A, Griese M, Kramer B. Successful weaning from mechanical ventilation in a patient with surfactant protein C deficiency presenting with severe neonatal respiratory distress. BMJ case reports. 2014;2014(bcr2013203053).
89. Chibbar R, Shih F, Baga M, Torlakovic E, Ramlall K, Skomro R, et al. Nonspecific interstitial pneumonia and usual interstitial pneumonia with mutation in surfactant protein C in familial pulmonary fibrosis. Mod Pathol. 2004;17(8):973-80.
90. Stevens PA, Pettenazzo A, Brasch F, Mulugeta S, Baritussio A, Ochs M, et al. Nonspecific Interstitial Pneumonia, Alveolar Proteinosis, and Abnormal Proprotein Trafficking Resulting from a Spontaneous Mutation in the Surfactant Protein C Gene. Pediatric Research. 2005;57:89-98.
91. Baldán Á, Tarr P, Vales CS, Frank J, Shimotake TK, Hawgood S, et al. Deletion of the Transmembrane Transporter ABCG1 Results in Progressive Pulmonary Lipidosis *. Journal of Biological Chemistry. 2006;281(39):29401-10.
92. de Aguiar Vallim TQ, Lee E, Merriott DJ, Goulbourne CN, Cheng J, Cheng A, et al. ABCG1 regulates pulmonary surfactant metabolism in mice and men [S]. Journal of Lipid Research. 2017;58(5):941-54.

93. Mora AL, Torres-Gonzalez E, Rojas M, Corredor C, Ritzenthaler J, Xu J, et al. Activation of Alveolar Macrophages via the Alternative Pathway in Herpesvirus-Induced Lung Fibrosis. American Journal of Respiratory Cell and Molecular Biology. 2006;35(4):466-73.
94. Puttur F, Gregory LG, Lloyd CM. Airway macrophages as the guardians of tissue repair in the lung. Immunology and cell biology. 2019;97(3):246-57.
95. Minutti CM, Knipper JA, Allen JE, Zaiss DMW. Tissue-specific contribution of macrophages to wound healing. Seminars in Cell & Developmental Biology. 2017;61:3-11.
96. Morales-Nebreda L, Misharin AV, Perlman H, Budinger GRS. The heterogeneity of lung macrophages in the susceptibility to disease. Eur Respir Rev. 2015;24:505-9.
97. Misharin AV, Morales-Nebreda L, Mutlu GM, Budinger GRS, Perlman H. Flow Cytometric Analysis of Macrophages and Dendritic Cell Subsets in the Mouse Lung. American Journal of Respiratory Cell and Molecular Biology. 2013;49(4):503-10.
98. Prasse A, Pechkovsky DV, Toews GB, Jungraithmayr W, Kollert F, Goldmann T, et al. A Vicious Circle of Alveolar Macrophages and Fibroblasts Perpetuates Pulmonary Fibrosis via CCL18. American Journal of Respiratory and Critical Care Medicine. 2006;173(7):781-92.
99. Hiemstra PS, McCray PB, Bals R. The innate immune function of airway epithelial cells in inflammatory lung disease. European Respiratory Journal. 2015;45(4):1150-62.
100. Hasenberg M, Stegemann-Koniszewski S, Gunzer M. Cellular immune reactions in the lung. Immunological Reviews. 2013;251(1):189-214.
101. Chaudhuri N, Sabroe I. Basic science of the innate immune system and the lung. Paediatric Respiratory Reviews. 2008;9(4):236-42.
102. Hartl D, Tirouvanziam R, Laval J, Greene CM, Habiel D, Sharma L, et al. Innate Immunity of the Lung: From Basic Mechanisms to Translational Medicine. Journal of Innate Immunity. 2018;10(5-6):487-501.
103. Gerard C, Rollins BJ. Chemokines and disease. Nature Immunology. 2001;2(2):108-15.
104. Sabroe I, Lloyd CM, Whyte MKB, Dower SK, Williams TJ, Pease JE. Chemokines, innate and adaptive immunity, and respiratory disease. European Respiratory Journal. 2002;19(2):350-5.
105. Panina-Bordignon P, D'Ambrosio D. Chemokines and their receptors in asthma and chronic obstructive pulmonary disease. Current Opinion in Pulmonary Medicine. 2003;9(2):104-10.
106. Owen C. Chemokine Receptors in Airway Disease: Which Receptors to Target? Pulmonary Pharmacology & Therapeutics. 2001;14(3):193-202.
107. Kruger P, Saffarzadeh M, Weber ANR, Rieber N, Radsak M, von Bernuth H, et al. Neutrophils: Between Host Defence, Immune Modulation, and Tissue Injury. PLOS Pathogens. 2015;11(3):e1004651.
108. Pabst R. Is BALT a major component of the human lung immune system? Immunology Today. 1992;13(4):119-22.
109. Lopez-Rodriguez E, Gay-Jordi G, Mucci A, Lachmann N, Serrano-Mollar A. Lung surfactant metabolism: early in life, early in disease and target in cell therapy. Cell and Tissue Research. 2017;367:721-35.
110. Gordon S. Alternative activation of macrophages. Nat Rev Immunol. 2003;3(1):23-35.
111. Gordon S, Martinez FO. Alternative Activation of Macrophages: Mechanism and Functions. Immunity. 2010;32(5):593-604.
112. Mills CD. M1 and M2 Macrophages: Oracles of Health and Disease. Crit Rev Immunol. 2012;32(6):463-88.
113. Moeller A, Ask K, Warburton D, Gauldie J, Kolb M. The bleomycin animal model: A useful tool to investigate treatment options for idiopathic pulmonary fibrosis? The International Journal of Biochemistry & Cell Biology. 2008;40(3):362-82.
114. Mouratis MA, Aidinis V. Modeling pulmonary fibrosis with bleomycin. Current Opinion in Pulmonary Medicine. 2011;17(5):355-61.
115. Lutz D, Gazdhar A, Lopez-Rodriguez E, Ruppert C, Mahavadi P, Guenther A, et al. Alveolar derecruitment and collapse induration as crucial mechanisms in lung injury and fibrosis. Am J Respir Cell Mol Biol. 2015;52:232-43.

116. Myers JL, Katzenstein AL. Ultrastructural evidence of alveolar epithelial injury in idiopathic bronchiolitis obliterans-organizing pneumonia. The American journal of pathology. 1988;132(1):102-9.
117. Bates JHT, Smith BJ. Ventilator-induced lung injury and lung mechanics. Annals of Translational Medicine. 2018:378.
118. Nieman GF, Andrews P, Satalin J, Wilcox K, Kollisch-Singule M, Madden M, et al. Acute lung injury: How to stabilize a broken lung. 2018. p. 136.
119. Autilio C, Perez-Gil J. Understanding the principle biophysics concepts of pulmonary surfactant in health and disease. Arch Dis Child - Fetal and Neonatal Edition. 2018;104(4):F443-F51.
120. Smith BJ, Bartolak-Suki E, Suki B, Roy GS, Hamlington KL, Charlebois CM, et al. Linking ventilator injury-induced leak across the blood-gas barrier to derangements in murine lung function. Frontiers in Physiology. 2017(466).
121. Hasan D, Blankman P, Nieman GF. Purinergic signalling links mechanical breath profile and alveolar mechanics with the pro-inflammatory innate immune response causing ventilation-induced lung injury. Purinergic signalling. 2017;13(3):363-86.
122. Petroulia V, Funke M, Zumstein P, Berezowska S, Ebner L, Geiser T, et al. Increased Expiratory Computed Tomography Density Reveals Possible Abnormalities in Radiologically Preserved Lung Parenchyma in Idiopathic Pulmonary Fibrosis. Investigative Radiology. 2018;53(1):45-51.
123. Todd NW, Atamas SP, Luzina IG, Galvin JR. Permanent alveolar collapse is the predominant mechanism in idiopathic pulmonary fibrosis. Expert Review of Respiratory Medicine. 2015;9(4):411-8.
124. Bachofen H, Schurch S. Alveolar surface forces and lung architecture. 2001;129(1):183-93.
125. Ma B, Suki B, Bates JHT. Effects of recruitment/derecruitment dynamics on the efficacy of variable ventilation. Journal of Applied Physiology. 2011;110(5):1319-26.
126. Bilek AM, Dee KC, Gaver DP. Mechanisms of surface-tension-induced epithelial cell damage in a model of pulmonary airway reopening. Journal of Applied Physiology. 2003;94(2):770-83.
127. Cassidy KJ, Halpern D, Ressler BG, Grotberg JB. Surfactant effects in model airway closure experiments. Journal of applied physiology (Bethesda, Md : 1985). 1999;87(1):415-27.
128. Ghadiali SN, Gaver DP. Biomechanics of liquid-epithelium interactions in pulmonary airways. 2008. p. 232-43.
129. Fehrenbach H. Alveolar epithelial type II cell: defender of the alveolus revisited. Respir Res. 2001;2:33-46.
130. Mouded M, Egea EE, Brown MJ, Hanlon SM, Houghton AMG, Tsai LW, et al. Epithelial cell apoptosis causes acute lung injury masquerading as emphysema. American Journal of Respiratory Cell and Molecular Biology. 2009;41(4):407-14.
131. Sisson TH, Mendez M, Choi K, Subbotina N, Courey A, Cunningham A, et al. Targeted injury of type II alveolar epithelial cells induces pulmonary fibrosis. American journal of respiratory and critical care medicine. 2010;181(3):254-63.
132. Hagimoto N, Kuwano K, Inoshima I, Yoshimi M, Nakamura N, Fujita M, et al. TGF-beta 1 as an Enhancer of Fas-Mediated Apoptosis of Lung Epithelial Cells. The Journal of Immunology. 2002;168(12):6470-8.
133. Korfei M, Ruppert C, Mahavadi P, Henneke I, Markart P, Koch M, et al. Epithelial endoplasmic reticulum stress and apoptosis in sporadic idiopathic pulmonary fibrosis. American Journal of Respiratory and Critical Care Medicine. 2008;178(8):838-46.
134. Zoz DF, Lawson WE, Blackwell TS. Idiopathic pulmonary fibrosis: a disorder of epithelial cell dysfunction. The American journal of the medical sciences. 2011;341(6):435-8.
135. Dreyfuss D, Martin-Lefvre L, Saumon G. Hyperinflation-induced lung injury during alveolar flooding in rats: effect of perfluorocarbon instillation. American journal of respiratory and critical care medicine. 1999;159(6):1752-7.
136. Cong X, Hubmayr RD, Li C, Zhao X. Plasma membrane wounding and repair in pulmonary diseases. 2017. p. L371-L91.
137. Kook S, Wang P, Young LR, Schwake M, Saftig P, Weng X, et al. Impaired Lysosomal Integral Membrane Protein 2-dependent Peroxiredoxin 6 Delivery to Lamellar Bodies Accounts for Altered

Alveolar Phospholipid Content in Adaptor Protein-3-deficient pearl Mice. The Journal of biological chemistry. 2016;291(16):8414-27.
138. Ozyilmaz E, Gunasti S, Kuyucu Y, Polat S, Gumurdulu D, Kuleci S, et al. Hermansky Pudlak Syndrome and pulmonary alveolar proteinosis at the same patient: First case report in the world literature. Sarcoidosis Vasculitis and Diffuse Lung Diseases. 2013;30(3):217-20.
139. Mao P, Li J, Huang Y, Wu S, Pang X, He W, et al. MicroRNA-19b Mediates Lung Epithelial-Mesenchymal Transition via Phosphatidylinositol-3,4,5-Trisphosphate 3-Phosphatase in Response to Mechanical Stretch. American journal of respiratory cell and molecular biology. 2017;56(1):11-9.
140. Sheppard D. Epithelial-mesenchymal interactions in fibrosis and repair: Transforming growth factor-beta activation by epithelial cells and fibroblasts. 2015;12:S21-S3.
141. Froese AR, Shimbori C, Bellaye P-S, Inman M, Obex S, Fatima S, et al. Stretch-induced Activation of Transforming Growth Factor-β1 in Pulmonary Fibrosis. American journal of respiratory and critical care medicine. 2016;194(1):84-96.
142. Khalil N, O'Connor R. The Role of TGF-β in Bleomycin Induced Pulmonary Fibrosis. In: Jakowlew SB, editor. Transforming Growth Factor-β in Cancer Therapy, Volume I: Basic and Clinical Biology. Totowa, NJ: Humana Press; 2008. p. 581-94.
143. Lopez-Rodriguez E, Echaide M, Cruz A, Taeusch HW, Perez-Gil J. Meconium impairs pulmonary surfactant by a combined action of cholesterol and bile acids. Biophysical Journal. 2011;100(3):646-55.
144. Lopez-Rodriguez E, Ospina OL, Echaide M, Taeusch HW, Perez-Gil J. Exposure to polymers reverses inhibition of pulmonary surfactant by serum, meconium, or cholesterol in the captive bubble surfactometer. Biophysical Journal. 2012;103(7):1451-9.
145. Cockshutt AM, Possmayer F. Lysophosphatidylcholine sensitizes lipid extracts of pulmonary surfactant to inhibition by serum proteins. Biochimica et Biophysica Acta (BBA) - Lipids and Lipid Metabolism. 1991;1086(1):63-71.
146. Fuchimukai T, Fujiwara T, Takahashi A, Enhorning G. Artificial pulmonary surfactant inhibited by proteins. Journal of Applied Physiology. 1987;62(2):429-37.
147. Holm BA, Venkitaraman AR, Enhorning G, Notter RH. Biophysical inhibition of synthetic lung surfactants. Chemistry and Physics of Lipids. 1990;52(3):243-50.
148. Holm BA, Enhorning G, Notter RH. A biophysical mechanism by which plasma proteins inhibit lung surfactant activity. Chemistry and Physics of Lipids. 1988;49(1):49-55.
149. Holm BA, Notter RH, Finkelstein JN. Surface property changes from interactions of albumin with natural lung surfactant and extracted lung lipids. Chemistry and physics of lipids. 1985;38(3):287-98.
150. Seeger W, Stohr G, Wolf HR, Neuhof H. Alteration of surfactant function due to protein leakage: special interaction with fibrin monomer. Journal of Applied Physiology. 1985;58(2):326-38.
151. Holm BA, Notter RH. Effects of hemoglobin and cell membrane lipids on pulmonary surfactant activity. Journal of Applied Physiology. 1987;63(4):1434-42.
152. Seeger W, Gunther A, Thede C. Differential sensitivity to fibrinogen inhibition of SP-C- vs. SP-B-based surfactants. American Journal of Physiology-Lung Cellular and Molecular Physiology. 1992;262(3):L286-L91.
153. Seeger W, Thede C, Günther A, Grube C. Surface properties and sensitivity to protein-inhibition of a recombinant apoprotein C-based phospholipid mixture in vitro — comparison to natural surfactant. Biochimica et Biophysica Acta (BBA) - Lipids and Lipid Metabolism. 1991;1081(1):45-52.
154. Taylor FB, Abrams ME. Effect of surface active lipoprotein on clotting and fibrinolysis, and of fibrinogen on surface tension of surface active lipoprotein: With a hypothesis on the pathogenesis of pulmonary atelectasis and hyaline membrane in respiratory distress syndrome of the newborn. The American Journal of Medicine. 1966;40(3):346-50.
155. Bubbles, Babies and Biology: The Story of Surfactant. The FASEB Journal. 2004;18(13):1624e-e.
156. Berry DD. Neonatology in the 1990's: Surfactant Replacement Therapy Becomes a Reality. Clinical Pediatrics. 1991;30(3):167-72.
157. Curstedt T, Halliday HL, Speer CP. A Unique Story in Neonatal Research: The Development of a Porcine Surfactant. Neonatology. 2015;107(4):321-9.

158. Speer CP, Robertson B, Curstedt T, Halliday HL, Compagnone D, Gefeller O, et al. Randomized European Multicenter Trial of Surfactant Replacement Therapy for Severe Neonatal Respiratory Distress Syndrome: Single Versus Multiple Doses of Curosurf. Pediatrics. 1992;89(1):13-20.
159. Fanaroff AA, Wright LL, Stevenson DK, Shankaran S, Donovan EP, Ehrenkranz RA, et al. Very-low-birth-weight outcomes of the National Institute of Child Health and Human Development Neonatal Research Network, May 1991 through December 1992. American Journal of Obstetrics & Gynecology. 1995;173(5):1423-31.
160. Hack M, Friedman H, Fanaroff AA. Outcomes of Extremely Low Birth Weight Infants. Pediatrics. 1996;98(5):931.
161. Avery ME, Mead J. Surface properties in relation to atelectasis and hyaline membrane disease. AMA J Dis Child. 1959;97(5, Part 1):517-23.
162. Fujiwara T, Konishi M, Chida S, Okuyama K, Ogawa Y, Takeuchi Y, et al. Surfactant Replacement Therapy With a Single Postventilatory Dose of a Reconstituted Bovine Surfactant in Preterm Neonates With Respiratory Distress Syndrome: Final Analysis of a Multicenter, Double-blind, Randomized Trial and Comparison With Similar Trials. Pediatrics. 1990;86(5):753-64.
163. Victorin LH, Deverajan LV, Curstedt T, Robertson B. Surfactant replacement in spontaneously breathing babies with hyaline membrane disease--a pilot study. Biol Neonate. 1990;58(3):121-6.
164. Ainsworth SB. Pathophysiology of Neonatal Respiratory Distress Syndrome. Treatments in Respiratory Medicine. 2005;4(6):423-37.
165. Taut FJH, Rippin G, Schenk P, Findlay G, Wurst W, Häfner D, et al. A Search for Subgroups of Patients With ARDS Who May Benefit From Surfactant Replacement Therapy: A Pooled Analysis of Five Studies With Recombinant Surfactant Protein-C Surfactant (Venticute). CHEST. 2008;134(4):724-32.
166. Baudouin SV. Exogenous Surfactant Replacement in ARDS — One Day, Someday, or Never? New England Journal of Medicine. 2004;351(9):853-5.
167. Robertson B. Surfactant inactivation and surfactant replacement in experimental models of ARDS. Acta Anaesthesiologica Scandinavica. 1991;35(s95):22-8.
168. Parimon T, Yao C, Stripp BR, Noble PW, Chen P. Alveolar Epithelial Type II Cells as Drivers of Lung Fibrosis in Idiopathic Pulmonary Fibrosis. International Journal of Molecular Sciences. 2020;21(7):2269.
169. Goss V, Hunt AN, Postle AD. Regulation of lung surfactant phospholipid synthesis and metabolism. Biochimica et Biophysica Acta (BBA) - Molecular and Cell Biology of Lipids. 2013;1831(2):448-58.
170. Wright JR, Clements JA. Metabolism and Turnover of Lung Surfactant. American Review of Respiratory Disease. 1987;136(2):426-44.
171. Wright JR, Dobbs LG. Regulation of Pulmonary Surfactant Secretion and Clearance. Annual Review of Physiology. 1991;53(1):395-414.
172. Hawgood S, Poulain FR. The Pulmonary Collectins and Surfactant Metabolism. Annual Review of Physiology. 2001;63(1):495-519.
173. Baker AD, Malur A, Barna BP, Kavuru MS, Malur AG, Thomassen MJ. PPARgamma regulates the expression of cholesterol metabolism genes in alveolar macrophages. Biochem Biophys Res Commun. 2010;393:682-7.
174. Baker AD, Malur A, Barna BP, Ghosh S, Kavuru MS, Malur AG, et al. Targeted PPARgamma deficiency in alveolar macrophages disrupts surfactant catabolism. Journal of Lipid Research. 2010;51(6):1325-31.
175. Malur A, Baker AD, McCoy AJ, Wells G, Barna BP, Kavuru MS, et al. Restoration of PPARgamma reverses lipid accumulation in alveolar macrophages of GM-CSF knockout mice. American journal of physiology Lung cellular and molecular physiology. 2011;300(1):L73-L80.
176. Rebello CM, Jobe AH, Eisele JW, Ikegami M. Alveolar and tissue surfactant pool sizes in humans. American Journal of Respiratory and Critical Care Medicine. 1996;154(3):625-8.
177. Hamm H, Kroegel C, Hohlfeld J. Surfactant: a review of its functions and relevance in adult respiratory disorders. Respiratory Medicine. 1996;90(5):251-70.

178. Post M, Batenburg JJ, Schuurmans EAJM. The rate-limiting step in the biosynthesis of phosphatidylcholine by alveolar type ii cells from adult rat lung. Biochimica et Biophysica Acta (BBA) - Lipids and Lipid Metabolism. 1982;712(2):390-4.
179. Kennedy MA, Barrera GC, Nakamura K, Baldn A, Tarr P, Fishbein MC, et al. ABCG1 has a critical role in mediating cholesterol efflux to HDL and preventing cellular lipid accumulation. Cell Metabolism. 2005;1(2):121-31.
180. Out R, Hoekstra M, Hildebrand RB, Kruit JK, Meurs I, Li Z, et al. Macrophage ABCG1 deletion disrupts lipid homeostasis in alveolar macrophages and moderately influences atherosclerotic lesion development in LDL receptor-deficient mice. Arteriosclerosis, Thrombosis, and Vascular Biology. 2006;26(10):2295-300.
181. Wang N, Silver DL, Thiele C, Tall AR. ATP-binding cassette transporter A1 (ABCA1) functions as a cholesterol efflux regulatory protein. Journal of Biological Chemistry. 2001;276(26):23742-7.
182. Chroneos ZC, Abdolrasulnia R, Whitsett JA, Rice WR, Shepherd VL. Purification of a cell-surface receptor for surfactant protein A. Journal of Biological Chemistry. 1996;271(27):16375-83.
183. Kuroki Y, Mason RJ, Voelker DR. Alveolar type II cells express a high-affinity receptor for pulmonary surfactant protein A. Proceedings of the National Academy of Sciences. 1988;85(15):5566-70.
184. Jain D, Dodia C, Fisher AB, Bates SR. Pathways for clearance of surfactant protein A from the lung. American journal of physiology Lung cellular and molecular physiology. 2005;289(6):L1011-L8.
185. Wissel H, Lehfeldt A, Klein P, Mller T, Stevens PA. Endocytosed SP-A and surfactant lipids are sorted to different organelles in rat type II pneumocytes. American journal of physiology Lung cellular and molecular physiology. 2001;281(2):L345-L60.
186. Crowther JE, Schlesinger LS. Endocytic pathway for surfactant protein A in human macrophages: binding, clathrin-mediated uptake, and trafficking through the endolysosomal pathway. American journal of physiology Lung cellular and molecular physiology. 2006;290(2):L334-L42.
187. Koth LL, Alex B, Hawgood S, Nead MA, Sheppard D, Erle DJ, et al. Integrin beta 6 mediates phospholipid and collectin homeostasis by activation of latent TGF-beta 1. American Journal of Respiratory Cell and Molecular Biology. 2007;37(6):651-9.
188. Munger JS, Huang X, Kawakatsu H, Griffiths MJD, Dalton SL, Wu J, et al. A Mechanism for regulating pulmonary inflammation and fibrosis: The integrin alpha-v beta-6 binds and activates latent TGF-beta 1. Cell. 1999;96(3):319-28.
189. Glasser S, Senft A. Pulmonary surfactant homeostasis and altered macrophage function. Lung Macrophages in Health And Disease, ed S Hodge (Bentham: Science Publisher Ltd). 2009:1-13.
190. Herold S, Becker C, Ridge KM, Budinger GRS. Influenza virus-induced lung injury: pathogenesis and implications for treatment. European Respiratory Journal. 2015;45(5):1463-78.
191. Tyrrell C, McKechnie SR, Beers MF, Mitchell TJ, McElroy MC. Differential alveolar epithelial injury and protein expression in pneumococcal pneumonia. Experimental Lung Research. 2012;38(5):266-76.
192. Wiener-Kronish JP, Sakuma T, Kudoh I, Pittet JF, Frank D, Dobbs L, et al. Alveolar epithelial injury and pleural empyema in acute P. aeruginosa pneumonia in anesthetized rabbits. Journal of Applied Physiology. 1993;75(4):1661-9.
193. Kosmider B, Messier EM, Chu HW, Mason RJ. Human Alveolar Epithelial Cell Injury Induced by Cigarette Smoke. PLOS ONE. 2011;6(12):e26059.
194. Thorley AJ, Tetley TD. Pulmonary epithelium, cigarette smoke, and chronic obstructive pulmonary disease. Int J Chron Obstruct Pulmon Dis. 2007;2(4):409-28.
195. Brody AR, Hill LH, Warheit DB. Induction of early alveolar injury by inhaled asbestos and silica. Fed Proc. 1985;44(10):2596-601.
196. Kamp DW, Panduri V, Weitzman SA, Chandel N. Asbestos-induced alveolar epithelial cell apoptosis:Role of mitochondrial dysfunction caused by iron-derived free radicals. In: Vallyathan V, Shi X, Castranova V, editors. Oxygen/Nitrogen Radicals: Cell Injury and Disease. Boston, MA: Springer US; 2002. p. 153-60.

197. Miller BE, Gary ERH. Hypertrophy and Hyperplasia of Alveolar Type II Cells in Response to Silica and Other Pulmonary Toxicants. Environmental Health Perspectives. 1990;85:15-23.
198. Manning CB, Vallyathan V, Mossman BT. Diseases caused by asbestos: mechanisms of injury and disease development. International Immunopharmacology. 2002;2(2):191-200.
199. Selman M. From Anti-inflammatory Drugs Through Antifibrotic Agents to Lung Transplantation: A Long Road of Research, Clinical Attempts, and Failures in the Treatment of Idiopathic Pulmonary Fibrosis. CHEST. 2002;122(3):759-61.
200. Klingsberg RC, Mutsaers SE, Lasky JA. Current clinical trials for the treatment of idiopathic pulmonary fibrosis. Respirology. 2010;15(1):19-31.
201. Meduri GU, Eltorky MA. Understanding ARDS-associated fibroproliferation. Intensive Care Medicine. 2015;41(3):517-20.
202. Meduri GU, Belenchia JM, Estes RJ, Wunderink RG, Torky ME, Leeper KV. Fibroproliferative Phase of ARDS: Clinical Findings and Effects of Corticosteroids. Chest. 1991;100(4):943-52.
203. Vasarmidi E, Tsitoura E, Spandidos DA, Tzanakis N, Antoniou KM. Pulmonary fibrosis in the aftermath of the Covid-19 era (Review). Exp Ther Med. 2020;20(3):2557-60.
204. Ojo AS, Balogun SA, Williams OT, Ojo OS. Pulmonary Fibrosis in COVID-19 Survivors: Predictive Factors and Risk Reduction Strategies. Pulmonary Medicine. 2020;2020:6175964.
205. Bersani I, Kunzmann S, Speer CP. Immunomodulatory properties of surfactant preparations. Expert Review of Anti-infective Therapy. 2013;11(1):99-110.
206. Fernsler JG, Zasadzinski JA. Competitive Adsorption: A Physical Model for Lung Surfactant Inactivation. Langmuir. 2009;25(14):8131-43.
207. Lopez-Rodriguez E, Cruz A, Richter RP, Taeusch HW, Pérez-Gil J. Transient Exposure of Pulmonary Surfactant to Hyaluronan Promotes Structural and Compositional Transformations into a Highly Active State. Journal of Biological Chemistry. 2013;288(41):29872-81.
208. López-Rodríguez E, Ospina Olga L, Echaide M, Taeusch HW, Pérez-Gil J. Exposure to Polymers Reverses Inhibition of Pulmonary Surfactant by Serum, Meconium, or Cholesterol in the Captive Bubble Surfactometer. Biophysical Journal. 2012;103(7):1451-9.
209. Lu KW, Taeusch HW, Clements JA. Hyaluronan with dextran added to therapeutic lung surfactants improves effectiveness in vitro and in vivo. Experimental Lung Research. 2013;39(4-5):191-200.
210. Campbell H, Bosma K, Brackenbury A, McCaig L, Yao L-J, Veldhuizen R, et al. Polyethylene Glycol (PEG) Attenuates Exogenous Surfactant in Lung-injured Adult Rabbits. American Journal of Respiratory and Critical Care Medicine. 2002;165(4):475-80.
211. Beike L, Wrede C, Hegermann J, Lopez-Rodriguez E, Kloth C, Gauldie J, et al. Surfactant dysfunction and alveolar collapse are linked with fibrotic septal wall remodeling in the TGF-beta 1-induced mouse model of pulmonary fibrosis. Laboratory Investigation. 2019:830-52.
212. Veen Avt, Mouton JW, Gommers D, Lachmann B. Pulmonary surfactant as vehicle for intratracheally instilled tobramycin in mice infected with Klebsiella pneumoniae. British Journal of Pharmacology. 1996;119(6):1145-8.
213. Banaschewski BJH, Baer B, Arsenault C, Jazey T, Veldhuizen EJA, Delport J, et al. The Antibacterial and Anti-inflammatory Activity of Chicken Cathelicidin-2 combined with Exogenous Surfactant for the Treatment of Cystic Fibrosis-Associated Pathogens. Scientific Reports. 2017;7(1):15545.
214. Basabe-Burgos O, Zebialowicz J, Stichtenoth G, Curstedt T, Bergman P, Johansson J, et al. Natural Derived Surfactant Preparation As a Carrier of Polymyxin E for Treatment of Pseudomonas aeruginosa Pneumonia in a Near-Term Rabbit Model. Journal of Aerosol Medicine and Pulmonary Drug Delivery. 2018;32(2):110-8.
215. Venkataraman R, Kamaluddeen M, Hasan SU, Robertson HL, Lodha A. Intratracheal Administration of Budesonide-Surfactant in Prevention of Bronchopulmonary Dysplasia in Very Low Birth Weight Infants: A Systematic Review and Meta-Analysis. Pediatric Pulmonology. 2017;52(7):968-75.

216. McEvoy CT, Ballard PL, Ward RM, Rower JE, Wadhawan R, Hudak ML, et al. Dose-escalation trial of budesonide in surfactant for prevention of bronchopulmonary dysplasia in extremely low gestational age high-risk newborns (SASSIE). Pediatric Research. 2020;88(4):629-36.
217. Mirastschijski U, Dembinski R, Maedler K. Lung Surfactant for Pulmonary Barrier Restoration in Patients With COVID-19 Pneumonia. Frontiers in Medicine. 2020;7(254).
218. Anzueto A, Baughman RP, Guntupalli KK, Weg JG, Wiedemann HP, Raventós AA, et al. Aerosolized Surfactant in Adults with Sepsis-Induced Acute Respiratory Distress Syndrome. New England Journal of Medicine. 1996;334(22):1417-22.
219. Lewis JF, Ikegami M, Jobe AH, Tabor B. Aerosolized surfactant treatment of preterm lambs. Journal of Applied Physiology. 1991;70(2):869-76.
220. Guillamat-Prats R, Gay-Jordi G, Xaubet A, Peinado VI, Serrano-Mollar A. Alveolar type II cell transplantation restores pulmonary surfactant protein levels in lung fibrosis. The Journal of Heart and Lung Transplantation. 2014;33(7):758-65.
221. Serrano-Mollar A, Gay-Jordi G, Guillamat-Prats R, Closa D, Hernandez-Gonzalez F, Marin P, et al. Safety and tolerability of alveolar type II cell transplantation in idiopathic pulmonary fibrosis. Chest. 2016;150(3):533-43.
222. Serrano-Mollar A, Nacher M, Gay-Jordi G, Closa D, Xaubet A, Bulbena O. Intratracheal transplantation of alveolar type II cells reverses bleomycin-induced lung fibrosis. American journal of respiratory and critical care medicine. 2007;176(12):1261-8.
223. Alvarez-Palomo B, Sanchez-Lopez LI, Moodley Y, Edel MJ, Serrano-Mollar A. Induced pluripotent stem cell-derived lung alveolar epithelial type II cells reduce damage in bleomycin-induced lung fibrosis. Stem Cell Research & Therapy. 2020;11(1):213.
224. Curley GF, Hayes M, Ansari B, Shaw G, Ryan A, Barry F, et al. Mesenchymal stem cells enhance recovery and repair following ventilator-induced lung injury in the rat. Thorax. 2012;67(6):496-501.
225. Curley GF, Ansari B, Hayes M, Devaney J, Masterson C, Ryan A, et al. Effects of Intratracheal Mesenchymal Stromal Cell Therapy during Recovery and Resolution after Ventilator-induced Lung Injury. Anesthesiology. 2013;118(4):924-32.
226. Chimenti L, Luque T, Bonsignore MR, Ramírez J, Navajas D, Farré R. Pre-treatment with mesenchymal stem cells reduces ventilator-induced lung injury. European Respiratory Journal. 2012;40(4):939-48.

6 ACKNOWLEDGEMENTS

I would like to thank to my thesis supervisor, Prof.Dr. Jesus Perez-Gil, for introducing me to the amazing world of lung surfactant back in 2008. I would also like to thank Prof.Dr. Lars Knudsen and Prof.Dr. Matthias Ochs for their continuous support in this adventure of researching in lung surfactant from 2013. Special thanks to Prof.Dr. Matthias Ochs for his trust in me and help in developing my career. To the three of them. Thanks. Hoping that this is the beginning of the next chapter in lung surfactant research and that we all write it together.

I would also like to thank to the people that accompanied me along this trip. Thanks to all my lab colleagues, collaborators, lab friends and especially to my students (all current and StrucMeds).

Thanks to my friends, the ones that I left in Madrid and the ones who stayed in Hannover. Special thanks to the person who moved with me and supported me during all the changes, good and bad times and the writing of this work.

To my family for their continuous support, regardless of the distance between us.

7 ANNEX

7.1 EIDESSTTATLICHE ERKLÄRUNG

Erklärung

§ 4 Abs. 3 (k) der HabOMed der Charité

Hiermit erkläre ich, dass

- weder früher noch gleichzeitig ein Habilitationsverfahren durchgeführt oder angemeldet wurde,
- die vorgelegte Habilitationsschrift ohne fremde Hilfe verfasst, die beschriebenen Ergebnisse selbst gewonnen sowie die verwendeten Hilfsmittel, die Zusammenarbeit mit anderen Wissenschaftlern/Wissenschaftlerinnen und mit technischen Hilfskräften sowie die verwendete Literatur vollständig in der Habilitationsschrift angegeben wurden,
- mir die geltende Habilitationsordnung bekannt ist.

Ich erkläre ferner, dass mir die Satzung der Charité – Universitätsmedizin Berlin zur Sicherung Guter Wissenschaftlicher Praxis bekannt ist und ich mich zur Einhaltung dieser Satzung verpflichte.

……. …….

Datum Unterschrift